University of Strathclyde

Department of Naval Architecture and Marine Engineering

Reliability–Based Fatigue Analysis of Steel Catenary Riser with Seabed Interaction

by

Hany Elosta

A thesis presented in fulfillment of the requirements for the degree of

Doctor of Philosophy

Glasgow, United Kingdom

January 2013

The candidate confirms that the work submitted is his own and that appropriate credit has been given where reference has been made to the work of others.

Dedicated To My Parents

Table of Contents

List of Figures

List of Tables

Nomenclature

A_i, A_0	Inner and outer area of riser pipe [m^2]
API	American Petroleum Institute
a	Power law parameter
B	Random variable which quantifies modelling error
B_R	Modelling uncertainty factor applied to the fatigue resistance limit
B_S	Bias factor associated with the fatigue damage calculation itself
b	Power law parameter
C_a	Allowable stress factor
C_d	Drag coefficient
C_f	Design case factor
C_M	Inertia coefficient
COV	Coefficient of variation
D	Pipe diameter [m]
D_{fat}	Accumulated fatigue damage
DFF	Design Fatigue Factor
D_i	Linear damage accumulation, resulting from the application of n_i cycles of stress range S_i
E	Young's modulus of elasticity [kN/m^2]
e	Pipe eccentricity
F	Shear force [kN]
f_b	Soil buoyancy factor
FEA	Finite Element Analysis
FD	Frequency Domain
F_F	Sliding resistance force [kN/m]
f_i	Probability that a single stress range within sea state 'j' will have magnitude S_i (i.e., the fraction of the total stress cycles of a given sea state that are applied at stress range S_i)
F_L	Hydrodynamic lift force upon the pipe [kN/m]
FORM	First-Order Reliability Method
FP	Floating Platform
FPSO	Floating Production Storage Offloading vessel
F_R	Passive resistance or penetration dependent lateral soil resistance force [kN/m]
F_y	Total lateral soil resistance [kN/m]
$F_{y_{max}}$	Maximum seabed friction force [kN/m]

$(F_y)_{res}$	Constant residual soil resistance value [kN/m]
f_{suc}	Soil suction ratio
G(x)	Failure or limit state function
GUI	Graphical User Interface
HR	Hybride Riser
H_s	Significant wave height
I	Second moment of area [m^4]
j	Wave component number
K	Fatigue strength coefficient
k	Thickness exponent for fatigue calculations
K_{max}	Normalised maximum stiffness
k_s	Seabed shear stiffness [$kN/m/m^2$]
M	Bending moment [kN-m]
m	Fatigue strength exponent
MBR	Minimum bend radius
MCS	Monte-Carlo Simulation
MPP	Most Probable Point
N	Number of stress cycles to failure
N_c	Nondimensional bearing factor
NNS	Northern North Sea
$n(S_i)$	Number of stress cycles with stress range S_i
$N(S_i)$	Number of stress cycles to failure
NSR_j	Number of applied stress ranges during sea state '*j*'
N_T	Total number of cycles in time, *T*
P(H)	Long term probability that the wave height does not exceed *H*
p_f	Probability of failure
P_i	Internal pressure
P_0	External pressure
R	Structure resistance (or upper limit of strength/behaviour)
$1/R$	Riser curvature [m^{-1}]
RAOs	Response Amplitude Operators
R_e	Reynolds number
S	Structure serviceability (or calculated response distribution from load effects)
S_0	Nominal stress range [kN/m^2]
SCF	Stress concentration factor
SCR	Steel Catenary Riser
S_{end}	Material's endurance limit for the applied stresses
SFs	Safety factors
S_i	Denotes the applied stress level, ($i=1, 2, 3,\ldots,NSR_j$) [kN/m^2]
S-N	Stress-life curve approach

SORM	Second-Order Reliability Method
S_{R}	Length of the riser between the TDP and the floating platform [m]
SRA	Structural Reliability Analysis
S_{sw}	Stress at intersection of the two S-N curves [kN/m^2]
S_u	Soil strength [kN/m^2]
$S_{\mathrm{u}}(z)$	Undreamed seabed soil strength at depth z [kN/m^2]
S_{u0}	Shear strength of soil at the seabed level [kN/m^2]
S_{ug}	Shear strength gradient [kN/m]
T	Catenary effective tension at a point along a riser [kN]
t_1	Wall thickness (thinner tube) [m]
t_2	Wall thickness (thicker tube) [m]
TD	Time Domain
TDP	Touchdown Point
TDZ	Touchdown Zone
T_{eff}	Effective tension [kN]
t_{fat}	Pipe wall thickness for fatigue calculations [m]
T_j	Time frame during a sea state '*j*' [Seconds]
T_p	Wave peak period [Seconds]
T_{s}	Service life [Years]
T_t	Tension at the riser top end [kN]
TTR	Top-Tensioned Riser
t_{ref}	Reference wall thickness for fatigue calculations [m]
TSJ	Tapered Stress Joint
T_{w}	Wall tension in riser pipe
u	Input random variables transformed into standard normal space
V	Vertical seabed reaction force [kN/m]
VIV	Vortex-Induced Vibration
V_{u}	Ultimate bearing load [kN/m]
V_u/D	Ultimate net bearing pressure at that depth below seabed [kN/m^2]
V-z	Load/deflection relationship
w	Submerged riser pipe weight [kN/m]
X	Denotes modelling accuracy
x_i	A set of I random variables
y	Displacement from the un-sheared position in lateral direction [m]
z	Embedment depth of pipe below the seabed [m]
α	Pipe-soil boundary roughness
β	Reliability or safety index
β_{T}	Target reliability index
$\partial\beta/\partial u$	Probabilistic importance factors of the input random variables
Δ	Fatigue resistance limit (also known as Miner's index)
η	Soil strength profile with depth [m^2]

θ	Riser top angle to vertical
λ_{suc}	suction decay parameter
λ_{rep}	Re-penetration parameter
μ	Friction coefficient
μ_G	Mean value of G
ρ_{soil}	Saturated soil density [kg/m^3]
ρ_s	Steel density [kg/m^3]
ρ_w	Seawater density [kg/m^3]
σ_{p_e}	Extreme von Mises stress [kN/m^2]
σ_a	Basic allowable combined stress [kN/m^2]
σ_y	Material minimum yield strength [kN/m^2]
σ_{pr}	Radial stress [kN/m^2]
$\sigma_{p\theta}$	Hoop stress [kN/m^2]
σ_{pz}	Axial stress [kN/m^2]
Φ	Standard normal cumulative distribution function (CDF)
Ω	Stress parameter

Acknowledgement

This research work was carried out from October 2009 until June 2012 in the Department of Naval Architecture and Marine Engineering, University of Strathclyde. During this time, I have been privileged to receive support from many people.

Firstly, I would like to express my cordial gratitude to my supervisor, Professor Shan Huang, for his expert guidance, patience, encouragement, friendliness and all the things that would require a volume thicker than this to enlist. I feel my vocabulary is not extensive enough to articulate my feelings of gratefulness. Thank you very much for your invaluable assistance in writing this thesis and for introducing me to the fascinating field of Marine Risers. I am obliged to him for his critical comments and suggestions throughout the time.

I am also very grateful and truly indebted to my second supervisor, Professor Atilla Incecik, for his constructive comments, motivation and support during this research. If not for his trust and support during my scholarship application, I would not have been able to start my doctoral study and would not have carried it all the way through to this stage. Apart from my studies, I also enjoyed parental care from him during these three years in my personal life.

I express my sincere gratitude and thankful to Professor Nigel Barltrop for providing valuable discussion, support and advice on the fatigue reliability analysis.

Without the financial support provided to me from Scottish Overseas Research Student Awards Scheme (SORSAS) and Department of Naval Architecture and Marine Engineering, University of Strathclyde, I would not have been able to obtain this degree, and for this, I will be eternally grateful.

I would also like to express my thankfulness to my colleagues and administrative staff in the department for being of great help throughout the course of study and for providing a very friendly environment in the research centre. I express my sincere gratitude to Thelma Will for her immeasurable assistance, encouragement and lovely warm smile during my PhD studies.

With admiration, appreciation and apologies, I express my limitless thanks to my parents Abdel-Samie and Mona Elosta; your warm and tireless encouragement and belief in me always meant so much. For all of your love, I cannot thank you enough.

Abstract

This thesis models a Steel Catenary Riser (SCR) on soft clay and subjected to random waves. SCR–seabed interaction is modelled using a hysteretic non-linear model in the vertical seabed direction and Coulomb friction model in the lateral direction together with an improved model that includes the breakout soil resistance. The influence of the uncertainty in the geotechnical parameters and the development of the trench in the seabed on the dynamic response is determined. The structural behaviour and a probabilistic approach to fatigue performance in the touchdown zone is developed. The probabilistic model can be employed as a risk analysis tool for the SCR assessment, leading to a safer and more cost-effective design of the SCR system. It is noted that confidence in seabed interaction modelling and geotechnical parameter values is needed in order to have confidence in the final numerical analysis results.

Summary

A Steel Catenary Riser (SCR) attached to a floating platform at its upper end encounters oscillations in and near its Touchdown Zone (TDZ), which results in interaction with the seabed. The motions of the floating platform can induce severe riser responses, which must be predicted as accurately as possible to determine the dynamic structural strength and fatigue performance of the SCR in the TDZ. The challenges regarding the fatigue damage assessment of an SCR in the TDZ are primarily due to non-linear behaviour of SCR–seabed interaction, considerable uncertainty in SCR–seabed interaction modelling, and geotechnical parameters.

This thesis is concerned with the modelling of an SCR with seabed interaction on soft clay when subjected to random waves. Analysis techniques have been developed in the three main areas: SCR–seabed interaction modelling, influences of the uncertainty in the geotechnical parameters and the development of the trench in the seabed on the dynamic response, structural behaviour and fatigue performance of SCRs in the TDZ, and the probabilistic approach for fatigue assessment of SCRs in the TDZ.

Initially, this thesis discusses the significance of SCR–seabed soil interaction in the design of an SCR for deepwater applications and it reports the results of an analysis of an SCR on soft clay using the commercial code OrcaFlex for non-linear time domain simulation. In the study reported in this thesis the vertical

embedment and large lateral movements of the SCR in the TDZ were investigated. During the simulations the seabed has been modelled using a hysteretic non-linear model in the vertical seabed direction, as well as bi-linear and tri-linear soil models in the lateral seabed direction. The results of numerical simulations of the global responses of the SCR considering a critical point at the TDZ are presented.

In the next step, this study investigates the sensitivity of fatigue performance to geotechnical parameters through a parametric study. In this thesis, global analyses are performed in order to assess the influence of vertical linear seabed springs, the lateral seabed model, and the vertical non-linear seabed model, including trench evolution into the seabed, seabed normalised stiffness, re-penetration offset parameter and soil suction resistance ratio on the fatigue life of an SCR in the TDZ.

Finally, this study presents the probability of failure associated with fatigue analysis of SCRs in the TDZ. The probabilistic methodology for fatigue reliability is illustrated. Uncertainties in structural load and material properties are considered by assigning probability distributions and standard deviations to the deterministic stress levels. A first order reliability method (FORM) is used for predicting the fatigue reliability index. The influence of uncertainties associated with soil parameters on reliability-based fatigue is investigated. In addition, a sensitivity study of influential variables has been carried out.

It is evident that employing the improved lateral SCR-soil interaction model with accurate prediction of soil stiffness and riser penetration with cyclic loading enables us to obtain dynamic global riser performance in the TDZ with better accuracy. The fatigue analyses results prove that the confounding results indicated by the previous research studies on the SCR in the TDZ are due to different geotechnical parameters imposed with the soil model and trench development. The trench deepening and the gradual embedment of riser and soil stiffness have a substantial influence on the fatigue life of SCRs in the TDZ. The main benefit of employing a reliability-based fatigue analysis framework is to increase the confidence in analysis and to reduce the likelihood of the failure of the SCR with seabed interaction, thereby minimising the risk of the loss of the containment with the associated environmental impact.

Overall, it can be said that only with confidence in seabed interaction modelling and better calibration of geotechnical parameter values can one have confidence in the final analysis results. In this thesis, several techniques have been combined to achieve what is believed to be a realistic modelling of SCRs with seabed interaction. The developed probabilistic model can be employed as a risk analysis tool for the SCR analysis assessment, leading to a safer and more cost-effective design of the SCR system.

CHAPTER 1

INTRODUCTION

1.1 Introductory Remarks

This introductory chapter will present an overview of the multiple riser types with special focus on the background and merits of the Steel Catenary Risers (SCRs) as well as their interaction issues with the seabed. Thereafter, the issues at hand will be formulated as statements for clear understanding of the standing problems of SCR in the Touchdown Zone (TDZ). Finally, the structure of the thesis, with a brief depiction of each chapter, will be introduced to facilitate the following subsequent ideas and actions conducted during this thesis.

1.2 Background

A big proportion of onshore oil and gas reserves as well as those in shallow waters offshore have already been banged due to growing demand for energy worldwide as shown in Figure 1.2—1, with long-term forecasts predicting a 40 % increase in demand by 2030. Consequently, all activities for hydrocarbon exploration have recently been moved into deeper waters. Hydrocarbon development fields in deepwater have become feasible after the advancement in oil exploration and production technologies.

The definition of deepwater has evolved with technology: according to Mineral Management Service (MMS), water depths greater than 305 m are typically considered deepwater, and the ultra-deepwater is classified as water depths greater than 1524 m. Since 1995, over 980 deepwater exploration wells have

been drilled, of which at least 126 deepwater discoveries have been declared (MMS, 2009, Payne, 2007). Because the oil fields are moving towards deepwater regions, the floating production platform, such as semisubmersible, is being employed. However, as the development of oil fields moves into deeper waters, the harsh marine environment presents a great challenge for offshore hydrocarbon technology.

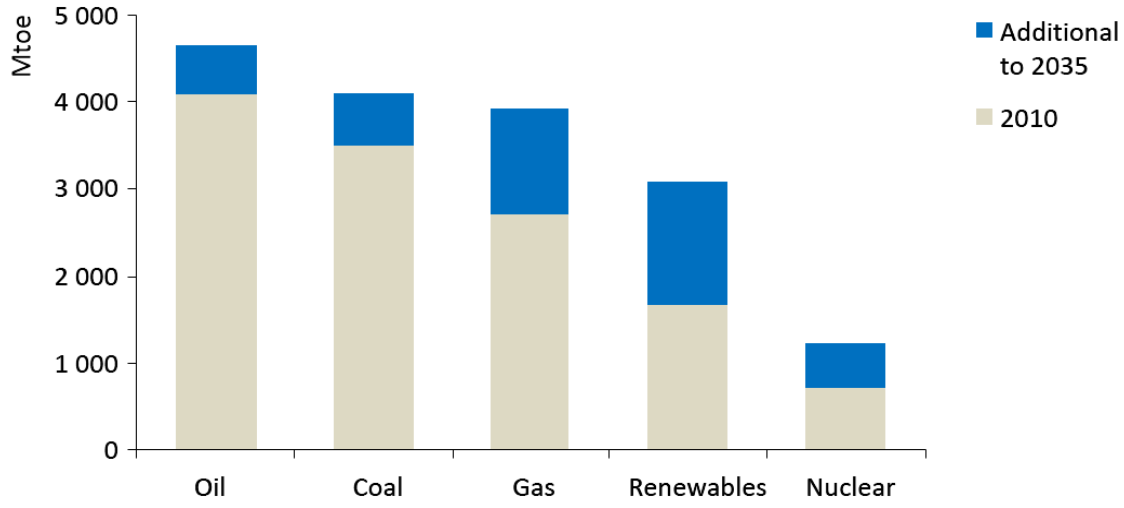

Figure 1.2—1 World primary energy demand (International Energy Agency, 2011)

The essential part of offshore equipment is the riser, which is currently facing new challenges. The floating platform can access the pipeline on the seabed through the risers. The riser is typically a conductor pipe which is connected to the seabed pipeline from the floating platform. The choice of the riser system depends on the environmental conditions, water depth and economic feasibility.

The different riser systems and their suitability are discussed in section 1.3. The compliant floating platforms for deepwater offshore hydrocarbon have advised the development of new systems of riser pipes to meet the demands of harsh operating conditions and economic benefits, which makes the SCR the system of choice due to simplicity in its arrangement and cost-effective riser system solution, see Figure 1.2—2. The use of SCR systems has increased with the progressive expansion of hydrocarbon production into deeper water. SCRs have been accompanied by floating platforms since the mid-1990s. It is a steel pipe suspended from the floating platform and smoothly extending down to the seabed at the Touchdown Point (TDP) in a catenary shape.

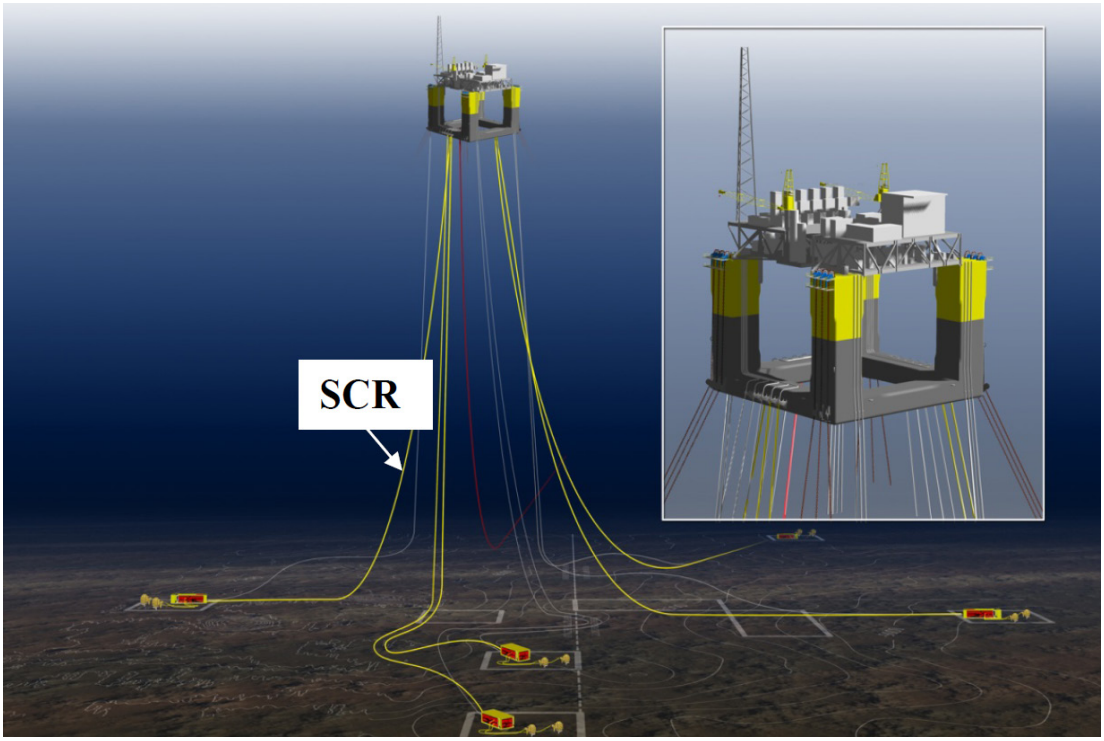

Figure 1.2—2 SCRs hanged from semisubmersible to the seabed (Song and Stanton, 2007)

1.3 Marine Risers

Marine risers are the structure systems that connect the subsea fields to the production and drilling units. Risers are pipes transferring hydrocarbons and production materials, such as injection fluids, between the wells and platforms. During a drilling operation, risers are used to provide transportation of necessary fluids, like drilling mud, to and from the well. They also support drilling strings, guide tools and auxiliary lines. Production and export risers are used to transfer the produced oil and gas to the floating unit. Risers are

normally made of steel or titanium, with the pipe having a wall thickness of less than one inch with an outer diameter of less than thirty inches. The length of the risers depends on how deep the oil production is moving into the water. Therefore, a riser is considered as a vital element for offshore oil platforms, as a failure in the riser will result in the stoppage of oil production and can also lead to pollution and spillage as well as very high economic and political consequences.

1.3.1 Riser Types

The selection of a riser system type depends on the metocean data and water depth. Several types of riser are available, extending from the flexible riser, SCR, and free-standing hybrid riser to the top-tensioned rigid riser, see Figure 1.3—1. There are primarily two main types of riser: rigid risers and flexible risers. A hybrid riser is a combination of these two (Bai and Bai, 2005, Bai, 2001). However, the most popular marine riser used in deepwater is the SCR which presents major merits over the conventional flexible or freestanding hybrid risers.

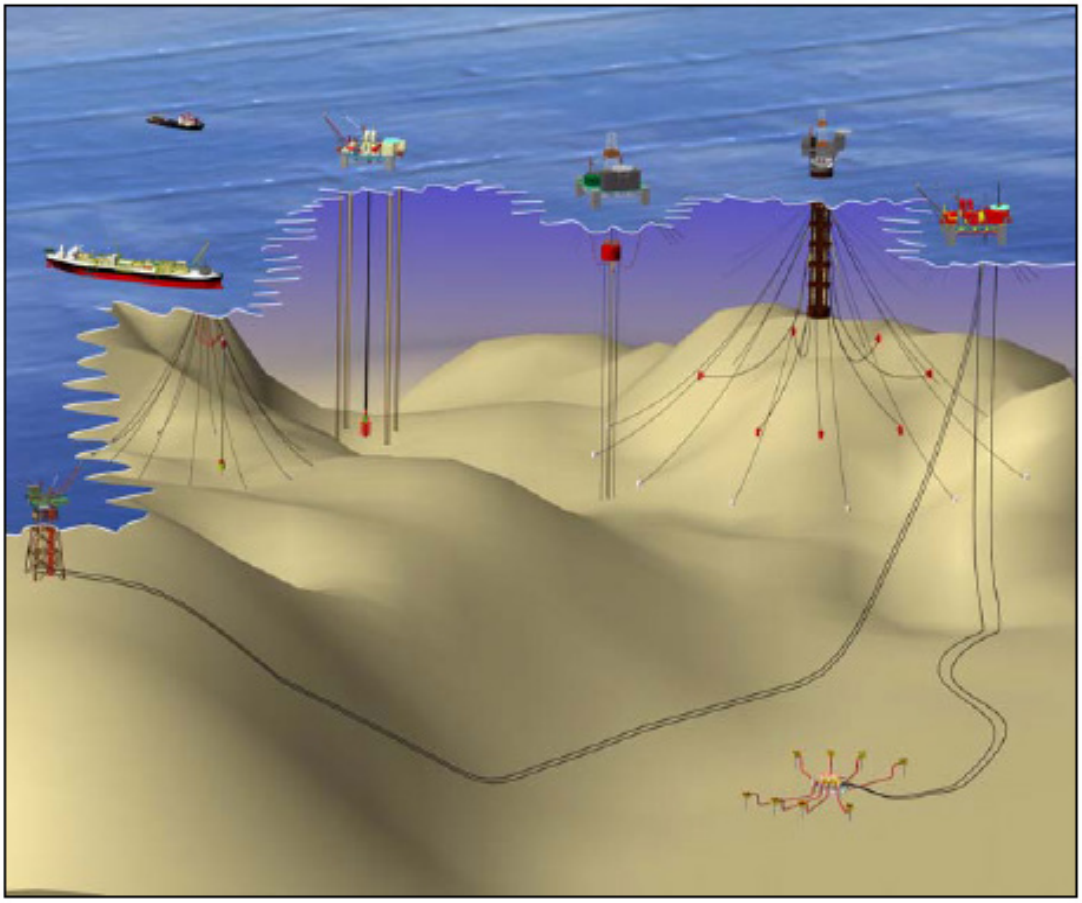

Figure 1.3—1 Multiple types of riser system (Song and Stanton, 2007)

Flexible risers

A flexible riser provides flexibility to cope with the floating unit motions. Flexible risers were found to be appropriate for offshore applications in the form of production and export risers. The application of a flexible riser has been deeded since the 1970s. The crucial characteristic of a flexible riser is its axial stiffness and relative bending. Flexible risers are characterised by their wall

structure, as shown in Figure 1.3—2. The structure of the flexible riser is made up of several different layers: an inner metallic carcass for collapse resistance; a plastic pressure sheath fluid containment that is leak-proof; a zeta and flat steel spiral for resisting internal pressure, external crushing loads and hoop stress resistance; steel armours to resist axial tensile loads; anti-wear layer to avoid friction; and a plastic outer sheath to prevent seawater penetration (SPARKS, 2008).

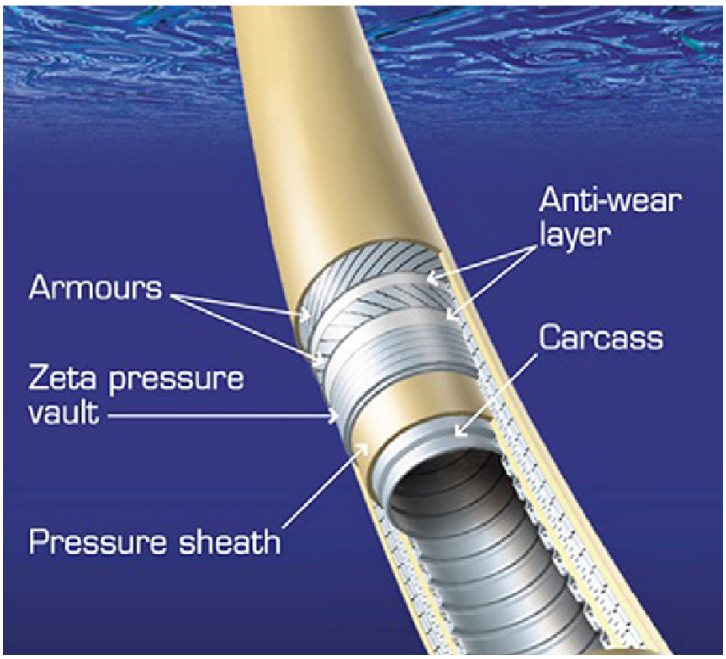

Figure 1.3—2 Typical cross section of flexible riser (Bai and Bai, 2010)

The flexibility system of a flexible riser is sustained by arranging the riser in a number of different standard configurations: Steep Wave, Lazy Wave, Free Hanging, Steep S, Lazy S, and Chinese Lantern, as shown in Figure 1.3—3. In addition, flexible risers are extending from the floating unit with a hang-off

angle of 5-6 degrees. Currently, flexible risers are being used as risers and flow-lines in water depths down to 2000 m.

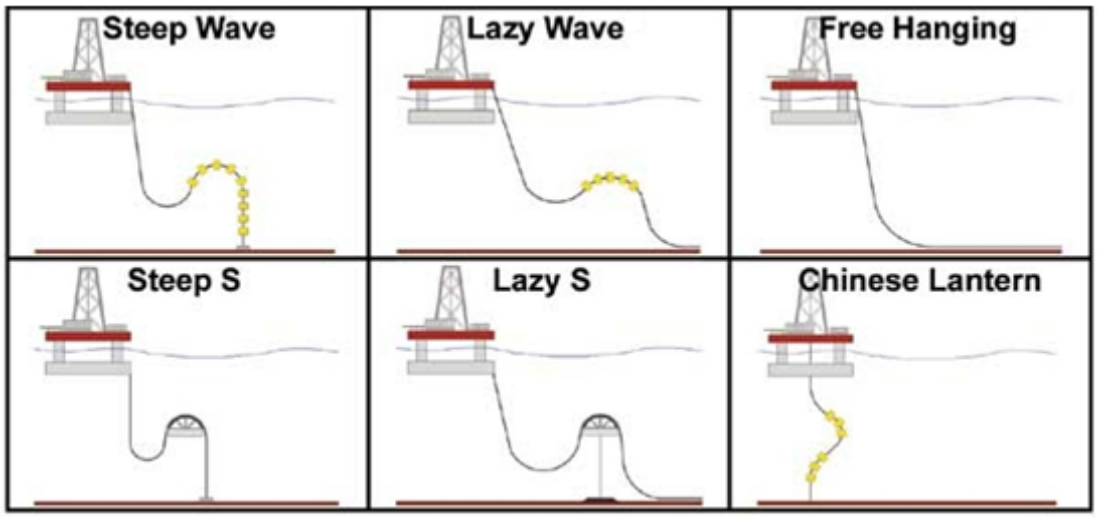

Figure 1.3—3 Standard flexible riser configurations (source: www.pennenergy.com)

Steel Catenary Risers (*SCRs*)

SCRs have recently joined the riser family, building on the catenary equation that has assisted in creating bridges across the world. SCRs are commonly used with TLPs, FPSOs, semisubmersibles and spars, as well as fixed structures, compliant towers and gravity structures. SCRs have been accompanied by floating platforms since 1994 and were first used as export risers for Auger TLP in an 872m (2860ft) water depth (Mekha, 2001, SPARKS, 2008). Since then, SCRs have been employed with many applications. The number of SCRs is increasing quickly because of its simplicity, economic effectiveness, and well-

known material properties. They can be hanged in longer lengths, eliminating the need for mid-depth arches or buoys due to the dead weight of its sag-bend. An SCR is a freely hanging pipe connected to a floating production vessel; it hangs at a prescribed top angle (8°-20°) and gradually extends down to the seabed at the TDP. An SCR consists of a steel pipe, with or without insulation and casing (Kenny, 2007), see Figure 1.3—4. In deeper waters, it can be more economical to install catenary-shaped risers.

While this curved riser can withstand some motion, excessive movement can cause problems. SCRs have similarities to free hanging flexible risers as they are the cheapest to install because they require minimal subsea infrastructure, and they also suffer from the same issues: large tension fluctuations due to vessel motions and cyclic movement of the TDP, which is leading to fatigue failure.

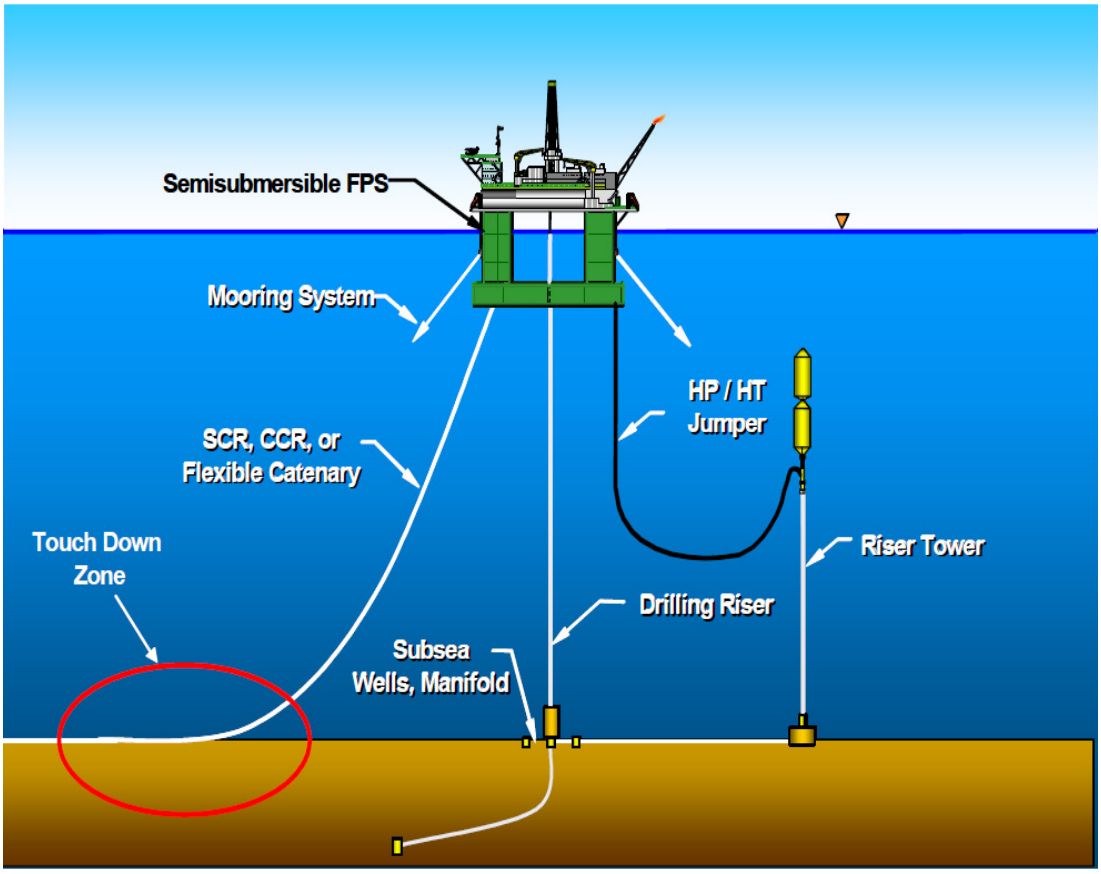

Figure 1.3—4 SCR connected to a semisubmersible (JIP, 2008)

Hybrid Risers (*HRs*)

A hybrid riser is the combination of rigid and flexible risers. The fundamental of a hybrid riser was developed based on the TTRs (Bai and Bai, 2010). A typical configuration of an HR consists of a vertical bundle of steel pipes supported by external buoyancy and flexible jumpers, connecting the top of the riser and the floating unit, and it is used to accommodate relative motion between the floater and riser bundle, as shown in Figure 1.3—5.

An HR introduces a compromise solution for deepwater and harsh environments. It can be used with a wide range of floaters as well as it has a compact subsea arrangement, excellent dynamic behaviour and low fatigue sensitivity. However, an HR is an expensive solution due to its complex components, such as a buoyancy can and riser bundle. Furthermore, an HR is installed as a single prefabricated item that is susceptible to risk during towing and installation.

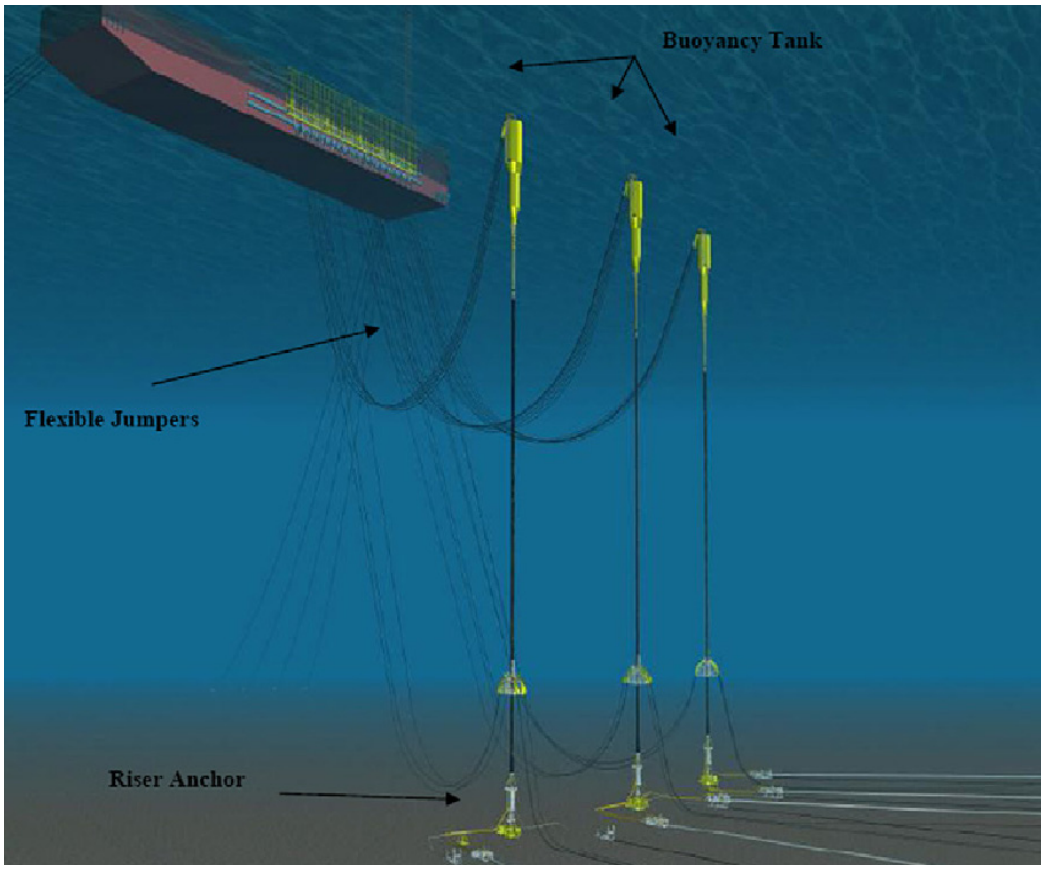

Figure 1.3—5 Hybrid riser system (Bai and Bai, 2010)

Top-Tensioned Risers (*TTRs*)

Permanent and not disconnectable TTRs were first used in 1984 for production/injection and export on the Hutton TLP. TTRs are a completely vertical riser system that terminates directly below the surface unit, such as TLPs and spars as shown in Figure 1.3—6. These floating units are able to move laterally with wind, waves and current even though they are moored.

While TTRs are fixed to the seabed, vertical displacement was introduced between the top of the riser and its connection point on the floating unit. Therefore, the common solution for these issues: a motion compensator can be included in the top-tensioning riser system; it can maintain constant tension on the riser by expanding and contracting with the motions of the floating unit and buoyancy cans which can be extended around the outside of the riser to keep it afloat.

The top of the rigid vertical top-tensioned riser is also connected to the floating unit by a flexible pipe in order to accommodate the motions of the floating unit. The rigid riser was tensioned to avoid buckling and excessive bending stress due to platform motion and Vortex-Induced Vibration (VIV). Therefore, TTRs require floating units with low or moderate motion response characteristics. The response of TTRs to the hydrodynamic loading is equivalent to a beam-column exposed to transverse loading.

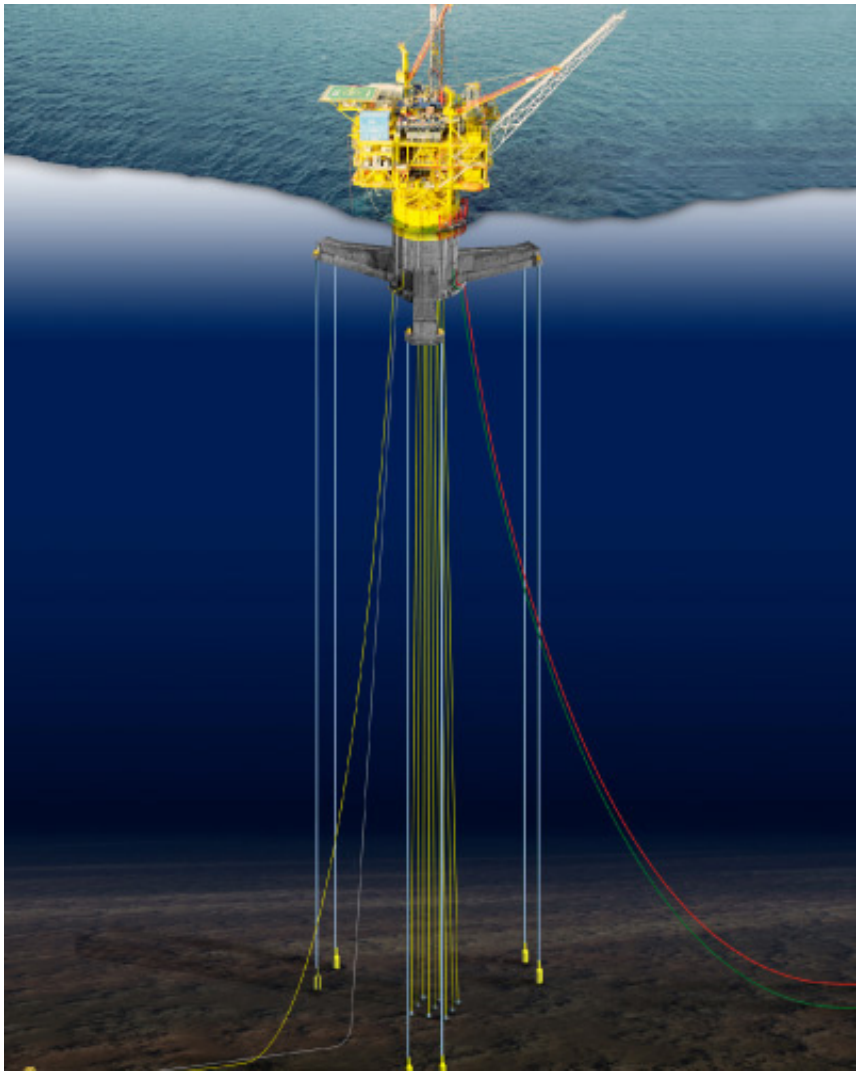

Figure 1.3—6 Top-tensioned risers (source: www.rigzone.com)

1.4 Why an SCR?

SCR systems have been recently exhibited to utilise hydrocarbon resources in deepwater around the world. SCRs introduce an economic alternative to rigid and flexible risers, which are used with all major floaters. Additionally, an SCR can be installed using the same lay vessel as the pipeline. The benefits of the SCR

compared to the TTR arrangements include eliminating the need for a hydropneumatic tensioner system and surface jumper hoses and substantially simplifying access. As an alternative to rigid pipe solutions on fixed platforms, jumper spool tie-ins and caisson risers can be eliminated with an associated reduction in the offshore operations required for installation. This configuration does not need heave compensation equipment when the riser is moved up and down together with the floater; the riser is simply lifted off or lowered down on the seabed (Bai, 2001, Bai and Bai, 2005). At the seabed, the riser base and base connector are eliminated. At the platform, the SCRs are connected to the pontoon by way of a flex joint, stress joint or pull tubes. Cost savings are made as a result of the simplified arrangement.

SCRs also offer benefits as an alternative to conventional flexible risers: they can be suspended in longer lengths, removing the need for mid-depth arches or buoys. They can be used at pressures, temperatures and diameters that cannot be achieved by a flexible pipe, allowing use of a smaller number of larger diameter lines, and they are less costly. Furthermore, steel catenaries are more congenial for design purposes, and steel pipes have better availability than a flexible riser (Howells, 1995).

SCRs introduce advantages over other riser concepts and have been widely used worldwide for deepwater oil and gas production. Additionally, SCRs are a more attractive solution for many deepwater fields compared to other deepwater

riser concepts because of their conceptual simplicity, relatively low cost, ease of fabrication and offshore installation, thereby encompassing different floater solutions, environmental conditions and water depths. To date, more than 100 SCRs for deepwater field developments have been installed, and the deepest SCR that has been installed is for an Independence Hub Facility (IHF) project at a water depth of 8000 ft (Song and Stanton, 2009).

However, riser spread is significantly changing with water depth. Generally, SCRs have a typical radial spread of 1 to 1.5 times the water depth (Howells and Hatton, 1997). In a 1000 m water depth, this would result in a total spread between diametrically opposed risers roughly of 2000 to 3000 m. In deepwater, the spread can affect the sizing of risers and the higher riser weight should be supported at the floater. Consequently, this is maximising the loading applied on the floating platform and require more attention to fatigue and fracture resistance. Therefore, rationalisation of the riser sizing is required to minimise the dynamic and loading effects on the floater. SCRs have been enjoying a widespread acceptability for many types of different deepwater floaters (see Figure 1.4—1), including Spar, Tension Leg Platform (TLP), Semisubmersible and Floating Production, storage and offloading (FPSO), in worldwide deepwater developing fields, such as the west of Africa, offshore Brazil, northern North Sea and the Gulf of Mexico. The main concerns for the design of SCRs hanged on floaters are the dynamic behaviour and fatigue performance of an SCR due to cyclic dynamic motion. However, SCR designs are very sensitive

to motion response of a host vessel as well as environmental loadings. Figure 1.4—2 shows typical heave natural period ranges and heave Response Amplitude Operators (RAOs) of Spar, TLP, Semisubmersible and FPSO. Therefore, SCR can be accompanied by all floaters without any constraints although motion optimisation is needed for Semisubmersible as well as mild environment operating condition for FPSO.

1.4.1 Why an SCR/Semisubmersible System?

As offshore hydrocarbon exploration is pushed into deeper and deeper water with the heavier payload, many innovative floating offshore structures are being proposed for economic savings. Figure 1.4—3 shows the combination of water depth and facility payloads influencing the choice between a TLP, Semisubmersible and Spar platform, which have proven to work well for SCRs in deepwater fields (Bell *et al.*, 2005). A semisubmersible floating system, see Figure 1.4—4, introduces a number of advantages, including less sensitivity to water depth, large payload capacity and the ability to relocate after field abandonment. This system consists of a buoyant floating facility moored to the seabed. Semisubmersible units offer reduced motions compared to FPSO. A semisubmersible has been applied in environments from harsh (e.g., North Sea) to the benign (e.g., Brazil). During the last decades, semisubmersibles with compliant risers have proven their excellence in use for deepwater development of oil/gas fields. Deepwater semisubmersibles with over fifty SCRs are being built nowadays (Huijs, 2007, Arnesen, 2006).

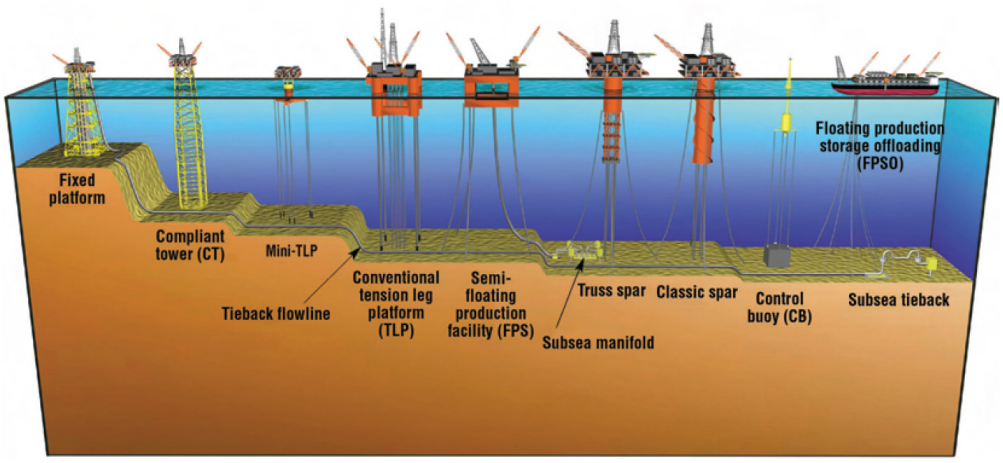

Figure 1.4—1 Deepwater field development platforms (Arnold, 2007)

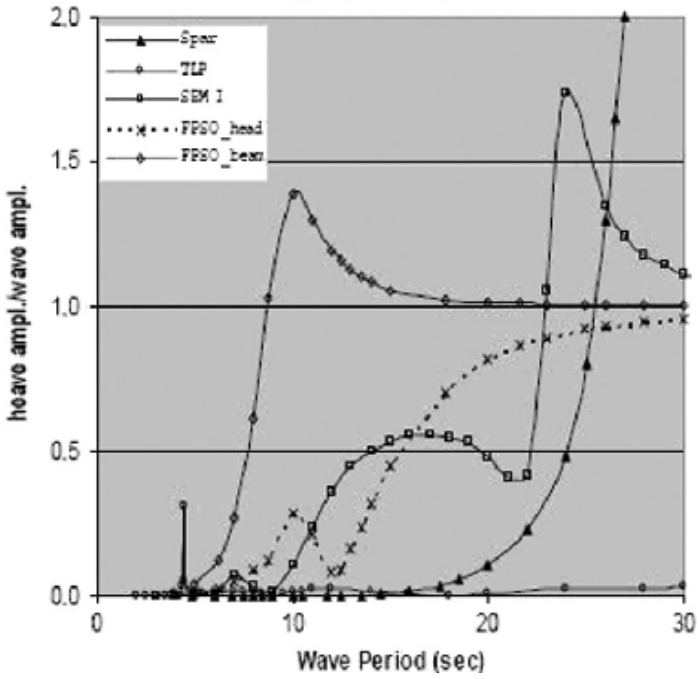

Figure 1.4—2 Typical heave RAOs for different floaters (Hansen *et al.*, 2004)

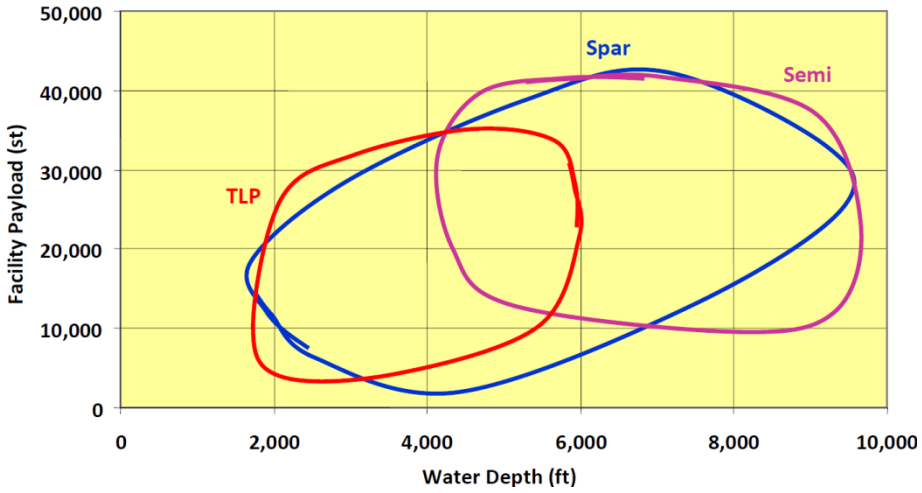

Figure 1.4—3 The influence of water depth and facility payload on the choice of platform (Barton, 2011)

Figure 1.4—4 Semisubmersible floating system (Arnold, 2007)

1.5 Considerations in SCR Analysis Modelling

To achieve a confident analysis modelling of SCRs, several design aspects should be investigated. As the SCR systems have been developed to exploit hydrocarbon resources in deepwater, there has been an increased need to understand the SCR dynamic behaviour and develop analysis techniques. A brief introduction to some aspects of the major concerns for the modelling of SCRs are characterised in the following sections, while expanding explanations, including state-of-the-art practices, are detailed in Chapter 3.

1.5.1 SCR Finite Element (FE) Model

An FE model of the SCR is created using the riser analysis software where the model is truncated and anchored with appropriate boundary conditions and sufficient length on the seabed beyond the TDP where the vessel is in the mean position. The finite element mesh (size/number of elements) takes into account the necessity for accuracy required in critical locations and the accuracy required for the type of analysis under consideration. The FE model includes all the relevant components and characteristics of the SCR (hang-off termination, coating, damping, etc.).

1.5.2 Modelling of SCR–Seabed Interaction

The vessel from which the SCR hangs is generally a floating platform and, as such, is subject to wave, current and wind loading. The floating platform is

subjected to six degrees of motion, which are classified as translation (i.e., Heave, surge and sway) and rotation (i.e., Yaw, roll and pitch), involving complex cyclic riser motion at the TDP due to the effects of random waves and currents. During normal operating conditions, the SCR is connected to the vessel via either a flex joint or a taper stress joint. These transfer the dynamic motions of the vessel directly to the top of the SCR, which causes the TDP to move along the riser in the touchdown region. The floating platform motions are directly interpreted into vertical and lateral cyclic motions in the TDZ, causing fatigue damage due to over-bend or compression. The floating platform motions are accommodated through the movement of the vessel to the near (i.e., vessel moves towards the TDP) or far (i.e., vessel moves far from the TDP in the opposite direction) positions; consequently, the riser is lowered down or lifted off the seabed, as shown in Figure 1.5—1. The TDZ is an area of particular interest and represents a fatigue hot spot due to the largest bending load occurring within this region.

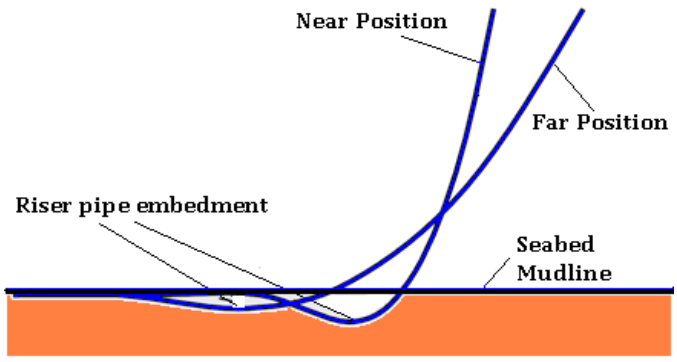

Figure 1.5—1 Schematic diagram of SCR pipe embedment in the TDZ

Modelling the SCR–seabed interaction in the riser touchdown area is an important analysis issue. Video evidence suggests that the deepest and widest part of the trench tends to be at the nominal vessel offset TDP position, where the most frequent riser motions occur (Thethi, 2001). The riser motion generally causes a trench to form; the depth of the trench is a function of several parameters, including the magnitude of the riser motion and diameter and soil properties. The relevant parameters include the soil vertical and lateral stiffness, suction effects and axial and lateral friction. The SCR interaction in the touchdown region with the seabed is an important factor for SCRs. An appropriate soil-pipe interaction model must be used. The sophistication of the model depends on the type of analysis under consideration and the accuracy required.

1.6 Formulating the Problem

SCR failure causes a reduction or interruption of revenue. It can also result in spillage or pollution and may endanger lives. An SCR attached to a floating platform at its upper end encounters oscillations in and near its TDZ that are interacting with the seabed as shown in Figure 1.6—1. The motions of the floating platform can induce severe riser responses which need to be predicted accurately to determine the structural behaviour of the SCR at the TDZ. Field observations and design analysis of SCRs show that the highest stress and greatest fatigue damage occurred near the TDP where the SCR first touches the

seabed soil. Many of the fresh discoveries in deepwater fields are in regions where soft clay is detected (Sen, 2007). ROV observations of installed SCRs have demonstrated deep trenches cutting into the seabed in the TDZ (Bridge, 2007; Thethi, 2001). Therefore, TDZ design must carry a high degree of reliability.

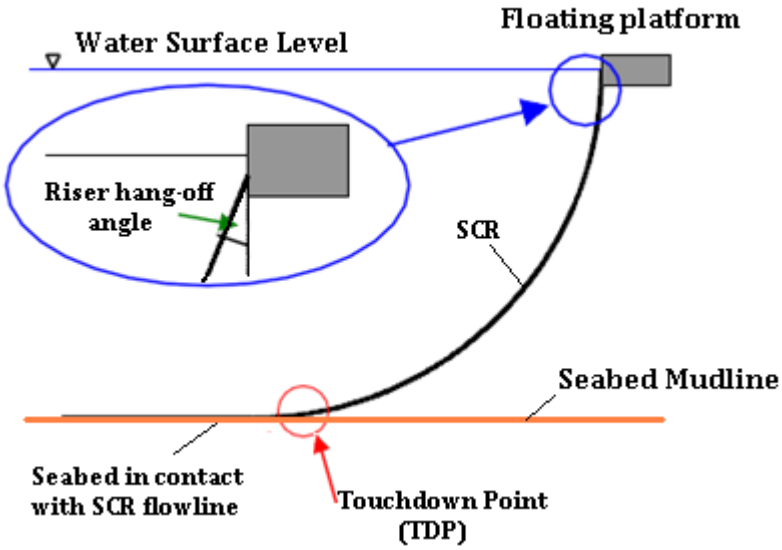

Figure 1.6—1 Illustration of the research problem

Current SCR–soil modelling practices are simplified compared with experimental data and field observations. Such experimental data are not available in the public domain. The present understanding of SCR–seabed interaction is limited; accordingly, there is an interest within the industry regarding the levels of conservatism and reliability of the SCR analysis.

Detailed analysis of SCRs can be performed using non-linear Finite Element Analysis (FEA) programs. The interaction models can vary in complexity from

using rigid seabed and friction coefficients to non-linear vertical and lateral stiffness and suction effects. The influence of soil stiffness, friction coefficients and suction effects can be reasonably significant to the dynamic and fatigue behaviour of the SCR. Specialised riser analysis codes employ either a rigid or linear elastic interaction surface to model the seabed and to simulate vertical soil resistance to pipe penetration, lateral friction resistance and axial friction resistance. A rigid seabed model generally gives a conservative result, since it is unyielding. Although the linear elastic contact is a better approximation of a seabed, it does not consider non-linear soil suction due to SCR–seabed interaction effects.

The issue of fatigue damage induced by the cyclic movements of the SCR with the seabed has acquired prominence with the TDP interaction in the TDZ. The challenges regarding the dynamic structural behaviour and fatigue damage assessment of the SCR in the TDZ are primarily because of the non-linear behaviour of SCR–seabed interaction, considerable uncertainty in SCR–seabed interaction modelling and geotechnical parameters. This uncertainty highlights the need to answer such a question: How safe is the fatigue performance of SCRs in the TDZ? This question leads directly to a reliability–based fatigue approach to tackle this probabilistic problem, which has yet not been investigated in the SCR design. Since the SCR–seabed response is critical for a reliable estimation of the fatigue life in the TDZ, it is important to develop a better understanding of the SCR–soil interaction response and geotechnical data in order to provide a

realistic technique for determining structural behaviour as well as fatigue performance in the TDZ.

The non-linear vertical and lateral seabed model as well as the influence of the trench shape is typically ignored in the traditional SCR design analyses. This is due to restrictions of seabed modelling to linear spring model approximation as well as uncertainty as to how the non-linear soil model will affect the fatigue performance of SCRs in the TDZ, which can lead to conservative fatigue damage. Therefore, the seabed parameters used in the SCR analysis can have a significant influence on the global riser response and the fatigue life in the TDZ. The seabed response model behaviour is an area where the understanding of the SCR behaviour must be improved in an attempt to reduce the number of accidents. In addition, the interaction model should have sufficient accuracy to give reliable estimates of fatigue life of SCRs in the TDZ.

This study will mainly focus on the significance of SCR–seabed soil interaction on the structural behaviour and fatigue life of SCRs in the TDZ, as it relates to the design of SCRs for deepwater fields. The investigation of vertical embedment and large lateral movements of the SCR in the TDZ enable us to obtain global riser dynamic performance in the TDZ with a better accuracy. Due to the demand for longer commitment of SCRs to a single location, as well as their use in deeper water and harsher environments, probabilistic reliability calculations are becoming increasingly important. With analysis techniques that

accurately reflect the physical processes occurring, a reduction of failure rates is possible.

1.7 Thesis Outline

The outline of this thesis broadly follows five topics: SCR analysis techniques, SCR–seabed vertical and lateral interaction model, global dynamic response of SCRs with seabed interaction under random loads, fatigue performance of SCRs and significance of seabed interaction on fatigue assessment and probabilistic fatigue reliability modelling and analysis of SCRs in the TDZ.

The structure of this research work is illustrated in Figure 1.7—1. The thesis has been divided into seven sections; a brief outline of each is given below:

- ***First Section (Formulating the Research Problem)***

Chapter 1 (*Introduction*): This chapter outlines the background of the study and describes and formulates the research problem tackled through this study. It initiates the research conducted in this thesis.

- ***Second Section* (*Research question and objectives*)**

Chapter 2 (*Aims and Objectives*): The second section describes the main aims and specific objectives to be achieved in this research. It is also highlighting the research question.

- ***Third Section* (*Review of the recent publications*)**

Chapter 3 (*Literature Review*): The third section presents a review of literature of the recent publications on the analysis techniques relevant to the analysis of the structural response of SCRs. This literature is covering SCRs, subsea seabed soils and SCR–seabed interaction. Whilst the state-of-the-art procedures in each modelling area are highlighted, emphasis is also focused on determining the level of complexity in each model component used for an individual study of the SCR response.

- ***Fourth Section* (*Adopted approach*)**

Chapter 4 (*Approach Adopted for SCR–Seabed Interaction Model*): This chapter defines the problem at hand and presents the approach adopted for an SCR–Seabed Interaction Model in a vertical and lateral direction.

- ***Fifth Section* (*Application*)**

Chapter 5 (*Global Riser Analysis Using a Seabed Interaction Model*): This chapter investigates the significance of SCR-seabed interaction on the global dynamic response of SCRs for deepwater applications and reports the results of an analysis of an SCR on soft clay in a 910 m depth of water. In the study reported in this chapter, the vertical embedment and large lateral movements of the SCR in the TDZ were investigated.

Chapter 6 (*Fatigue Performance of SCRs in the TDZ and Effects of Key Parameters*): This chapter examines the sensitivity of fatigue performance to geotechnical parameters through a parametric study. In this chapter, global analyses are performed in order to assess the influence of vertical linear seabed springs, the lateral seabed model and the non-linear seabed model, including trench evolution into the seabed, seabed normalised stiffness, re-penetration offset parameter and soil suction resistance ratio on the fatigue life of SCRs in the TDZ.

Chapter 7 (*Fatigue Reliability Analysis of SCRs in soft clay near the TDZ*): This chapter concentrates on probabilistic fatigue modelling and analyses of SCRs. The probabilistic methodology for fatigue reliability is illustrated. Variables that influence the fatigue assessment of SCRs are investigated by attributing their inherent statistical variability to a probabilistic distribution. Comparisons between using deterministic mean values and probabilistic distributions for these variables are drawn.

- ***Sixth Section* (*Main Findings and Contributions*)**

Chapter 8 (*Discussions and Recommendations for Future Research*): This chapter outlines the developments, discusses the findings and main contributions of this research and provides recommendations and scope for future further research.

- ***Seventh Section* (*Main Conclusion*)**

Chapter 9 (*Conclusions*): This chapter summarises the main conclusions of this research study.

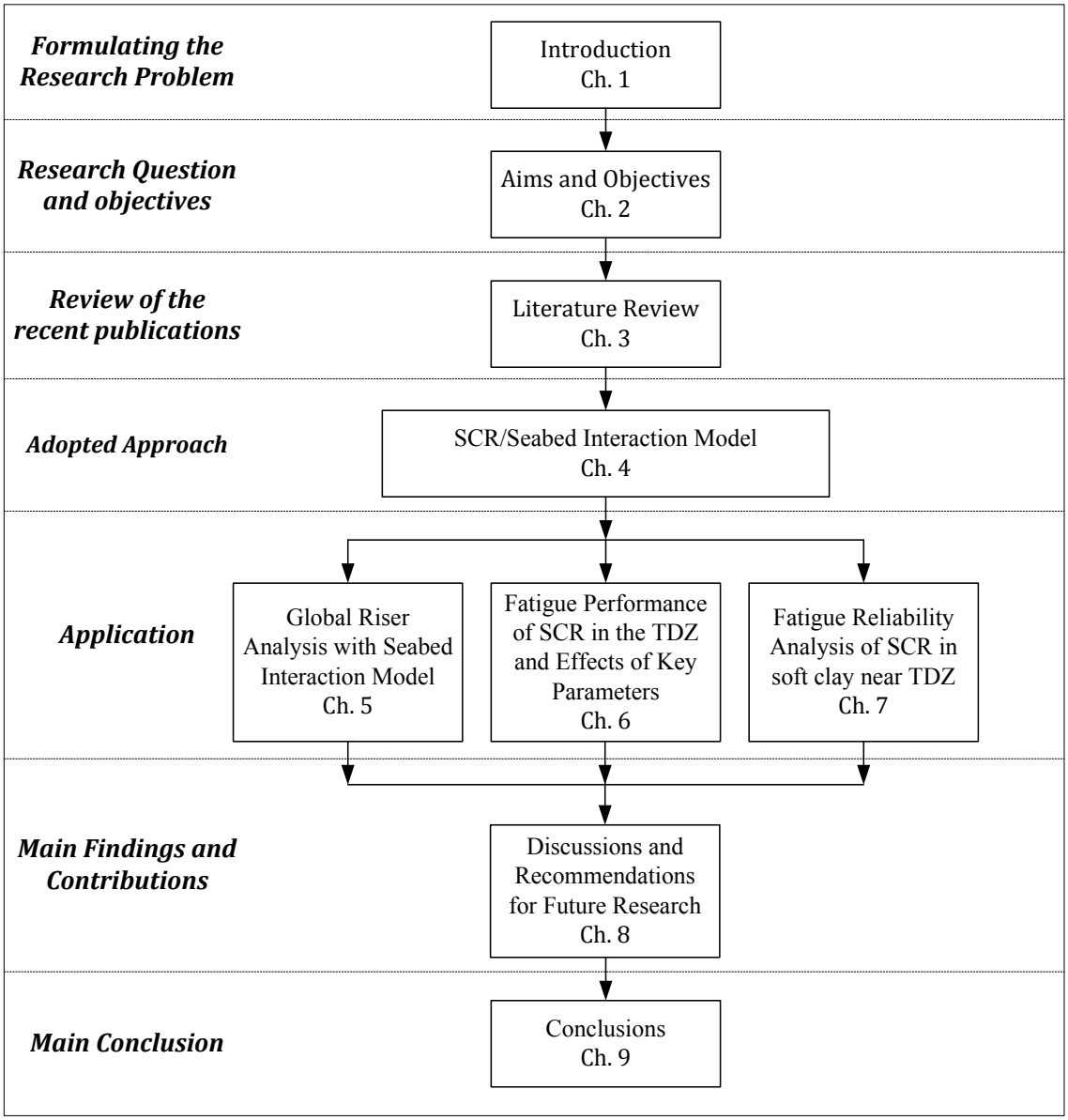

Figure 1.7—1 Thesis layout

1.8 Concluding Remarks

During this introductory chapter, an overview of marine riser systems is shown. SCRs offer a simple engineering concept and economical merits. In addition, the background and considerations in SCR modelling and analysis that initiated this research were presented and explained. The problem at hand was formulated and demonstrated. The main concept of the thesis focus was also revealed. It also summarised the structure outline of the thesis to smoothen the reading flow.

In this respect, the current thesis work will focus on the investigation and modelling on SCR–seabed interaction response under random waves and their consequences on the dynamic structural behaviour, and deterministic and probabilistic fatigue performance of SCRs in the TDZ.

The next chapter will be outlining the research question, aim and set of objectives of this thesis.

1.9 References

Arnesen, G., Kavaerner, A., Dalane, J. I., Aramanadka, S. S. B., Herfjord, K., Snell, R., and Stansberg, C. T. Integrated semi and steel catenary risers (SCRs) in deep water and harsh environment conditions. *In:* Offshore Technology Conference, OTC 18259, 2006 Houston, Texas, USA.

Arnold, K. E. 2007. *Petroleum engineering handbook, volume iii: Facilities and construction engineering*, Society of Petroleum Engineers.

Bai, Y. 2001. *Pipelines and risers*, Elsevier Science.

Bai, Y. & Bai, Q. 2005. *Subsea pipelines and risers*, Elsevier Science Ltd.

Bai, Y. & Bai, Q. 2010. *Subsea engineering handbook*, Gulf Professional Publishing.

Barton, C. M. 2011. PFC: Expanding facilities knowledge workshop-offshore concept selection. *FloaTec Company* [Online].

Bell, J. M., Chin, Y. D. & Hanrahan, S. 2005. State-of-the-art of ultra deepwater production technologies. *Offshore Technology Conference, OTC 17615.* Houston, Texas: Offshore Technology Conference.

Hansen, V., Wang, L., Sodahl, N. & Ward, E. Guidelines on coupled analyses of deepwater floating systems. *In:* Offshore Technology Conference, 2004 Houston, USA.

Howells, H. 1995. Advances in steel catenary riser design. *DEEPTEC.* Aberdeen.

Howells, H. & Hatton, S. A. 1997. Challenges for ultra-deep water riser systems. *Floating Production Systems IIR, London*.

Huijs, F. A. The influence of steel catenary risers on the first order motions of a semi submersible. *In:* Proceedings of the Seventeenth (2007) International Offshore and Polar Engineering Conference, July 1-6 2007 Lisbon, Portugal.

International Energy Agency, I. 2011. World energy outlook 2011. London.

JIP, S. T. Z. 2008. New touch down zone (TDZ) solutions for steel catenary risers (SCRs) - development and qualification of alternative design solutions. Houston, USA.

Kenny, J. P. 2007. Deepwater riser design, fatigue life and standards study report. Houston, USA.

Mekha, B. B. 2001. New frontiers in the design of steel catenary risers for floating production systems. *Journal of Offshore Mechanics and Arctic Engineering,* 123**,** 153.

MMS 2009. Deepwater gulf of mexico 2009: Interim report of 2008 highlights. U.S. Department of the Interior, Minerals Management Service, Gulf of Mexico OCS Region.

Payne, M. L. 2007. Deepwater activity in the us gulf of mexico continues to drive innovation and technology. Drilling & Well Technology.

Song, R. & Stanton, P. Advances in deepwater steel catenary riser technology state-of-the-art: Part I—design. *In:* Proceedings of the 26th International

Conference on Offshore Mechanics and Arctic Engineering, 2007 San Diego, California, USA. ASME.

Song, R. & Stanton, P. Advances in deepwater steel catenary riser technology state-of-the-art: Part II—analysis. *In:* Proceedings of the ASME 2009 28th International Conference on Ocean, Offshore and Arctic Engineering, 2009 Honolulu, Hawaii, USA. ASME.

SPARKS, C. 2008. *Fundamentals of marine riser mechanics: Basic principles & simplified analysis*, PennWell.

Thethi, R., and Moros, T. Soil interaction effects on simple catenary riser response. *In:* Proceeding Conference on Deepwater Pipeline & Riser Technology, 2001 Houston, Texas.

CHAPTER 2

AIMS AND OBJECTIVES

2.1 Introductory Remarks

This is a brief chapter that introduces the research question as well as the aims and objectives of this research study.

2.2 Research Question

The main research question of this thesis study may be put together as:

"How do the non-linearity in the response model of the SCR–seabed interaction and the uncertainty in geotechnical parameters influence the dynamic structural behaviour and the reliable estimates of the fatigue damage of the SCR in the TDZ?"

2.3 Research Aims

The formulation of the problem in Chapter 1 gives a comprehensive description of the research problem that needs to be tackled in this study. This thesis is concerned with the dynamic response modelling of SCRs on soft clay in deepwater when subjected to random waves. The primary aim of this study is to investigate the importance of the SCR–seabed interaction model response and its effects on the dynamic structural behaviour and fatigue life assessment in the TDZ. This can be carried out using a non-linear soil model in vertical and lateral seabed direction. This study aims to extend knowledge of analysis techniques of SCRs in three key areas:

- SCR–seabed interaction modelling,
- Effects of the uncertainty in the geotechnical parameters and the development of the trench in the seabed on the dynamic response, structural behaviour and fatigue performance of SCRs in the TDZ, and
- Probabilistic approach for fatigue assessment of SCRs in the TDZ.

The basic philosophy is to investigate the SCR–seabed interaction issues identified in Chapter 1, using deterministic tools, within a probabilistic reliability-based fatigue framework which accounts for inherent uncertainties. The purpose of the probabilistic approach is to achieve better understanding of SCR behaviour and to increase confidence in all the components affecting the SCR–seabed response.

2.4 Research Objectives

The aforementioned aims of this research are pursued through the following objectives:

- To critically review the literature relevant to SCR analysis techniques as well as SCR–seabed interaction modelling, in an endeavour to improve the understanding and analysis modelling of seabed soil interaction with the SCR.
- To develop and apply advanced non-linear SCR–seabed vertical and lateral interaction models with the cyclic motions of the SCR using a

finite element model. These models can be used to analyse the soil resistance to SCR movements under hydrodynamic loading and to determine the interaction influence on the global riser structural dynamic behaviour as well as the fatigue performance with a better accuracy by investigating and assessing the large lateral soil resistance to SCR's movements and vertical embedment of a riser pipe in the TDZ.

- To identify and gain better insight into the key geotechnical and non-linear seabed modelling parameters and to investigate the influence of trench deepening and the main seabed soil parameters under dynamic cyclic motions on the evaluation of the structural dynamic behaviour and fatigue performance of SCRs in the TDZ through conducting a parametric study.
- To develop and advise a framework for an effective reliability-based fatigue assessment methodology to determine the impact of the deterministic and probabilistic modelling of the SCR on the fatigue life in the TDZ and also to define the sources of uncertainty associated with fatigue life calculations. The objective of reliability-based fatigue methodology is to increase the confidence and safety in the design of SCR in the TDZ, to provide a means to quantify the reliability of SCRs in the TDZ and to develop further understanding of the response behaviour of SCR–seabed interaction.
- To quantify and investigate the influence of the uncertainties parameters, which have inherent randomness associated with the riser

on the reliability level of the riser through the evaluation of the reliability safety index or the probability of failure of the SCR in the TDZ, and to carry out a sensitivity study of the influential variables affecting the performance of the SCR.

2.5 Chapter Summary

This chapter has dwelled on clarifying the research question along with the aims and objectives of this thesis. The next chapter will be reviewing the SCR analysis techniques and the literature related to various aspects of the SCR–seabed interaction modelling.

CHAPTER 3

LITERATURE REVIEW

3.1 Introductory Remarks

The TDZ often proves to be a spot where cyclic bending stresses are the largest and is therefore a critical location for fatigue. SCRs are subject of much ongoing research, particularly with respect to their fatigue life, which is strongly influenced by seabed soil conditions in the TDZ. This chapter reviews literature of the recent publications that might have an impact on the methodologies and approaches relevant to the global analysis techniques of SCRs, with particular reference to the SCR–Seabed interaction. The review starts by looking at the SCR general arrangement and then the issues and challenges of an SCR for deepwater application. Thereafter, the focus moves to the review of the recent research that studied the interactions between deepwater SCRs and the seabed, both analytically and experimentally. In addition, the review went over the analysis techniques of the SCR, including the modelling philosophy and models for seabed response. This chapter also presents an overview of the riser dynamic analysis program named OrcaFlex, which is used in this thesis.

3.2 SCR General Arrangement

The essential steel catenary concept is simple. A free-hanging simple catenary riser is connected to a floating production vessel and the riser hangs at a prescribed top angle. The riser is free-hanging and gently curves down to the seabed at the TDP. At the TDP, the SCR pipe embeds itself in a trench and then evenly rises to the surface where it rests, and is effectively a static pipeline. SCRs

may be described as consisting of three portions (Bridge, 2003), as shown in Figure 3.2—1 below:

- Catenary zone, where the riser suspends in a catenary section
- Buried zone, where the riser pipe penetrates into a trench
- Surface zone, where the riser pipeline rests on the seabed

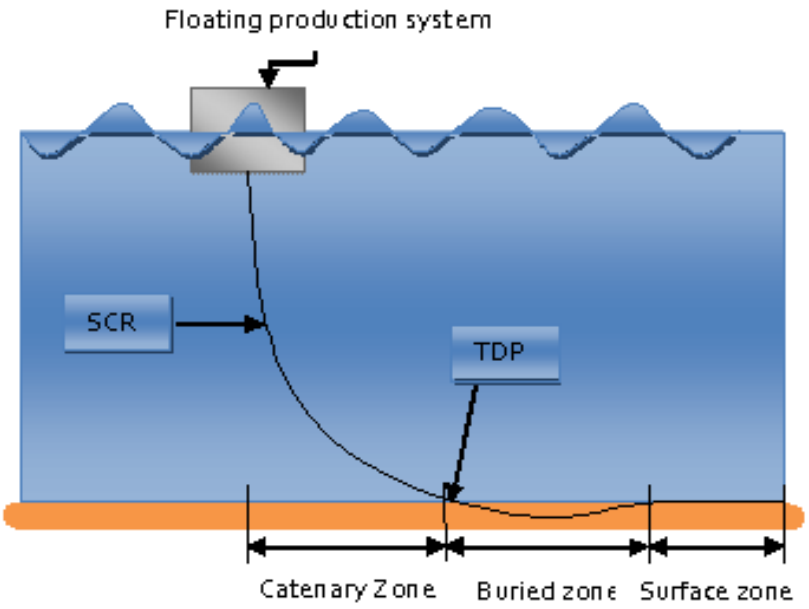

Figure 3.2—1 General SCR Arrangement

3.3.1 SCR Hang–Off System

SCRs are very sensitive to dynamic environmental loading. Vessel motions and wave actions near the water surface produce bending and tension stress at the top end of the SCR. High bending moments can be generated in an SCR's top end due to severe vessel motion response. Therefore, the SCR is using hang-off

system termination at the vessel in order to accommodate bending moments of the SCR due to excessive vessel motions. A better understanding of the hang-off system is essential in evaluating maximum stresses and fatigue life of the SCR near the water surface.

SCRs can be attached to the floating vessel by way of a hang-off system. Generally, three hang-off systems have been used: flex joint, Taper Stress Joint (TSJ) and pull tube, as shown in Figure 3.2—2 and Figure 3.2—4 respectively. SCR hang-off systems typically include a porch structure on the hull or pull tubes and connection of the top of the SCR to the porch structure. A porch utilises a receptacle-type structure consisting of a basket that accommodates the flexing mechanism and a welded-plate structure that connects the basket to the hull near the water surface (Chang *et al*., 2010). In addition, a porch can hold both flexible joints and stress joints. As an SCR is attached to the lower end of a flex joint or a stress joint, a spool piece attaches the upper end of the flexing mechanism to the piping system of the floating vessel.

The functional requirement of an SCR governs the selection of the hang-off system, in terms of the required angular deflection, SCR size and the expected riser's top tension. Porch termination, which is used to accommodate a flex joint or TSJ, is preferred to a designer's perspective, as it can accommodate both flexing mechanisms, hold multiple SCR dimensions and can afford the potential riser hang-off angle change.

Schematics of the flex joint configuration are given in Figure 3.2—2. The flex joint incorporates elastometer/alternating laminations of spherically shaped rubber and steel components within a steel bellow support structure, which involves an extension of welding to the main riser. Therefore, a flex joint simulates a hinge and allows the SCR to rotate with a minimum bending moment imposed onto the vessel hull structure under severe environmental conditions. A better understanding of flex joint stiffness is necessary in determining strength behaviour and fatigue performance at the SCR top end.

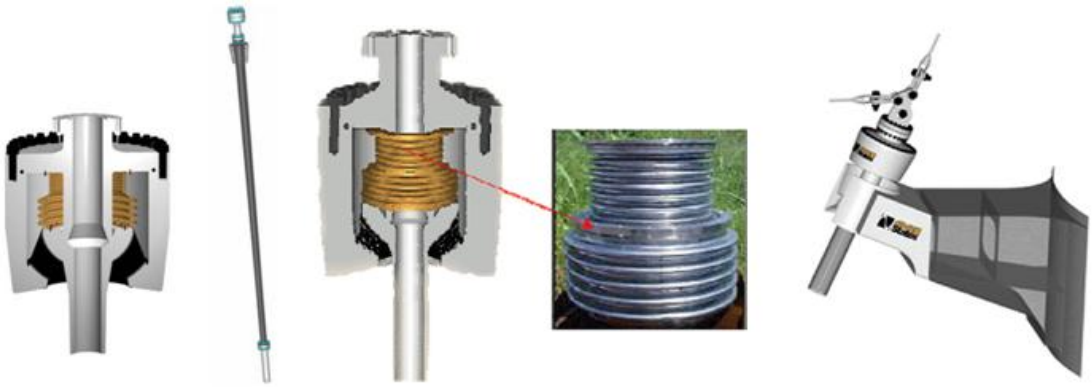

Figure 3.2—2 SCR hang-off systems: Flex Joint and Stress Joint (Bai and Bai, 2010, Song and Stanton, 2007)

A TSJ is typically a tapered tubular system as shown in Figure 3.2—3. A TSJ simulates a rigid attachment and may be used in place of flex joints but reveals larger bending loads to the floating vessel. In addition, it is a simple, solid metal structure and is able to cope with high pressure. It can be made from steel or titanium. Flanges are required at both ends of a titanium TSJ due to the

transition from a titanium to steel riser on the lower end and the transition to steel hull piping on the upper end.

Alternatively, pull tubes have been used with spars to guide SCRs through the spar truss while the SCR is hanged from the top of the spar. The pull tubes serve as a continuous curved guide for the SCR passing through the hull of the spar and hanging on the top spar deck as shown in Figure 3.2—4. Pull tubes can extend from either inside or outside the hull of a spar. Figure 3.2—4 shows a pull tube attached to a spar and extending outside the truss of the hull. Generally, a stress joint is required at the lower end of the pull tube to accommodate bending moments under environmental conditions.

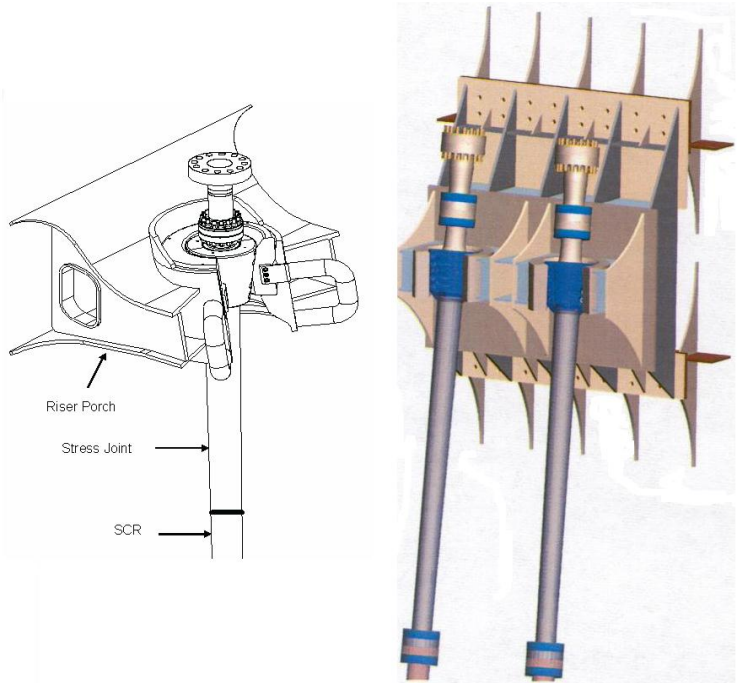

Figure 3.2—3 Tapered stress joints at porch hang-off (Chang *et al.*, 2010, Kenny, 2007)

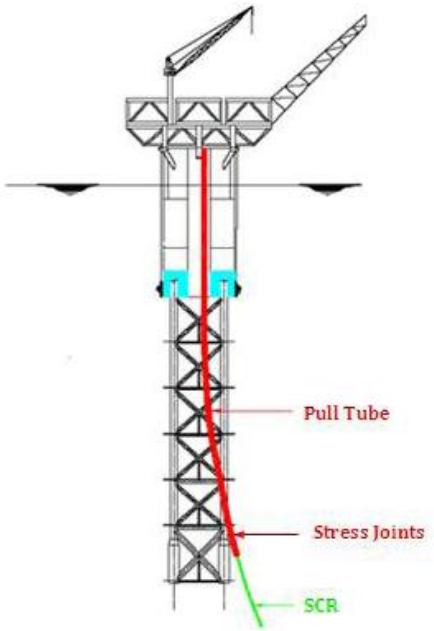

Figure 3.2—4 Spar with pull tube hang-off (Chang *et al.*, 2010, Luk and Chang, 2011, Shi *et al.*, 2011)

3.3 History of SCR Development

SCRs were initially installed on fixed platforms. SCRs were firstly installed on Shell's Auger TLP in the Gulf of Mexico in 1994 and since then have been widely used in deepwater oil/gas fields and attached to different floaters. Recently, an SCR has been installed on FPSO in the west of Africa. This section presents a brief review of some installation instances (Bai and Bai, 2005):

1994 The first SCRs were installed on Auger TLP in the Gulf of Mexico.

1997 The first SCRs were installed on a semisubmersible in Marlim field.

2001 The first SCRs were installed on truss spars located at Boomvang and Nansen fields in the Gulf of Mexico.

2004 The first SCRs were installed on an FPSO unit in the west of Africa.

3.4 SCR Challenges in Deepwater Environment

Recently, deepwater exploration and production activities have significantly increased in different locations of the world, such as the west of Africa, Brazil, Gulf of Mexico and Northern North Sea (NNS) (Song and Stanton, 2007). While the development of oil and gas fields extended to deeper waters, new deepwater environmental issues and challenges were introduced. Risers are one of the substantial parts of a floating system affected by a deepwater environment. Challenges of riser applications due to a deepwater environment are evaluated below.

3.4.1 Water Depth

Riser system arrangement is significantly affected by the increase in deepwater depths and by the increase in riser length. Therefore, the riser weight is increased due to the increase in riser length, resulting in an increase in riser tension and hydrodynamic drag loading (Howells, 1997). A pipe lay vessel shall afford a high riser's top tension, which will restrict the number of appropriate vessels. In addition, the increase in riser weight can cause an increase in the development cost. A further influence of deepwater is the alteration in riser spread in the case of an SCR, which is affecting riser system arrangement selection.

3.4.2 Severe Currents

A deepwater environment increases the sophistication of riser arrangement selection. Large current speeds may be experienced in deepwater field applications that produce larger riser curvatures and which result in an increase in top tension to maintain the same operating condition limits (Howells and Bowman, 1997). In addition, high currents produce VIV, which can increase hydrodynamic drag loading and generate high levels of fatigue damage.

3.4.3 Severe Waves

Larger wave heights increase riser loading and floating unit dynamic motions. Large floating unit motions will have a significant influence on riser behaviour, since a riser system has to accommodate floating unit motions. Selection of riser system configuration is highly dependent on vessel offset motions due to severe waves and currents (Hatton, 1999). The dynamic motions of the floating platform, through the wave-induced vessel motions, are transferred directly to the SCR at the touch-down area. These motions at the TDP cause the greatest stress fluctuation in the TDZ, thereby highlighting the SCR–seabed interaction issue. The seabed response due to riser loading and the trench formation phenomenon are of great significance for safe and economic riser design.

3.5 A State-of-the-Art Review of SCR–Seabed Interaction

A number of researches have been directed towards understanding the soil–riser interaction. Better predictions of the SCR's fatigue life require an accurate characterisation model of seabed stiffness as well as a realistic description of the load/deflection curve. Therefore, this section gives a state-of-the-art review of the recent research on soil–riser interaction models. Briefly, a series of previous work associated with seabed-riser interaction mechanism and simulation models, as well as load/deflection models, will be described and discussed. Several model tests related to this area will be presented and described.

3.5.1 Model Tests

A full-scale model test of an SCR was conducted by (Willis, 2001) as part of the STRIDE III JIP by 2H Offshore Engineering Ltd to investigate the effects of fluid/riser/soil interaction on SCR response and to develop finite element analysis techniques to predict the measured response. A 110 m-long (360 ft) and 0.1683 m-diameter (6 inch) SCR was suspended from an actuator on the harbour wall to an anchor point at the Watchet Harbour in the west of England. The harbour seabed soils have properties similar to deepwater Gulf of Mexico seabed soils. The seabed is described by soft clay, with the undrained shear

strength of 3 to 5 kPa and a plasticity index of 39% (i.e., is the numerical difference between the liquid limit and the plastic limit).

The top end of the riser was programmed to simulate the wave and vessel drift motions of a spar platform in a 1,000 m (3,300 ft) water depth. The riser was fully instrumented with 13 sets of strain gauges measuring vertical and horizontal bending strain and load cells measuring the tensions and shear forces at the actuator and the tension at the anchor. The objectives of this test were to assess the effects of seabed–riser interaction and to identify key soil modelling parameters for simulation of this interaction.

The results from the harbour test are given as bending moment versus actuator position at strain gauge locations. In addition, each test measurement from a strain gauge location was compared to an analogous point on the analytical model. The computed bending moments were bracketed by analytical predictions considering the effect of suction force. The results of this comparison showed good agreement, as illustrated in Figure 3.5—1 and Figure 3.5—2.

Bridge and Willis (2002) utilised a pipe–soil model for soil suction to estimate and analyse the response of the harbour test riser of 2H Offshore Engineering Ltd. The soil suction curve utilised in the analytical modelling was the upper bound curve established upon the preceding STRIDE 2D pipe–soil interaction study (Willis, 2001). They declared that the soil suction curve in Figure 3.5—3

comprises of three parts: suction mobilisation, suction plateau and suction release.

The authors also compared pull-up and lay-down responses to investigate the difference in bending moments between the two responses due to soil suction. The results of these comparisons are as follows:

- A sudden vertical displacement of an SCR at its TDP after a period at rest can drive a peak in the bending stress that travels along the riser.
- Soil suction forces are subject to hysteresis effects.
- The soil suction force is related to the consolidation time.
- Soil suction can drive effects such as a suction kick.
- Pull-up velocity does not strongly correlate with the bending moment response on a remolded seabed.

Bridge *et al*. (2003) reviewed the results of a full-scale riser test and concluded that the soil suction force, repeated loading, pull-up velocity and the length of the consolidation time can affect the riser–soil interaction from the test data. In addition, they declared the possible causes of trench formation mechanisms, as follows:

- The dynamic motions of the riser applied by an actuator can cause trench formation. In addition, water rushing out from beneath the riser can scour out a trench.

- Scouring and washing away of the sediments around the riser may be caused by the flow of the tides.
- The high frequency motions caused by vortex-induced vibration will slowly cut into the seabed.

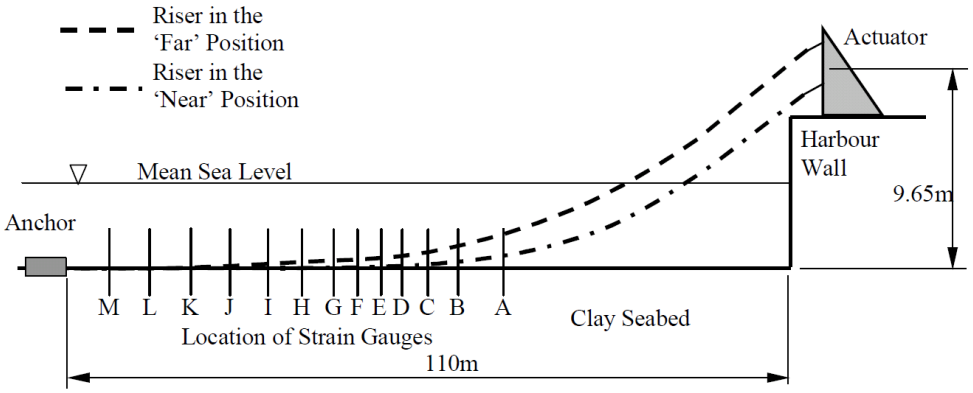

Figure 3.5—1 Schematic of the harbour tests and locations of strain gauges A to M conducted by (Bridge and Willis, 2002)

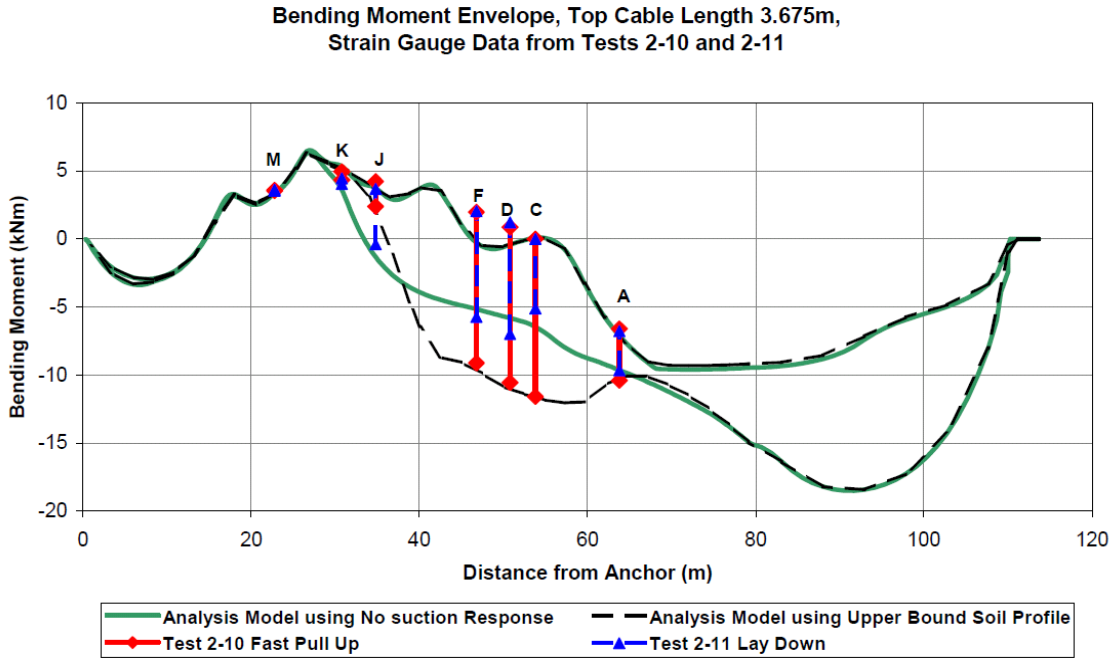

Figure 3.5—2 Comparison of Test Data and Analytical Bending Moment Envelope (Bridge and Willis, 2002)

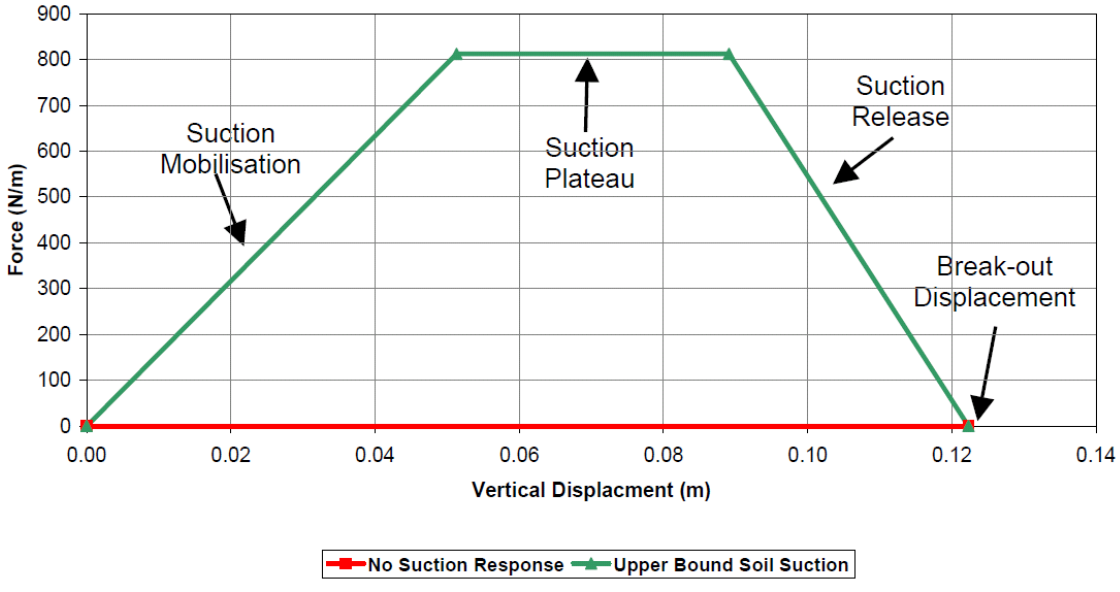

Figure 3.5—3 Soil Suction Models (Bridge and Willis, 2002)

Thethi (2001) considered three mechanisms of riser–soil interaction: the effect of riser motions on the seabed associated with the vertical movement of the riser, the effect of the water on the seabed relating to pumping action, and the effect of the seabed on the riser relating to vertical, lateral and axial soil resistance. As a consequence of the complexity of the problem, the authors recommend that trench depth and width profiles were selected in the riser analysis based on the deepest trenches and conservative soil strength assumptions.

Riser–soil response curves can be presented in terms of a seabed soil spring. The shape of the spring may change with time from a virgin curve of soil response to a degraded response. Riser–soil response curves may be described as a load path bounded by the backbone curve as shown in Figure 3.5—4. The characteristics of this riser–seabed load/deflection curve depend on the burial depth as well as the soil and riser properties.

Bridge *et al*. (2004) presented a seabed response model due to vertical loading. The model was based on published data and the test data from the STRIDE and CARISIMA JIPs. They described an example of the development of the pipe–soil interaction curve with an unloading and reloading cycle as well as the mechanism of pipe and soil interaction described below:

- The pipe is originally in contact with a virgin soil.

- The pipe penetrates the soil, plastically deforming it. The pipe–soil interaction curve follows the backbone curve.
- The pipe moves up and the soil behaves elastically. The pipe and soil interaction curve moves apart from the backbone curve; the force decreases over a small displacement.
- The pipe continues penetrating the soil, deforming it elastically. The pipe–soil interaction curve follows an elastic curve.
- The pipe keeps delving into the soil, plastically deforming it. The pipe–soil interaction curve meets again with the backbone curve and follows it.

Bridge also showed that the riser experiences a downward resistance (suction resistance) during the uplift, limited to the maximum mobilised suction resistance. Once maximum suction force is reached; there is a gradual decay in the suction resistance, followed by breakout. The riser re-penetrates the soil, tracking the re-penetration curve and ultimately following the backbone curve beyond the maximum penetration depth attained during the previous downward loading. The force/displacement curve associated with the suction effect is shown in Figure 3.5—5 and illustrated below:

(1) Penetration: The pipe penetrates the soil to a depth where the soil force equals the penetration force.

(2) Unloading: The penetration force reduces to zero, allowing the soil to swell.

(3) Soil suction: As the pipe continues to elevate, the adhesion between the soil and the pipe causes a tensile force, resisting the pipe motion; the adhesion force quickly increases to a maximum then decreases to zero as the pipe pulls out of the trench.

(4) Re-penetration: The re-penetration force and displacement curve have zero force when the pipe enters the trench again, only increasing the interaction force when the pipe re-contacts the soil. The pipe–soil interaction force then increases until it retorts the backbone curve at a lower depth than the previous penetration.

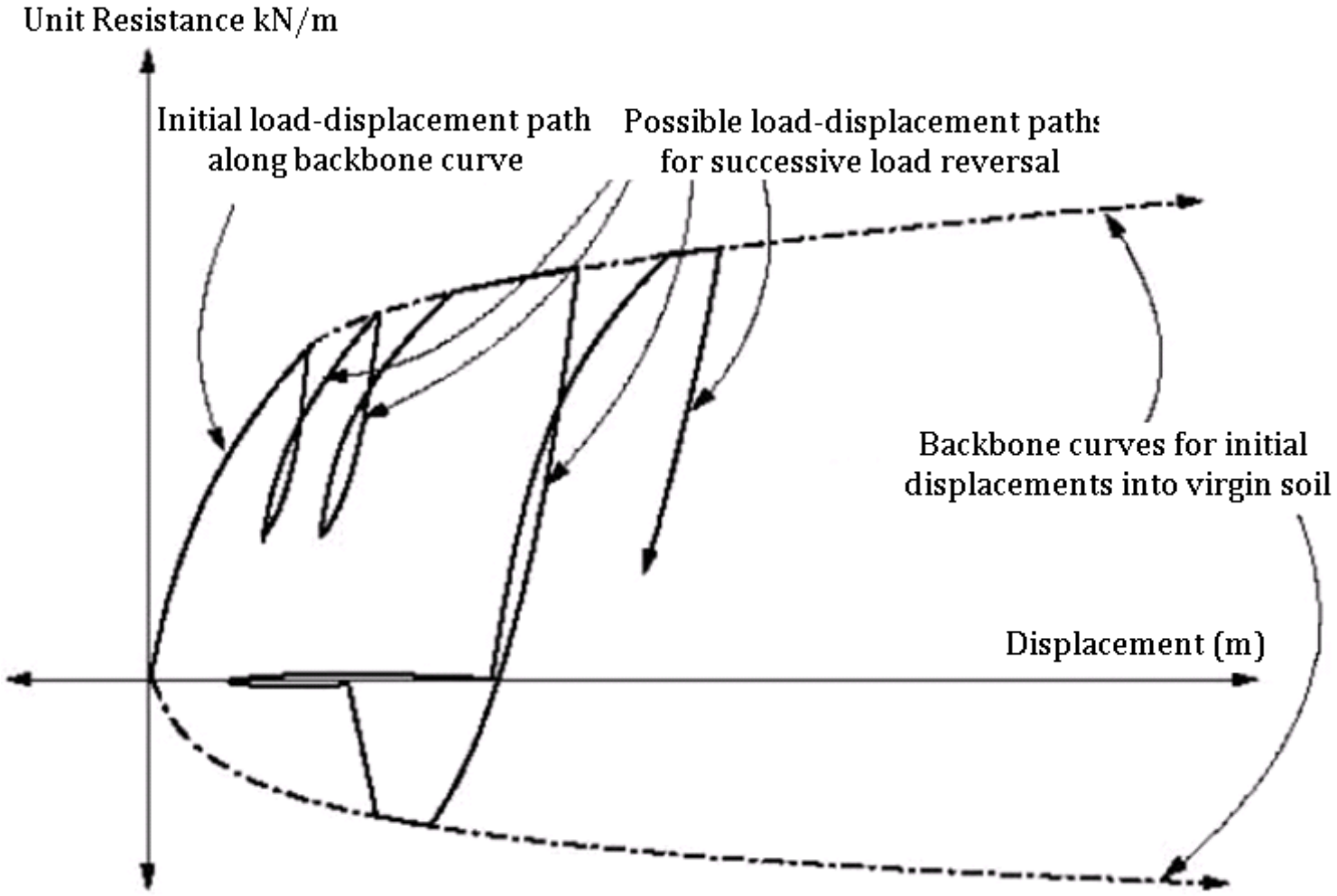

Figure 3.5—4 Concept of Backbone & Load-Displacement Curves (Thethi, 2001)

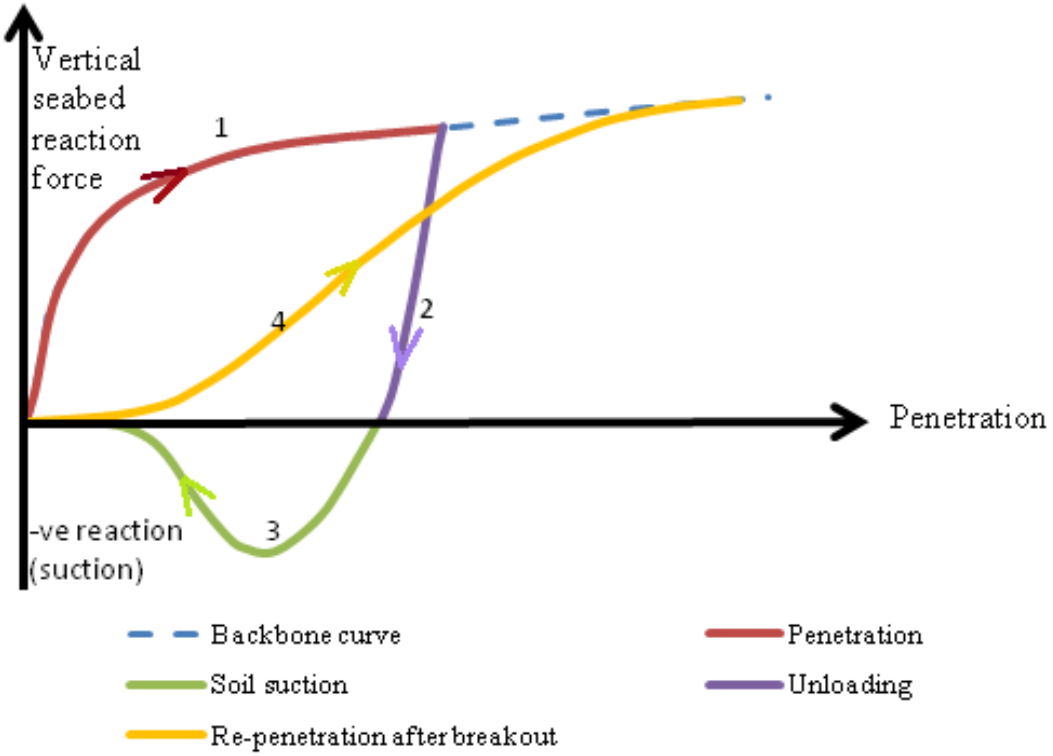

Figure 3.5—5 Pipe/soil interaction curves after Bridge *et al.* (2004)

Dunlap (1990) carried out laboratory model tests of vertically loaded horizontal pipes in sediment to simulate pipeline/sediment interaction under cyclic load conditions. The model pipe was a 0.5ft-diameter, 5ft-long aluminium tube with a 3/8in-wall thickness. The test basin had a 6ft x 6ft cross section and was 4ft deep. The sediment was a green-grey calcium bentonite mixture. The liquid limit of the sediment was 101 and the plasticity index was 62, which classified it as highly plastic clay.

The test program includes two series: force-controlled cyclic tests and displacement-controlled cyclic tests. Force-controlled tests were performed by applying cyclic loads with constant maximum and minimum force levels of

about a median load. While the displacement-controlled test represents a force test, as the pipe was loaded with reinforcing bars to a predetermined weight and allowed to settle freely under its own weight during the downward stroke of the lever arm and on the upward stroke of the arm, the pipe was pulled free of the sediment under constant cyclic displacement loads. Thus, displacement-controlled tests closely reproduced the actual behaviour of pipes that may be alternately pulled completely free of the sediment and then pushed into the sediment. The results of displacement-controlled tests are shown in Figure 3.5—6. A summary of Dunlap results are presented in section 3.6.5.

After two hours of cyclic loading, the backbone curve (i.e., presents how the seabed reaction force per unit length varies with the riser pipe penetration depth below the mudline) was established as the embedment of the pipe due to 1, 10, 100, 1000, and 3000 cycles being plotted versus soil forces. The comparison of the 1st and 3000th cycles also exhibited the degradation effects of the sediment strength under the influence of cyclic loading. These test data produce the general load/deflection pattern for soil-riser interaction and necessary information for the validation of the *V*-z models as well as the determination of parameters used in the model.

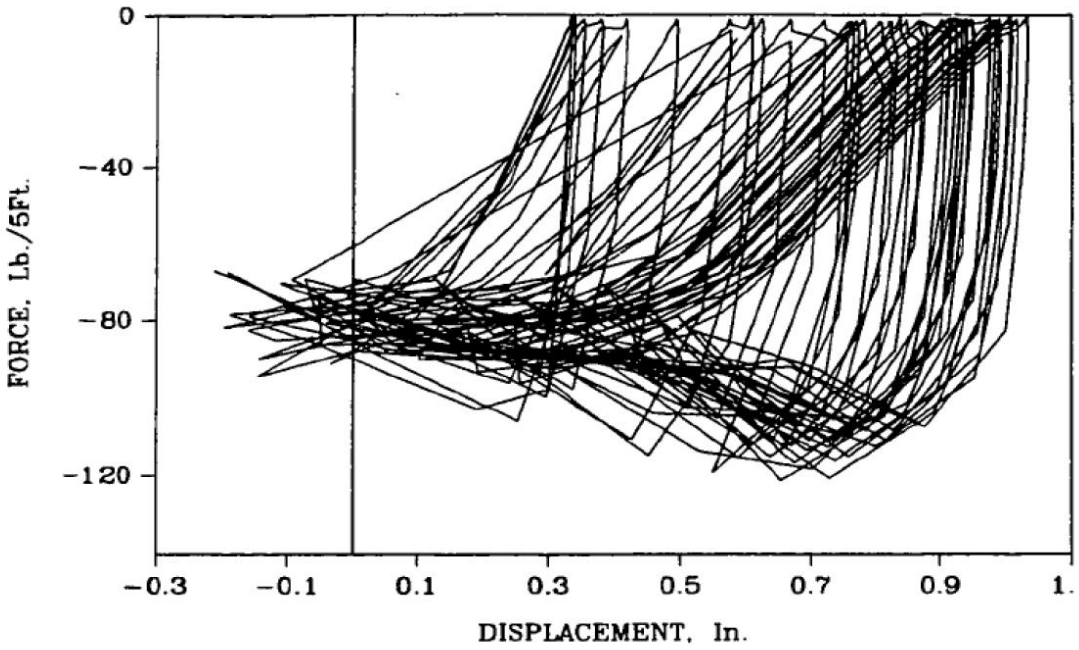

Figure 3.5—6 Load/Deflection Curve for Displacement-Controlled Test

(Dunlap *et al.*, 1990)

3.5.2 Analytical Models

Pesce *et al*. (1998) investigated a soil rigidity effect in the touchdown boundary layer of a riser on a static problem. They developed analysis by considering a linearly elastic soil, which performed on the catenary riser TDP static boundary-layer problem. Although linear elastic seabed models (e.g., Pesce *et al*., 1998) give very useful insights about soil-riser interactions, they cannot fully identify complex interaction problems including trench formation, non-linear soil stiffness, soil suction, breakaway of the riser from the seabed, and cyclic degradation of soil stiffness, as exhibited by full-scale experimental testing (Bridge and Willis 2002; Bridge *et al*., 2004). Palmer (Palmer, 2008) extends the rigid seabed analysis to a rigid plastic seabed (i.e., where the seabed is assumed to have plastic deformation, and hence reaction forces developed will remain when the riser moves from one offset to another). He also derived an analytical solution, which can be used to predict the additional load that occurs in the TDZ based on the pipeline configuration and lay tension.

Bridge *et al*. (2004) introduced three types of soil stiffness to be utilised in modelling soil–riser interaction: static stiffness, large deflection dynamic stiffness, and small deflection dynamic stiffness. Static stiffness is used to estimate the initial penetration of an SCR into a virgin seabed. Small deflection dynamic stiffness is used to model soil–riser interaction under unloading and reloading conditions. Large deflection dynamic stiffness is used to model the soil–riser interaction during large riser motions, where the pipe breaks away

from the soil and is typically a modified secant stiffness that accounts for the plastic deformation when soil–riser separation occurs. Section 3.6.5 illustrates and describes the static stiffness, small deflection dynamic stiffness and large deflection stiffness.

Aubeny *et al*. (Aubeny *et al.*, 2006, Aubeny and Biscontin, 2009) have presented a seabed/riser interaction model based on an elastic pipe supported on non-linear springs (see Figure 3.5—7). Spring stiffness is identified in terms of load/deflection (*V*-z) relationships that form a critical component of the model. They proposed a non-linear load/deflection *V*-z model based on the observation of laboratory model tests of vertically loaded pipes in weak sediment (Bridge *et al.*, 2004, Dunlap *et al.*, 1990). The *V*-z model is formulated in terms of a backbone curve describing initial plastic penetration into the seabed, a bounding loop describing load/deflection behaviour under conditions of extreme deflection, and a series of rules for describing load/deflection behaviour within the bounding loop (Aubeny *et al.*, 2006). The soil spring component of the model involves solution of a fourth-order, ordinary, non-linear differential equation. In addition, trench formation also has a significant effect on seabed–riser response. Aubeny *et al*. (2006) have indicated that the trench depth, trench width and roughness at the soil-riser surface could affect soil resistance. Soil resistance force would increase with trench increasing and it would decrease as the trench becomes wider. Seabed soil with a rough interface would have a larger resistance than a smooth case.

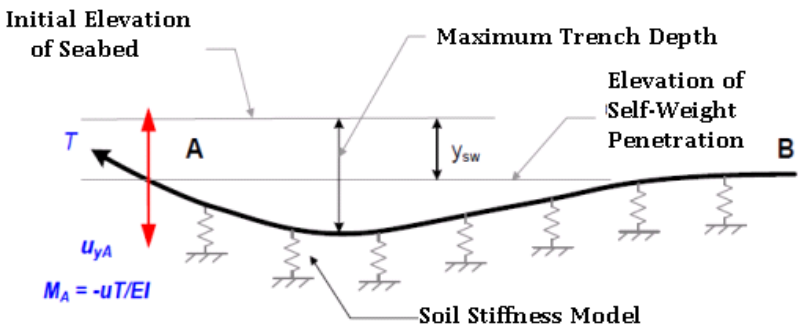

Figure 3.5—7 Seabed–riser interaction model (Aubeny and Biscontin, 2009, You, 2008)

You (2008) introduced an analytical framework for simulating seabed–riser interaction as a linearly elastic pipe on a series of non-linear soil springs. The soil model follows the *V*-z model proposed by Aubeny and Biscontin (2006), but it includes the effects of the degradation in stiffness due to cyclic loading, as exhibited by cyclic load tests of model pipes supported on soil (Dunlap *et al.*, 1990). Although lateral motions of the riser affect riser performance (Morris, 1988, Hale, 1992), the proposed seabed–riser interaction model regards only the vertical riser motions. In addition, they adopted small displacement beam analysis in the analytical problem to treat the interaction problem. The model is utilised to perform parametric studies to assess the effects of soil stiffness, soil strength, trench geometry and amplitude of pipe displacements.

The seabed non-linear soil model has been implemented in Orcina (2010) based on the Randolph and Quiggin (2009) model, as it models the vertical pipe–soil interaction on soft clay according to the dynamic aspects more accurately than a linear seabed model (Randolph, 2009). The non-linear penetration resistance is

established on a power law expression for the nominal bearing capacity factor, $N_c = V/Ds_u$, with V being the vertical force per unit length, D the pipeline diameter and S_u the undrained shear strength at the pipeline invert, indicated by Aubeny *et al*. (2005) as:

$$N_c = a\left(\frac{z}{D}\right)^b$$

Equation 3.5—1

where z is the pipeline penetration into the seabed. The OrcaFlex default values of a = 6 and b = 0.25 were adopted.

3.5.3 Summary

The seabed response due to riser loading and the trench formation phenomenon are of great significance for safe and economic riser design. Current studies of SCR technology focused on better understanding of the TDZ and its interaction with the seabed soil. The soil–riser interaction involves a number of complexities, including non-linear soil behaviour, trench width and depth variability and softening of the seabed soil under cyclic loading. The seabed–riser interaction modelling allows the effect of physical phenomena, such as lateral resistance, soil suction forces and vertical seabed stiffness on the SCR performance to be identified and quantified. Non-linear seabed–riser model interaction will determine the influence of the seabed profile on SCR fatigue. A

small change in seabed stiffness can result in a small change in bending stress, but this causes a significant change in fatigue life. Therefore, the need for seabed–riser interaction modelling to be as realistic as possible is evident. In this section, a comprehensive review of the recent researches on the SCR–seabed interaction is introduced.

3.6 SCR Analysis Techniques

The SCR is a promising solution for deepwater applications. Due to their economic importance, ease of installation and fabrication within the offshore industry, there has been a steady increase in demand for their use in a deeper water environment. To be confident of their use in deepwater environments, there has been a need for changes in analysis techniques to make them more accurate, avoiding unessential conservatisms that were once commonplace.

More realistic SCR's models depend on the relevant physical processes that have been developed in a number of areas, the most significant being:

- Dynamic Effects,
- Environmental Wave Loading,
- SCR Design and Analysis Philosophy,
- Modelling of SCR,
- Riser/Seabed Interaction – Models for Seabed Response.

Many individual studies have been published on SCR response. Rather than detailing the strengths and weaknesses of each assessment, a review of the developments of each area, highlighting the current state-of-the-art procedures, will be given. In section 3.6.8, a table summarising the application of these developments in a representative set of SCR studies is presented. It is shown that while many studies utilise state-of-the-art procedures for one or two aspects, there are a few that bring all components to the same level of complexity.

3.6.1 Dynamic Effects

The need to consider dynamic effects of marine risers has been acknowledged (Egeland *et al.*, 1982, Kirk *et al.*, 1979, Burke, 1973, Ljuština *et al.*, 2004, Chakrabarti and Frampton, 1982). Detailed reviews of previous studies were presented by Patel and Seyed (1995). Debate exists as to the proper method of accounting for the dynamic effects of an SCR. The main techniques that have been applied are time domain and frequency domain. The preferred technique is a function of the accuracy-required computational efficiency. The SCR's behaviour is non-linear in nature (Mekha, 2001). The SCR analysis includes inherent non-linearities due to drag, damping, riser–vessel attachment, riser–soil interaction, etc. Time domain techniques give the adequately complete analysis option with the capability to reflect the actual physical processes and non-linearities within the riser system. However, they are computationally

time-consuming. The frequency domain techniques offer a more numerically efficient solution, but as the non-linearities' behaviour of the SCR must be linearised either by dropping higher order terms in the equation of motion or using appropriate approximations, some physical processes become inaccurately modelled. These include the non-linearities in loading from riser-seabed interaction and Morison's drag effects.

In summary, time domain analysis is inherently more accurate than frequency domain analysis; however, frequency domain analysis is considerably faster (Chakrabarti, 1987). Time domain analysis is the preferred option for detailed analysis on complex riser systems to capture possible non-linear effects, associated wave forces and structural motions of SCR response.

3.6.2 Environmental Wave Loading

Extreme storm analysis can be performed using either regular or random waves. Deterministic regular wave theories, which include Airy and Stokes V, are a good option for preliminary design, as required design changes can be quickly evaluated. Therefore, deterministic wave analysis is sufficient for early feasibility checks (Chakrabarti, 2005). Moreover, regular wave theories assume all wave energy is assembled in one frequency component rather than the broad spectrum of the sea environment and hence give an unrepresentative dynamic response of SCRs.

For dynamically responding structures, such as SCRs, it is important to simulate all of the random, spectral and non-linear properties of wave loading. The dynamic response of an SCR depends not only upon the load being currently applied, but also on the load history. Therefore, the most accurate estimation of the extreme response is based on random time domain simulation of the sea surface and corresponding kinematics. For severe environmental conditions, response statistics are typically evaluated over a 3-hour period. However, random time domain simulation is computationally time-consuming in order to achieve confidence in results. Random wave analysis is typically established by selection of spectrum type and parameters, associated current and directional data based on available metocean data.

Time simulation procedures are often used for irregular wave dynamic analysis. A structural dynamic analysis of the SCR including the non-linear effects is performed using a small time-step. The main drawback in this method is that only a limited number of time simulations, each covering a few hours, can be carried out due to the excessive computational costs. Therefore, time series from irregular wave simulations must be processed to obtain extreme values for storm duration of interest using Weibull or Rayleigh distribution.

3.6.3 SCR Design and Analysis Philosophy

SCRs are designed to withstand the influences of the environmental, hydrodynamic and geotechnical loadings. Analysis of an SCR is aimed to

determine the structural strength behaviour, the fatigue performance as well as vortex-induced vibration, which are considered as the key activities of the SCR design. Herein, these key aspects of SCR's design are discussed after highlighting the current SCR code design and material selection.

a. Overview of SCR Code Deign

Different design codes for the SCR's designing in deepwater. The most widely applied codes for design of deepwater risers are API RP 2RD (API, 1998), API RP 1111 (API, 1999), DNV RP F201 (DNV, 2001-amended 2009), (DNV, January 2001), and DNV RP F204 (DNV, 2005). The design codes are divided into two categories according to the fundamental design approaches: Working Stress Design (WSD) and Limit State Design (LSD) (Kavanagh *et al*., 2003). WSD is the conventional approach for steel design, which relates the allowable loading to the yield stress of the steel pipe, while the LSD is an ultimate strength approach that relates allowable loading to the ultimate strength of the steel pipe. The WSD approach is widely acknowledged and relatively easier than the LSD approach. It is desirable to follow one approach for SCR design to produce a consistent design and safety level.

b. Material Selection

The common materials for an SCR include carbon steel pipe, clad steel pipe, steel forgings and titanium. Carbon steel line pipe is the less expensive and most

commonly used material for SCRs. Normally, API X52 through X80 line pipe has been widely used for SCR pipe, see Figure 3.6—1 (API, 2004). Alternatively, other high-strength steel such as 13% *Cr* or super-duplex may be applied. Titanium alloys are also very attractive to deepwater applications (Bai, 2001). The flow-line risers will internally be exhibited to the well fluids, which will be corrosive due to CO_2. The Corrosive Resistant Alloy is discussed in detail by Karunakaran *et al.* (2005).

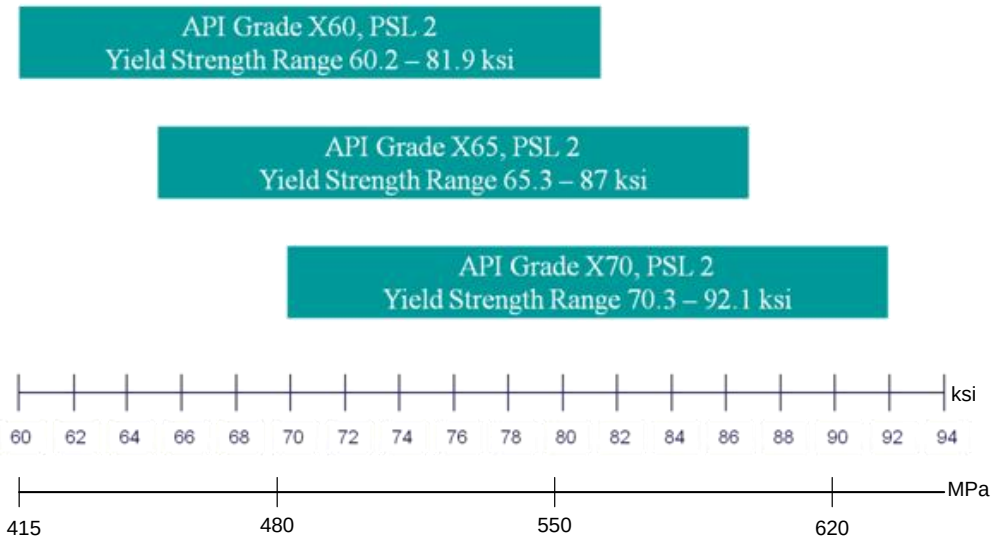

Figure 3.6—1 API standard grades yield strength

c. SCR Strength Analysis

The SCR's strength performance is determined using an extreme loading condition (10-year and 100-year current and sea-state return condition) and intact and accidental design load cases (i.e., intact and failed mooring condition respectively) for stress utilisation checks as per API RP 2RD (API, 1998). The

dynamic response (i.e., effective tension, stresses, deflections, etc.) of an SCR is assessed by using a random wave simulation of 3-hour duration. For permanent operational conditions with duration in excess of 12 months, a 100-year return period is used. The most severe loading condition, when the data about the joint probability of waves and current is not known, can be approximated by the following combinations (DNV, 2009):

- The 100-year return condition of waves combined with the 10-year return condition for current.
- The 10-year return condition for waves combined with the 100-year return condition for current.

d. SCR Wave Fatigue Analysis

The main contributor to fatigue damage of the SCRs comes from the wave-induced fatigue. As the SCRs are attached to the floating platform, the SCR's fatigue life is assessed by involving the fatigue damage from the first and second order motions of the facility as well as the fatigue damage from VIV (Campbell, 1999). A sufficient number of sea-state fatigue bins (statistical representation of individual wave conditions which exist during a given period, e.g., 3 hours (Barltrop *et al.*, 1991) representative of the wave scatter diagram are used to determine the wave-induced fatigue damage. Fatigue analysis can be performed using the rain-flow counting method presented by Ariduru (2004); it can be

performed to calculate the fatigue damage from the stresses driven from the first and second order loading.

e. Vortex–Induced Vibrations (VIV)

Oil and gas production in deep and ultra-deep water depths introduces many challenges, one of them being the VIV and its influences on the fatigue life. VIV is an important design issue for deepwater SCR systems operating in locations where severe current loading is expected. SCRs may experience an oscillatory force when seawater flows past an SCR's pipe, which results in shed alternating vortices. Higher current speeds can generate VIV that results in high rates of riser fatigue damage accumulation. As riser development moves into deeper water, VIV behaviour introduces one of the biggest uncertainties challenging riser engineers (Lim and Howells, 2000). Limitation of VIV-induced fatigue damage in SCRs may require the use of suppression devices, such as strakes along the critical area of the riser. On the other hand, strakes will increase the hydrodynamic drag forces.

3.6.4 Modelling of SCR

Numerical models of SCRs are used to determine the riser static and dynamic response. The catenary mathematical equation is used to give the riser configuration and the static response. Generally, non-linear Finite Element Analysis (FEA) is used to determine the dynamic response of SCRs. There are

many riser finite element software packages, both riser specific and general purpose. SCRs are typically analysed using a non-linear time domain FEA to assess the SCR's static and dynamic response. This study selects the most notable and widely used packages for briefly reviewing their usage, efficiency and the limit of the analysis (Table 3.6—1). SCRs can be modelled by a finite element model using a series of line segments. Since the sections highlighted the SCR/floating platform interface and the touchdown area as hotspots for the design and analysis of an SCR, a robust mesh of the segment length should be suitably used at these sections.

Riser analysis can be carried out using many FEA packages, as described in Table 3.6—1. The boundary conditions of the SCR are the SCR/vessel interfacing and the interaction with the seabed. The floating platform can be modelled using Response Amplitude Operators (RAOs), which define the floating platform motions. Generally, the seabed soil model is modelled as either a rigid or linear surface with lateral and axial friction coefficients. All FEA packages listed are using a stiffness matrix and for solving the equation of motion, either explicit or implicit integration schemes are used.

Table 3.6—1 Riser pipe analysis software packages

Software	Vendor	Dynamic Approach		Use	References
		TD	FD		
OrcaFlex	Orcina	√	√	Riser Specific	(Orcina, 2010, Borgen, 2002, Borgen *et al.*,

Software	Vendor	Dynamic Approach		Use	References
		TD	FD		
					2003)
RIFLEX	MARINTEK (the Norwegian Marine Technology Institute)	√	√	Riser Specific; No GUI	(Chatjigeorgiou, 2008, Rustad *et al.*, 2008)
FREECOM	Marine Computation Services, Ltd		√	Riser specific; (Less accurate than TD)	(DNV, 2011, Serta, 1996)
FLEXCOM	Marine Computation Services, Ltd	√		Riser Specific	(DNV, 2011, Serta, 1996)
OFFPIPE	OFFPIPE	√		Offshore Pipeline	(Robert and Malahy, 1996)
SAGE PROFILE 3D	Fugro GeoConsulting	√		Subsea Pipeline	(Bayirli, 2009)
ABAQUS	Dassault Systemes Simulia	√	√	General Purpose	(Hodder, 2010b, Pasqualino *et al.*, 2002)
ANSYS	ANSYS, Inc.	√	√	General Purpose	(Natarajan *et al.*, 2008, Sánchez and Salas, 2005)
ANFLEX	developed jointly by COPPE and PETROBRAS	√	√	Riser Specific	(Dantas *et al.*, 2005, Sagrilo *et al.*, 2002)
Deeplines	PRINCIPIA	√	√	Riser Specific	www.principia.fr (Chatjigeorgiou, 2008)

Note: FD, TD, and GUI denote frequency domain, time domain, and graphical user interface, respectively.

a. Catenary Shape Equation

The catenary is the shape of a perfect cable suspended by its ends and acted upon by a uniform gravitational force. Its equation was obtained by Leibniz and Johann Bernoulli in 1691 (Leibniz, 1691a, Leibniz, 1691b). It assumes that the

cable/riser catenary has zero bending stiffness and zero current load. Figure 3.6—2 shows the axes and the forces acting on a simple catenary, with origin at the TDP. Angle θ is measured from the horizontal; T is the catenary effective tension at a point along a riser; T_t is the tension at the riser top end with vertical component V and horizontal component H; w is the apparent weight per unit length and is equal to the submerged mass per unit length multiplied by acceleration due to gravity; S_R is the length of the riser between the TDP and the floating platform; and S is the arc length measured from the TDP to a point on the riser. The catenary equation is only applicable in the catenary zone (i.e., from the riser top end at the floating platform to the TDP), as it does not involve the riser interaction with the seabed. The equation of the catenary is derived from the geometric constraint,

$$ds = \sqrt{dx^2 + dy^2} \quad \text{then} \frac{\text{ds}}{\text{dx}} = \sqrt{1 + \left(\frac{dy}{dx}\right)^2}$$

Equation 3.6—1

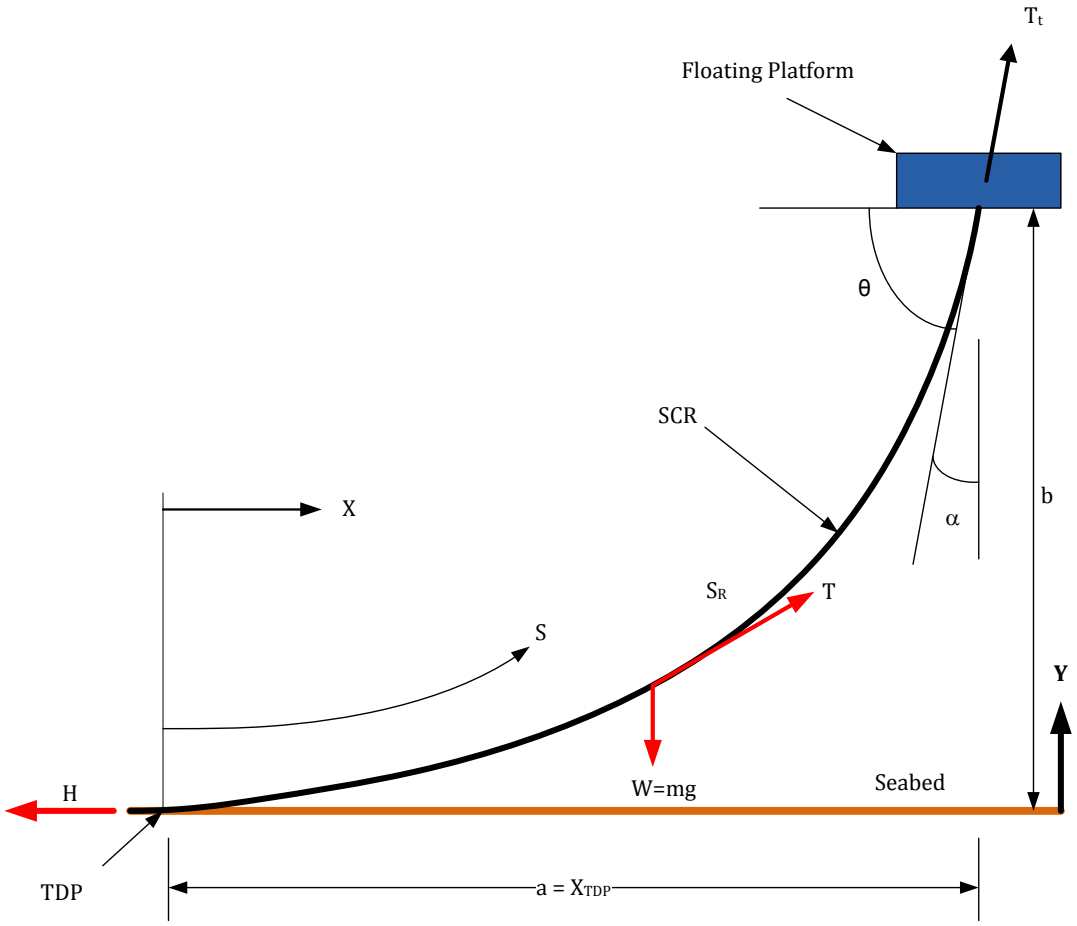

Figure 3.6—2 Catenary axes and symbols

This can be solved (see Appendix A for the derivation in detail), and hence the catenary equation is given by:

$$y = \frac{H}{mg}\cosh\left(\frac{mg}{H}x\right)$$

Equation 3.6—2

Equation 3.6—2 allows the calculation of a point on the SCR above the seabed, given the distance from the TDP, apparent weight per unit length and the horizontal tension at the TDP.

The curvature and bending moment distribution for the catenary shape is derived from curvature relationships given below:

$$\frac{d\theta}{ds} = \frac{1}{R} = \frac{d^2y/dx^2}{\left[1+\left(dy/dx\right)^2\right]^{3/2}}$$

Equation 3.6—3

$$M = \frac{EI}{R}$$

Equation 3.6—4

where $(1/R)$ is the curvature, E is Young's modulus of elasticity, I is the second moment of area and M is the bending moment. The riser's curvature in the catenary zone depends on the riser effective weight and tension, as presented by Equation 3.6—3.

Therefore, the bending moment distribution is given by:

$$\frac{M}{EI} = \frac{1}{c}\frac{1}{\left[\cosh\frac{a}{c}\right]^2} \quad \text{where } c = (H/mg).$$

Equation 3.6—5

The bending stress resulting from this moment can be established using a fundamental relationship:

$\sigma_b = \frac{M}{z}$ where z is the section modulus.

Equation 3.6—6

b. SCR Configuration Design

The catenary riser length is estimated using simple geometric considerations, as following (Hatton, 1999):

$$\text{Total Riser Length} = \left(\frac{D-(MBR)A}{\cos\theta}\right) + \left(0.5\pi(MBR)A\right)$$

Equation 3.6—7

where D is a water depth, A is a factor depending on severity of environment (1.0 for mild environments and 1.2 for severe environments), θ is the Riser top angle to vertical, typically between 10 and 25 degrees depending on severity of environment and water depth, and *MBR* is minimum bend radius based on 80% material yield strength (typically API grade X65 shown in Table 3.6—2). An additional riser pipeline length of approximately 750m should be included to allow for TDP movement between near and far offset conditions, see Figure 3.6—3.

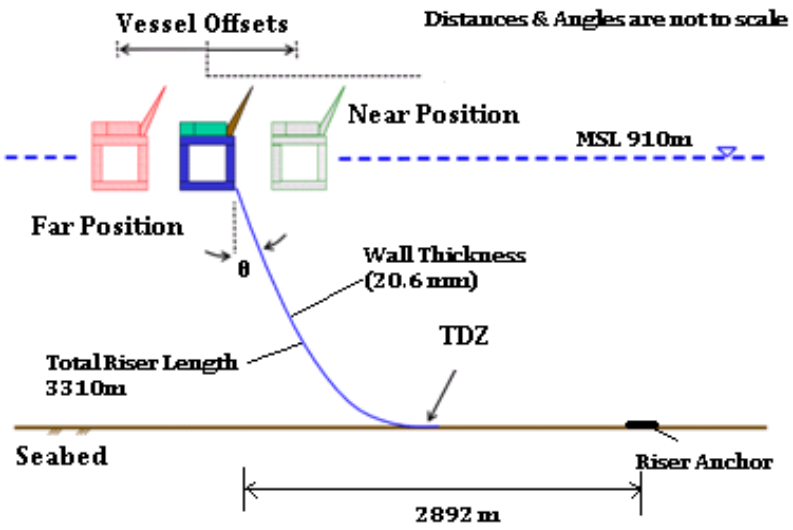

Figure 3.6—3 Schematic of SCR configuration and vessel offsets

Therefore, allowable minimum bend radii of different pipe sizes should be considered, see Table 3.6—2. Based on the Equation 3.6—7, the approximate minimum water depths, in which steel catenaries of different diameters can be used, can be taken as twice the MBR.

Table 3.6—2 Steel pipe MBR (Howells, 1995)

Pipe OD (inch)	Minimum Bend Radius (m)
6	43
8	58
12	87
20	147
30	220
Assumes X65 material, allowable stress of 0.8 yield stress	

The main parameters clarifying the SCR configuration design are wall thickness, top hang-off angle and riser length to the TDP, see Figure 3.6—3. These were selected initially based on sizing and static and dynamic analysis.

c. SCR Static Profile and Analysis

The initial stage of any analysis of an SCR is the computation of its configuration under a set of static forces. The catenary equation gives a good first approximation for this, but in their basic formulation it only involves loads due to riser weight and assumes a riser pipe of zero bending stiffness, as presented before. However, the SCR static analysis is a large deflection non-linear behaviour problem with the influences of bending and tensional stiffness included. Therefore, many approaches have been developed to handle this problem using a combination of catenary equations and numerical techniques through iterative analysis. A review of existing approaches can be found in (Patel and Seyed, 1995). The SCR's static configuration must be determined before carrying out dynamic analysis. Figure 3.6—4 shows an example of static configuration of an SCR in a 910-m water depth with a hang-off angle of 20° and a 273 mm (10.75 inch) outer diameter connected to the floating platform (FP) in the zero mean offset position (i.e., the FP is in its initial position without drifting in any direction), which is calculated using OrcaFlex/FEA software.

Generally, SCRs have a limited amount of additional pipeline length available to accommodate the FP motions. Alterations in the catenary suspended length are

obtained by the riser either being picked up or laid down on the seabed. Limitations are approached when either the SCR tension at the FP becomes too great as the FP drifts away from the TDP (far load case, as shown before in Figure 3.6—2) or when the bending stresses near the seabed become too great as the FP drifts towards the touchdown point (near load case). SCRs are less appropriate for FPSO applications where vessel offsets are considerably higher. Figure 3.6—5 shows the effect of the horizontal vessel offset on the horizontal projection of the TDP. While the top of the SCR has the highest tension and lowest bending moment, the TDP has the lowest tension and the highest bending moment. The maximum bending stress and effective tension along the SCRs' arc length within the vessel offsets and the horizontal projection of the TDP are presented in Figure 3.6—6 and Figure 3.6—7 respectively.

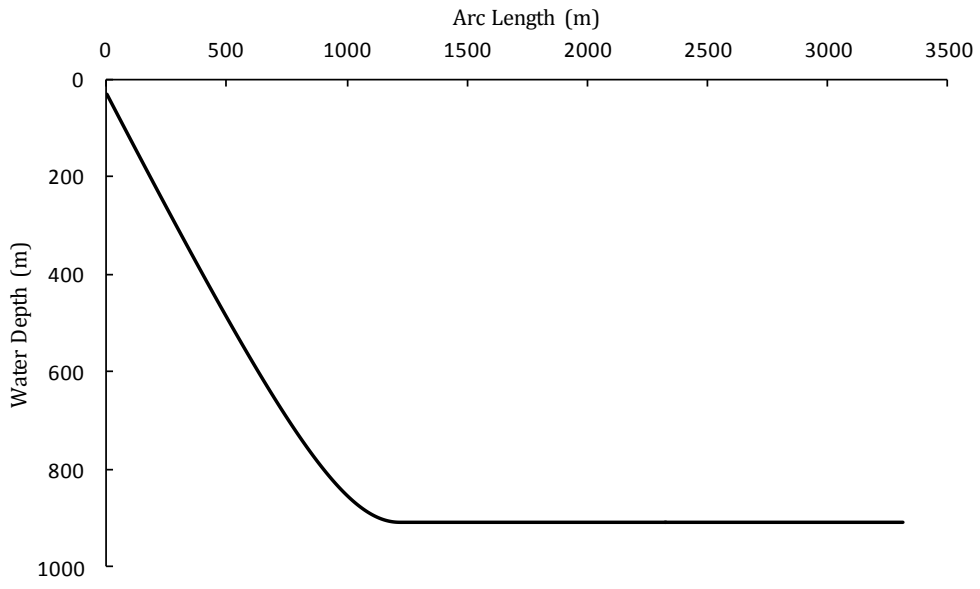

Figure 3.6—4 Static configuration of SCR model

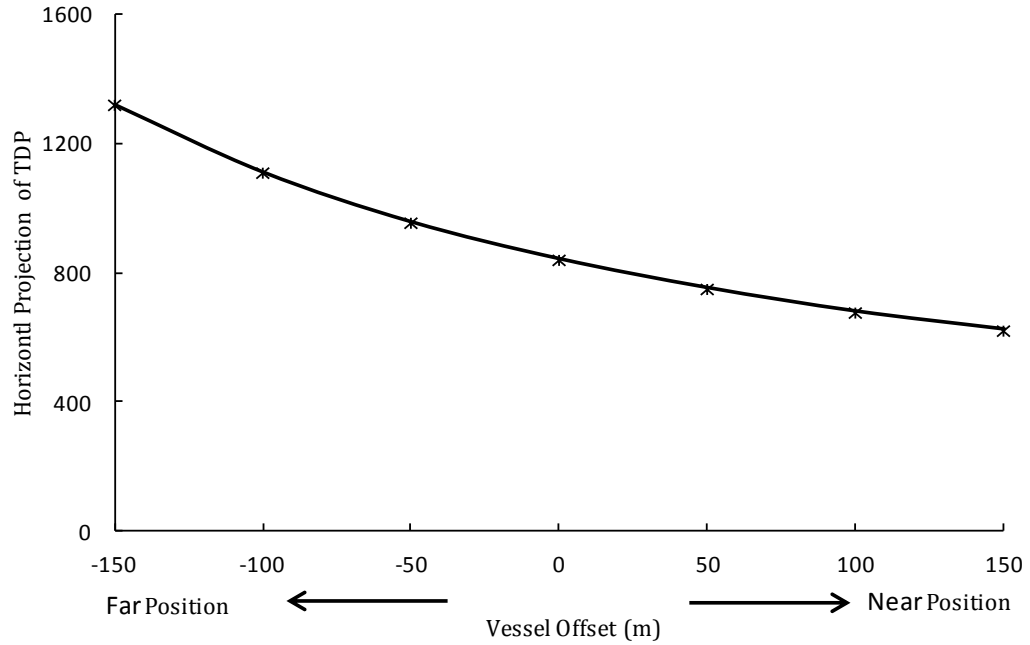

Figure 3.6—5 Effect of the vessel offsets on the horizontal projection of the TDP

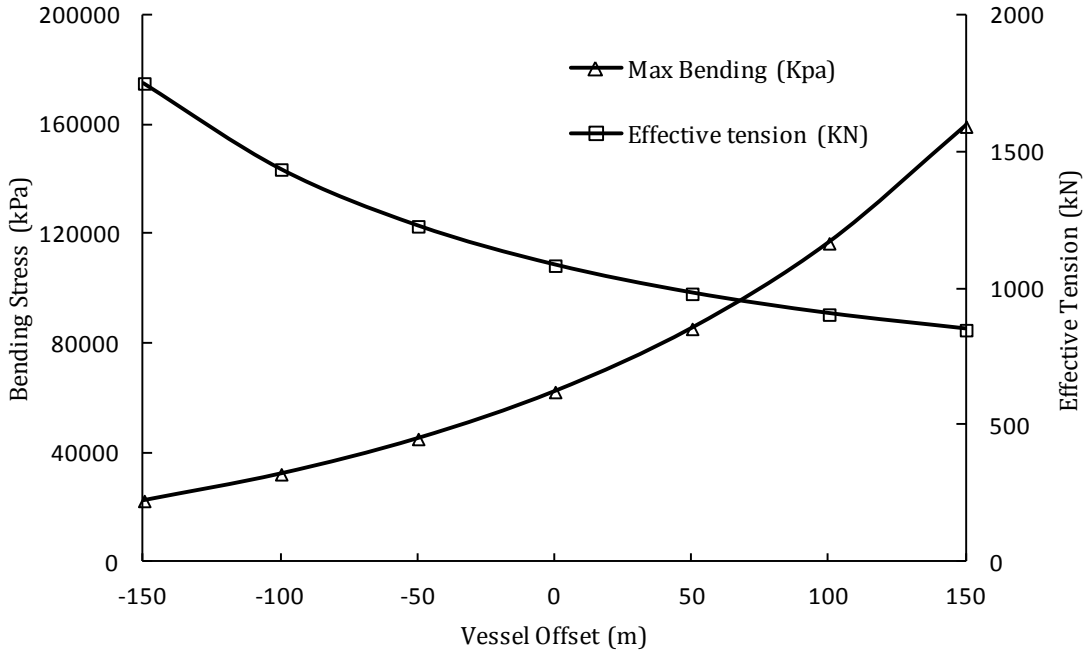

Figure 3.6—6 Alterations of maximum bending stress and maximum effective tension with the horizontal vessel offset

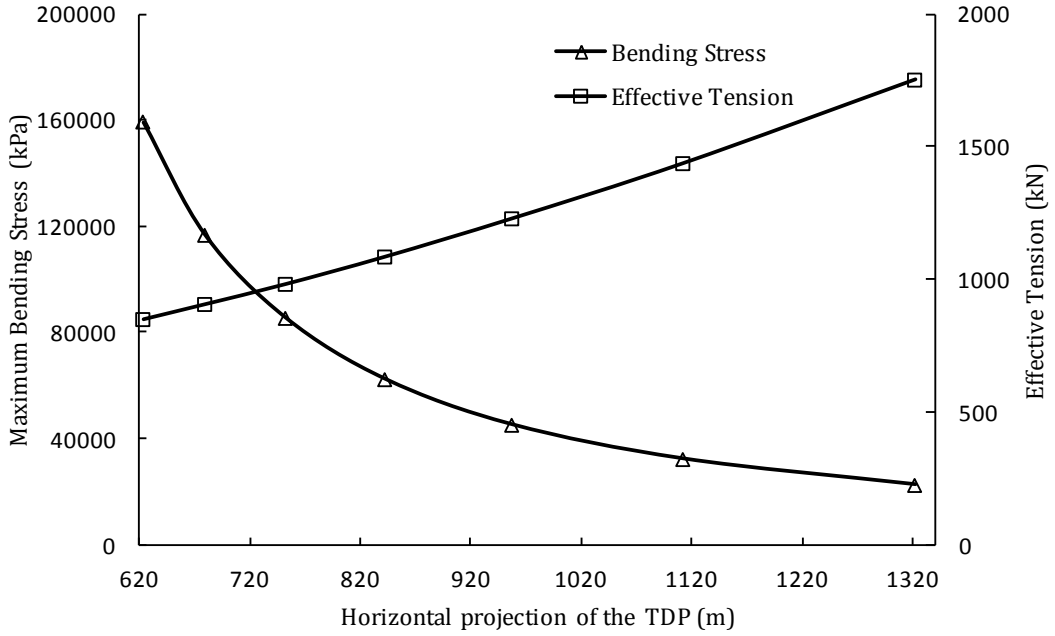

Figure 3.6—7 Alterations of maximum bending stress and effective tension with the horizontal projection of the TDP

The vessel offset governs the maximum bending stress at the TDP and also the maximum tension at the riser's top end. In the left region of Figure 3.6—7, where the vessel drifts towards the TDP (near load case), the bending stress at the TDP is increased rapidly within small change in the vessel offset. In the intermediate region, the bending stress and tension are slightly increased with the vessel offset. In the right region, where the vessel drifts away from the TDP (far load case), the bending stress slightly decreased, while the tension increased. Therefore, the conclusion from these results is that the vessel mean position should be offsetting the TDP with a roughly distance of 0.75 to 1.5 of the water depth. Furthermore, the catenary equation is a simple implementation tool to figure out the load distribution, geometric properties

and static loads on an SCR. The specialist non-linear/FEA is implemented for the SCR design to tackle the complex nature of non-linear, large deflection behaviour of SCRs and to be post-processed quickly. The evaluation of the forces and behaviour of SCRs in the TDZ need more sophisticated methods.

d. SCR Dynamic Modelling

The riser dynamics modelling can be simulated using the lumped mass method in the time domain. This modelling approach involves the lumping of all forces and masses at a finite number of nodes along the riser. These nodes are connected through springs and dampers, see Appendix B for dynamic modelling of lines. Hydrodynamic loads are calculated using Morison's Equation, comprising of drag force and inertia force. Generally, the riser dynamic model is conducted to determine stresses and displacements due to dynamic motions by utilising RAOs for the evaluation of the structure strength sufficiency as well as subsequent calculation of the riser fatigue life.

3.6.5 SCR/Seabed Vertical Interaction – Models for seabed response

The application of SCR systems has increased with the progressive development of hydrocarbon production further offshore and into deeper waters. The seabeds of deepwater hydrocarbon fields often consist of soft clay. The SCR–soil interaction at touchdown with the seabed is a major key factor for SCRs. An SCR is subjected to oscillatory motions from the host vessel and wave action.

Therefore, the SCR experiences a complex interaction between the riser and seabed in the touchdown area, and deep trenches thus cut into the seabed in the buried zone beyond the TDP (Thethi, 2001, Karunakaran *et al.*, 2005a, Karunakaran *et al.*, 1999).

An appropriate SCR–seabed interaction model must be used. The TDZ is one of the key locations where the fatigue damage happens. The sophistication of the interaction model depends on the type of analysis and accuracy required. These interaction models vary from a simple rigid seabed with soil friction coefficients to more sophisticated ones, including vertical and lateral stiffness, friction and suction.

a. Rigid Seabed

A potential fatigue damage of the SCR in the TDZ is related to maximum bending stress in the SCR, which relies on the soil stiffness of the seabed and the motions of the SCR. For example, the SCR on a soft seabed will have reduced bending stresses when a load is applied, while the one on a rigid seabed will have more critical bending stresses. A rigid surface generally contributes a conservative result, since it is unyielding, while the non-linear soil model is a better approximation of a seabed. Extreme offsets of the floating production unit with soft seabed model may then give higher stresses than those calculated on rigid seabed stiffness, since the catenary pipeline must be broken out of the seabed soil and high suction forces must be overcome. Figure 3.6—8 shows a schematic

of an SCR close to the TDP with the forces acting on a rigid seabed. The shear force *F* in the near horizontal segment close to the TDP is given by:

$$F = \frac{dM}{dx} = \frac{d}{dx}\left[EI\left(\frac{d^2 y}{dx^2} \right) \right] = EI\left(\frac{d^3 y}{dx^3} \right)$$

Equation 3.6—8

See Appendix A for details, then $d^3y/dx^3 = (w/H)ke^{-kx}$. The shear force close to the TDP is thus given by:

$$F = EI\left(\frac{w}{H} \right) k e^{-kx}$$

Equation 3.6—9

The bending moment at the TDP diminishes from the catenary bending moment to zero, and there is a concentrated reaction force. Since $k = \sqrt{H / EI}$, the TDP shear force that is transmitted to the soil (SPARKS, 2008, Palmer, 2008) is given by:

$$F_{TDP} = w\sqrt{EI / H}$$

Equation 3.6—10

where F_{TDP} is the concentrated reaction at the TDP, assuming a rigid surface seabed, F_f is the reaction to the pipe resting on the seabed, see Figure 3.6—8.

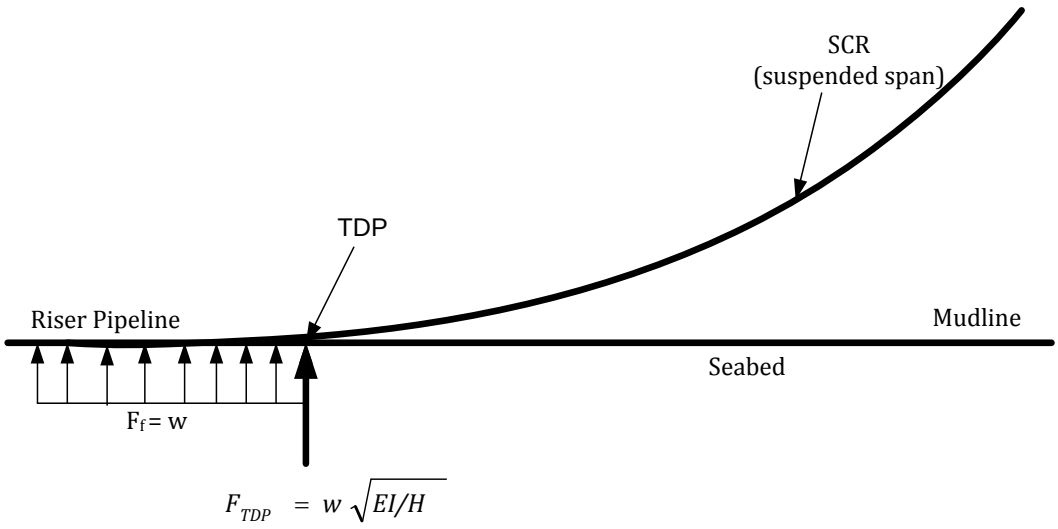

Figure 3.6—8 Configuration of SCR close to TDP with a rigid seabed

b. Elastic Seabed

Configuration of an SCR close to the TDP is shown in Figure 3.6—9 by representing a seabed with a linear elastic model. The curvature in the suspended length is given by Equation 3.6—3, while the curvature in the surface zone (i.e., while the pipeline is resting on the seabed) is zero. In the TDZ, the riser's pipe is resting on linear elastic foundations. The solution for a beam element resting on an elastic foundation can be found in (Jones, 1997, Hetényi and Michigan, 1946), who introduced solutions that can be implemented for SCR–seabed interaction.

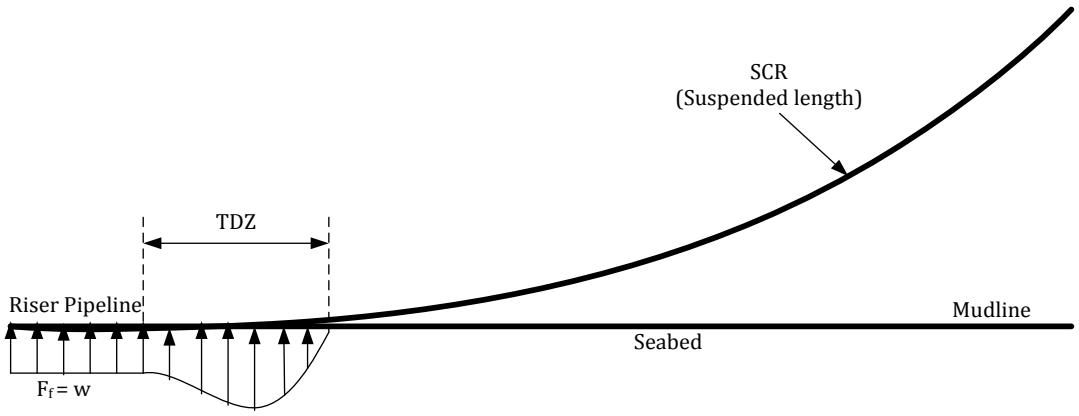

Figure 3.6—9 SCR's Configuration close to TDZ with linear elastic seabed

c. Non-linear Load/Deflection Model

The current practice for the FEA of SCR–seabed interaction response is to model this interaction as structural soil springs (Thethi 2001) by using the developed models for buried pipelines and strip foundation theory. The conventional modelling of riser–seabed interaction use the non-linear elastic load/deflection curves, as presented in Figure 3.6—10. Since the resistance force does not exceed the friction resistance limit (μV), the soil spring has a constant stiffness coefficient, *K*. The load/deflection model has zero resistance force at zero displacement, as the pipe displacement is increasing the resistance force also increases linearly until the peak seabed resistance is approached. When the seabed friction exceeds the limit friction force, the resistance force becomes constant with changing pipe displacement (large displacements occur without a further increase in the friction resistance force) and the spring stiffness becomes zero (i.e., slip occurs). The maximum seabed resistance load is given by

the backbone curve (Dunlap *et al.*, 1990), which corresponds to virgin penetration of the riser pipe into the seabed.

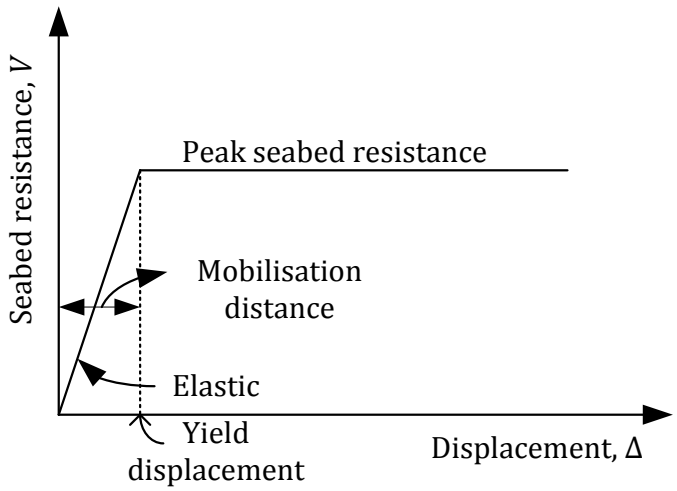

Figure 3.6—10 Description of load/deflection model of pipe-seabed interaction (Chen and Han, 1985)

d. Seabed Stiffness

Linear soil stiffness can be used by FEA codes to model the non-linear riser–seabed interaction curves. Linear soil stiffness is defined as the ultimate bearing load divided by the riser pipe displacement, as given below:

$$K = \frac{V}{\Delta}$$

Equation 3.6—11

where K is the soil stiffness per unit length; V is the force per unit length; Δ is the riser pipe displacement. Different approaches are used to characterise the

linear seabed stiffness, such as secant, tangent and Young's modulus stiffness, for more details see Barltrop *et al.* (1991). Herein, the secant stiffness type is considered because it is more stable than the tangent stiffness approach and is being used to model the load/deflection curve. The secant stiffness is the average stiffness between two points, typically the origin and the point in question, see Figure 3.6—11.

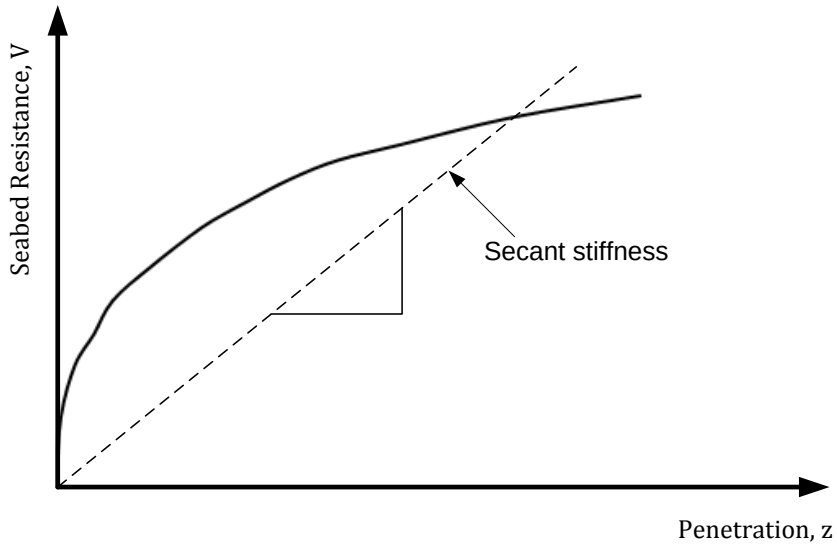

Figure 3.6—11 Secant stiffness for non-linear seabed *V-z* model

Regarding the SCR–seabed interaction response, two types of seabed stiffness are required: the static and dynamic seabed stiffness. The static seabed stiffness is used to model the initial riser penetration, and the dynamic seabed stiffness is used to model the dynamic SCR–seabed interaction.

Static seabed stiffness is using a linear stiffness to represent the backbone curve in riser–seabed interaction analysis. It is assumed that the riser will penetrate

into the seabed until the bearing load equals the submerged riser pipe weight; $w=V_u$ where w is the submerged riser pipe weight, and V_u is the ultimate bearing load, as shown in Figure 3.6—12.

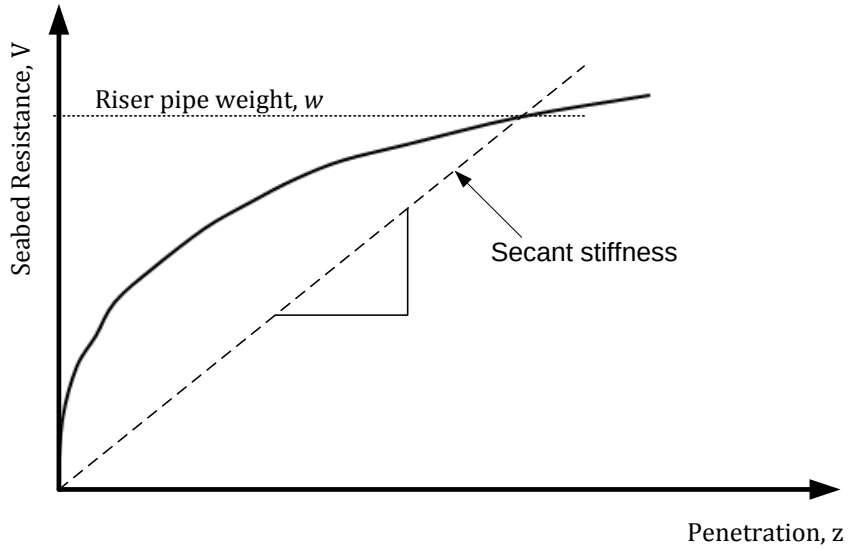

Figure 3.6—12 Static seabed stiffness

Figure 3.6—13 shows the dynamic seabed stiffness, which is used to model the dynamic riser–seabed interaction. Experimental studies have presented that the seabed will be plastically deformed around the riser pipe after the initial penetration (Bridge *et al.*, 2004). The dynamic stiffness is greater than the static stiffness because the seabed soil has plastically deformed under the influence of dynamic riser motions that create deep trenches into the seabed. As shown in Figure 3.6—13 the mobilisation distance is an important factor to estimate the dynamic stiffness. The mobilisation distance is distance over which the force changes from zero to the maximum (Bridge *et al.*, 2004). The linear stiffness is

thus obtained using Equation 3.6—11, where $\Delta = z_u$ mobilisation distance and V = soil resistance.

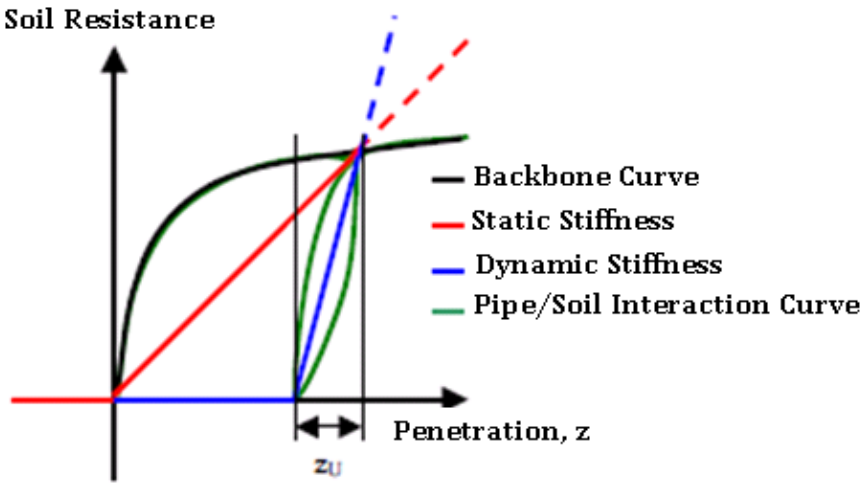

Figure 3.6—13 Dynamic seabed stiffness (Bridge *et al.*, 2004)

e. SCR–Seabed Cyclic Loading

The motions at the FP can induce severe riser response, leading to difficulty in achieving strength and fatigue criteria at the TDZ. The cyclic influence of pipe–seabed interaction in soft clay has been investigated by many authors; Dunlap (1990), Bridge *et al.* (2004), Aubeny *et al.* (2008) and Langford and Aubeny (2008). The influence is that as the number of interaction cycles increases, the seabed stiffness reduces (i.e., stiffness degradation). Seabed stiffness degradation has an important influence on the SCR's fatigue performance in the TDZ, as presented by Clukey (2007). Therefore, seabed degradation should be accurately modelled and illustrated by the *V-z* model of riser-seabed interaction. It has been found that of all the vessel motions, heave causes the largest SCR

stress fluctuations in the TDZ (Bridge *et al*., 2003). Different results from previous studies on vertical cyclic loading in soft clay will be demonstrated in this section.

Dunlap *et al*. (1990) carried out experiments to investigate the cyclic pipe–seabed interaction, as explained before in section 3.5. They used a 0.152m-diameter pipe to penetrate clay soils up to a one-pipe diameter. These experiments were performed using both force- and displacement-controlled tests. Dunlap *et al*. (1990) introduced the results in the form of normalised soil stiffness, K_C, for 1, 10, 100, 1000 and 3000 cycles, in the formulation that follows:

$$K_c = a\left(\frac{z}{D}\right)^b$$

Equation 3.6—12

where *a*, *b* are empirically derived constants. A summary of the empirical factors *a* and *b* determined by Dunlap *et al*. (1990) are presented in Table 3.6—3 and are represented graphically as dynamic backbone curves in Figure 3.6—14 for the load control tests. These tests introduced that as the number of cycles increased, the pipe seabed interaction force decreases.

Table 3.6—3 Summary of coefficients *a* and *b* for non-dimensional backbone curves (Dunlap *et al.*, 1990)

Cycle	Load-Controlled Tests				Displacement-Controlled Tests	
	K_C^+ (load increase)		K_C^- (load decrease)		K_C	
	a	*b*	*a*	*b*	*a*	*b*
1	8.332	0.615	6.855	0.727	7.388	0.645
10	8.350	0.612	6.823	0.730	5.408	0.555
100	8.324	0.631	6.650	0.732	4.93	0.624
1000	8.480	0.660	6.695	0.757	5.674	0.835
3000	9.330	0.710	7.284	0.773	5.919	0.934

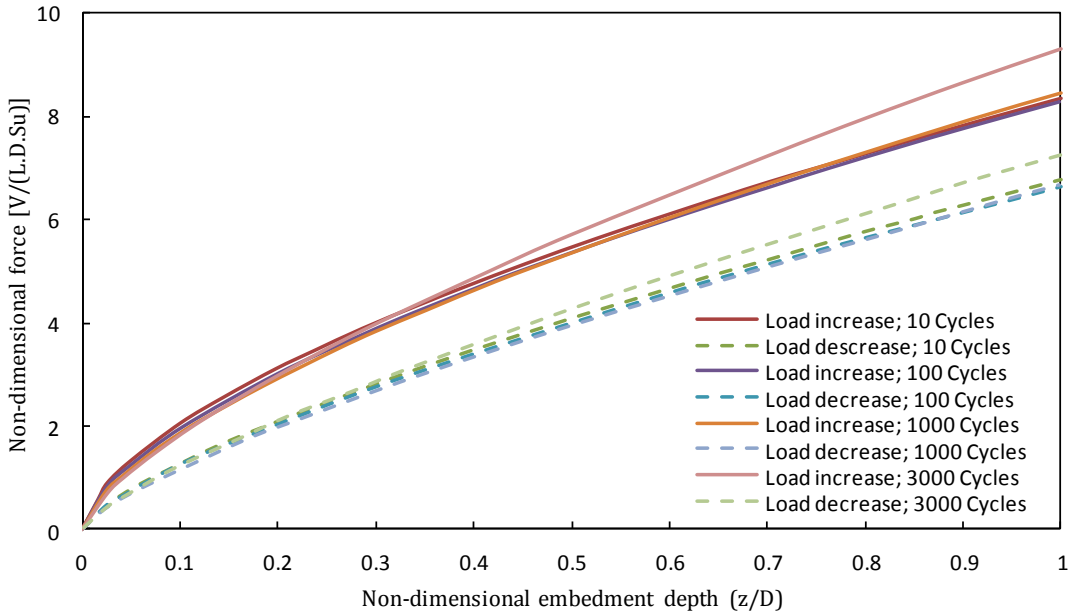

Figure 3.6—14 Summary of non-dimensional bearing capacity factors from load-controlled tests (Dunlap et al., 1990)

Bridge *et al.* (2004) introduced the state-of-the-art models developed using published data from pipe–seabed interaction tests carried out in the STRIDE and CARISIMA JIP. The author presented the behaviour of the backbone curve (soil resistance force versus pipe displacement) of pipe–seabed interaction at

different stages of riser pipe embedment and uplift. The authors have proposed a model of seabed degradation that is characterised by the change in the secant stiffness shown in Figure 3.6—15. The pipe penetration and the corresponding seabed soil resistance, denoted as backbone and soil suction curves in Figure 3.6—15, would change as the number of load cycles increases. The proposed model assumes the breakout displacement of trench depth. The model parameters are derived empirically from model experiment results.

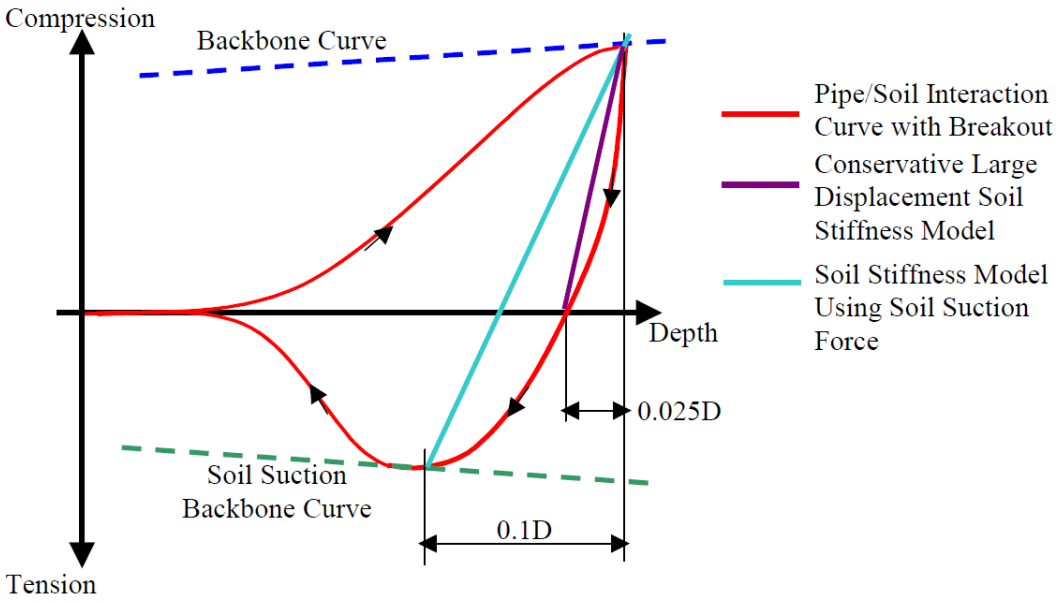

Figure 3.6—15 Displacements of unloading and soil suction curves of pipe-seabed interaction (Bridge *et al.*, 2004)

Clukey *et al.* (2008) carried out experiments to examine the pipe–seabed response under loading conditions that cause the fatigue damage for an SCR. These tests aimed at investigating the cyclic loads and displacements. The tests were conducted on a one-inch (0.0254m) in diameter pipe and was six inches

(0.1524m) in length; it was subjected to a series of load- and displacement-controlled cyclic loads and displacements.

They have been presenting the seabed soil stiffness values as non-dimensional stiffness ratios to compare the results with different sequences of loading conditions. The soil stiffness is computed by dividing the measured stiffness (k) (from cyclic load/cyclic displacement) per unit length by the bearing capacity factor, N_c, times the undrained shear strength, S_u. The non-dimensional stiffness, K_{stiff}, is then represented using the following expression:

$$K_{stiff} = \frac{K}{N_c S_u}$$

Equation 3.6—13

The bearing capacity factor, N_c, is computed using the proposed equation by Skempton (1984):

$$N_c = 5.14\left(1 + 0.23\left(\frac{z}{B}\right)^{0.5}\right)$$

Equation 3.6—14

where B is the width of the pipe in contact with soil. The load and displacement control tests carried out by Clukey *et al.* (2008) show similar results in which the stiffness ratio decreases to a value of less than 10. Consequently,

considerable attention has been focused on the seabed stiffness values that are typically expressed as a factor, K_{stiff}, times the bearing resistance, $N_c S_u$. Typical values of K_{stiff} range from a maximum of about 200 at very small displacement amplitudes down to below 10 for amplitudes exceeding 10% of a riser pipe diameter. The authors also observed the gap formation underneath the pipe under cyclic motions and that the characteristic shape of the load/deflection curve changes appreciably.

Aubeny *et al*. (2008) has presented a stiffness degradation model during the cyclic loading of pipe–seabed interaction. The authors stated that at the given load cycle, the reload stiffness is less than the unload stiffness. They introduced a numerical model based on and empirically fitted to finite element predictions proposed by Aubeny *et al.* (2005) for pipe embedment in seabed clay soil of less than one-half diameter (z/D <0.5), as following:

$$N_c = a\left(\frac{z}{D}\right)^b$$

$$N_c = \frac{V}{S_u(z)D}$$

Equation 3.6—15

where $S_u(z)$ is the undrained seabed soil strength at depth z. The bending moment of the pipe is determined numerically by involving Equation 3.6—15, the degradation soil model and the 4th order differential equation describing the vertical displacements for a pipe resting on a bed of springs. It is observed that

the stiffness degradation is occurred under the cyclic displacement, which leads to a significant decline in the soil stiffness between the seabed and riser.

The seabed response model can be modelled using hyperbolic functions (Randolph and Quiggin, 2009) for the decrease in stiffness with the increase in the displacement amplitude. For such a model, the key characteristics are illustrated in Chapter 4. The model uses data such as the pipe diameter, the seabed soil shear strength profile with depth and the soil density.

f. Seabed Condition and Field Observation

SCRs are typically used in deepwater and ultra-deepwater. The development of deepwater fields has led to discoveries. Many of these fresh discoveries are in regions where soft clay is detected, as shown by Dunlap *et al.* (1990) and Sen (2007). Typically, the undreamed shear strength at the mud-line is roughly in the range of 1–4 kPa (Willis, 2001, Nakhaee, 2009). The undrained shear strength is also noticed to increase linearly with depth below the seabed mudline and can be given as:

$$S_u = S_{u_0} + S_{ug} z$$

Equation 3.6—16

where S_{u0} is the undrained shear strength at the seabed mudline; S_{ug} is the undrained shear strength gradient; and z is the penetration depth below the

seabed mud-line. Trenches have been observed even after SCR installation within few months. The trench profile is very difficult to be predicted, which depends on the FP motions and the environmental loading (Thethi, 2001, Bridge, 2007).

3.6.6 SCR/Seabed Lateral Interaction

One of the main issues encountered with the use of the SCR is the large lateral movements on the seabed due to the FP motions and marine environment. Thus, better understanding of the lateral soil resistance to SCR pipe movements must be considered for SCR design. Many researchers had focused on studying and investigating the pipe-seabed lateral interaction response (Wagner *et al.*, 1987, Bruton, 2008, Morris, 1988, Cheuk and Bolton, 2006, White, 2008, Brennodden *et al.*, 1989).

The lateral interaction of an un-trenched pipeline placed on clay soil is modelled using Coulomb friction. The proposed lateral friction coefficients for sand (non-cohesive) and clay (cohesive) soils are given in Table 3.6—4. The studies published by Lyons (1973) and Wagner *et al*. (1987) have suggested that Coulomb friction is not suitable to describe the lateral pipe sliding on soft clays, as the pipe will penetrate the seabed. This is because the lateral soil resistance on the pipeline should be a function of soil and pipe properties. Numerous experimental studies on the lateral movement of un-trenched pipelines have been conducted with cyclic actuator loading methods (Wagner *et al.*, 1987,

Brennodden *et al.*, 1989, Schotman and Stork, 1987, Bruton, 2008, Morris, 1988).

Among these, Wagner *et al.* (1987) improved the Coulomb friction theory into an empirical pipe-soil interaction model, in which the total lateral seabed resistance was assumed to be the sum of the Coulomb friction component and the soil passive resistance component. Brennodden *et al.* (1989) further suggested an energy-based pipe-soil interaction model, in which the soil passive resistance component is related to the work done by a pipe during its movement on the soil. In brief, the aforementioned studies indicated that the conventional design method based on Coulomb friction theory was too conservative compared to the experimental results. However, the SCR pipeline on the seabed is an issue of the interaction between a riser pipe, seabed soil and marine environment, as described in Figure 3.6—16.

Table 3.6—4 Typical lateral soil resistance friction coefficients (DNV, 2007)

Soil Type	Minimum	Maximum
Sand	0.6	1.0
Clay	0.2	1.0

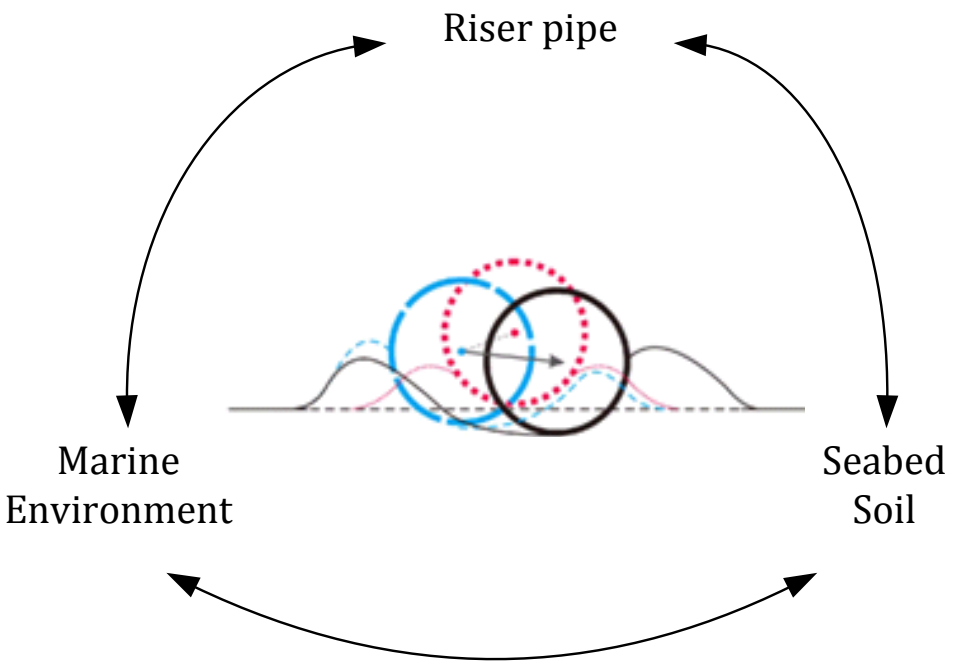

Figure 3.6—16 Tripartite interaction between the riser pipe, seabed and marine environment

A series of pipe-soil interaction tests that used a half pipe section mounted onto a rigid frame allowing either motion or force to be applied laterally and vertically were performed by Wagner *et al.* (1987). The pipe was embedded into virgin clay soil that was contained within a large test tank, see Figure 3.6—17.

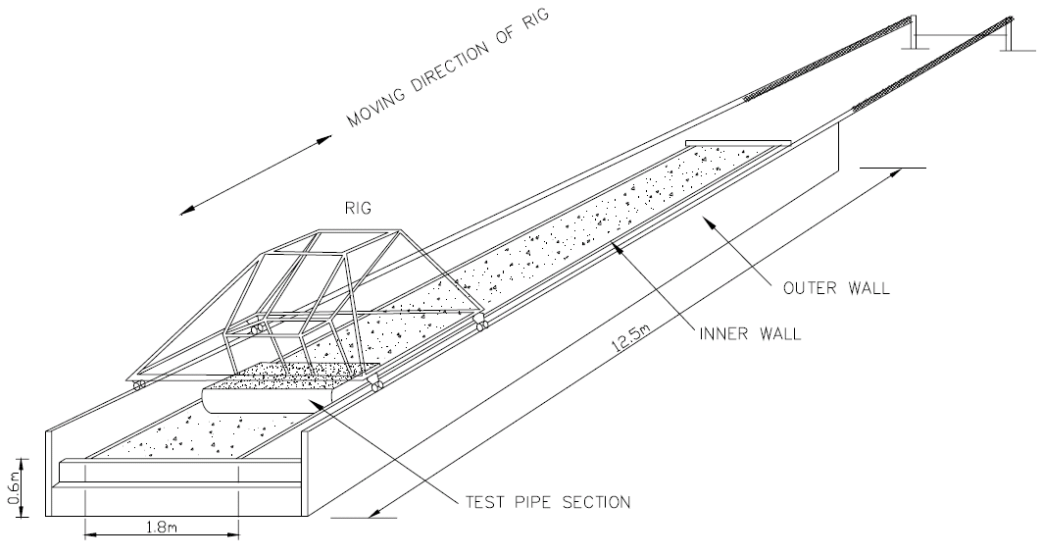

Figure 3.6—17 Typical test facility for pipe-soil interaction (Wagner *et al.*, 1987)

An empirical formula was developed for modelling the soil resistance to lateral pipe movement based on the pipe soil interaction model and energy-based pipe–soil interaction model proposed by Wagner *et al.* (1987) and Brennodden *et al.* (1989) respectively. In both models, the total lateral resistance, F_y, consists of two resistance forces, one is the sliding resistance component, F_F, due to friction and the second is the soil passive resistance component, F_R, due to soil cohesion, i.e.,

$$F_y = F_F + F_R$$

Equation 3.6—17

where

$$F_F = \mu(W_s - F_L)$$
$$W_s = \rho_s \frac{\pi}{4}\left(D_o^2 - D_i^2\right)g - \rho_w \frac{\pi}{4} D_o^2 g$$

Equation 3.6—18

Where μ is the sliding resistance coefficient and is set at 0.2 for clay regardless of clay shear strength, W_s is the submerged pipe weight per unit length; ρ_s and ρ_w are densities of steel pipe and seawater respectively; D_o and D_i are the outer and inner diameter of the pipe respectively; g is the acceleration due to gravity; and F_L is the hydrodynamic lift force upon the pipe.

The difference between the two models (i.e., Brennodden *et al.* (1989) and Wagner *et al.* (1987)) is the methodology of estimating the passive soil resistance component. The passive resistance component was indicated by Wagner *et al.* (1987), was used by Morris (1988), and the empirical formula is expressed as follows:

$$F_R = \beta S_u A / D$$

Equation 3.6—19

where β is an empirical passive resistance coefficient, it is a function of the pipe displacement and the lateral loading history; A is one half the embedded area of the pipe or the characteristic area (i.e., one half the contact area between the

pipeline and soil); and D is the pipe diameter. The methodology and approach used in this thesis to model the lateral seabed resistance, which is based on the empirical formulas derived from previous experiments, are presented in Chapter 4. In addition, different formulations for passive soil resistance are presented in Chapter 4.

3.6.7 SCR/Seabed Axial Interaction

The axial soil resistance for SCR movement is typically modelled using the Coulomb friction model, which is adopted to evaluate the axial resistance of a partially embedded riser pipe, and is expressed as Cathie (2005), Oliphant and Maconochie (2007):

$$F_x = \mu_A W_s$$

Equation 3.6—20

where F_x is the axial soil resistance and μ_A is the coefficient of axial coil friction. The typical values for axial friction have been reported to vary between 0.2 and 0.5 for clay soil (DNV, 2007).

3.6.8 Overall SCR–Seabed Interaction Technique – A Summary of Models Used

A number of scientific papers have been published on the study of soil–riser interaction. Table 3.6—5 details the level of complexity used in the analysis of SCR–seabed interaction response in a representative set of studies published in the last twenty-five years, with six areas previously highlighted as conventionally conservative and broken into components of increasing degree of sophistication and accuracy. This table presents the considerable diversity in the level of complexity used in the SCR–seabed interaction analyses. All components in Table 3.6—5 have been assessed for appropriate modelling of the physical SCR–seabed interaction process and graded with a three categories system: α represents state-of-the-art practice, β a compromise solution (adequate under some circumstances) and γ an inadequate method (which usually produces an overly conservative response).

General comments:

SCR–Seabed Interaction Models: The majority of experimental studies carried out in recent years have presented the non-linear behaviour of SCR–seabed interaction and trenching effects in the TDZ. An SCR in the TDZ was recently identified as a fatigue hotspot that substantially increased fatigue damage under the SCR–seabed interaction phenomenon. Better understanding of the significance of SCR–seabed interaction behaviour and soil properties improves

the fatigue life prediction in the TDZ. Most of the existing riser models unrealistically simplified SCR–seabed interaction behaviour by assuming a rigid or linearly elastic seabed. Trench formation and trench deepening have also significant influence on SCR–seabed response.

Pipe–seabed Interaction Models: Experimental model tests and analytical models of vertically loaded horizontal pipes in clay sediment provided valuable information for better awareness of SCR–seabed interaction in the TDZ. These experimental and analytical data produce the general load/deflection curve for pipe–seabed interaction and necessary information for validation of *V-z* model and determination of geotechnical parameters used in the model. Randolph and Quiggin (2009) introduced a mathematical model of the reaction force normal to the seabed, experienced by a pipeline or catenary riser in contact with the seabed. The model uses data such as the pipe diameter, the seabed soil shear strength profile with depth and the soil density. There are four different penetration modes in this seabed model, namely Not-in-Contact, Initial Penetration, Uplift and Re-penetration modes, as discussed later in Chapter 4. Different *V-z* functions are used for the initial penetration, for uplift and for re-penetration. In addition, the function parameters are updated each time a penetration reversal occurs. This enables the model to capture the hysteretic behaviour of the seabed soil response and the increasing penetration of the pipe under cyclic loading in the vertical plane. The model was validated against laboratory and field-scale experiments with reasonable accuracy shown. This

model has been implemented in OrcaFlex software, which is widely used for riser response analysis. This model is particularly suitable, as it models the vertical pipe–soil interaction on soft clay according to the dynamic aspects more accurately than a linear seabed model.

Different approaches can be considered for determining the lateral soil resistance of partially embedded pipelines. The Coulomb friction approach and the two-component soil resistance models approach for the assessment of SCR's global response are presented in Chapter 4.

Cyclic Loading: SCR–seabed interaction processes should cover vertical and lateral responses to cyclic loading. Movement and oscillation of the SCR in the TDZ will cause trenching and dynamic embedment of the SCR into the seabed. Seabed stiffness degradation due to cyclic oscillations has a significant influence on the behaviour of an SCR in the TDZ, and especially on the SCR's strength and fatigue performance. After the seabed soil approaches the maximum strength throughout the applied cyclic loading, the seabed soil tends to lose strength and stiffness with the increase in plastic embedment during cyclic oscillations. The seabed soil stiffness degradation mechanism comprises stiffness reduction presented in uplift, suction, and separation as well as the re-penetration process. The degradation of soil stiffness with cyclic loading is best captured by the non-linear seabed model.

Wave loading: The use of regular wave theories does not adequately represent wave loading on SCRs. However, when used, the level of sophistication in

random wave loading is highly variable. For example, the length of simulation used to estimate response levels differs widely. Most studies use simplifying assumptions due to the extensive computational time needed to perform random time domain simulation properly.

Analysis (Coupled vs. Uncoupled): SCRs have a relative effect on the motions of a floating unit, which in turn affects the SCR fatigue life. In a coupled analysis, the floating unit and SCR are modelled together including their mass, stiffness and damping. Coupled analysis is computationally demanding, especially for robust finite element mesh size. In uncoupled analysis, platform wave frequency is computed in separate models by different programs. Once the floating unit motions are obtained, either from coupled or uncoupled analysis, they are imported as input into the riser analysis software for the uncoupled riser analysis. In uncoupled analysis, the riser is considered to have no effect on the platform at its top. These effects are usually negligible, and an uncoupled analysis is adequate.

Fatigue Analysis & Reliability-Based Fatigue: SCR's Fatigue life in the TDZ is affected by SCR–seabed interaction. Accurate estimation of the fatigue life and riser response is a function of the applied seabed interaction modelling, cyclic dynamic loading and wave model. Therefore, realistic predictions of the SCR's fatigue life require an accurate characterisation model of seabed stiffness as well as a realistic description of the load/deflection curve.

Table 3.6—5 Level of complexity used in SCR-seabed interaction technique

Author	Year	SCR-Seabed Interaction Models				Pipe-Seabed Interaction Models				Cyclic Loading		Wave Loading		Analysis		Fatigue Analysis	Reliability-based Fatigue
		Model tests	Analytical Models	Deg. of Complexity		Model tests	Analytical Models	Deg. of Complexity		α		α	β	α	β		
										Vertical	Lateral	Irregular	Regular	Coupled	Uncoupled		
				γ	Rigid Seabed			γ	Rigid Seabed								
				β	Linear Seabed			β	Linear Seabed								
				α	Non-linear Seabed			α	Non-linear Seabed								
				α	Trenching effects			α	Trenching effects								
(Sharma and Aubeny, 2011)	2011		√	√						√		√			√	√	
(Cao, 2010)	2010			√										√	√	√	
(Cardoso and silveira, 2010)	2010					√					√				√		
(Hodder, 2010a)	2010					√				√					√		
(Jin *et al*, 2010)	2010					√					√				√		
(Kimiaei *et al.*, 2010)	2010				√								√		√		
(Nakhaee, 2008, Nakhaee and Zhang, 2010)	2008& 2010									√			√		√		
(Aubeny *et al.*, 2006a, Aubeny and Biscontin, 2009)	2006& 2009									√					√		
(Randolph and Quiggin, 2009)	2009									√		√			√	√	
(Oliphant, 2009)	2009					√					√				√		
(Bruton *et al.*, 2006, Bruton, 2008)	2006& 2008					√					√				√		
(Clukey *et al.*, 2008)	2008					√				√					√		
(Palmer, 2008)	2008				√										√		
(Sen, 2006, Sen, 2008)	2008			√										√		√	√
(Xia, 2008a)	2008			√								√		√		√	√

Author	Year	SCR-Seabed Interaction Models							Pipe-Seabed Interaction Models							Cyclic Loading		Wave Loading		Analysis		Fatigue Analysis	Reliability-based Fatigue
		Model tests	Analytical Models	Deg. of Complexity					Model tests	Analytical Models	Deg. of Complexity					Vertical	Lateral	Regular	Irregular	Uncoupled	Coupled		
				γ	β	α	α	Trenching effects			γ	β	α	α	Trenching effects	α	α	β	α	β	α		
				Rigid Seabed	Linear Seabed	Non-linear Seabed					Rigid Seabed	Linear Seabed	Non-linear Seabed											
(Akpan *et al.*, 2007)	2007		√																		√	√	√
(Karunakaran *et al.*, 2005b)	2005				√														√		√	√	√
(Bridge *et al.*, 2004)	2004								√			√	√		√	√				√			
(Giertsen, 2004)	2004								√							√						√	
(Bridge, 2003)	2003	√														√					√		
(Langner, 2003)	2003		√																√		√	√	√
(Bridge and Willis, 2002)	2002	√														√					√	√	√
(Thethi, 2001)	2001	√														√					√	√	√
(Willis, 2001)	2001	√														√					√	√	√
(Pesce, 1998)	1998				√															√			
(Verley and Lund, 1995)	1995								√								√			√			
(Hale, 1992)	1992								√							√	√			√			
(Dunlap *et al.*, 1990)	1990								√							√							
(Brennodden *et al.*, 1989)	1989								√								√			√			
(Morris, 1988)	1988								√								√			√			
(Wagner *et al.*, 1987)	1987								√								√			√			

3.7 Research Gap

The SCR is proving to commonly be the system of choice to transmit the hydrocarbon products from the seabed to the FP in deepwater. An SCR connecting to an oscillating floating structure at its upper end experiences oscillations in and near its TDZ that are constrained by and interact with the seabed soil. The literature review introduced in this chapter reveals that the SCR motion at the TDP is predominantly lateral, vertical and cyclic in nature. SCRs are the subject of much ongoing research, particularly with respect to fatigue and interaction with the seabed at the TDP.

The current SCR's analysis is performed using simplified pipe–seabed interaction models and disregards the SCR's embedment into the seabed as well as soil suction effects in the TDZ; this will affect the predicted SCR response. Previous experiments showed that the soil suction effect can increase the bending stress of SCRs in the TDZ. The predominant offshore soil condition in a deepwater environment is soft clay soil with small undrained shear strength. Field observations have introduced that the trench is a common feature due to the SCR pipe penetration into the seabed. However, there are few published literatures that investigate the trenching effects of the riser pipe in the TDZ on the SCR's dynamic structural behaviour and fatigue performance.

Seabed stiffness degradation due to cyclic motion is an important parameter in order to estimate the SCR fatigue in the TDZ. This aspect is not well investigated

and the seabed is traditionally not properly modelled in the current SCR fatigue analysis. Existing literature has introduced that fatigue damage is highly sensitive to the soil model utilised in the fatigue estimation calculation. The seabed non-linear model, to simulate the SCR–seabed interaction, has been shown to be more sophisticated compared to those SCR–seabed interactions with linear soil springs.

It can be concluded from the summary of models presented in the existing literature survey that:

a. Although the linear seabed model is commonly used for seabed response modelling of SCRs, (Xia, 2008a, Grealish *et al.*, 2007, Karunakaran *et al.*, 2005a), it is too simplified to capture the nature of the highly non-linear physical behaviour involved. For better understanding of SCR behaviour and reliable prediction of the fatigue life in the TDZ, a numerical study and analysis of SCRs with vessel motions should be performed;
b. Fatigue performance assessment of the SCR in the TDZ remains a serious design challenge for SCR behaviour. Despite some research papers presenting a reduction in fatigue damage (Sharma and Aubeny, 2011, Langner, 2003, Nakhaee, 2008) due to riser embedment in the TDZ, other studies have proposed an increase in fatigue damage (Giertsen, 2004, Leira *et al.*, 2004). These confounding results due to different geotechnical parameters have been imposed with synthesis trenches. The trench deepening, gradual embedment of the riser and soil stiffness

have an important influence on the SCR's fatigue life in the TDZ. Furthermore, the soil parameters used in riser–seabed analysis can have a significant effect on fatigue life of SCRs. Therefore, SCR's fatigue damage in the TDZ is a critical design aspect where geotechnical consideration becomes important;

c. Although lateral movements of the SCR can influence the riser performance, as suggested by Giertsen (2004) and Aubeny and Biscontin, (2009), the adduced SCR–seabed interaction analytical models regard only the vertical SCR motions and neglect lateral soil friction, as presented by Nakhaee (2008) and Nakhaee and Zhang (2010); and

d. It is shown that while many studies regard the SCR's fatigue performance, there are few which regard the probability of failure associated with the current design practices of fatigue analysis of SCRs. Among these studies, Akpan *et al.* (2007), Sen (2008), Xia *et al*. (2008 b) studied the uncertainties associated with fatigue performance of SCRs. However, seabed modelling is ignored in studies by both Akpan *et al*. and Sen *et al*., but Xia *et al*. have utilised a linear seabed model. In terms of fatigue, SCRs are very sensitive to seabed modelling. Reliability-based fatigue behaviour provides a means to quantify the reliability of SCRs in the TDZ and to develop further understanding of the response behaviour of SCR-seabed interaction.

3.8 Overview of OrcaFlex – The Analysis Program Used in Thesis

An overview of the components of the dynamic structural analysis program used in this thesis is described in Appendix B. Named OrcaFlex, it is capable of considering the major non-linearities in marine riser response. OrcaFlex is the world's leading package for the dynamic analysis of offshore marine systems. In addition, validation of OrcaFlex software against API Bulletin 16J is given in Appendix B. However, there are several software packages that are currently available for the analysis and design of risers; the most widely used are presented in section 3.6.4.

3.9 Concluding Remarks

After reviewing the different parts of literature relevant to this study, some of the required knowledge to be used in this research is acquired and some other existing gaps in the field are identified. This chapter has presented a review of the state-of-the-art SCRs with seabed interaction as well as SCR analysis techniques, including the SCR global modelling and analysis and seabed response models. It has also discussed the existing theories for modelling SCR–seabed interaction with detailed explanation of currently used methods for evaluating the SCR structural performance in the TDZ. It then presented a brief overview of the riser dynamic (OrcaFlex) program used in this study and a

validation of this software against API Bulletin 16J. Finally, the chapter concluded by identifying the research gap.

The next chapter will be outlining the approach adopted for this research.

3.10 References

Akpan, U., Koko, T., Rushton, P., Tavassoli, A. & Else, M. Probabilistic fatigue reliability of large diameter steel catenary risers (SCR) for ultra-deepwater operations. *In:* Proceedings of the 26th International Conference on Offshore Mechanics and Arctic Engineering, 2007 California, USA. ASME.

API, 1998. API RP 2RD: Design of risers for floating production systems (FPSs) and tension-leg platforms (TLPs). American petroleum institute

API, 2004. 5l, specification for line pipe. *Edition March*.

API, 1999. 1111 design, construction, operation, and maintenance of offshore hydrocarbon pipelines (limit state design). *Design, Construction, Operation, and Maintenance of Offshore Hydrocarbon Pipelines (Limit State Design), of 3rd Ed*.

Ariduru, S. 2004. *Fatigue life calculation by rainflow cycle counting method.* Master of Science, The Graduate School of Natural and Applied Sciences of Middle East Technical University.

Aubeny, C., Gaudin, C. & Randolph, M. 2008. Cyclic tests of model pipe in kaolin. *SPE Projects, Facilities & Construction,* 3**,** 1-6.

Aubeny, C., Shi, H. & Murff, J. 2005. Collapse loads for cylinder embedded in trench in cohesive soil. *International Journal of Geomechanics,* Vol. 5, No. 4.

Aubeny, C. P., Biscontin, G. a. & Zhang, J. 2006. Seafloor interaction with steel catenary risers. Texas: Offshore Research Centre, Texas A&M University, College Station, Houston, Final Project Report to Minerals Management Service,Offshore Technology Research Centre Industry Consortium, OTRC Library Number 9/06A173

Aubeny, C. P. a. & Biscontin, G. 2009. Seafloor-riser interaction model. *International Journal of Geomechanics,* Vol. 9, No. 3.

Bai, Y. 2001. *Pipelines and risers*, Elsevier Science.

Bai, Y. & Bai, Q. 2005. *Subsea pipelines and risers*, Elsevier Science Ltd.

Bai, Y. & Bai, Q. 2010. *Subsea engineering handbook*, Gulf Professional Publishing.

Barltrop, N. D. P. & Adams, A. J. 1991. *Dynamics of fixed marine structures*, Butterworth-Heinemann Oxford.

Bayirli, S. 2009. Corridor survey of both existing and new to be built pipelines on land using lidar scanning. *4th Pipeline Technology conference.* Hannover, Germany

Borgen, J. E. 2002. Large diameter steel riser for semi submersible floater in harsh environment. *Deep Offshore Technology.* New Orleans, USA.

Borgen, M. J., Fosterud, M. E. & Larsen, M. T. L-riser: Steel dynamic riser for severe vessel motions. *In*: Offshore Technology Conference 2003, Houston, Texas.

Brennodden, H., Lieng, J., Sotberg, T. & Verley, R. 1989. An energy-based pipe-soil interaction model. *Offshore Technology Conference.* Houston, Texas, USA.

Bridge, C., Howells, H., Toy, N., Parke, G. and Woods,R. Full scale model tests of a steel catenary riser. *In:* Proceding of International Conference on fluid Structure Interaction, 2003 Cadiz, Spain.

Bridge, C., Laver, K. & Clukey, E. Steel catenary riser touchdown point vertical interaction models. *In:* Offshore Technology Conference, OTC 16628, 2004 Houston, Texas.

Bridge, C. & Willis, N. Steel catenary risers–results and conclusions from large scale simulations of seabed interactions. *In:* International Conference on Deep Offshore Technology, 2002 New Orleans, USA. PennWell.

Bridge, C. D. a. H., H.A. Observations and modeling of steel catenary riser trenches. *In:* International Society of Offshore and Polar Engineers (ISOPE) 2007 Lisbon.

Bruton, D., White, D., Cheuk, C., Bolton, M. & Carr, M. Pipe/soil interaction behavior during lateral buckling, including large-amplitude cyclic displacement tests by the safebuck JIP. *In:* Offshore Technology Conference, 2006 Houston, USA.

Bruton, D. A. S., White, D. J., Carr, M., and Cheuk, J. C. Y. Pipe-soil interaction during lateral buckling and pipeline walking - the safebuck JIP. *In:* Offshore Technology Conference, OTC 19589, 5-8 May 2008 Houston, Texas.

Burke, B. An analysis of marine risers for deep water. *In*: Offshore Technology Conference, 1973, Houston, Texas.

Cao, J. Fatigue analysis technique of deepwater steel catenary risers. *In:* 29th International Conference on Ocean, Offshore and Arctic Engineering, OMAE 2010, 6-11June 2010 Shanghai, China. ASME.

Cardoso, C. & silveira. Pipe-soil interaction behavior for pipelines under large displacements on clay soils-a model for lateral residual friction factor. *In*, Offshore Technology Conference, OTC 20767, 2010 Houston, Texas.

Campbell, M. The complexities of fatigue analysis for deepwater risers. *In:* Deepwater Pipeline Conference, March 1999 New Orleans, USA.

Cathie, D., Jaeck, C., Wintgens, J-F and Ballard, J-c 2005. Pipeline geotechnics - state of the art. *Proc. International Symposium on Frontiers in Offshore Geotechnics (ISFOG).* Perth, Australia.

Chakrabarti, S. K. 1987. Hydrodynamics of offshore structures: Mathematical theory and its applications in structures.

Chakrabarti, S. K. 2005. *Handbook of offshore engineering*, Elsevier.

Chakrabarti, S. K. & Frampton, R. E. 1982. Review of riser analysis techniques. *Applied Ocean Research,* 4**,** 73-90.

Chang, S. H. M., Stanton, P., Kuriakose, S. & Thompson, H. Sleeved stress joint for steel catenary riser application. *In:* 29th International Conference on Ocean, Offshore and Arctic Engineering, 2010. ASME.

Chatjigeorgiou, I. K. 2008. A finite differences formulation for the linear and nonlinear dynamics of 2D catenary risers. *Ocean Engineering,* 35**,** 616-636.

Chen, W. F. & Han, D. J. 1985. *Tubular members in offshore structures*, Pitman Publishing Inc.

Cheuk, C. & Bolton, M. A technique for modelling the lateral stability of on-bottom pipelines in a small drum centrifuge. *In*: Physical Modelling in Geotechnics - 6th ICPMG, 2006 London.

Clukey, E., Ghosh, R., Mokarala, P., and Dixon, M. 2007. Steel catenary riser (SCR) design issues at touch down area. *Proceedings of the 17th (2007) International Offshore and Polar Engineering Conference*.

Clukey, E., Young, A., Dobias, J. & Garmon, S. Soil response and stiffness laboratory measurements of SCR pipe/soil interaction. *In*: Offshore Technology Conference, 2008 Houston, USA.

Dantas, C. M. S., de Siqueira, M. Q., Torres, A. L. F. L., Ellwanger, G. B. & Mourelle, M. M. A frequency domain approach for the random fatigue analysis of SCR considering bimodal/bidirectional characteristic of campos basin sea states. *In*, 2005. ASME.

DNV 2001-amended 2009. DNV-OS-F201: Dynamic risers. Det Norske Veritas.

DNV 2005. Riser fatigue. *Recommended Practice DNV-RP-F204.* Det Norske Veritas.

DNV 2007. DNV-RP-F113: Recommended practice pipeline subsea repair. Det Norske Veritas

DNV 2009. Dnv-rp-f109: Recommended practice on-bottom stability design of submarine pipelines (with amendments, april 2009).

DNV 2011. Offshore riser systems. *Offshore Service Specification DNV-OSS-302.* Det Norske Veritas.

DNV January 2001. Dynamic risers. *DNV-OS-F201 amended in October 2009.* Det Norske Veritas.

Dunlap, W. A., Bhojanala, R. P. a. & Morris, D. V. Burial of vertically loaded offshore pipelines in weak sediments. *In:* Offshore Technology Conference, 7th-10th March 1990 Houston, Texas.

Egeland, O., Wiik, T. & Natvig, B. 1982. Dynamic analysis of marine risers. *Offshore South East Asia Show,* Singapore.

Giertsen, E., Verley, R. and Schroder, K. 2004. Carisima: A catenary riser/soil interaction model for global riser analysis. *23rd International Conference on Offshore Mechanics and Arctic Engineering, OMAE2004-51345*, Vancouver, British Columbia, Canada.

Grealish, F., Kavanagh, K., Connaire, A. & Batty, P. Advanced nonlinear analysis methodologies for SCRs. *In:* Offshore Technology Conference, OTC 18922, 30Aril-3May, 2007 Houston, Texas.

Hale, J. R., Morris, D. V., Yen, T. S., and Dunlap, W. A. Modelling pipeline behaviour on clay soils during storms. *In:* Offshore Technology Conference, OTC 7019, May 4-7 1992 Houston, Texas.

Hatton, S. 1999. Update on the design of steel catenary riser systems. *Society of Underwater Technology,* Newcastle, UK.

Hetényi, M. & Michigan, U. o. 1946. *Beams on elastic foundation*, The Univ. of Michigan Press.

Hodder, M. S., and Byrne, B. W. 2010a. 3D experiments investigating the interaction of a model SCR with the seabed. *Applied Ocean Research*.

Hodder, M. S., and Cassidy, M. J. 2010b. A plasticity model for predicting the vertical and lateral behaviour of pipelines in clay soils. *Geotechnique 60, No. 4***,** 247-263.

Howells, H. 1995. Advances in steel catenary riser design. *DEEPTEC.* Aberdeen.

Howells, H. & Bowman, J. 1997. Drilling riser/well system interaction in deep water, harsh environments. *Advances in Subsea Technology*, 997.

Jin, J., Audibert, J. M. & Kan, W. C. 2010. Practical design process for flowlines with lateral buckling. *In*: Proceedings of the ASME 29th International Conference on Ocean, Offshore and Arctic Engineering, OMAE2010-20478, 2010 Shanghai, China. ASME.

Jones, G. 1997. *Analysis of beams on elastic foundations: Using finite difference theory*, Inst of Civil Engineers Pub.

Karunakaran, D., Lund, K. M. & Nordsve, N. T. 1999. Steel catenary riser configurations for north sea field developments. *Offshore Technology Conference.* Houston, Texas.

Karunakaran, D., Meling, T., Kristoffersen, S. & Lund, K. Weight-optimized SCRs for deepwater harsh environments. *In:* Offshore Technology Conference, 2-5 May 2005 Houston, TX, USA.

Kavanagh, W., Lou, J. & Hays, P. Design of steel risers in ultra deep water-the influence of recent code requirements on wall thickness design for 10,000 ft water depth. *In*: Offshore Technology conference, OTC 15101, 2003 Houston, Texas.

Kenny, J. P. 2007. Deepwater riser design, fatigue life and standards study report. Houston, USA.

Kimiaei, M., Randolph, M. & Ting, I. A parametric study on effects of environmental loadings on fatigue life of steel catenary risers (using a nonlinear cyclic riser-soil interaction model). *In:* Proceedings of the ASME 2010 29th International Conference on Ocean, Offshore and Arctic Engineering, 2010 Shanghai, China. ASME.

Kirk, C., Etok, E. & Cooper, M. 1979. Dynamic and static analysis of a marine riser. *Applied Ocean Research,* 1**,** 125-135.

Langford, T. & Aubeny, C. Model tests for steel catenary riser in marine clay. *In:* Offshore Technology Conference, 2008 Houston, USA.

Langner, C. G. 2003. Fatigue life improvment of steel catenary risers due to self-trenching at the touchdown point. *Offchore Technology Confernce.* Houston, Texas, USA.

Leibniz, G. W. 1691a. *The string whose curvature is described by bending under its own weight and the remarkable resources that can be discovered from it by however many proportional means and logarithms. Acta eruditorum,*

leipzig. Translated by pierre beaudry [Online]. Acta Eruditorum, Leipzig. Translated by Pierre Beadudry. Available: WWW.schillerinstitute.org [Accessed].

Leibniz, G. W. 1691b. *Solutions to the problem of the catenary, or funicular curve, proposed by m. Jacques bernoulli in the acta of june 1691. Acta eruditorum, leipzig. Translated by pierre beaudry* [Online]. Acta Eruditorum, Leipzig. Translated by Pierre Beaudry. Available: WWW.schillerinstitute.org. [Accessed].

Leira, B. J., Passano, E., Karunakaran, D., Farnes, K. A. & Giertsen, E. Analysis guidelines and application of a riser-soil interaction model including trench effects. *In:* 23rd International Conference on Offshore Mechanics and Arctic Engineering, OMAE2004-51527, 2004 Vancouver, British Columbia, Canada. ASME.

Lim, F. & Howells, H. Deepwater riser VIV, fatigue and monitoring. *In:* Deepwater Pipeline & Riser Technology Conference, 2000 Houston.

Ljuština, A. M., Parunov, J. & Senjanović, I. Static and dynamic analysis of marine riser. *In*: Proceedings of the 16th Symposium "Theory and Practice of Shipbuilding"Zagreb, 2004.

Luk, C. & Chang, S. H. M. Elastic-plastic pull-in strength and damage analyses of steel catenary risers in deepwater. *In*: ASME Conference Proceedings 2011 2011. ASME.

Lyons, C. Soil resistance to lateral sliding of marine pipelines. *In:* Offshore Technology Conference, 1973 Texas, USA.

Mekha, B. B. 2001. New frontiers in the design of steel catenary risers for floating production systems. *Journal of Offshore Mechanics and Arctic Engineering,* 123**,** 153.

Morris, D. V., Webb, R. E., and Dunlap, W. A. 1988. Self-burial of laterally loaded offshore pipelines in weak sediments. *Offshore Technology Conference, OTC 5855.* Huston, Texas.

Nakhaee, A., and Zhang, J. 2008. Effects of the interaction with the seafloor on the fatigue life of a SCR. *Proceedings of the 18th (2008) International Offshore and Polar Engineering Conference*.

Nakhaee, A., and Zhang, J. 2009. Trenching effects on dynamic behaviour of a steel catenary riser. *Ocean Engineering*.

Nakhaee, A. & Zhang, J. 2010. Trenching effects on dynamic behavior of a steel catenary riser. *Ocean Engineering,* 37**,** 277-288.

Natarajan, S., Nguyen, C. & Walters, D. Advances in deepwater top tensioned riser design consideration. *In*: International Society of Offshore and Polar Engineers 2008, P. O. Box 189, Cupertino, CA, 95015-0189, USA.

Oliphant, J. & Maconochie, A. 2007. The axial resistance of buried an unburied pipelines. *OFFSHORE SITE INVESTIGATION AND GEOTECHNICS, Confronting New Challenges and Sharing Knowledge*.

Oliphant, J., Maconochie, A., White, D. and Bolton, M. 2009. Trench interaction forces during lateral SCR movement in deepwater clays *Offshore Technology conference.* Houston, Texas, USA.

Orcina 2010. Orcaflex user manual *Orcina,* version 9.4a, UK.

Palmer, A. 2008. Touchdown indentation of the seabed. *Applied Ocean Research***,** 235-238.

Pasqualino, I. P., Valeriano, I. A. & Alves, T. M. J. Crack growth prediction in girth welds of steel catenary risers. *In*: Proceedings of The 12th International Offshore and Polar Engineering Conference, 2002. 192-197.

Patel, M. & Seyed, F. 1995. Review of flexible riser modelling and analysis techniques. *Engineering structures,* 17**,** 293-304.

Pesce, C. P., Aranha, J. A. P. and Martins, C. A. 1998. The soil rigidity effect in the touchdown boundary-layer of a catenary riser: Static problem. *Proceedings of the 8th International Offshore and Polar Engineering Conference.* Monterial, Canada.

Randolph, M., and Quiggin, P. 2009. Non-linear hysteretic seabed model for catenary pipeline contact. *28th International Conference on Ocean, Offshore and Arctic Engineering, OMAE* Proceedings of the ASME 2009

Randolph, M. & Quiggin, P. 2009. Non-linear hysteretic seabed model for catenary pipeline contact. *28th International Conference on Ocean, Offshore and Arctic Engineering, OMAE*

Robert, C. & Malahy, J. 1996. Offpipe user's guide.

Rustad, A. M., Larsen, C. M. & Sørensen, A. J. 2008. Fem modelling and automatic control for collision prevention of top tensioned risers. *Marine Structures,* 21**,** 80-112.

Sagrilo, L., Siqueira, M., Ellwanger, G., Lima, E., Ferreira, M. & Mourelle, M. 2002. A coupled approach for dynamic analysis of calm systems. *Applied Ocean Research,* 24**,** 47-58.

Sánchez, H. A. S. & Salas, C. C. Riser stability under external pressure and axial compression observing geometrical imperfections. *In:* ASME 2005 24th International Conference on Offshore Mechanics and Arctic Engineering (OMAE2005) , 2005, Greece ASME.

Schotman, G. J. & Stork, F. G. 1987. Pipe-soil interaction: A model for laterally loaded pipelines in clay. *Offshore Technology conference.* Houston, Texas, USA.

Sen, T. K. 2006. Probability of fatigue failure in steel catenary riser in deep water. *Journal of Engineering Mechnics*.

Sen, T. K., and Hesar, M. Riser soil interaction in soft clay near the touchdown zone. *In:* Offshore Technology Confernce, 30 April-3 May 2007 Huston, Texas, USA. OTC.

Sen, T. K., Brown, K. and Root 5-8 May 2008. Fatigue in deep water steel catenary risers - a probabilistic approach for assessment of risk. *Offshore Technology Conference.* Houston, Texas, USA.

Sen, T. K., Brown, K. and Root 2008. Fatigue in deep water steel catenary risers - a probabilistic approach for assessment of risk. *Offshore Technology Conference.* Houston, Texas, USA.

Serta, O. B., Petrobras, S. A., Mourelle, M. M., Petrobras, S. A., Grealish F. W., Harbert, S. J. and Souza, L. F. A. Steel catenary riser for the marlim field

FPS P-XVIII. *In:* Offshore Technology Conference, 1996 Houston, Texas, 6-9 May.

Sharma, P. & Aubeny, C. Advances in pipe-soil interaction methodology and application for SCR fatigue design. *In:* Offshore Technology Conference, 2011 Houston, USA.

Shi, S., Mao, C., Yang, J. & Kurup, N. New design configuration of steel catenary risers with pull-tube for spars. In: ASME 2011 30th International Conference on Ocean, Offshore and Arctic Engineering, OMAE2011-50303, 2011, Netherlands, ASME.

Skempton, A. 1984. The bearing capacity of clays. *Selected Papers on Soil Mechanics*, 50.

Song, R. & Stanton, P. Deepwater tieback SCR: Unique design challenges and solutions. *In*: Offshore Technology Conference, 2007 Houston, Texas.

SPARKS, C. 2008. *Fundamentals of marine riser mechanics: Basic principles & simplified analysis*, PennWell.

Thethi, R., and Moros, T. Soil interaction effects on simple catenary riser response. *In:* Proceeding Conference on Deepwater Pipeline & Riser Technology, 2001 Houston, Texas.

Verley, R. & Lund, K. M. A soil resistance model for pipelines placed on clay soils. *In*, 1995. American Society of Mechanical Engineers, 225-225.

Wagner, D., Murff, J., Brennodden, H. & Sveggen, O. Pipe-soil interaction model. *In:* Offchore Technology Confernce, April 27-30 1987 Houston, Texas, USA. OTC.

White, D. J., and Cheuk, C. Y. 2008. Modelling the soil resistance on seabed pipelines during large cycles of lateral movement. *Marine Structures,* 21, 59-79.

Willis, N. R. T., and West, P. T. J. Interaction between deepwater catenary risers and a soft seabed: Large scale sea trials. *In:* Offshore Technology Conference, 2001 Houston, Texas OTC 13113.

Xia, J., Das, P. K. and Karunakaran, D. 2008. A parametric design study for a semi/SCR system in northern north sea. *Ocean Engineering*, Ocean Engineering35(2008)1686–1699.

Xia, J. a. D., P. K. 2008b. Probabilistic fatigue reliability analysis of deepwater steel catenary risers. *Proceedings of the ASME 27th International Conference on Offshore Mechanics and Arctic Engineering.* Estoril, Portugal: OMAE.

You, J., Biscontin, G., and Aubeny, C. P. Seafloor interaction with steel catenary risers. *In:* International Offshore and Polar Engineering Conference, July 6-11 2008 Vancouver, BC, Canada. The International Society of Offshore and Polar Engineers (ISOPE).

CHAPTER 4

APPROACH ADOPTED FOR SCR–SEABED INTERACTION MODEL

4.1 Introductory Remarks

An SCR is a form of connection between the seabed and a floating facility. SCRs are subjected to cyclic motions from the floating facility and also from currents. The fatigue damage of the SCR in the TDZ, caused by cyclic interaction of the SCR with the seabed, is a critical design aspect where geotechnical considerations become significant. Therefore, the better clarification of the SCR–soil interaction process will provide a realistic technique for determining structural strength behaviour as well as reliable evaluation of fatigue performance in the TDZ. The fatigue issue is impelled by cumulative cycles of stress change during the lifetime of an SCR, largely due to fluctuations in the bending stress. In the TDZ, the maximum cyclic bending stress range presents in the region of maximum shear force, and sequentially the maximum shear force value is highly affected by the stiffness of the seabed (Randolph, 2008). Since fatigue concepts relate the fatigue damage to a high power of cyclic stress range, relatively small changes in cyclic stress amplitude can have a considerable effect on the evaluated fatigue life. Therefore, appropriate characterisation of seabed soil behaviour is significant in order to achieve a realistic estimation of fatigue behaviour.

The riser–seabed interaction problem engages a number of complex non-linear processes, including non-linear soil stiffness, soil suction, riser uplift and riser trenching effects. Such interaction is currently often modelled using simplified

seabed interaction models. Present SCR models that approach the seabed by means of rigid or linear elastic disregard the nature of trenching development process into seabeds and the awareness of non-linear interaction in the TDZ.

This chapter discusses the adopted modelling approach of the SCR–seabed interaction relating to the design of SCRs for deepwater development fields. Various design approaches pertaining to the lateral pipe–soil resistance model are discussed. The techniques that can be used to cover these aspects and to develop an advanced SCR–seabed lateral interaction model have been outlined. These techniques have been applied in the FE model, see Chapter 5, which can be used to analyse the lateral SCR–seabed interaction under hydrodynamic loading.

4.2 Problem Description of an SCR Pipe Embedment

A complex interaction between the SCR and seabed is experienced when the SCR is subjected to oscillatory motions. For SCRs, the most critical fatigue hotspot occurs in the TDZ. The SCR–seabed interaction is an essential key factor that should be considered in strength and fatigue assessment. How to precisely model this interaction response is still an issue and has been a hot field for academic research.

Current SCR–seabed interaction modelling approaches the seabed as a rigid or linear elastic model with friction coefficients appointed in the axial and lateral

directions relative to the axis of the SCR. The use of a rigid seabed model presents higher maximum fatigue damage of the SCR in the TDZ in comparison with a linear seabed, as will be shown later in Chapter 6. However, the linear seabed model does not simulate the actual behaviour of the seabed. Therefore, several studies have recently focused on load/deflection (V-z) curves for the response of SCR–seabed interaction, where V stands for the resistance force of soil and z stands for the vertical penetration of the SCR's pipe. Researchers determined the empirical equations for (V-z) curves from experiments.

SCR pipe penetration is defined as the depth of penetration of the pipe invert (bottom of pipe), relative to the undisturbed seabed as shown in Figure 4.2—1. Pipe penetration affects the riser pipe–seabed contact area, which subsequently affects the axial and passive soil resistance against the riser. Consequently, the passive soil resistance influences the lateral breakout force. Heave of seabed soil during embedment increases the local penetration of the SCR pipe by raising the soil surface level against the shoulders of the pipe. The typical geometry of heave produced during vertical embedment of an SCR pipe is such that the nominal penetration is approximately 50% less than the local embedment relative to undisturbed seabed surface (Bruton, 2008).

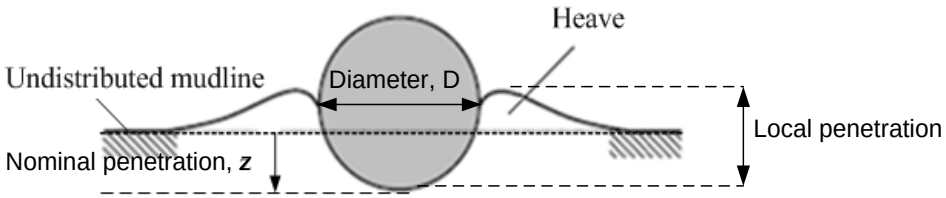

Figure 4.2—1 Initial penetration of an SCR pipe

SCR–seabed interaction should involve vertical and lateral responses to cyclic loading. Movement and oscillation of the SCR in the TDZ will cause trenching and dynamic embedment of the SCR into the seabed. A typical schematic illustration of the SCR–seabed interaction and trench formation in the TDZ are shown in Figure 4.2—2. Several researches have been directed towards understanding the SCR–seabed interaction (Aubeny and Biscontin, 2009, Aubeny, 2006, Willis, 2001, Bridge *et al.*, 2004, Bridge, 2007, Thethi, 2001).

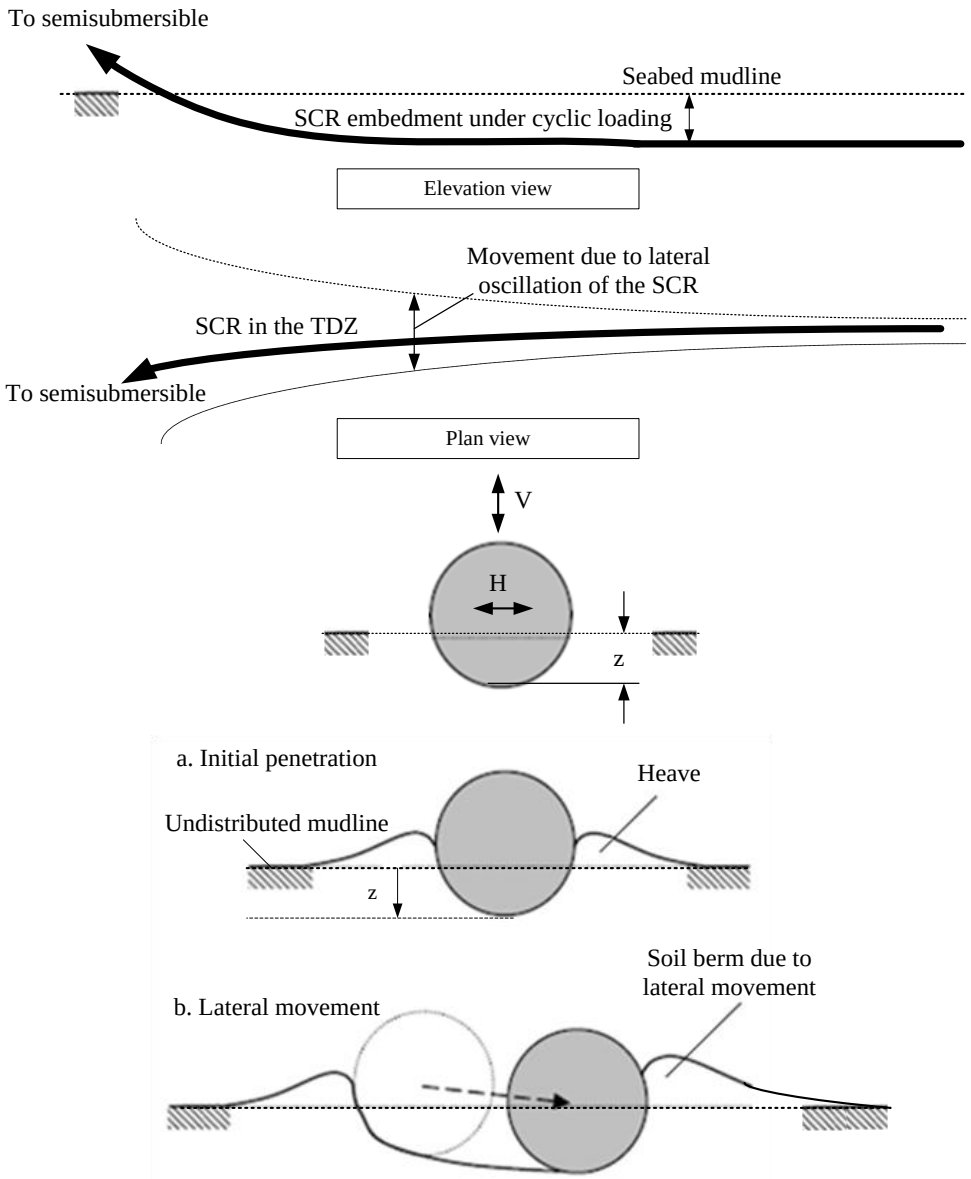

Figure 4.2—2 Schematic illustration of the SCR–seabed interaction in the TDZ

4.3 SCR–Seabed Vertical Interaction

As the SCR touches down, plastic deformation of the soil occurs until the penetration is sufficient to resist the penetrator, i.e., it continually occurs until

the bearing area is large enough to provide the necessary resistance. If the soil loading at the TDZ is greater than the SCR weight, the soil then experiences unloading as the SCR oscillations continue.

The entrenched flow-line endures loads as the riser is uplifted from the trench due to the weight of soil backfill on top of the entrenched riser, as well as suction and adhesion. Bridge *et al.* (2004) presented the non-linear force/deflection curve for an entrenched pipe experiencing suction. The suction force is a function of the SCR diameter, bearing width of the riser, riser penetration and the undrained shear strength of the soil.

The non-linear soil model is based on a hyperbolic secant stiffness formulation proposed by Bridge *et al.* (2004), Aubeny *et al.* (2006), and Randolph and Quiggin (2009). The non-linear seabed model is more sophisticated than the linear model, in that it models the non-linear hysteretic behaviour of the seabed in the vertical direction, including modelling of suction effects when the SCR rises up sufficiently. Different functions are used for the initial penetration, for uplift and for re-penetration, whilst the function parameters are updated each time a penetration reversal occurs. This enables the model to capture the hysteretic behaviour of the seabed soil response and the increasing penetration of the pipe under cyclic loading in the vertical plane.

4.3.1 Process of Pipe–Soil Vertical Interaction

The typical *V*-*z* curve patterns, see Figure 4.3—1, of pipe–soil interaction are produced by laboratory model experiments (Dunlap *et al.*, 1990) of vertically loaded horizontal pipes in weak sediment. These curves can be divided into four different paths. The pipe–soil interaction process is described in Table 4.3—1, and the depiction of the development of the interaction curve is given in Figure 4.3—1, associated with the uplift/re-penetration cycle.

If the riser pipe continues to experience oscillatory loading movement, the *V*-*z* interaction curve will repeat the loop enclosed by path 1-2-3-1 under the assumption of a non-degradation model.

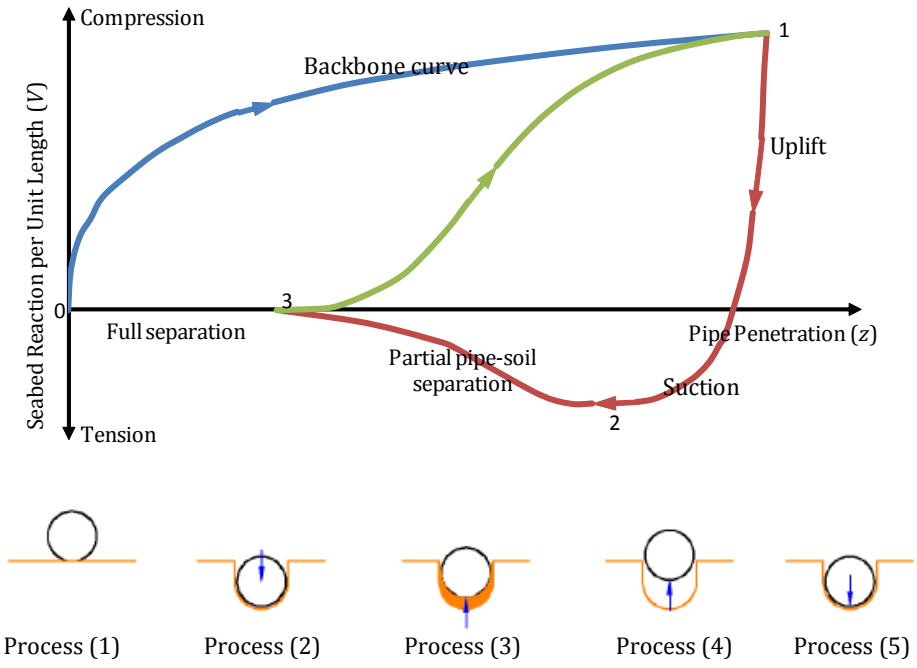

Figure 4.3—1 Depiction of typical V-z behaviour

Table 4.3—1 Illustration of pipe–soil interaction

Process No.	Location on P-y curve	Description
Process (1)	Point (0)	The pipe is initially laid on virgin soil and z=0.
Process (2)	Path 0-1	The pipe initially penetrates the seabed and follows along the backbone curve from point 0 to 1.
Process (3)	Path 1-2	The pipe moves upwards (uplift), and soil resistance is reduced quickly over a small displacement. After the soil resistance reaches zero, the soil suction loading increases to the peak rapidly.
Process (4)	Path 2-3	The pipe continues uplift, and the soil suction gradually tends towards zero, as indicated by model tests. The riser pipe starts to separate from the seabed at point 2, when an adequate large magnitude of uplift motion is reached. When a pipe is continued uplift, the riser pipe is completely separated from the seabed.
Process (5)	Path 3-1	The pipe again penetrates the seabed. The soil resistance follows along the curve from point 3 to 1 and rejoins the backbone curve. Previous data (Dunlap *et al.*, 1990, Bridge *et al.*, 2004) indicate that soil resistance does not mobilise abruptly upon pipe–seabed re-penetration; instead, soil resistance mobilises gradually, as described by the S-shaped Path 3-1.

4.3.2 Modelling of SCR–Seabed Interaction

Recent SCR–soil interaction models are too simplified to simulate the complex interaction between the seabed and riser pipe. Several studies investigate the mechanism of pipe–soil interaction by model experiments and give various equations. One famous experiment is STRIDE JIP's full-scale harbour experiment (Willis, 2001). This experiment experiences 3 months at a harbour in the west of England. Bridge developed advanced SCR–seabed interaction models using published data and pipe-soil interaction experiments conducted by the STRIDE and CARISIMA JIP (Bridge and Laver, 2004). The seabed reaction force can be divided into two phases: seabed resistance and seabed suction. This part indicates the related concepts of the non-linear vertical interaction model theory.

Randolph and Quiggin (2009) introduced a non-linear mathematical model for cyclic SCR–Seabed interaction in the TDZ, which is established on hyperbolic secant stiffness formulation, such as those indicated by Bridge *et al.* (2004) and Aubeny *et al.* (2006). The soil stiffness will vary along the TDZ within a non-linear soil model depending on the amplitude of cyclic displacement. The model uses data such as the pipe diameter, the seabed soil shear strength profile with depth and the soil density. As shown in Figure 4.3—2 there are four different penetration modes in this seabed model, namely Not in Contact, Initial Penetration, Uplift and Re-penetration modes. Different formulas are utilised for the initial penetration, for uplift and for re-penetration, and the function

parameters are updated each time a penetration reversal happens. Main features of this model are as follows:

- The backbone curve gives the relation between the ultimate compressive soil resistance per unit length and penetration depth for the first time. Typically, backbone curve formulation is based on collapse load computations (Aubeny *et al.*, 2005, Murff, 1989) for a horizontal cylinder, and bearing capacity theory (Bridge *et al.*, 2004, Aubeny, 2006), see Figure 4.3—3. The backbone curve is typically governed by Equation 4.3—1:

$$V_u(z) = N_c(z).S_u(z).D$$

Equation 4.3—1

where:

z is the penetration of a riser's pipe invert (i.e. bottom of the outer surface of the pipe);

$V_u(z)$ is the ultimate penetration resistance at penetration z. This is the highest soil reaction force per unit length of a riser pipe that the seabed soil can give;

$N_c(z)$ is the dimensionless bearing factor at penetration z;

$S_u(z)$ is the undrained soil shear strength at penetration z;

$S_u(z) = S_{u0} + S_{ug}.z$, S_{u0} is the soil shear strength at the mud-line and S_{ug} is the shear strength gradient with respect to z; and

D is the riser pipe outer diameter.

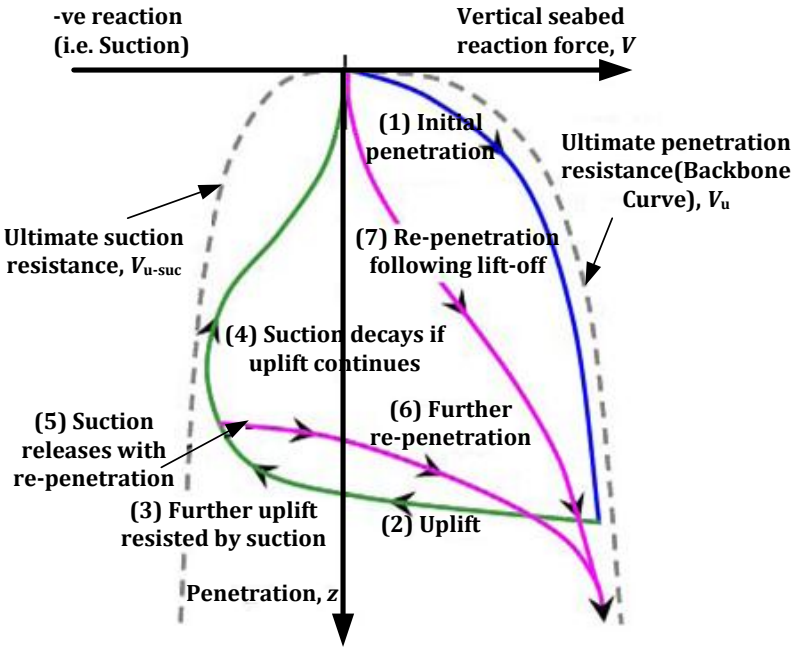

Figure 4.3—2 Soil model characteristics for different modes (Randolph 2009)

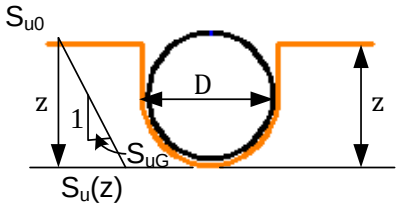

Figure 4.3—3 Characteristics of riser trench into seabed

A non-linear seabed model has been implemented in OrcaFlex (version 9.4b), as it models the dynamic behaviour of the vertical SCR–seabed interaction on soft clay more precisely than a linear seabed model. The bearing factor $N_c(z)$ is sensitive to soil trench geometry (Aubeny, 2006), involving riser pipe diameter, depth of embedment and trench width, and the roughness of soil-riser surface. The non-linear penetration resistance is established on an empirical power law expression for the nominal bearing factor that is based on finite element simulations data, $N_c(z) = V(z)/D.S_u$, with V being the vertical force per unit length at penetration z, expressed by Aubeny *et al.* (2005) as:

$$N_c(z) \approx a\left(\frac{z}{D}\right)^b$$

Equation 4.3—2

Fitted values of the power law expression, a and b, relied on the relative roughness of the pipe-soil boundary and the strength profile with depth η, $\eta = S_{ug}D/S_{u0}$. The pipe-soil roughness boundary was modelled by Merifield *et al.* (2009) and Aubeny *et al.* (2005) using an boundary roughness α, where the maximum shear stress at the pipe-soil boundary $\tau_{\max} = \alpha S_u$. The rough and smooth extreme boundaries have been modelled using α = 1 and α = 0 respectively. Values of the power law coefficient, a and b, in Equation 4.3—2,

which provide a reasonable fit to the numerical results throughout the range of $0 \le \eta \le \infty$, are shown in Table 4.3—2.

Table 4.3—2 Power law coefficients

Boundary	$z/D \le 0.5$	$z/D > 0.5$
Smooth	a = 4.97, b = 0.23	a = 4.88, b =0.21
Rough	a = 6.73, b = 0.29	a = 6.15, b = 0.15

In brief, the critical characteristics of the backbone curve involve riser diameter, penetration depth, and the roughness at the riser–soil interface. As the riser pipe penetration depth z increased, the bearing resistance $N_c(z)$ will increase, which is often associated with an increase in the soil undrained shear strength $S_u(z)$. The non-linear seabed model is using a depth-dependent bearing factor, as indicated in Equation 4.3—2. This model also includes the effects of a linearly increasing shear strength profile by considering the undrained shear strength at penetration z, as shown in Figure 4.3—3.

A sample backbone curve for an initial penetration process is presented in Figure 4.3—4, with riser and soil parameters as follow: riser diameter = 0.4 m; soil shear strength = 2.6 kPa, shear strength gradient = 1.25 kPa/m. For a couple of power coefficients a and b: a = 4.88, b = 0.21 and a = 6.15, b = 0.15.

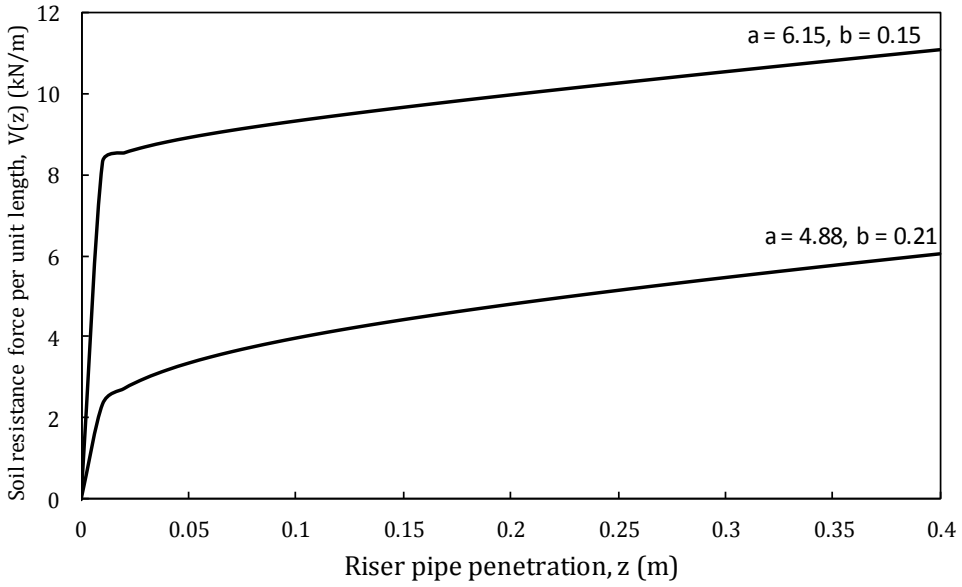

Figure 4.3—4 Sample of backbone curves for two different couples of power law coefficients

- Seabed stiffness: the SCR pipe–seabed interaction model is used to calculate the seabed stiffness and is summarised in this section. The SCR–seabed interaction in the TDZ can extend over a considerable distance across the seabed as shown in Figure 4.3—5. Therefore, the seabed stiffness effects are not efficiently characterised by a single soil spring, but rather by a series of springs, and extending over the length of the TDZ.

  A laboratory model test carried out at the Norwegian Geotechnical Institute (NGI) (Langford and Aubeny, 2008, Sharma and Aubeny, 2011) presents the typical measures of a relationship between vertical soil

resistance and riser pipe penetration, as shown before in Figure 4.3—1, which involves a number of complexities such as plastic penetration, soil suction, riser uplift and stiffness degradation. A non-linear seabed model is a rigorous approach to the model load-displacement process. The seabed soil stiffness utilised to model the SCR pipe–seabed interaction is based on *V*-*z* curves. An equivalent secant stiffness is employed to define the soil spring during unload and reload cycles.

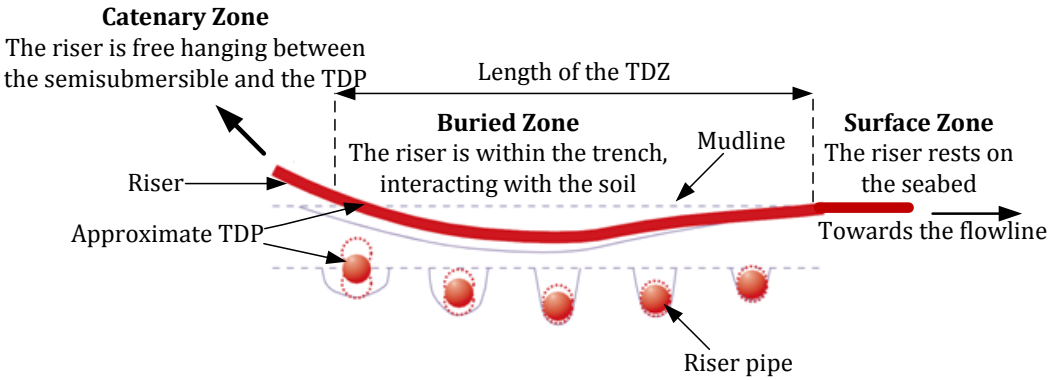

Figure 4.3—5 Overview of trench definitions and development in the TDZ

The normalised secant stiffness, K_{max}, is the pipe-soil stiffness, see Figure 4.3—6, normalised by the ultimate net-bearing pressure at that depth, which is a measure of the effective stiffness since the last reversal in penetration or since penetration started, and is given by:

$$K_{\max} = \frac{\text{Pipe-soil stiffness}}{\text{Ultimate net bearing pressure}} = \frac{K_{su}}{(V_u/D)} = \frac{\Delta V/\Delta z}{N_c(z).S_u}$$

Equation 4.3—3

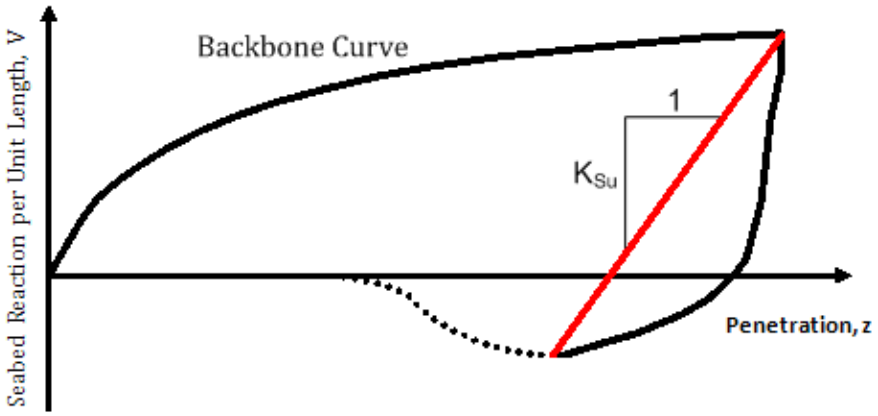

Figure 4.3—6 Seabed resistance model and definition of pipe–soil stiffness

It has been found that the maximum normalised secant stiffness, K_{max}, has the typical range of values as shown in Table 4.3—3 (Bridge *et al.*, 2004, Clukey *et al.*, 2008, Randolph and Quiggin, 2009, Aubeny and Biscontin, 2008).

Table 4.3—3 Typical range of normalised secant stiffness values

K_{max}	Cyclic displacement ($\Delta z/D$)
150 to 400	~0.1%
~100	~0.5%
~40	~2.5%
~10	~10%

- In each penetration mode, the seabed reaction force per unit length, $V(z)$, is modelled using an analytic function of the non-dimensional penetration z/D. $V(z)$ is modelled, in contact modes including the initial penetration, uplift and re-penetration, by applying different non-linear hyperbolic functions, $H_{IP}(\zeta)$, $H_{UL}(\zeta_0-\zeta)$ and $H_{RP}(\zeta-\zeta_0)$, to the ultimate penetration resistance $V_u(z)$ or the ultimate suction resistance $V_{u\text{-}suc}(z)$, which are given as:

$$V(z)=\begin{cases} H_{IP}(\zeta).V_u(z) & \text{Initial Penetration Mode} \\ V_0-H_{UL}(\zeta_0-\zeta).(V_0-V_{u-suc}(z)) & \text{Uplift Mode} \\ V_0+H_{RP}(\zeta-\zeta_0).(V_u(z)-V_0) & \text{Re - penetration Mode} \end{cases}$$

Equation 4.3—4

$$H_{IP}(\zeta)=\frac{\zeta}{(1+\zeta)}$$

Equation 4.3—5

$$H_{UL}(\zeta_0-\zeta)=\frac{(\zeta_0-\zeta)}{\left[\frac{(V_0-V_{u-suc}(z))}{V_u(z_0)}+(\zeta_0-\zeta)\right]}$$

Equation 4.3—6

$$H_{RP}(\zeta-\zeta_0)=\frac{(\zeta-\zeta_0)}{\left[\frac{(V_u(z)-V_0)}{V_{u^*}}+(\zeta-\zeta_0)\right]}$$

Equation 4.3—7

$$\zeta=\frac{z}{(D/k_{\max})}$$

Equation 4.3—8

where V_0 and ζ_0 are the soil resistance and non-dimensional penetration at the latest episode of this contact mode started, respectively, and $V_{U^*}=V_u(z)$ if $V_0\le 0$, i.e., if this re-penetration started from zero or negative resistance, while $V_{U^*}=V_u(z^*)$ if $V_0>0$ where z^* is the penetration when the preceding episode of uplift started. The maximum normalised stiffness of the pipe–soil interaction following reversal of motion is used to derive non-linear hyperbolic functions that model the seabed resistance force as a function of the penetration.

- For each mode, the analytical formulae use a term of hyperbolic form, as indicated by Equation 4.3—4, which provides a high stiffness response for small reversals of motion, but assures that the resistance $V(z)$ asymptotically approaches the seabed ultimate penetration resistance (for penetration) or ultimate suction resistance (for uplift) as the

penetration z increases or decreases from its magnitude when this episode of penetration or uplift started, see Figure 4.2—2. The ultimate penetration and suction asymptotic limits are given by:

$$V_u(z) = N_C(z).S_u(z).D$$

Equation 4.3—9

$$V_{u-suc}(z) = -f_{suc}.V_u(z)$$

Equation 4.3—10

where f_{suc} is the suction resistance ratio. The suction resistance depends partly on the local soil strength and riser pipe velocity, as indicated by Randolph and Quiggin (2009). Therefore, the use of a constant factor f_{suc} in Equation 4.3—10 is a simplification.

The non-linear soil model parameters control the maximum suction, f_{suc}, the displacement over which the suction decays, λ_{suc}, and the delay in mobilising full resistance during re-penetration, λ_{rep} (Randolph and Quiggin, 2009). Throughout the uplift, the suction resistance has been found to rely on the rate at which the catenary pipe is lifted up, the time during which upward motion is sustained and the recent history of cyclic motion (Bridge *et al*., 2004). Nevertheless, despite the availability of limited experimental data, the model has utilised a specific suction

resistance ratio, f_{suc}, which can be designated anywhere within the range from zero to unity, although an upper limit of about 0.7 is most likely realistic. The suction decay parameter, λ_{suc}, can be adopted so that the uplift resistance eventually becomes small, within an uplift displacement of about 1 diameter. Values within the range from 0.2 to 0.6 are appropriate for this. The final parameter, λ_{rep}, controls the delay in mobilising the ultimate resistance curve during re-penetration for which a value in the range 0.1 to 0.5 reasonably matches experimental data (Randolph and Quiggin, 2009).

This enables the model to capture the hysteretic behaviour of the seabed soil response and the increasing penetration of the pipe under cyclic loading in the vertical plane. The model was validated against laboratory and field-scale experiments with reasonable accuracy shown. This model has been implemented in OrcaFlex software, which is widely used for riser response analysis (Orcina, 2010), as it models the vertical pipe–soil interaction on soft clay according to the dynamic aspects more accurately than a linear seabed model (Randolph, 2009).

4.4 Pipe–Seabed Lateral Interaction Models

4.4.1 Lateral Soil Resistance Approaches for a Partially Embedded SCR

The lateral soil resistance of the partially embedded pipeline must be determined at the design stage. For lateral movement considerations, one of the principal factors is the ability to model lateral movements with cyclic motions. Three different approaches (Cathie, 2005, Dendani, 2008) can be considered for determining the lateral soil resistance of partially embedded pipelines:

1. a single friction factor "Coulomb friction model" approach, where the lateral soil resistance is related to the submerged weight of the pipeline and the soil type. This approach is fairly simplified, as it does not pertain to pipe embedment;
2. a two-component model, where the lateral soil resistance consists of a sliding resistance component and a lateral passive pressure component (Verley and Lund, 1995, Brennodden *et al.*, 1989, Wagner *et al.*, 1987); and
3. a plasticity model approach: Zhang *et al.* initially developed the plasticity model for calcareous sand and clays (Zhang *et al.*, 2002). However, the clay's model is established on the behaviour of shallow flat footings in which a large lateral movement does not occur.

Therefore, the Coulomb friction approach and the two-component soil resistance models for the assessment of SCR global response are presented in this thesis.

4.4.2 Coulomb Friction 'Bilinear' Model

Present industry procedure is to evaluate the soil resistance with a Coulomb friction model, as shown in Figure 4.4—1, which expresses the lateral resistance as the product of the effective submerged pipeline vertical force (submerged pipe weight minus hydrodynamic lift force) and a soil friction coefficient that depends solely on soil type. Recommended values of the Coulomb friction coefficient, μ, lie in the range 0.2–0.8, while the displacement to mobilise this resistance is typically 0.1 pipe diameters (Lyons, 1973, Brennodden *et al.*, 1989, Wagner *et al.*, 1987, White, 2008).

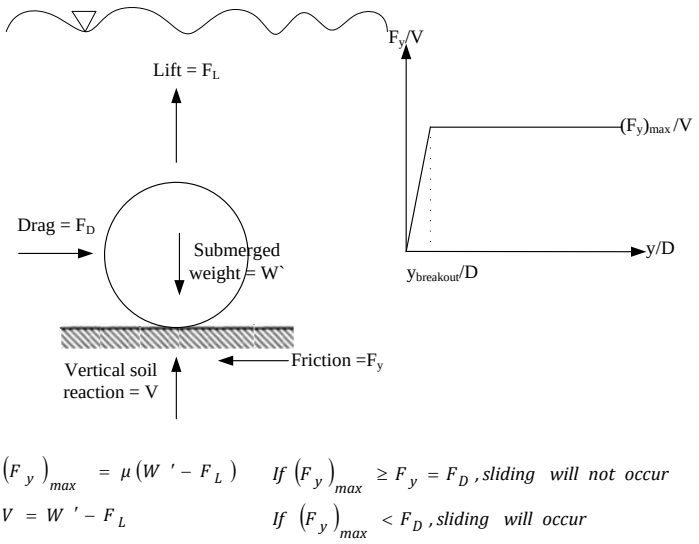

Figure 4.4—1 Coulomb friction model analysis

4.4.3 Improved 'Tri-linear' Pipe–Seabed Interaction Model

The experiment results show that the pipe–soil lateral motion is far more complicated than simple coulomb friction. An improved model is essential in order to mimic the effects of soil strength and the load history of the catenary pipeline as well as the associated pipe embedment on the lateral seabed soil resistance. The improved empirical model utilises two components to predict the seabed resistance to lateral pipeline movements, resulting in the improved so-called 'two-component model'.

The two-component model uses an empirical formula to assess the soil resistance to lateral pipeline motions. The first component depends on the vertical pipe weight (pipe weight minus hydrodynamic lift force) and imitates

the sliding resistance of the pipeline along the soil surface, while the second component depends on the pipe penetration and soil strength.

Generally, the two-component models are based on empirically fitting laboratory test data. A summary of some of the proposed formulas is given in Table 4.4—1. The peak lateral soil resistance is a key parameter for the on-bottom pipeline movement. Several reported methods (Brennodden *et al.*, 1989, Wagner *et al.*, 1987, Verley and Lund, 1995, Bruton *et al.*, 2006) have been published for the assessment of the lateral soil resistance. These determined resistances were then compared with the results of the available pipe model tests.

Table 4.4—1 Lateral resistance models of partially embedded pipelines in soft clay

Author	Lateral soil resistance formulas	Comments
Wagner *et al.* (Wagner *et al.*, 1987)	$F_y = \mu(W' - F_L) + \beta S_u A / D$	Monotonic $\mu = 0.2$ $\beta = 39.3$
	F_y = Lateral soil resistance μ = Sliding resistance coefficient W' = Submerged pipe weight F_L = Hydrodynamic lift β = Empirical soil passive resistance coefficient S_u = Undrained shear strength of the	Cyclic (oscillations below the monotonic breakout load [<static failure]) Penetration x 2 $\beta = 31.4$
		Cyclic

Author	Lateral soil resistance formulas	Comments
	clay A = 0.5 x embedded area	(large displacement oscillations) Penetration x 2.5 $\beta = 15.7$
Brennodden *et al.* (Brennodden *et al.*, 1989)	$F_y = \mu(W' - F_L) + F_R$	$\mu = 0.2$ F_R calculated considering accumulated energy
Verley & Lund (Verley and Lund, 1995)	$F_y = F_C + F_R$ $F_y = \mu(W' - F_L) + F_R$ $F_R = 4.13 D S_u \left(\frac{S_u}{\gamma' D}\right)^{-0.392} \left(\frac{z}{D}\right)^{1.31}$	Clays (S_u<70 kPa) $\mu = 0.2$
Bruton *et al.* (Bruton *et al.*, 2006)	$(F_y)_{\text{dimensionless}} = \mu v + \frac{3}{\sqrt{\frac{S_u}{\gamma' D}}} \frac{z_{init}}{D}$ $(F_y)_{\text{dimensionless}} = \frac{F_y}{S_u D}$ $\frac{z_{init}}{D}$ = normalised initial pipe penetration $v = \frac{V}{D S_u}$ normalised vertical load due to the effective pipe weight $\frac{(f_y)_{res}}{v} = 1 - 0.65\left[1 - \exp\left(-\frac{1}{2}\frac{s_u}{\gamma' D}\right)\right]$	Soft Clays (0.15<S_u<8 kPa) $\mu = 0.2$

Figure 4.4—2 shows the lateral load response from steps 0 to 3, characterised as follows (Bruton *et al.*, 2005):

(0-1) First load breakout, with elastic response characterised by the mobilisation displacement and a peak that is dependent on the initial pipe embedment;

(1-2) Suction release phase and elevation correction, depending on initial pipe embedment;

(2-3) Steady state of residual friction.

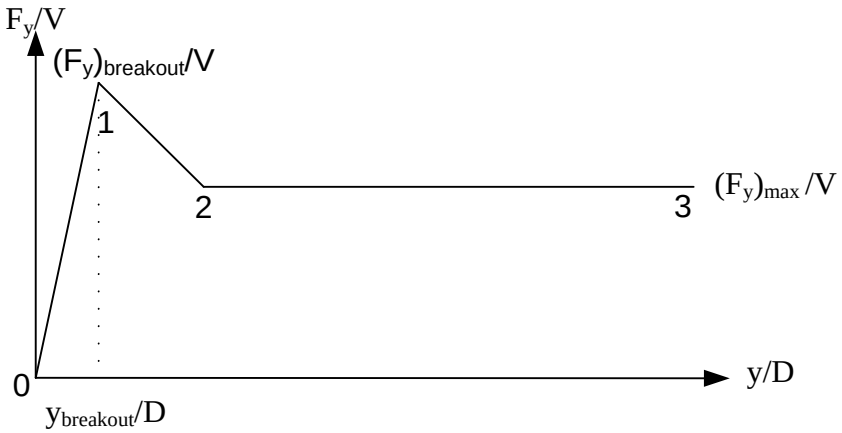

Figure 4.4—2 Schematic of the tri-linear soil resistance model

4.5 Concluding Remarks

Non-linear soil models have been presented for SCR–seabed interaction. The SCR–seabed interaction analyses engage the effect of physical phenomena, such as soil suction forces, and lateral and vertical seabed stiffness on the SCR performance, to be identified and quantified and also provide a better understanding of the complex physical process of SCR-soil-fluid interaction. These models were validated against a laboratory test with reasonable accuracy

shown. Riser-soil-fluid interaction modelling and analyses reduce the need for expensive experiment facilities and intricate design complications. An outline of the SCR–seabed interaction methodology utilised in this thesis was presented.

This chapter also introduced the basic concepts of SCR–seabed interaction and described the adopted modelling approach for vertical and lateral interaction, which will be used in this study. Equations for the backbone curve, the secant seabed stiffness, different modes of pipe penetration and lateral breakout resistance are also presented.

Better understanding and modelling of the seabed interaction will present more accurate estimation of the fatigue life of an SCR at the TDP. The SCR–seabed interaction and geotechnical parameters are the key issues for the assessment of strength behaviour and fatigue performance. To improve the understanding of SCRs behaviour and increase the confidence in its fatigue design at the TDZ, a numerical study is performed in this thesis.

The next chapter will present and discuss the significance of SCR–seabed soil interaction on the dynamic structural behaviour of SCRs for deepwater applications.

4.6 References

Aubeny, C. & Biscontin, G. 2008. Interaction model for steel compliant riser on soft seabed. *Offshore Technology Conference.* Houston, USA: Society of Petroleum Engineers.

Aubeny, C., Shi, H. & Murff, J. 2005. Collapse loads for cylinder embedded in trench in cohesive soil. *International Journal of Geomechanics,* Vol. 5, No. 4.

Aubeny, C. P., and Shi, H. 2006. Interpretation of impact penetration measurements in soft clays. *Journal of Geotechnical and Geoenvironmental Engineering,* Vol. 132, No. 6.

Aubeny, C. P., Biscontin, G. a. & Zhang, J. 2006. Seafloor interaction with steel catenary risers. Texas: Offshore Research Centre, Texas A&M University, College Station, Houston, Final Project Report to Minerals Management Service,Offshore Technology Research Centre Industry Consortium, OTRC Library Number 9/06A173

Aubeny, C. P. a. & Biscontin, G. 2009. Seafloor-riser interaction model. *International Journal of Geomechanics,* Vol. 9, No. 3.

Brennodden, H., Lieng, J., Sotberg, T. & Verley, R. 1989. An energy-based pipe-soil interaction model. *Offshore Technology Conference.* Houston, Texas, USA.

Bridge, C., Laver, K. & Clukey, E. Steel catenary riser touchdown point vertical interaction models. *In:* Offshore Technology Conference, OTC 16628, 2004 Houston, Texas.

Bridge, C. D. a. H., H.A. Observations and modeling of steel catenary riser trenches. *In:* International Society of Offshore and Polar Engineers (ISOPE) 2007 Lisbon.

Bruton, D., Carr, M., Crawford, M. & Poiate, E. The safe design of hot on-bottom pipelines with lateral buckling using the design guideline developed by the safebuck joint industry project. *In:* Deep Offshore Technology Conference, 2005 Espirito Santo, Brazil.

Bruton, D., White, D., Cheuk, C., Bolton, M. & Carr, M. Pipe/soil interaction behavior during lateral buckling, including large-amplitude cyclic displacement tests by the safebuck JIP. *In:* Offshore Technology Conference, 2006 Houston, USA.

Bruton, D. A. S., White, D. J., Carr, M., and Cheuk, J. C. Y. Pipe-soil interaction during lateral buckling and pipeline walking - the safebuck JIP. *In:* Offshore Technology Conference,OTC 19589, 5-8 May 2008 Houston, Texas.

Cathie, D., Jaeck, C., Wintgens, J-F and Ballard, J-c 2005. Pipeline geotechnics - state of the art. *Proc. International Symposium on Frontiers in Offshore Geotechnics (ISFOG).* Perth, Australia.

Clukey, E., Young, A., Dobias, J. & Garmon, S. Soil response and stiffness laboratory measurements of SCR pipe/soil interaction. *In:* Offshore Technology Conference, 2008 Houston, USA.

Dendani, H., and Jaeck, C. Flowline and riser: Soil interaction in plastic clays. *In:* Offshore Technology Conference, 5-8 May 2008 Houston, Texas, USA.

Dunlap, W. A., Bhojanala, R. P. a. & Morris, D. V. Burial of vertically loaded offshore pipelines in weak sediments. *In:* Offshore Technology Conference, 7th-10th March 1990 Houston, Texas.

Langford, T. & Aubeny, C. Model tests for steel catenary riser in marine clay. *In:* Offshore Technology Conference, 2008 Houston, USA.

Lyons, C. Soil resistance to lateral sliding of marine pipelines. *In:* Offshore Technology Conference, 1973 Texas, USA.

Merifield, R., White, D. & Randolph, M. 2009. The ultimate undrained resistance of partially embedded pipelines. *Ge´otechnique 58, No. 6***,** 461-470.

Murff, J. D., Wagner, D. A., and Randolph, M. F. 1989. Pipe penetration in cohesive soil. *Geotechnique,* 39**,** 213-229.

Orcina 2010. Orcaflex user manual *Orcina,* version 9.4a, UK.

Randolph, M., and Quiggin, P. 2009. Non-linear hysteretic seabed model for catenary pipeline contact. *28th International Conference on Ocean, Offshore and Arctic Engineering, OMAE* Proceedings of the ASME 2009

Randolph, M. & Quiggin, P. 2009. Non-linear hysteretic seabed model for catenary pipeline contact. *28th International Conference on Ocean, Offshore and Arctic Engineering, OMAE*

Randolph, M. F., and White, D. J. Pipeline embedment in deep water: Processes and quantitative assessment. *In:* Offshore Technology Confernce, 5-8 May 2008 Huston, Texas, USA.

Sharma, P. & Aubeny, C. Advances in pipe-soil interaction methodology and application for SCR fatigue design. *In:* Offshore Technology Conference, 2011 Houston, USA.

Thethi, R., and Moros, T. Soil interaction effects on simple catenary riser response. *In:* Proceeding Conference on Deepwater Pipeline & Riser Technology, 2001 Houston, Texas.

Verley, R. & Lund, K. M. A soil resistance model for pipelines placed on clay soils. *In*, 1995. American Society of Mechanical Engineers, 225-225.

Wagner, D., Murff, J., Brennodden, H. & Sveggen, O. Pipe-soil interaction model. *In:* Offchore Technology Confernce, April 27-30 1987 Houston, Texas, USA. OTC.

White, D. J., and Cheuk, C. Y. 2008. Modelling the soil resistance on seabed pipelines during large cycles of lateral movement. *Marine Structures,* 21**,** 59-79.

Willis, N. R. T., and West, P. T. J. Interaction between deepwater catenary risers and a soft seabed: Large scale sea trials. *In:* Offshore Technology Conference, 2001 Houston, Texas OTC 13113.

Zhang, J., Stewart, D. & Randolph, M. 2002. Modeling of shallowly embedded offshore pipelines in calcareous sand. *Journal of Geotechnical and Geoenvironmental Engineering,* 128**,** 363.

CHAPTER 5

GLOBAL RISER ANALYSIS USING A SEABED INTERACTION MODEL

5.1 Introductory Remarks

An SCR is a prolongation of subsea flow-line pipes connected to a floating platform in a catenary shape. The motions of the floating platform and random waves cause oscillations in and near its TDZ which results in interaction with the seabed. These riser motions in the TDZ could induce severe riser responses, leading to difficulty in meeting structural strength criteria at the TDZ. The development of deepwater fields has led to new research areas and discoveries.

Applying advanced non-linear SCR–seabed vertical and lateral interaction models that incorporate the SCR's cyclic motions using a finite element model can provide a realistic technique for predicting the dynamic response and structural behaviour of the SCR in the TDZ. These models can be used to analyse soil resistance to SCR movements under hydrodynamic loading and determine the interaction's influence on the global riser structural dynamic behaviour as well as the fatigue performance with a better accuracy. This chapter reports on a study investigating and assessing the vertical embedment and large lateral movements of the riser pipe in the TDZ.

A number of published research studies have focused on elaborating the SCR–seabed interaction (Bridge *et al.*, 2004, Aubeny and Biscontin, 2009, Thethi, 2001, Willis, 2001). The most common SCR vertical models that model the seabed with rigid or linear surfaces disregard the nature of the trenching

development process into the seabed and the passive soil resistance to the SCR's lateral movement in the TDZ.

In the other hand, the lateral soil resistance of the partially embedded pipeline must also be modelled at the design stage. One of the principal factors in lateral movement modelling is the ability to model lateral movements with cyclic motions. The different approaches available for modelling lateral seabed resistance have already been introduced in Chapter4.

The Coulomb friction approach and the two-component soil resistance models are used in this thesis for the assessment of the SCR's global response. The goal of this chapter is to discuss the significance of the SCR–seabed soil interaction in the design of SCR for deepwater applications and reports the results of an analysis of a SCR on soft clay in 910 m of water using the commercial code OrcaFlex for a non-linear time domain simulation with a robust meshing technique. Vertical embedment and large lateral SCR movements in the TDZ are investigated. The numerical results of the SCR's global response when considering a critical point in the TDZ are presented, for which the seabed is modelled using a hysteretic non-linear model proposed by Randolph and Quiggin (2009) in the vertical seabed direction, and bilinear (Brennodden *et al.*, 1989, Wagner *et al.*, 1987, White, 2008) and tri-linear soil models in the lateral seabed direction. The results show that the TDZ response involves the degradation of the seabed soil stiffness due to cyclic loading. Furthermore, the more highly adopted and applied lateral SCR-soil interaction model improves

the dynamic response of the soil stiffness and riser penetration which affects the global riser dynamic performance in the TDZ.

Cyclic degradation is generally thought to affect the ability of structural systems to resist failure under a cyclic loading condition. Seabed stiffness degradation due to cyclic loading has a significant impact on the structural dynamic behaviour of SCRs in the TDZ, especially on the riser's resistance to fatigue. Seabed soil degradation must be incorporated into soil models when attempting to capture dynamic cyclic loading on the SCR's response.

5.2 Design Criteria for SCRs

The following design codes are commonly employed for the design and analysis of deepwater SCR:

- API RP 2RD (API, 1998),
- DNV-RP-F204 (DNV, 2005)
- DNV-OS-F201 (DNV, 2001-amended 2009)

SCR design must comply with the design criteria, which means that the developed configurations must meet the Serviceability Limit State (SLS), Ultimate Limit State (ULS), Accidental Limit State (ALS) and Fatigue Limit State (FLS).

According to API RP 2RD, the SCR strength is verified in terms of the maximum stress according to the following relationship:

$$\left(\sigma_p\right)_e < C_f \sigma_a$$

Equation 5.2—1

Where $\left(\sigma_p\right)_e$ is the extreme von Mises stress; $\sigma_a = C_a \sigma_y$ is the basic allowable combined stress; C_a is the allowable stress factor equal to 2/3; σ_y is the material's minimum yield strength, defined for steel or titanium as the tensile stress required to produce a total elongation of 0.5% of the test specimen gauge length; and C_f is the design case factor, which measures 1.2 for extreme condition (100 years) and 1.5 for survival conditions (1000 years).

In plain round pipe, where transverse shear and torsion are negligible, the three principal stress components of the primary membrane stress (average stress across the pipe wall) are σ_{pr}, $\sigma_{p\theta}$, and σ_{pz}, where *r*, θ and *z* refer to the radial, hoop and axial stresses respectively (API, 1998). Thus:

$$\left(\sigma_p\right)_e = \max\left[\frac{\left(\sigma_{pr} - \sigma_{p\theta}\right)^2 + \left(\sigma_{p\theta} - \sigma_{pz}\right)^2 + \left(\sigma_{pz} - \sigma_{pr}\right)^2}{2}\right]^{1/2} \leq C_f \sigma_a$$

Equation 5.2—2

5.3 Modelling and Analysis

5.3.1 SCR Modelling

The SCR strength analysis is developed by satisfying the ULS design conditions. The dynamic analysis is performed for the 0°, 90° and 180° wave directions (representing the in-plane and lateral load cases). The response analysis is specified by the following steps:

- The SCR is modelled with a finite element model. The riser is divided into a series of line segments, which are then modelled by straight massless model segments with a node at each end.
- The SCR's static configuration is established.
- A non-linear dynamic time domain response analysis is used, for which the SCR configuration and tension are calculated at each time step with an iterative procedure and the SCR systems's dynamic response is estimated using the integration scheme (i.e., forward Euler with a constant time step). The dynamic analysis is a time simulation of the model's motions over a specified period of time, starting from the position derived by the static analysis.

5.3.2 SCR–Seabed Interaction Modelling

The SCR–seabed interaction response characteristic is a highly non-linear phenomenon. It is important not to restrict the modelling of this interaction to a

linear seabed model approximation and the riser analysis techniques must be improved by refining the riser–seabed interaction (Leira *et al.*, 2004). SCR–seabed interaction modelling should involve vertical and lateral soil responses to the cyclic loading oscillations of the SCR in the TDZ, which can cause trenching and dynamic embedment of the SCR into the seabed. The SCR–seabed interaction problem and modelling technique, based on the adopted approach presented in Chapter 4, are shown in Figure 5.3—1.

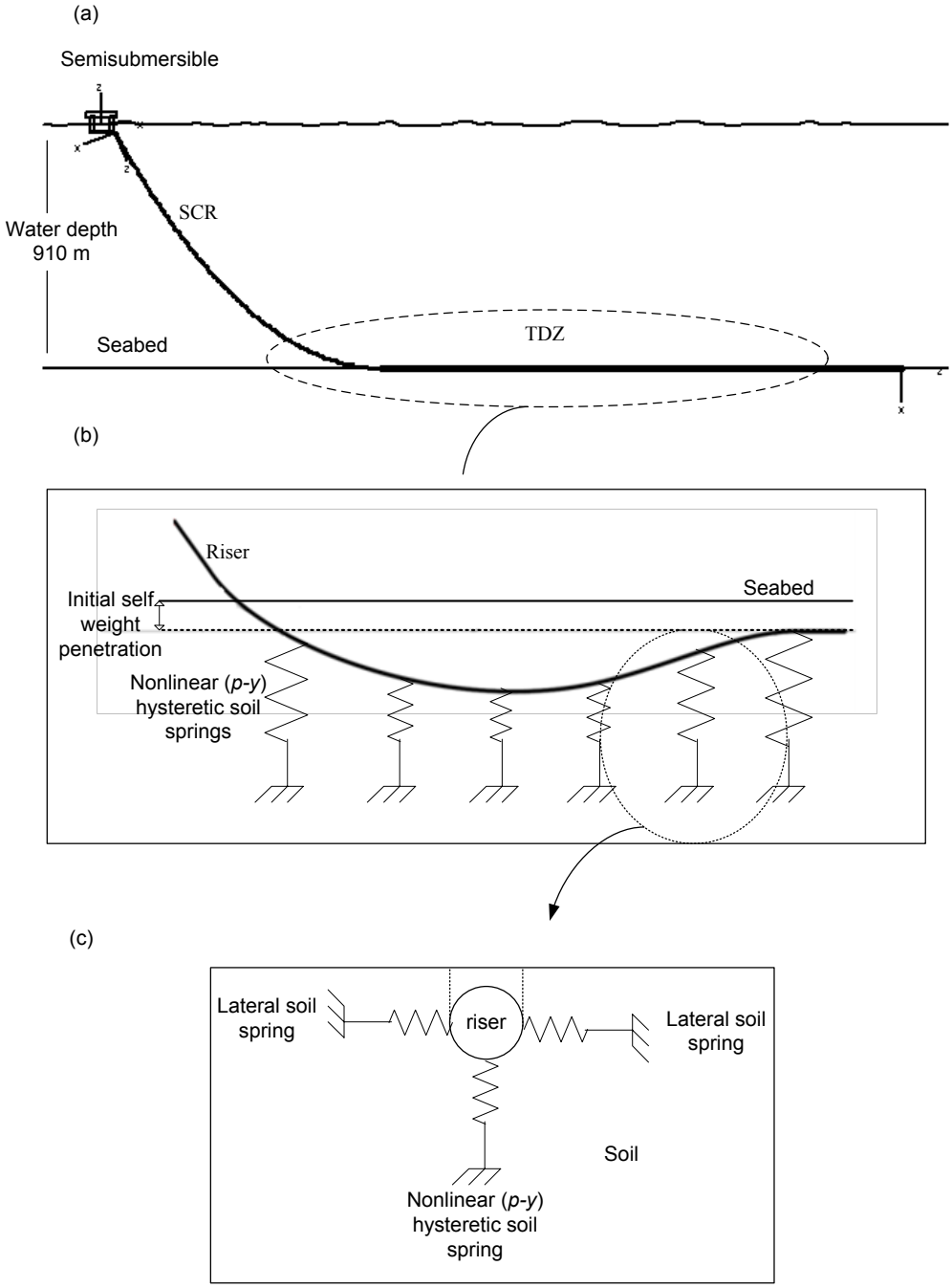

Figure 5.3—1 (a) SCR–seabed interaction problem (b) schematic of the TDZ attached with hysteretic non-linear soil springs, and (c) riser-soil model

a. SCR–Seabed Vertical Interaction Model

Recent studies (Aubeny *et al.*, 2006, Randolph and Quiggin, 2009, Bridge *et al.*, 2004) have developed an advanced non-linear SCR–seabed interaction in the TDZ. The non-linear seabed model includes features such as pipe embedment, cyclic loading motions, and soil suction which highlight the level of conservatism in the current linear model approximation of the seabed. The SCR's stresses in the TDZ are of prime importance in the evaluation of the dynamic response and structural behaviour of the SCR's global response. These stresses and their locations in the TDZ are very sensitive to the seabed model's interaction response.

The seabed stiffness is a key factor in the modelling and analysis of the SCR–seabed interaction and is characterised by *V-z* curves. In this study, the SCR–soil interaction is modelled as a "lumped mass" finite element model resting on non-linear seabed model at the touchdown for cyclic riser–seabed interaction. The non-linear seabed model is based on a hyperbolic secant stiffness formulation and is presented in Chapter 4. The seabed soil stiffness is characterised by the non-linear seabed model based on *V-z* curves.

The non-linear seabed model is appropriate for modelling soft clays, and is particularly suitable for deepwater cases where the mudline undrained shear strength measures is low and where the contact behaviour is govered by plastic penetration rather than an elastic response (Orcina, 2010).

b. SCR–Seabed Lateral Interaction Models

Bilinear friction model: The conventional riser–soil design procedure is to model the interaction with spring links at intervals along the riser flow-line. These links provide a bilinear soil resistance in the lateral direction, as shown in Figure 5.1—1. Common design practice dictates the assumption of frictional behaviour, so that the limiting horizontal force on the pipe is proportional to the pipe weight, as shown in Equation 5.3—1:

$$\left(F_y\right)_{\max} = \mu V$$

Equation 5.3—1

The seabed friction force has a magnitude of up to μV, where μ is the friction coefficient and V is the seabed reaction force, and acts tangential to the seabed plane. A linear model of the friction force is employed and given by $F = -k_s * A * y$ to a magnitude of no more than μV, where y is the displacement from the un-sheared position, k_s is the seabed shear stiffness, and A is the contact diameter multiplied by the length of the line represented by the node. The Coulomb friction models the friction force of $-\mu V$ to $+\mu V$ which occurs as a linear variation over the deflection range $-y_{breakout}$ to $+y_{breakout}$. Here $y_{breakout}$ is given by $y_{breakout} = \mu V / k_s A$.

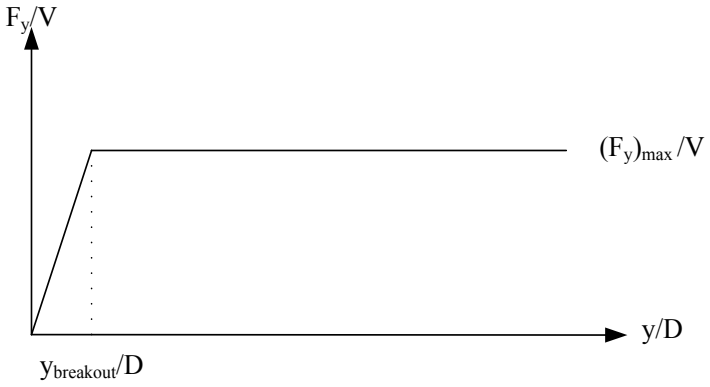

Figure 5.3—2 Coulomb friction 'bi-linear' model

Tri-linear friction model: The next degree of sophistication in pipe–soil response modelling beyond a simple bilinear frictional model, is to use empirical expressions evaluated from previous model tests (e.g., Wagner *et al.*, 1987; Brennodden *et al.*, 1989; Verley *et al.*, 1995; Bruton *et al.*, 2006) to assess the lateral soil resistance F_y required for a pipe to move laterally. Generally, these empirical expressions divide the ultimate lateral soil resistance into two contributions: a frictional component linked to the pipe weight and a passive component linked to the soil strength S_u and pipe embedment depth z. The total lateral soil resistance, F_y, is divided into the two components given below:

$$F_y = F_F + F_R$$

Equation 5.3—2

where F_y is the total lateral soil resistance, F_F is the sliding resistance force equal to a sliding resistance coefficient multiplied by the vertical pipe weight and F_R is the passive resistance (i.e., a penetration-dependent soil resistance force). The

lateral response is modelled using independent values of soil–pipe breakout friction, $(f_y)_{breakout}/V$, and residual soil resistance $(f_y)_{res}/V$ using the tri-linear response shown in Figure 5.3—3 and Chapter 4.

Bruton *et al.*, (2006) have examined a large database of test results and deduced that normalised breakout soil resistance, $\left(F_y\right)_{\dim ensionless} = F_y / S_u D$ depends on the current normalised vertical load, $v = V/DS_u$, the initial embedment depth, z_{init}/D, and the dimensionless ratio of soil strength to weight, $S_u/\gamma'D$. A relationship using these variables have been suggested by Verley and Lund (Cathie, 2005) and consists of a frictional component of the seabed soil resistance below the SCR, and a passive component required the lifting and deformation of the soil in the vicinity and in front of the catenary pipeline. Their model has been reappraised by Bruton *et al.* (2006) based on a new experimental database, introducing the following formula for breakout seabed soil resistance:

$$\left(F_y\right)_{\dim ensionless} = 0.2v + \frac{3}{\sqrt{\frac{S_u}{\gamma' D}}}\frac{z_{init}}{D}$$

Equation 5.3—3

The lateral seabed soil resistance changes to a constant residual soil resistance value $(F_y)_{res}$ after breakout in the tri-linear model. Bruton *et al.* (2006) have reviewed the experimental results and recognised that the residual seabed

friction factor, $(F_y)_{res}/V$, depends on the soil strength–weight ratio, $S_u/\gamma'D$, and have proposed the following expression (White, 2008):

$$\frac{(F_y)_{res}}{V} = 1 - 0.65\left[1 - \exp\left(-\frac{1}{2}\frac{s_u}{\gamma' D}\right)\right]$$

Equation 5.3—4

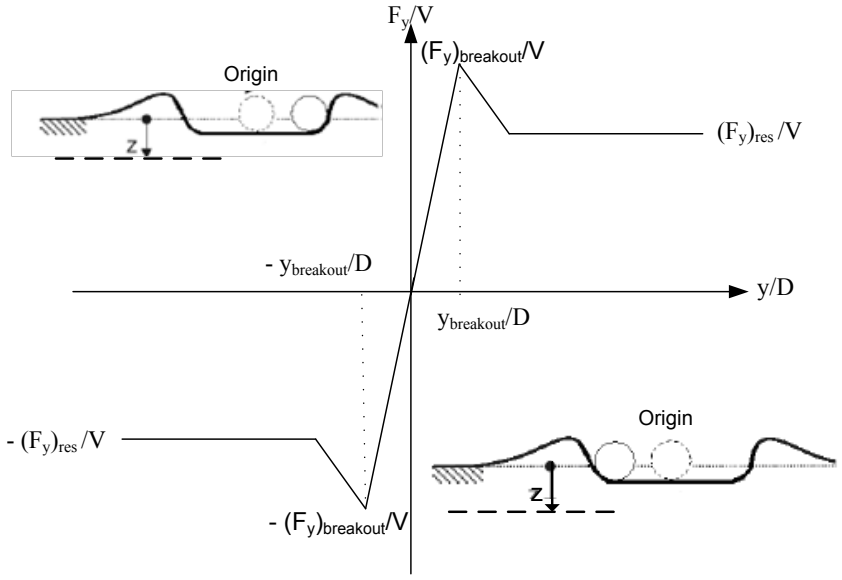

Figure 5.3—3 Lateral pipe–soil interaction using a tri-linear model

The improved soil resistance model can be applied with the current capabilities of the OrcaFlex program by using a combination of seabed friction, see Figure 5.3—2, and a pure damper-type link to provide the additional resistance present at the start of motion, Figure 5.3—4. The breakout (mobilisation) displacement occurs at very small riser movement approximately 0.1 of the pipe diameter as stated in DNV (2009). The damper is set to apply a force over a

small velocity range but to apply nothing once a limiting velocity is exceeded. The sliding resistance component represents the constant resistance that the SCR encounters in the TDZ once it has overcome the initial peak in resistance and the load has settled.

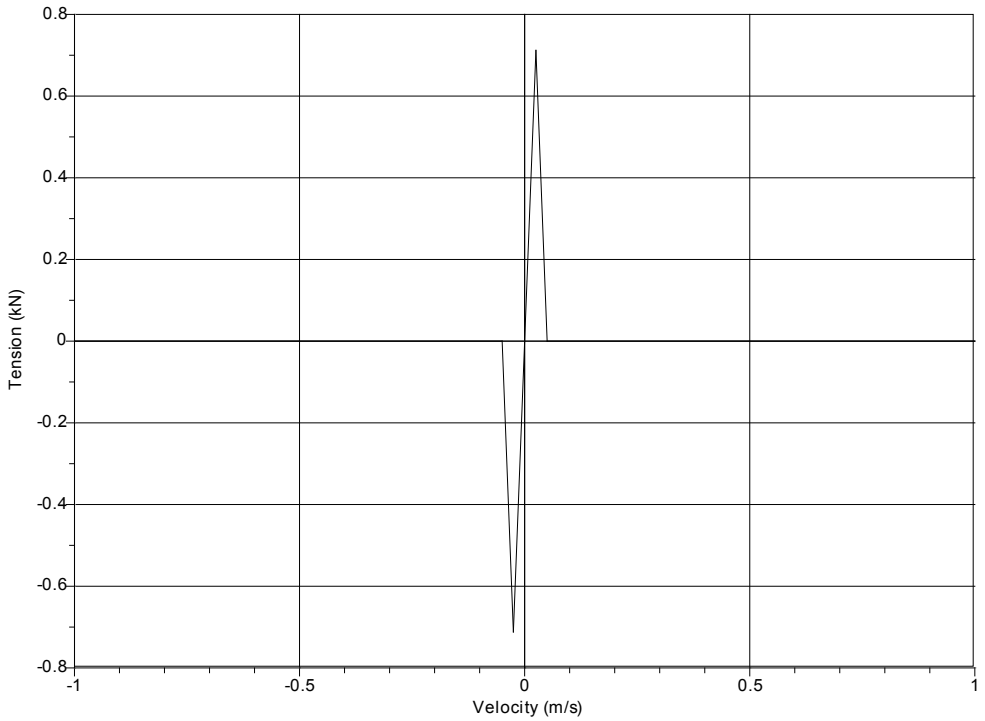

Figure 5.3—4 Resistance applied by the damper-type link

The force applied by the damper represents the additional force over and above the constant value. The small velocity range is intended to account for the fact that this additional force is applied only at the very start of motion. The model accounts for the cyclic nature of the motion because it is applied each time the pipe moves. It should be noted that the links must be long so that small changes in the line node positions do not lead to significant changes in the angle of the link (because the link force must remain perpendicular to the direction of the

line axis at all times). The disadvantage of this type of scheme is that it most likely requires a large number of links to appropriately restrain the seabed section of the line.

5.3.3 Analysis Technique

The stresses occurring in the TDZ are crucial to the evaluation of the SCR strength and are very sensitive to the behaviour of the SCR–seabed interaction. The most critical excitation levels in the TDZ are the ULS and FLS, as illustrated in Figure 5.3—5. The TDZ located closest to a semi-submersible is subjected to the highest stresses during moderate excitation levels. Because these excitation levels correspond to frequently occurring environmental conditions, they make the highest contributions to the FLS. At higher excitation levels corresponding to the critical condition in the ULS, the cross-sections of the SCR with the highest stresses moves farther away from the floating production unit (Giertsen, 2004).

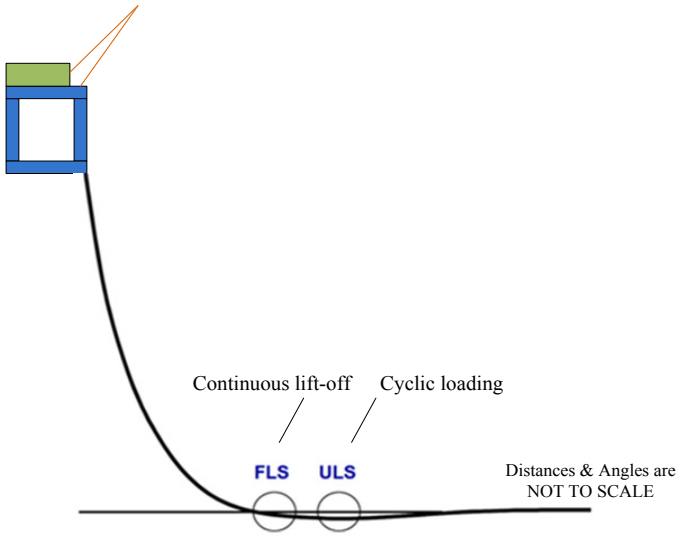

Figure 5.3—5 ULS and FLS zones in the touchdown area

5.4 Numerical Implementation for Dynamic Analysis

OrcaFlex and its non-linear time-domain finite element analysis, a commercial software package for the numerical analysis of offshore marine systems, are used to model the semi-submersible and SCR motions. The environmental data inputted into the analysis is based on a typical NNS scatter diagram. OrcaFlex implements implicit integration scheme. For implicit solver, OrcaFlex uses generalised-α integration scheme, which is unconditionally stable, to solve the system equation at the end of the time-step. In this study, the nonlinear time domain simulation time-step of 0.05 seconds is utilised in the dynamic analysis.

The normalized secant stiffness is the pipe-soil stiffness, dV/dz, normalized by the ultimate net bearing pressure at that depth, V_u/D which presented in Chapter 4. The normalized secant stiffness has typical soft clay values ranging from 150 to 250 (Bridge *et al.*, 2004). The non-linear soil model parameters have been discussed by Randolph and Quiggin (2009).

5.5 Case Study

5.5.1 SCR Model Description

The SCR descends from a semi-submersible pontoon in a simple catenary configuration, transitioning to a flow-line after 1260 m, and the SCR is connected to a semi-submersible at a mean top angle of 20° to the vertical, as shown in Figure 5.5—1. The riser is constructed of line pipe, in accordance with

API Spec 5L, of grade X70 steel with 551.58 MPa of yield stress. The outside diameter is 273 mm (10.75 in) with a wall thickness of 20.6 mm (0.812 in) and a total riser length of 3310 m (Serta, 1996). The SCR line is divided into 1022 elements. The element length of 0.5 m is chosen for the TDZ and 5 m for other zones. In the global analysis, the top-end is modelled as pinned, which means it is free to rotate. The SCR pipe is bundled with a normal coating for preliminary design purposes (Deka *et al.*, 2010, Bai and Bai, 2005):

- Coating thickness 75 mm
- Normal coating density 800 kg/m^3

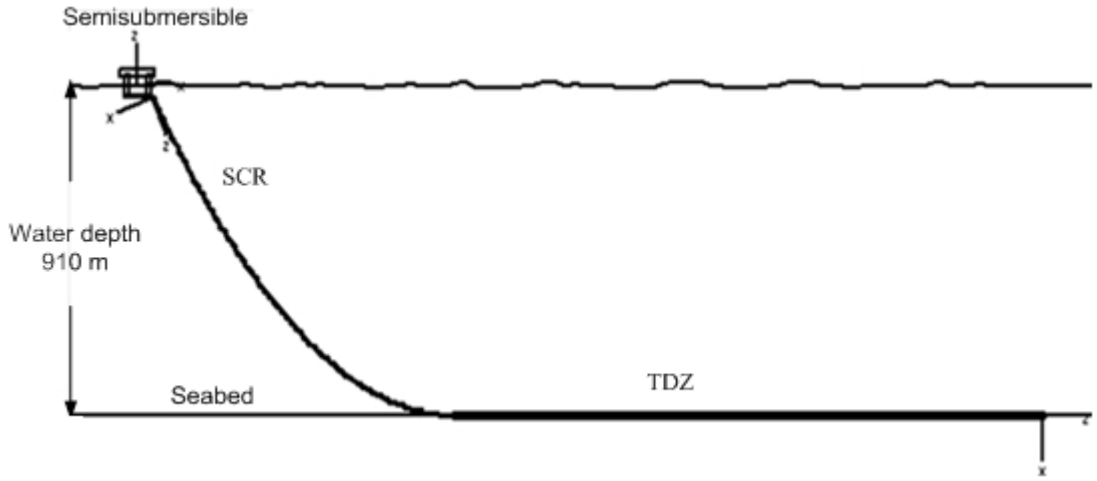

Figure 5.5—1 SCR design configuration

The drag coefficient, C_d, can be specified to vary with the Reynolds number, R_e. The variable data table specifies the drag coefficient as a function of the Reynolds number, C_d (R_e), as shown in Figure 5.5—2. The inertia coefficient C_M used in this analysis is 2.0, and the added mass coefficient C_a = 1.0.

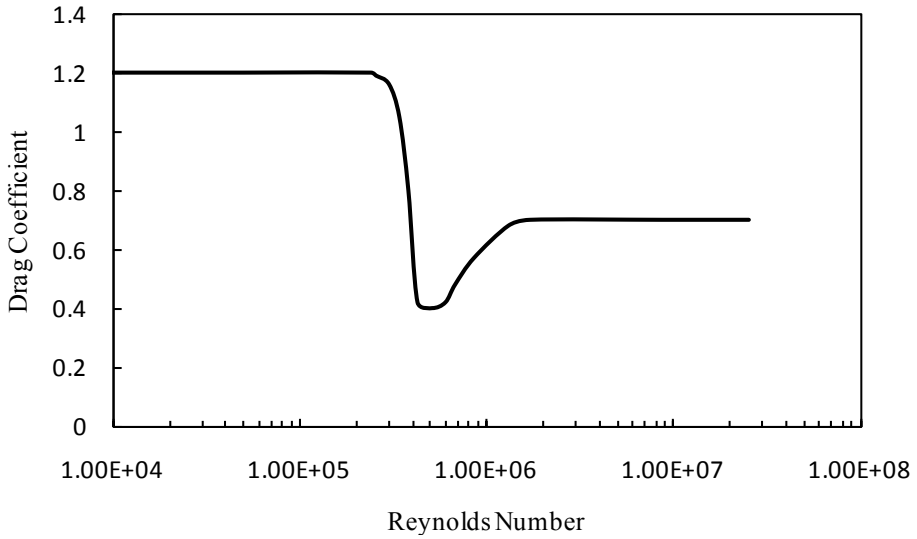

Figure 5.5—2 Drag coefficient variations with the Reynolds number (Barltrop *et al.*, 1991)

5.5.2 Environmental Conditions & Geotechnical Data

For design purposes and to verify the strength, the SCR is designed for a 100-year wave condition combined with a 10-year current profile, which is defined as a severe condition by the DNV (DNV, 2009). The wave data represent a typical NNS location and the water depth is set at 910 m in this location. The extreme sea state is modelled by irregular waves.

To establish a long-term sea state prediction of the NNS, we must use the joint frequency of the significant wave height (H_s) and the peak wave period, as given by the scatter diagram presented by Faltinsen (Faltinsen, 1999). The scatter diagram can be used to acquire long-term statistics on the wave height, as shown in Appendix E.

An appropriate approximation to the probability density function for the maximum wave elevation can be acquired from the Rayleigh distribution, and we can obtain the long-term probability using a simple summation:

$$P(H) = 1 - \sum_{j=1}^{M} e^{\left(\frac{-2H^2}{\left(H_s^{(j)}\right)^2}\right)} p_j$$

Equation 5.5—1

where $P(H)$ is the long term probability that the wave height will not exceed H, j is the wave component number, H_s is the significant wave height, M is the number of significant wave height upper intervals (see Appendix E) and p_j is the probability of the wave component in the scatter table.

Therefore, the 100-year sea state is:

- significant wave height H_s 15.6 m
- corresponding wave peak period T_p 16 s

the corresponding 10-year current profile has been given by Bitner-Gregersen (2005), Leira *et al.* (2002) and Xia *et al.* (2008), see Table 5.5—1.

Many of deepwater fields have recently been discovered in regions where soft clay is detected (Sen, 2007). Table 5.5—2 gives the ranges of shear strength in soft clay (Willis, 2001, Sen, 2007).

Table 5.5—1 Water depth vs. current speed

Water depth (m)	Current speed (m/s)
0 at water surface	1.0
50	0.68
300	0.47
910	0

Table 5.5—2 Typical ranges of shear strength in the seabed (soft clay)

Soil rank	S_{u0} (kPa)	S_{ug} (kPa/m)
Lower range	1.2	0.8
Median range	2.6	1.25
Upper range	3.8	2.0

Note: S_{u0} is the shear strength of the soil at the seabed level, and S_{ug} is the shear strength gradient.

5.5.3 Vessel RAO Data

SCRs are being considered for production units in deepwater environments such as the NNS. When used in conjunction with a semi-submersible in harsh deepwater environments, however, SCRs present significant design challenges. The large vertical motions of the semi-submersible induce a severe riser response, which causes difficulty in achieving the strength criteria at the hang-off and TDP locations. The RAOs of a semi-submersible's center of gravity are shown in Figure 5.5—3, Figure 5.5—4 and Figure 5.5—5. The static vessel offset

for the extreme response analysis is 10% of the water depth for intact mooring and 12% when one mooring line failure condition occurs.

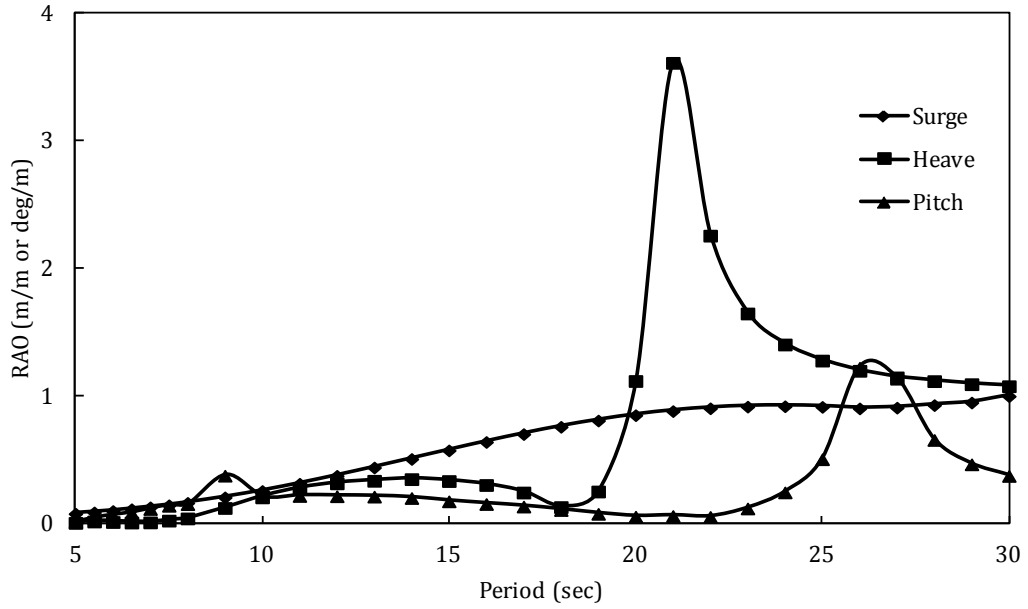

Figure 5.5—3 Semi-submersible RAOs in head seas – wave heading = 0°

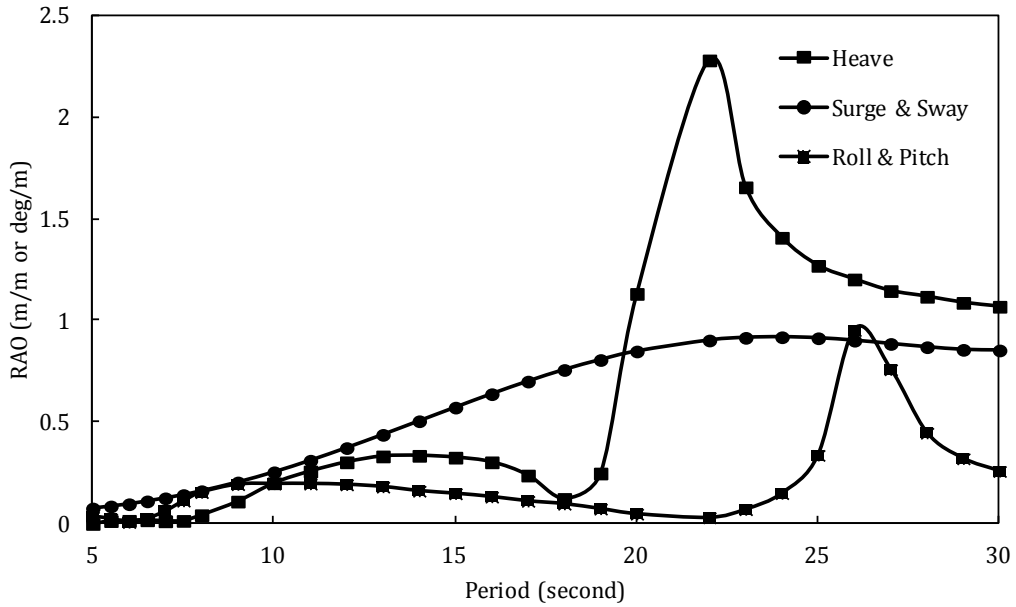

Figure 5.5—4 Semi-submersible RAOs in starboard bow quarter seas – wave heading = 45°

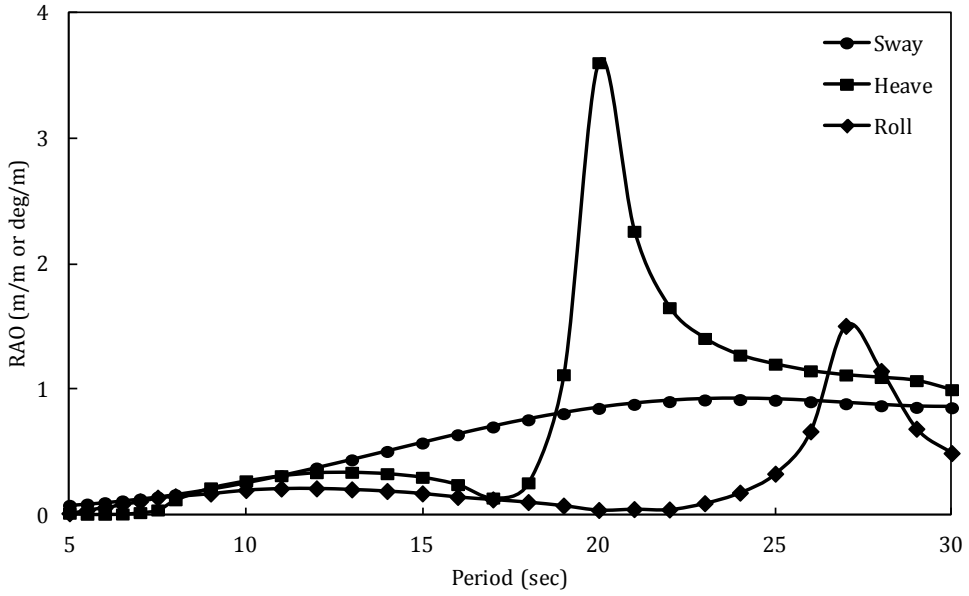

Figure 5.5—5 Semi-submersible RAOs in beam seas – wave heading = 90°

5.6 Results and Discussion

5.6.1 Global SCR Response

The SCR is analysed for the extreme operating intact mooring conditions. The extreme analyses are conducted for the load cases defined by API RP 2RD and the strength analysis is performed for near (i.e., when the FPU offsets closest to the TDP, see Figure 5.6—1), far (i.e., when the FPU drifts away from the TDP) and transverse vessel position offsets and a 100-year wave combined with a 10-year current, which is defined as a severe condition by the DNV (DNV, 2009). The median range of the soil shear strength is utilised in the strength analyses, as stated in Table 5.5—2.

The SCR configuration possesses adequate strength capacity for extreme operating intact conditions. The summary of these strength analyses is presented in Table 5.6—1 and Table 5.6—2. The most critical section for the von Mises stress occurs at the TDZ and the von Mises stress utilisation presented in Table 5.6—1 is calculated by normalising the calculated maximum von Mises stress with the yield stress, which is compared with 0.8 times the yield stress for intact mooring line extreme condition.

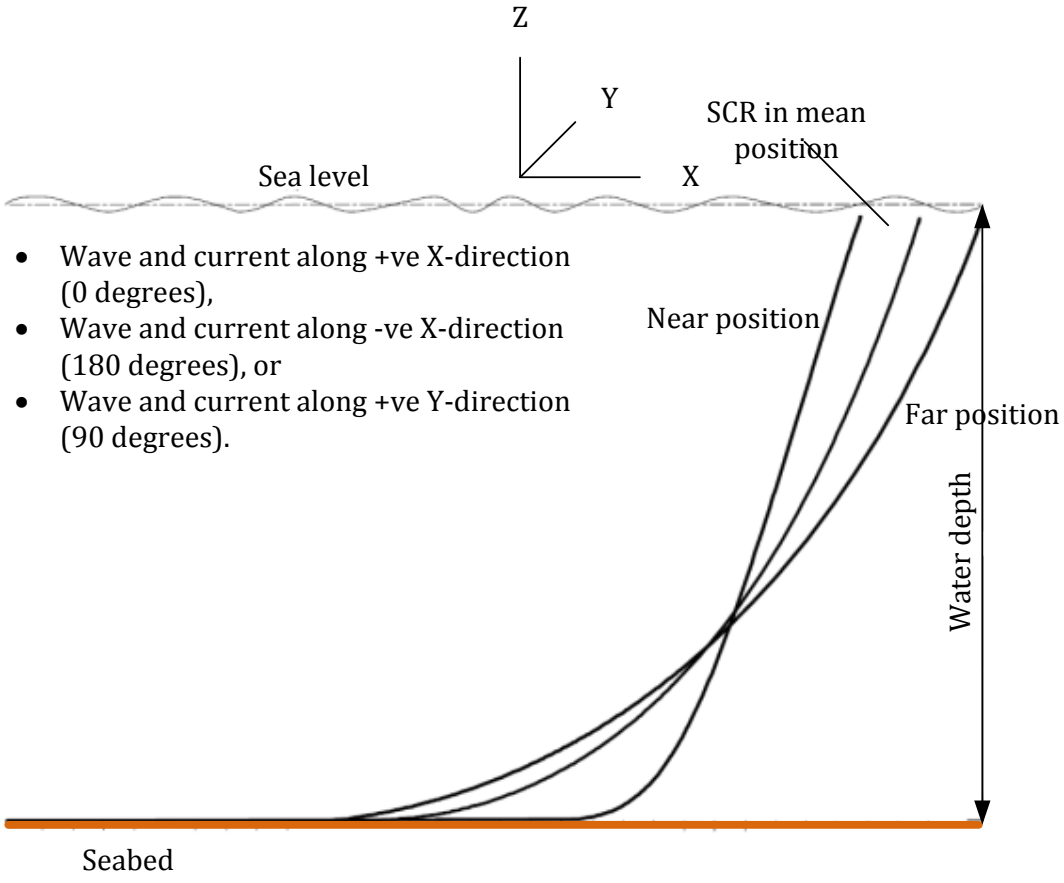

Figure 5.6—1 Vessel position definition

Table 5.6—1 Strength analyses results (3-hour simulation time)

Wave &current direction	Mooring condition	Riser offset position	Max. z/D	Max.von Mises stress /σ_y at TDP	Allowable stress/ σ_y
0 °	Intact	Near	0.13	0.74	0.8
		Mean	0.11	0.58	
		Far	0.10	0.57	
90 °	Intact	Transverse +Y	0.37	0.79	0.8
		Mean	0.19	0.71	
		Transverse -Y	0.14	0.63	
180 °	Intact	Near	0.12	0.67	0.8
		Mean	0.10	0.54	
		Far	0.59	0.79	

Table 5.6—2 Summary of SCR strength analysis results (3-hour simulation time)

Soil model	Environment	Wave &current direction	Riser offset position	Max bending moment (kN-m)	Max wall tension (kN)
Non-linear soil in vertical direction & Coulomb friction in lateral direction	100-year wave +10-year current	0 °	Mean	317.1	2255.2
		90 °	Mean	385.2	2368.9
		180 °	Mean	287.7	2483.5

The von Mises stresses along the riser length are shown in Figure 5.6—2 for the 0°, 90° and 180° wave and current directions when the semi-submersible is in the mean position. The floating production unit offset and dynamic motions in a harsh environment influence the stresses in the TDZ. The most critical section

for the von Mises stress occurs at the TDZ, and the numerical simulations exhibit the maximum variation in the bending moment near the TDZ, which depends on the excursion and cyclic motions of the floating production unit. The semi-submersible offset governs the maximum von Mises stress at the TDP and the maximum tension at the SCR's top end. The seabed interaction model has an influence on the calculated von Mises stresses. Commercially available software for SCR analysis is mostly limited to calculating the soil's linear or rigid response, although non-linear soil response capabilities are being developed. For example, the case study 0° wave and current direction, intact mooring and near offset gives von Mises utilisation with value of 0.74 when the non-linear soil model is used while a value of 0.61 and 0.8 are introduced in case of employing the linear and rigid surfaces for seabed model respectively. Therefore, the evaluation of the dynamic response depends on the employed soil model. However, the soil parameters govern the behaviour of non-linear soil model and consequently the evaluated global SCR's dynamic response.

Although the results show that the SCR has a sufficient margin for strength performance, it is essential to note that the strength analyses are carried out with the same floating production unit offsets, wave and current data for the near, far and transverse positions and intact mooring lines.

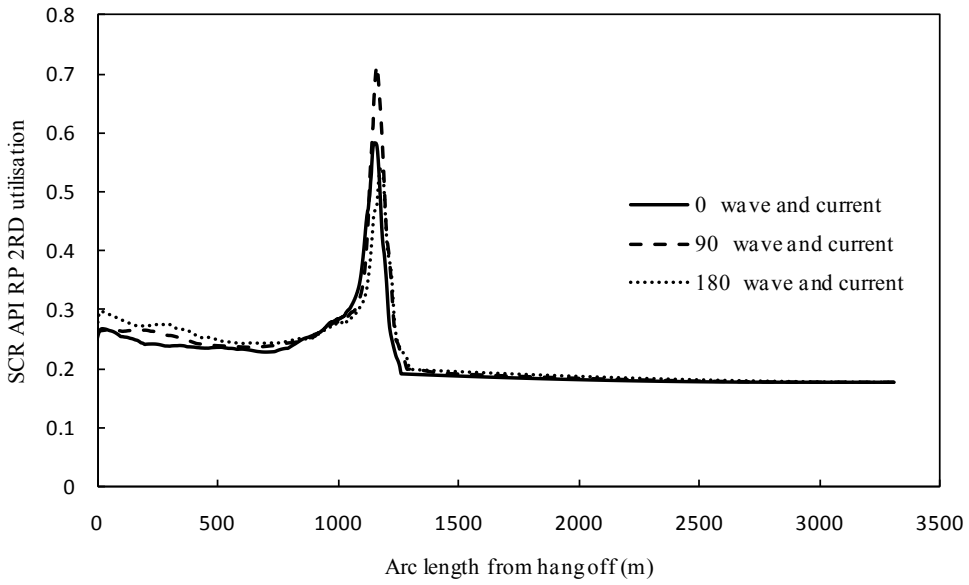

Figure 5.6—2 API RP 2RD utilisation along the SCR arc length in the mean position

5.6.2 Riser–Soil Response

The seabed soil's non-linear response is modelled using a hyperbolic approach and the model parameters are listed in Table 5.6—4. The riser-soil static response, including the penetration, declination angle, bending moment, effective tension, shear force and vertical soil resistance is presented in Figure 5.6—3 as a function of the SCR arc length measured from the floating production unit. The SCR arc length scale is decreased for the penetration and seabed resistance graphs to highlight the zone of seabed contact. The static TDP is located at an arc length of nearly 1083 m in the near load case and 1490 m in the far load case, as measured from the semi-submersible, with a maximum static seabed penetration of 0.018*D* occurring 8 m behind the TDP and

corresponding to the maximum seabed resistance of 3.84*D* kPa, compared with 8.2*D* kPa and 2*D* kPa when rigid seabed and linear seabed surface are employed respectively, at the near load case.

The dynamic pipeline-seabed penetration, expressed as seabed penetration/*D*, and dynamic seabed contact resistance, expressed as seabed resistance/*D*, are shown in Figure 5.6—4 and Figure 5.6—5 for a 3-hour simulation time, a 180° wave and current direction. The initial penetration of 0.01*D* corresponds to a local seabed contact force of 2.42*D* kPa (hence a secant stiffness of k = 2.42/0.01 = 242 kPa). The maximum envelope of the pipeline profile increases to approach a penetration of 0.8*D* at an arc length to the TDP of 1445 m during the cycles of vertical motion. The seabed resistance's maximum envelope approaches a local maximum of 19.4*D* kPa (nearly eight-times the static value of 2.42*D* kPa) compared with seabed resistance with a value of 4.7*D* kPa and 76*D* kPa when linear and rigid seabed are employed respectively, while the minimum seabed resistance/*D* "soil suction resistance/*D*" approaches a value of -9.84*D* kPa.

Table 5.6—3 Non-linear soil model parameters

Parameters	Symbol	Value
Pipe diameter	D	0.273 m
Mudline shear strength (median range)	S_{u0}	2.6 kPa
Shear strength gradient (median range)	S_{ug}	1.25 kPa/m
Saturated soil density	ρ_{soil}	1.5 t/m^3
Power law parameters	a	6.15
Power law parameters	b	0.15

Parameters	Symbol	Value
Normalised maximum stiffness	K_{max}	200
Suction ratio	f_{suc}	0.7
Suction decay parameter	λ_{suc}	0.6
Re-penetration parameter	λ_{rep}	0.3

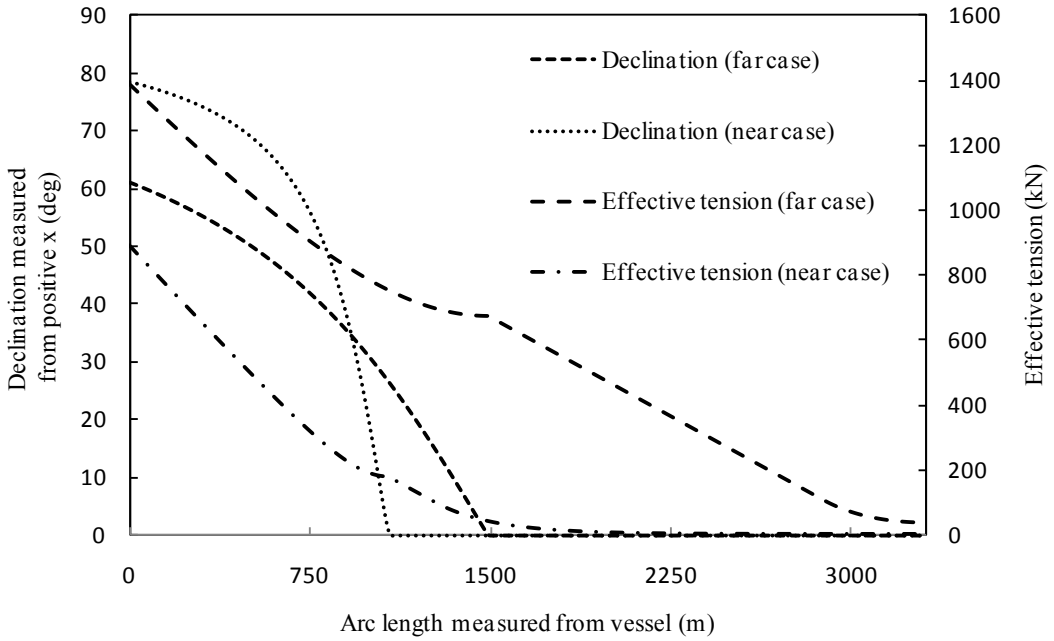

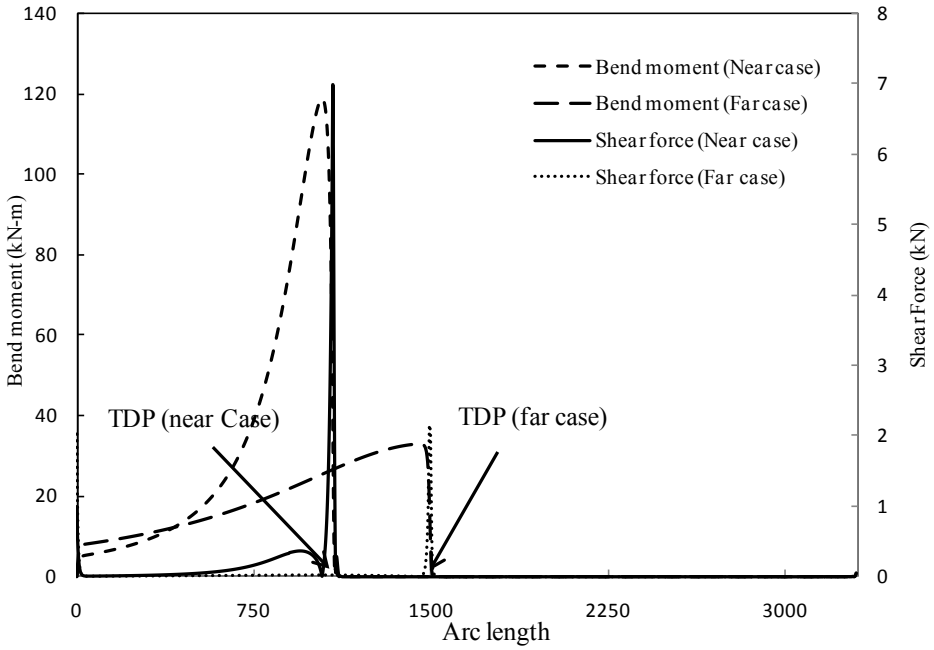

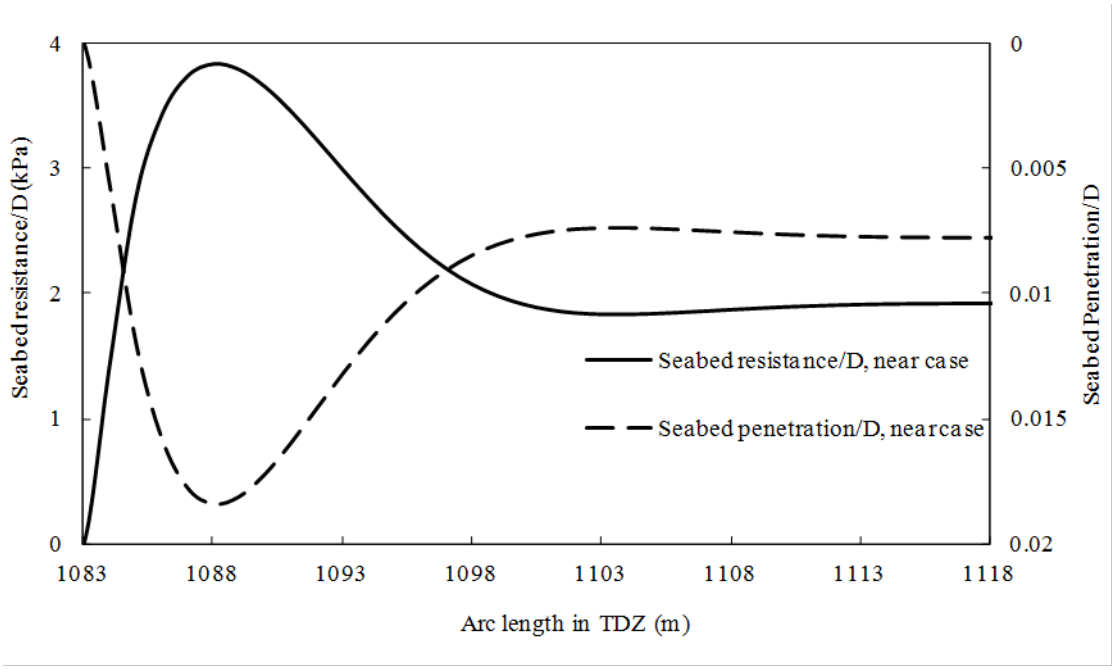

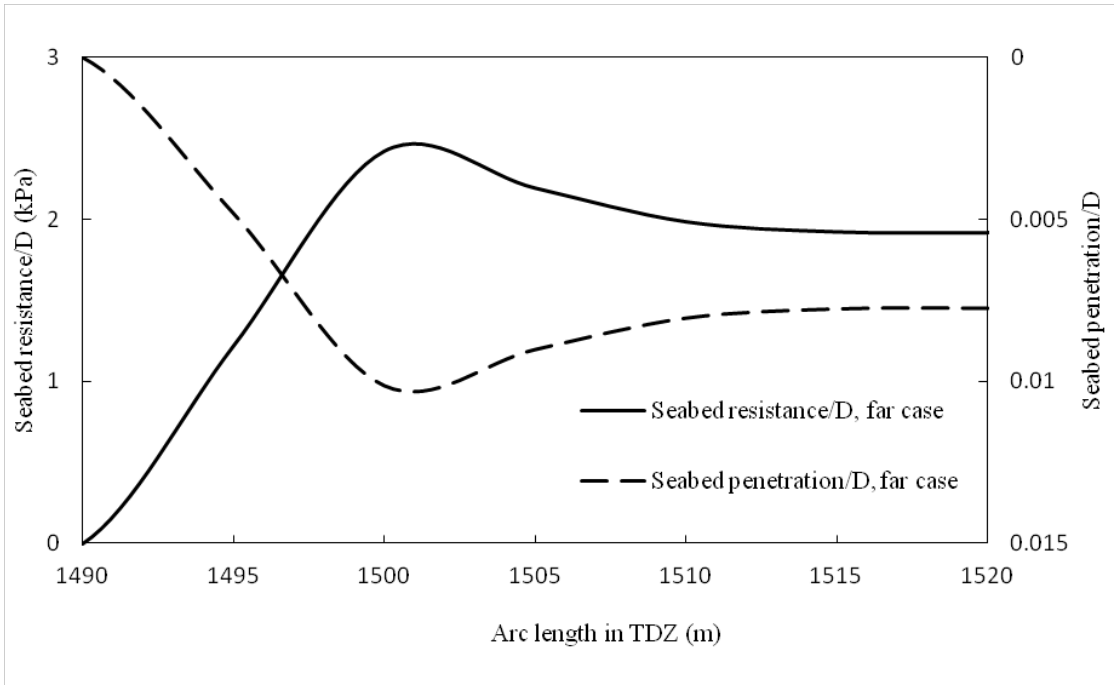

Figure 5.6—3 Riser-soil static response for the 180° wave and current direction

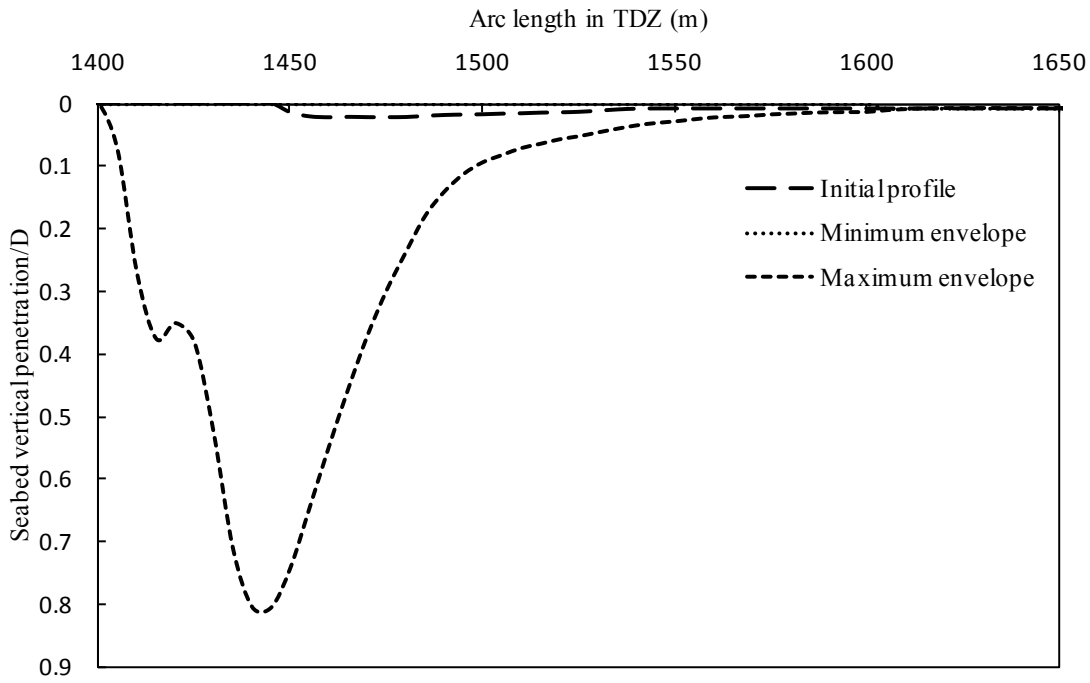

Figure 5.6—4 Dynamic SCR penetration profile in the far load case

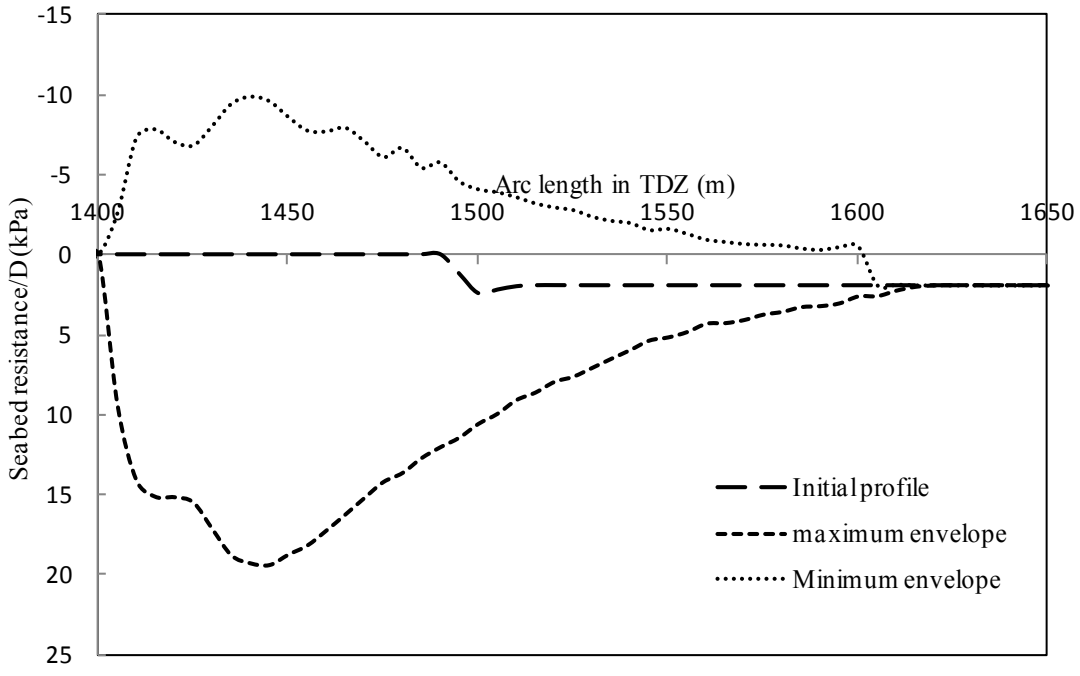

Figure 5.6—5 Dynamic SCR-soil contact resistance in the far load case

Non-linear hysteretic SCR–seabed contact model response

The initial dynamic TDP identified at an arc length of nearly 1400 m, measured from the top end of the SCR at the semi-submersible for the 180° extreme accidental wave and current direction and in the far load case (extreme accidental condition is proven to have sufficient margin for strength performance criteria). Figure 5.6—6 presents the calculated cyclic response at a 1410 m arc length in the TDZ during simulated cyclic motion. The non-linear hyperbolic model, which experiences a delay in rejoining the preceding maximum resistance during re-penetration, produces an incremental embedment of the SCR from an initial penetration of 0.16*D* to a maximum value in excess of 0.8*D* at an arc length of 1445 m. The non-linear soil model captures, as shown in Figure 5.6—6, the varying soil stiffness and soil cyclic degradation, allowing the representation of re-penetration, uplift and suction effects. The dynamic cyclic motions of the SCR within the TDZ increase the SCR's embedment beyond that produced by the static load. The results show evidence of the dynamic SCR's penetration behaviour under cyclic loading.

The seabed stiffness degradation due to cyclic oscillations has a significant influence on the behaviour of the SCR in the TDZ and especially on the SCR's structural dynamic behaviour. After the seabed soil approaches its maximum strength during the applied cyclic loading, the seabed soil tends to lose strength and stiffness with the increase in plastic embedment during the cyclic oscillations. The seabed soil stiffness degradation mechanism can only be

represented by non-linear hysteretic seabed model which is based on experimental results and is comprised of the stiffness reduction presented by the uplift, suction, and separation as well as the re-penetration process. The seabed soil degradation must be involved in the soil modelling efforts to capture the dynamic cyclic loading on the SCR's response. The degradation of the soil stiffness with cyclic loading is best captured by the non-linear seabed model.

The SCR–seabed response in the TDZ follows the general characteristics of non-linear soil behaviour illustrated and the asymptotic merging of the limiting resistances curves $V_u(z)$ and $V_{u\text{-}suc}(z)$ as explained before in Chapter 4. The penetration parameter z for the ultimate resistance limits increases in the penetration motion and decreases in the uplift motion. The ultimate penetration and suction resistance's asymptotic limits are given by $V_u(z) = N_c S_u(z) D$ and $V_{u-suc}(z) = -f_{suc} . V_u(z)$.

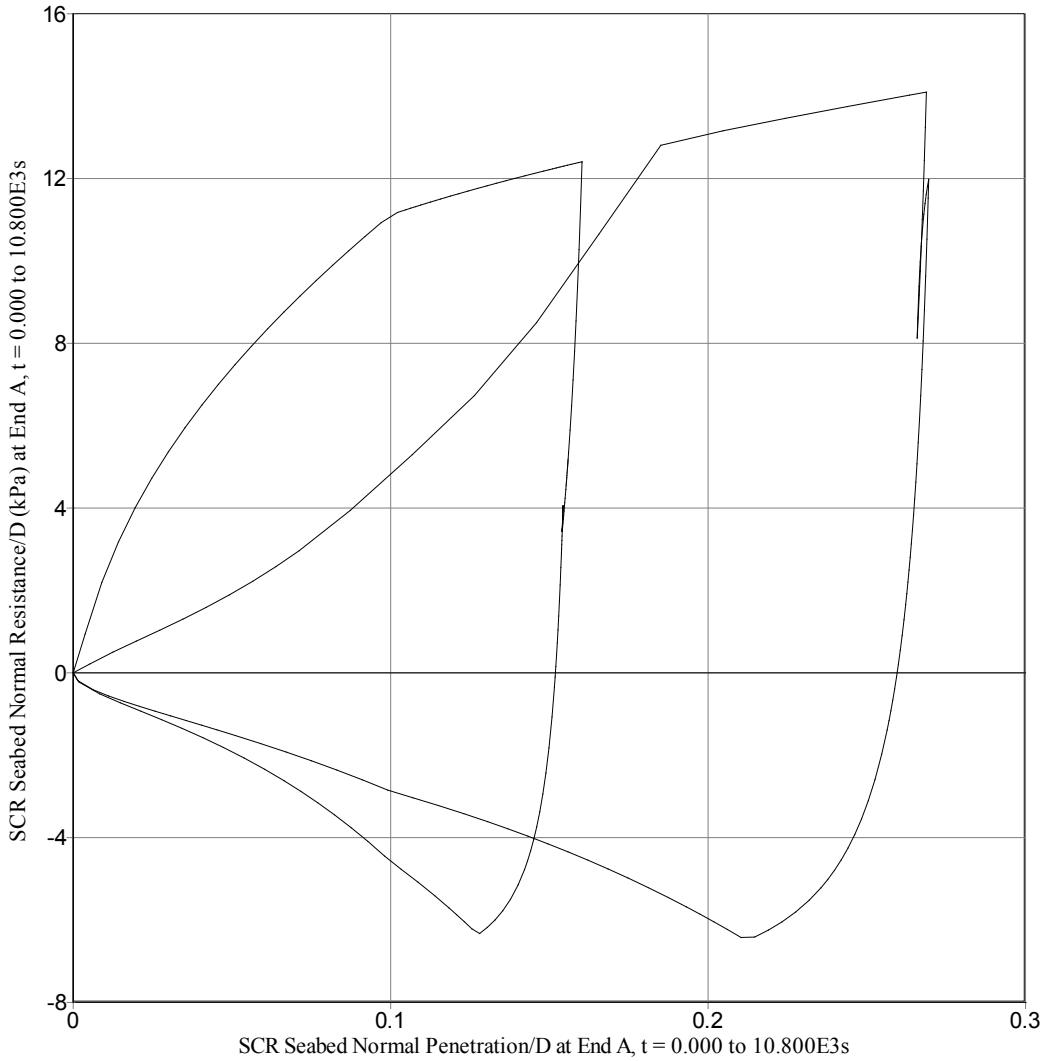

Figure 5.6—6 SCR–seabed interaction response in the TDZ at a 1410 m arc length

5.6.3 SCR–Seabed Lateral Interaction Response

A non-linear seabed soil model is used to investigate the vertical SCR–seabed interaction in soft clay and is integrated with the lateral SCR–seabed interaction models; the Coulomb friction (bilinear) model and the improved (tri-linear) soil model. The SCR is modelled using a coarse mesh in the sag-bend and flow-line

and a finer mesh in the TDZ. The von Mises stress utilisation is shown in Figure 5.6—7 and Figure 5.6—8 for the 100-year combined wave and current and 100-year wave combined with a 10-year current applied, respectively, in the lateral direction (i.e., 90° wave and current directions). The calculated maximum von Mises stress is normalised by the yield stress, being compared with 0.8 times the yield stress for the intact mooring line extreme condition. It is clearly shown that for 100-year wave combined with 10-year current applied in the lateral direction, the difference between biliniear and tri-linear models are negligible, as shown in Figure 5.6—8, while in harsh environment (i.e., 100-year combined wave and currents) the SCR encounters large movements in the TDZ and, therefore, higher von Mises stress due to lateral soil passive resistance, as shown in Figure 5.6—7.

The lateral SCR-seabed resistance models also affect the maximum effective tension along the SCR's arc length, as shown in Figure 5.6—9 for 100-year wave and 10-year current extreme operational condition. Figure 5.6—9 presents the effective tension along SCR by using a non-linear seabed model in vertical direction and bilinear and tri-linear model alternatively for the lateral direction. The effective tension is given by $T_{eff} = T_w - P_i A_i + P_0 A_0$, where T_{w} is the wall tension in the riser pipe, P_{i} is the internal pressure, P_0 is the external pressure and A_{i} and A_0 are the inner and outer areas respectively. The lateral SCR–seabed interaction affects the axial strain of the riser pipe. As the wall tension is a

function of the total axial strain, therefore, the lateral riser movement on the seabed can influence the effective tension.

The model is used to assess the SCR's response by extracting its lateral displacement. This lateral displacement on the seabed, using the severe environmental condition of a 100-year wave combined with a 10-year current, are presented in Figure 5.6—10 and Figure 5.6—11. The analysis is performed using the Coulomb friction model (bilinear soil resistance) and the improved model (tri-linear soil resistance). The lateral oscillation amplitude, y/D, is defined as half of the difference between the maximum and minimum calculated out-of-plane SCR lateral displacements divided by the SCR's diameter, as shown in Figure 5.6—10. For the lateral load case study, the lateral SCR oscillation, y/D, is generally around ±22 within the TDZ when using Coulomb friction model for lateral soil resistance compared with ±29 when using the improved soil model. Figure 5.6—11 shows the influence of bilinear and tri-linear soil models on the specified arc length (1225 m) of the SCR in the TDZ during 3-hour simulation time. The lateral SCR's movement (displacement) in the TDZ obtained with the improved soil model is smaller than that obtained with the Coulomb friction model for the same sliding friction factor (μ=0.2) due to the effect of the passive soil resistance.

Furthermore, the SCR's lateral cyclic oscillation has a significant effect on the soil stiffness in the TDZ. The improved soil model in the lateral direction is essential to model the effects of the load history, soil strength and sliding

resistance on the riser embedment and seabed soil resistance. The influence of the lateral soil models on the riser embedment is shown in Figure 5.6—12. It is shown that the riser's pipe penetration into the seabed is reduced when the soil lateral passive resistance is introduced. The SCR Y-shear force over the entire 3600 seconds simulation in the TDZ is as shown in Figure 5.6—13 for a 100-year wave and current along the positive y-direction with a static vessel offset of 10% of the water depth. The SCR's shear force in the TDZ obtained by using the improved soil model is larger than that obtained with the Coulomb friction model for the same sliding friction factor due to the increase in the seabed resistance (passive resistance). The SCR's displacement and cyclic force/displacement curve are shown at the TDP in Figure 5.6—14, Figure 5.6—15 and Figure 5.6—16 for simulation times ranging from 2040 to 2060 seconds. It is clearly shown that the seabed resistance force is increased while the riser's pipe displacement is decresed when the improved soil model is used, while the riser's pipe displacement is increased and seabed resistance force is decreased when the Coulomb friction model is applied in lateral direction.

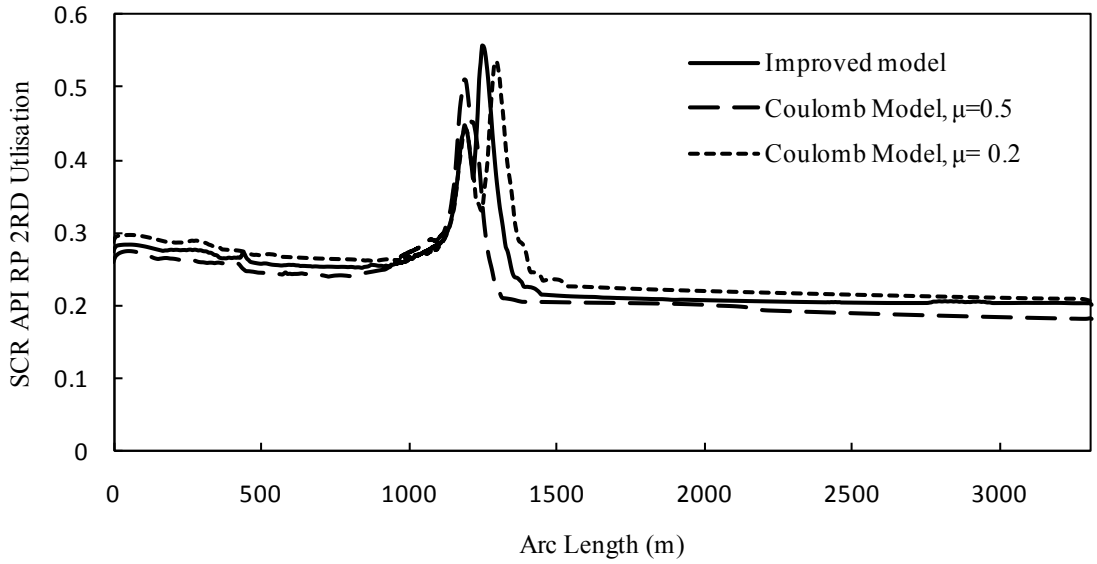

Figure 5.6—7 API RP 2RD utilisation along the SCR (100-year wave/current)

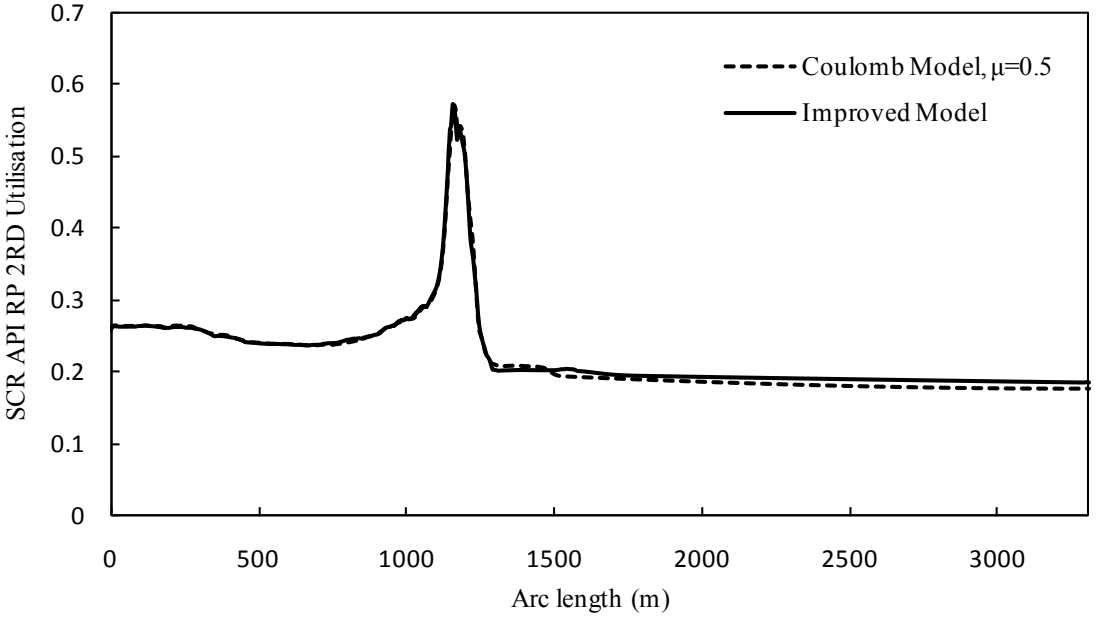

Figure 5.6—8 API RP 2RD utilisation along the SCR (100-year wave and10-year current)

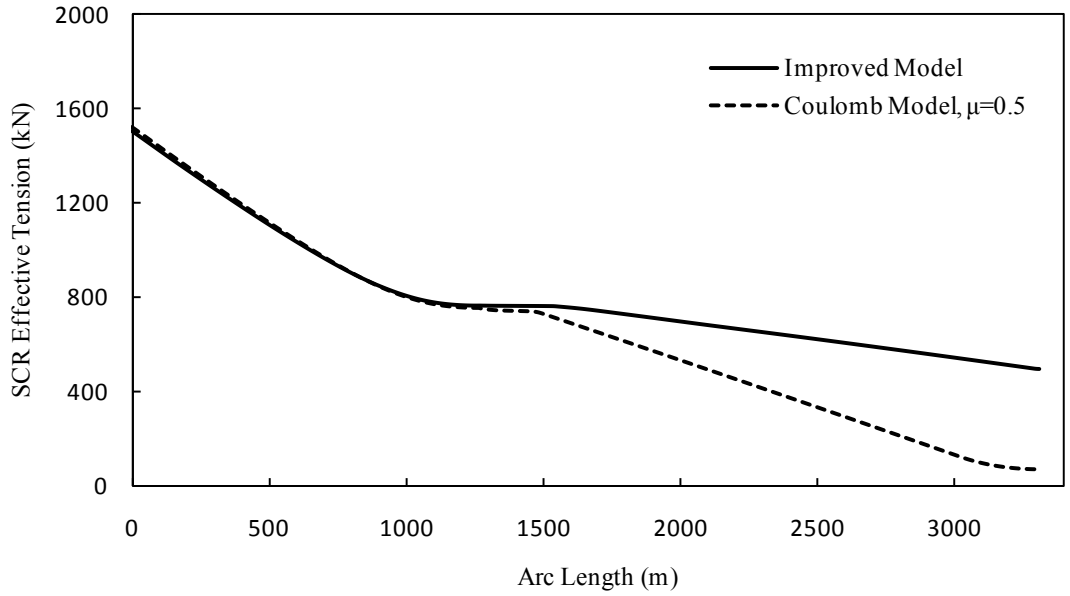

Figure 5.6—9 Maximum effective tension along the SCR for two alternative soil models in lateral direction

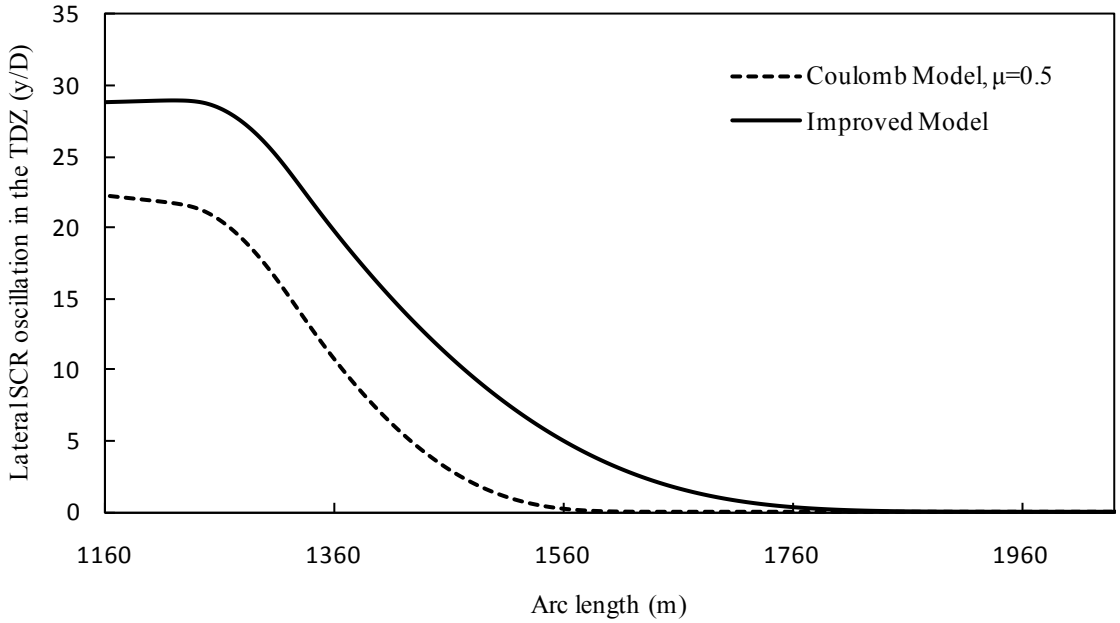

Figure 5.6—10 Dynamic SCR lateral oscillation for beam seas in the TDZ (3-hour simulation)

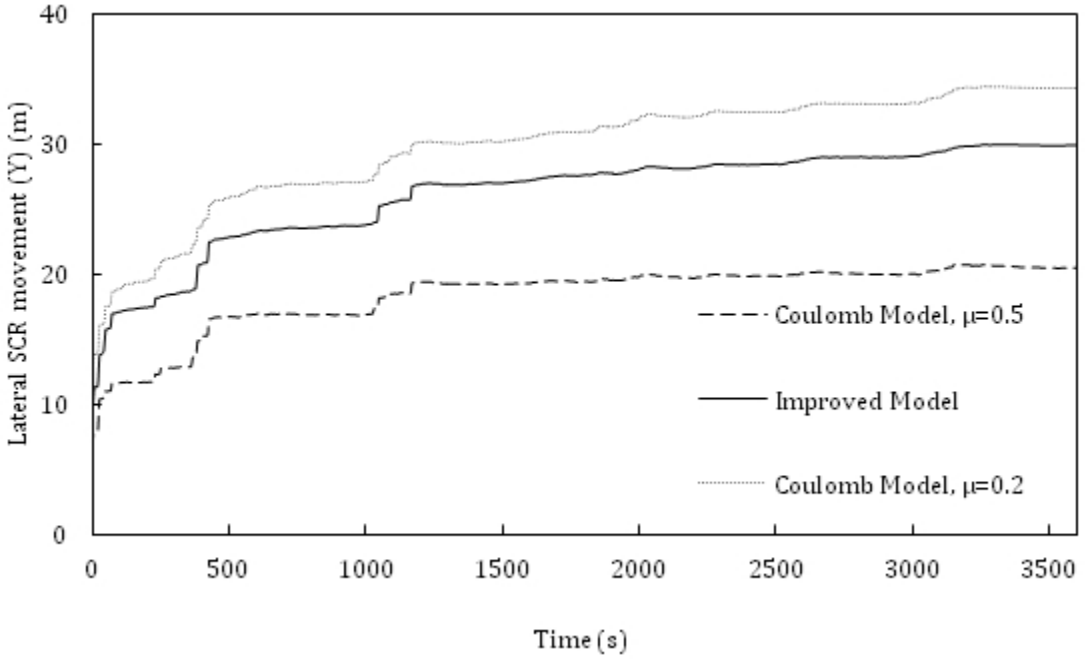

Figure 5.6—11 SCR–seabed lateral interaction at an arc length of 1225m

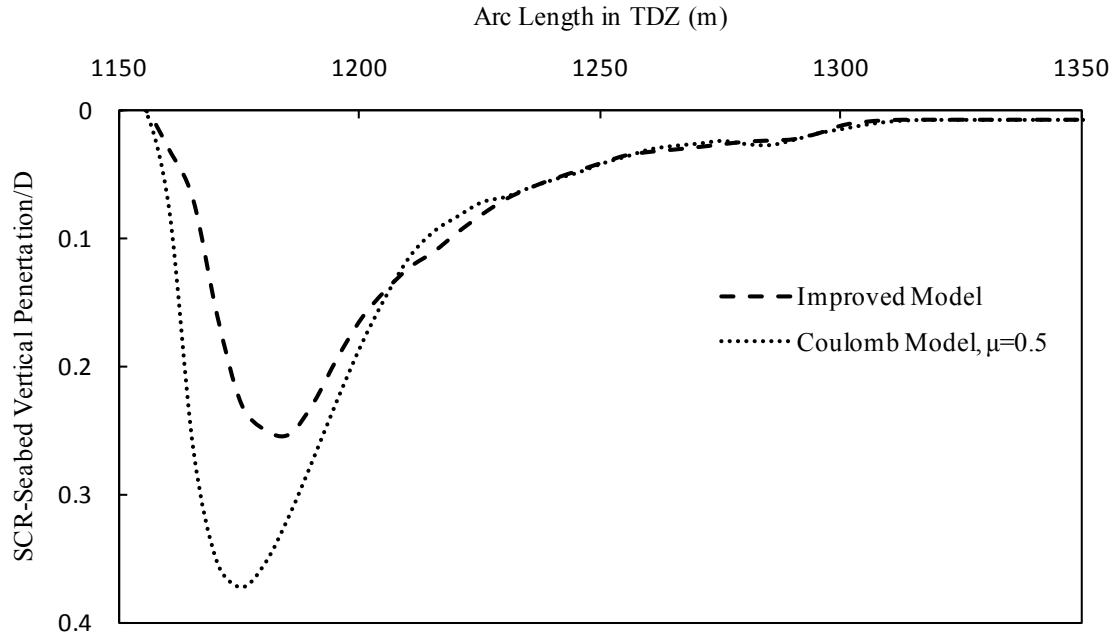

Figure 5.6—12 Influence of the lateral soil models on the riser embedment

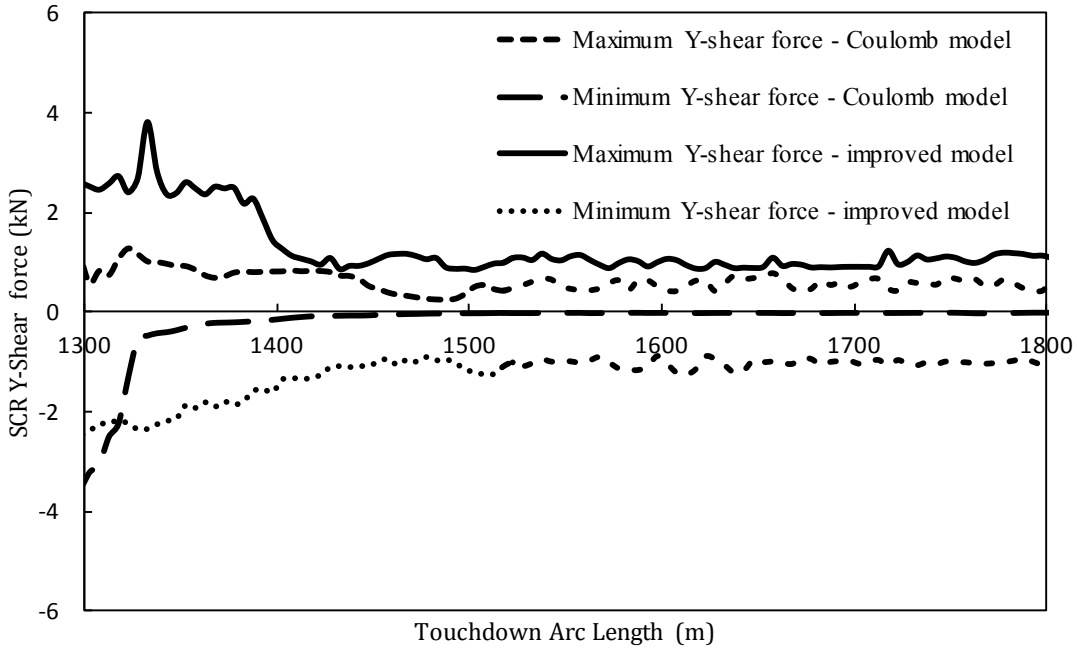

Figure 5.6—13 SCR Y-shear force in the TDZ

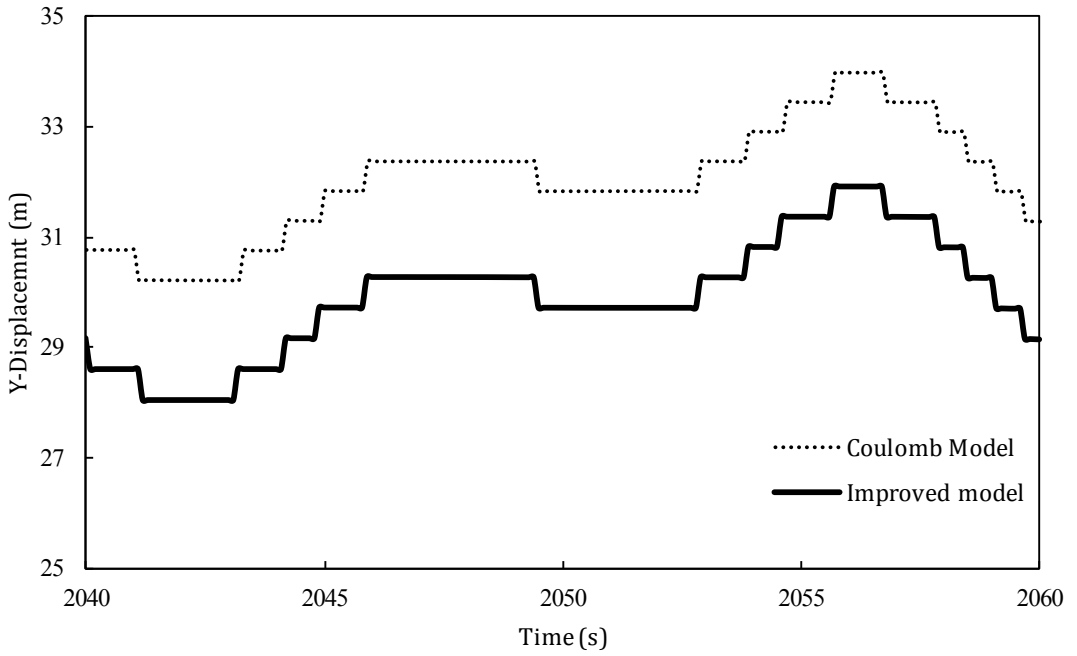

Figure 5.6—14 Y–displacement of SCR at the TDP (t=2040 to 2060 s)

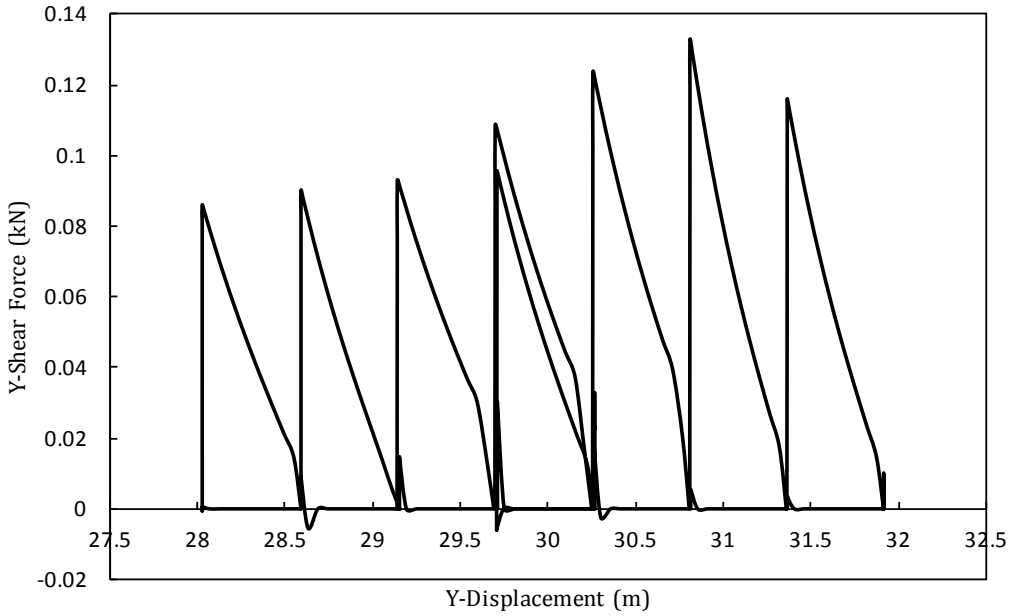

Figure 5.6—15 Cyclic force/displacement obtained with the improved model at the TDP

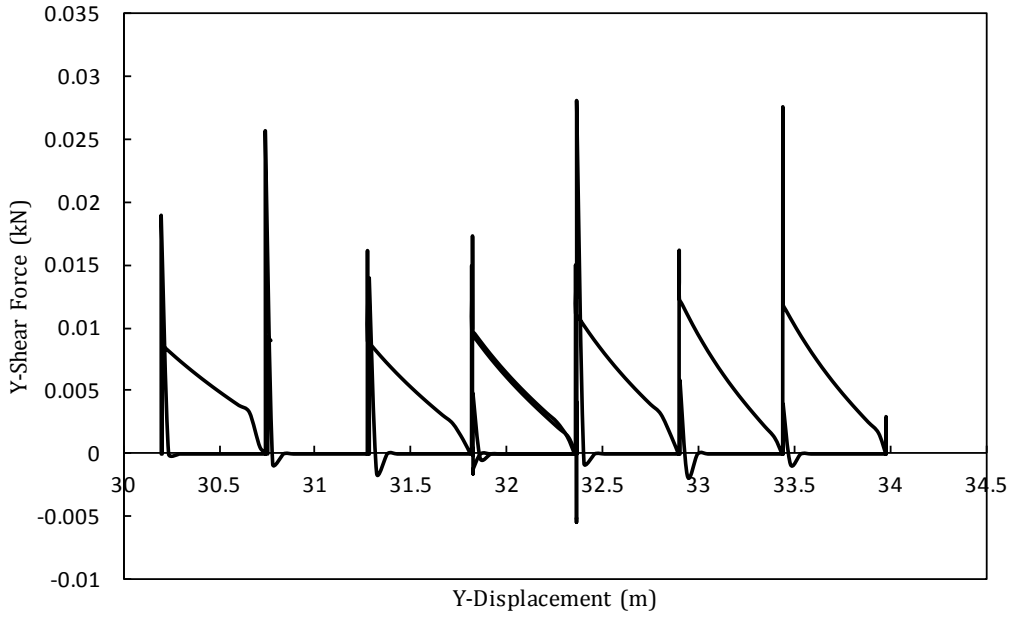

Figure 5.6—16 Cyclic force/displacement obtained with the Coulomb model at the TDP

It has been noted and shown earlier that the difference between the Coulomb (bilinear) model and improved (tri-linear) model approach is the passive resistance part which adds more resistance to the SCR movement on the seabed in lateral direction. This is clearly captured by the developed model, as shown in Figure 5.6—14, which can be considered as primary validation for the developed model. The SCR movement behaviour on the seabed is the same for Coulomb and improved models except additional resistance (due to passive soil resistance) applied to the SCR movement in the lateral direction. The passive resistance effect has experimentally proven before by Wagner *et al.* (1987), Brennodden *et al.* (1989), Bruton (2008), Verley and Lund (1995), and this study developed and applied a lateral soil interaction model to be used for the assessment of SCR dynamic analysis based on a previously developed experimental formula. The developed finite element interaction model is an effort to capture the effects of seabed interaction proved by the experiments and to improve the accuracy of the predicted dynamic response of SCRs in the TDZ numerically, while the previous efforts dedicated for riser–seabed interaction modelling that use rigid or linear soil model in vertical direction and Coulomb friction model in lateral direction.

It is clearly drawn from these results that the dynamic performance of SCR is affected by the vertical and lateral seabed model. Seabed interaction model can influence the accuracy of SCR's dynamic response assessment such as the von Mises stresses, seabed vertical resistance and the maximum effective tension

along SCR. The applied lateral improved model is accounting for the dynamic cyclic loading and involving the influence of riser penetration as well as the lateral soil resistance in the TDZ. Therefore, Coulomb friction (bilinear) soil model is more conservative compared to the improved (tri-linear) model. The adoption of the tri-linear model for lateral seabed interaction modelling, which is proven to be the realistic behaviour of the lateral pipe–soil interaction by previous experiments as shown in Chapter 4, can effectively capture the lateral behaviour of seabed soil and their influences on the global dynamic performance of the SCR.

5.7 Conclusion

This chapter describes a detailed strength analysis of the SCR connected to a semisubmersible in the NNS performed for the extreme operating intact mooring conditions in a harsh environment. The dynamic analysis is performed for wave and current directions of 0°, 180° (in-plane load cases) and 90° (out-of-plane load case). The significance of the SCR–seabed interaction on the global dynamic response of SCR is highlighted. An outline of this study's methodology and results are presented and the SCR flow-line embedment, soil cyclic degradation and lateral movement are discussed.

The SCR–seabed interaction analysis allows for the effects of physical phenomena such as soil suction forces and lateral and vertical seabed stiffness on the SCR's performance to be identified and quantified, and it provides a

better understanding of the SCR–soil–fluid interaction's complex physical process. The non-linear soil model characterise the variation (i.e., degradation) in soil stiffness during the dynamic riser–soil interaction as the seabed soil tends to lose strength and stiffness with an increase in embedment during cyclic oscillations after the seabed approaches its maximum strength during applied cyclic loading. The TDZ response, which involves the degradation of the seabed soil stiffness due to cyclic loading, is addressed by the analyses performed in this study.

This study also highlights potential lateral soil resistance models. The major conclusion identified on the SCR–seabed lateral interaction studies is that the soil's resistance to lateral SCR motions is more complex than that represented by simple Coulomb friction. The techniques that can be used to incorporate these aspects and develop an advanced SCR–seabed lateral interaction model are outlined. Furthermore, these techniques are applied in an FE model that can be used to analyse the lateral SCR–seabed interaction under hydrodynamic loading. Dynamic finite element analysis is performed on the SCR in beam seas during extreme environmental conditions, and various aspects of a dynamic SCR–seabed lateral interaction are investigated. The SCR has sufficient allowances for strength in both the Coulomb friction and improved soil resistance models. The main benefits achieved by applying the improved SCR–seabed interaction model to assess the lateral behaviour of an SCR in the TDZ are as follows:

- The improved tri-linear soil model mimics of a catenary pipeline's soil strength and load history and the associated pipe embedment on the lateral seabed soil resistance.
- It is concluded that the lateral SCR–seabed displacement obtained with an improved tri-linear soil model is smaller than that obtained with a Coulomb friction model due to passive soil resistance. The lateral SCR-soil displacement can affect the SCR's strength performance under extreme environmental conditions.
- Developing a better lateral SCR-soil interaction model improves the prediction of dynamic response of soil stiffness and riser penetration, which affect the global riser dynamic performance in the TDZ.

Furthermore, the improved SCR–soil interaction model, which predicts soil stiffness and riser penetration, enables us to obtain the global riser dynamic performance in the TDZ more accurately. The SCR's dynamic cyclic motions within the TDZ increase the riser penetration beyond that generated by the static case, and the increase in the seabed soil's riser embedment is caused by the cyclic impact of the SCR in the seabed. Riser-soil-fluid interaction modelling analyses minimise the need for expensive experimental facilities and complicated designs. The next chapter investigates the significance of seabed interactions on the fatigue assessment of SCR in the TDZ.

5.8 References

API 1998. API RP 2RD: Design of risers for floating production systems and tension-leg platforms. American Petroleum Institute

Aubeny, C., Biscontin, G. & Zhang, J. 2006. Seafloor interaction with steel catenary risers. Texas: Offshore Technology Research Center, Texas A&M University, College Station, Houston, Final Project Report to Minerals Management Service, OTRC Library Number 9/06A173.

Aubeny, C. P. A. & Biscontin, G. 2009. Seafloor-riser interaction model. *International Journal of Geomechanics,* Vol. 9, No. 3.

Bai, Y. & Bai, Q. 2005. Subsea pipelines and risers, Elsevier Science Ltd.

Barltrop, N. D. P. & Adams, A. J. 1991. Dynamics of fixed marine structures, Butterworth-Heinemann Oxford.

Bitner-Gregersen, E. 2005. Joint probabilistic description for combined seas. *24th International Conference on Offshore Mechanics and Arctic Engineering, OMAE2005-67382.* Halkidiki, Greece: ASME.

Brennodden, H., Lieng, J., Sotberg, T. & Verley, R. 1989. An energy-based pipe-soil interaction model. *Offshore Technology Conference.* Houston, Texas, USA.

Bridge, C., Laver, K. & Clukey, E. Steel catenary riser touchdown point vertical interaction models. *In:* Offshore Technology Conference, OTC 16628, 2004 Houston, Texas.

Bruton, D., White, D., Cheuk, C., Bolton, M. & Carr, M. Pipe/soil interaction behavior during lateral buckling, including large-amplitude cyclic displacement tests by the safebuck JIP. *In:* Offshore Technology Conference, 2006 Houston, USA.

Bruton, D. A. S., White, D. J., Carr, M., and Cheuk, J. C. Y. Pipe-soil interaction during lateral buckling and pipeline walking - the safebuck JIP. *In:* Offshore Technology Conference,OTC 19589, 5-8 May 2008 Houston, Texas.

Cathie, D., Jaeck, C., Wintgens, J. F. and Ballard, J. C. 2005. Pipeline geotechnics - state of the art. *Proc. International Symposium on Frontiers in Offshore Geotechnics (ISFOG).* Perth, Australia.

Deka, D., Campbell, M., Kakar, K. & Hays, P. Advances in deepwater riser technology: Gulf of mexico wet tree deepwater riser concepts with sour service. *In:* Offshore Technology Conference, 2010 Houston, USA.

DNV 2001-amended 2009. DNV-OS-F201: Dynamic risers. Det Norske Veritas.

DNV 2005. Riser fatigue. *Recommended Practice DNV-RP-F204.* Det Norske Veritas.

DNV 2009. DNV-RP-F109: Recommended practice on-bottom stability design of submarine pipelines (with amendments, April 2009).

Faltinsen, O. M. 1999. *Sea loads on offshore structures,* Cambridge, Cambridge University Press.

Giertsen, E., Verley, R. and Schroder, K. 2004. Carisima: A catenary riser/soil interaction model for global riser analysis. *23rd International Conference on Offshore Mechanics and Arctic Engineering, OMAE2004-51345,* Vancouver, British Columbia, Canada.

Leira, B., Holmås, T. & Herfjord, K. 2002. Estimation of extreme response and fatigue damage for colliding risers. *21st International Conference on Offshore Mechanics and Arctic Engineering*, *OMAE 2002-28435,* Oslo, Norway.

Leira, B. J., Passano, E., Karunakaran, D., Farnes, K. A. & Giertsen, E. 2004. Analysis guidelines and application of a riser-soil interaction model including trench effects. *23rd International Conference on Offshore Mechanics and Arctic Engineering, OMAE2004-51527,* Vancouver, British Columbia, Canada.

Orcina 2010. Orcaflex user manual *Orcina,* version 9.4a, UK.

Randolph, M. & Quiggin, P. 2009. Non-linear hysteretic seabed model for catenary pipeline contact. *28th International Conference on Ocean, Offshore and Arctic Engineering, OMAE2009-79259.* Honolulu, Hawaii, USA

Sen, T. K., and Hesar, M. Riser soil interaction in soft clay near the touchdown zone. *In:* Offshore Technology Conference, 30 April-3 May 2007 Huston, Texas, USA. OTC.

Serta, O. B., Petrobras, S. A., Mourelle, M. M., Petrobras, S. A., Grealish F. W., Harbert, S. J. and Souza, L. F. A. Steel catenary riser for the marlim field FPS P-XVIII. *In:* Offshore Technology Conference, 1996 Houston, Texas, 6-9 May.

Thethi, R., and Moros, T. Soil interaction effects on simple catenary riser response. *In:* Proceeding Conference on Deepwater Pipeline & Riser Technology, 2001 Houston, Texas.

Verley, R. & Lund, K. M. A soil resistance model for pipelines placed on clay soils. *In*, 1995. American Society of Mechanical Engineers, 225-225.

Wagner, D., Murff, J., Brennodden, H. & Sveggen, O. Pipe-soil interaction model. *In:* Offshore Technology Conference, April 27-30 1987 Houston, Texas, USA.

White, D. J., and Cheuk, C. Y. 2008. Modelling the soil resistance on seabed pipelines during large cycles of lateral movement. *Marine Structures,* 21**,** 59-79.

Willis, N. R. T., and West, P. T. J. Interaction between deepwater catenary risers and a soft seabed: Large scale sea trials. *In:* Offshore Technology Conference, 2001 Houston, Texas OTC 13113.

Xia, J., Das, P. K. & Karunakaran, D. 2008. A parametric design study for a semi/scr system in northern north sea. *Ocean Engineering***,** Ocean Engineering35(2008)1686–1699.

CHAPTER 6

FATIGUE PERFORMANCE OF SCR IN THE TDZ AND EFFECTS OF KEY PARAMETERS

6.1 Introductory Remarks

Challenges regarding SCR fatigue damage assessment in the TDZ are primarily due to non-linear behaviour of SCR–seabed interaction, considerable uncertainty in SCR–seabed interaction modelling, and geotechnical parameters. Since the SCR–seabed response is critical for reliable estimation of the fatigue life in the TDZ, it is significant to develop a better understanding of the SCR–soil interaction mechanism and to provide a realistic technique for determining strength behaviour and fatigue performance in the TDZ.

Several studies have focused on understanding the SCR–seabed interaction (e.g., Aubeny and Biscontin (2009), Aubeny *et al.* (2006), Willis (2001), Bridge and Willis (2002), Bridge and Howells (2007) and Thethi and Moros (2001)). The interaction of the SCR with the seabed is not fully understood. However, the seabed response can be depicted from SCR field observations or large-scale tests (Cardoso and silveira, 2010, Clukey *et al*., 2008, Willis, 2001, Bridge and Willis, 2002). As noted earlier, present SCR models represent the seabed by means of a rigid surface (Palmer, 2008) or linear springs (Xia *et al.*, 2008, Grealish *et al.*, 2007, Karunakaran *et al.*, 2005) disregard the non-linearity nature of seabed interaction in the TDZ. Recently, a number of vertical non-linear soil models have been suggested by Aubeny and Biscontin (Aubeny and Biscontin, 2009) and Randolph and Quiggin (Randolph and Quiggin, 2009), which are based on the experimental results and the analytical models.

Recently, despite the fact that research studies on fatigue assessment of SCRs in the TDZ have presented a reduction in fatigue damage (Sharma and Aubeny, 2011, Langner, 2003, Nakhaee, 2008) due to riser embedment in the TDZ, other studies have proposed an increase in fatigue damage (Giertsen, 2004, Leira *et al*., 2004). These confounding results are due to different geotechnical parameters imposed with the developed trenches.

The non-linear seabed model, as well as the influence of the trench shape, is typically ignored in the traditional SCR design analyses. This is due to uncertainty as to how the non-linear soil model will affect the SCR fatigue performance in the TDZ and also geotechnical parameters, which can lead to conservative fatigue damage. Therefore, the seabed parameters used in SCR analysis can have a significant influence on the global riser response and the fatigue life in the TDZ. In addition, the interaction model should have sufficient accuracy to give a reliable estimate of SCR's fatigue life in the TDZ.

This chapter discusses the significance of SCR–seabed soil interaction on the fatigue life of SCRs in the TDZ as it relates to the design of SCRs for deepwater developments. It also details the analyses of an SCR on soft clay in a 910 m depth of water. The SCR–seabed interaction is investigated using an non-linear time domain finite element model along with a robust meshing technique. This study investigates the sensitivity of fatigue performance to geotechnical parameters using the non-linear soil model presented in Chapter 5. Numerical

results for parametric study of the fatigue performance of SCRs in the TDZ are presented here. Successions of numerical analyses of an SCR/semisubmersible in an irregular sea are performed. These are accompanied by a hysteretic non-linear model in the vertical seabed direction as well as bilinear (e.g., White (2008), Wagner *et al*. (1987), Brennodden *et al*. (1989) and Lyons (1973)) and tri-linear (e.g., Verley and Lund (1995), Wagner *et al*. (1987), Brennodden *et al*. (1989) and Bruton *et al*. (2006)) soil model alternatives in the lateral seabed direction. The reason for these analyses is to examine how the main seabed soil parameters influence the fatigue performance of SCRs in the TDZ.

Vertical embedment and large lateral movements of the SCR in the TDZ are investigated. Parametric studies for fatigue performance in the TDZ are conducted by examining the effects of lateral, vertical linear and non-linear seabed models. The main non-linear soil model parameters considered are normalised maximum stiffness, soil suction resistance ratio, normalised re-penetration offset parameter and trenching effects. This study summarises how these parameters affect the fatigue performance of SCRs in TDZ. It has been found that the type of seabed model and geotechnical parameters have a substantial influence on the fatigue performance in the TDZ.

6.2 SCR Fatigue Evaluation Methodology

6.2.1 Background

In the design and analysis of SCRs, different limit states should be investigated. The fatigue limit state is one of these limit states that should be carefully considered in the analysis of SCRs. Fatigue load is the progressive and localised structural damage that a material experiences when subjected to a cyclic stress loading history. Fatigue failure is more likely to occur in SCRs and is usually one of the most challenging design considerations because they are exposed to sea waves that involve a great number of fluctuating loads during the service lifetime of the structure. The fluctuating loads can cause fatigue damage at a stress level usually well below the design allowable of the material. Fatigue failure is a progressive failure process that, unless detected and remedied, can affect the component reliability of SCRs and can lead to a catastrophic rupture. Therefore, the fatigue analysis should be included in the SCR analysis.

Wave loading fatigue can significantly affect the total fatigue performance through wave-induced floating platform motions. The fatigue damage of SCRs is mainly due to the random sea-state waves. The resulting stresses and the corresponding structural dynamic response due to environmental loading are random in nature, as shown in Figure 6.2—1. Generally, the greatest wave loading fatigue damage of SCRs occurs in the wave zone (near to vessel/riser interface) and at the TDP on the seabed. Each sea-state is performed using

virgin seabed clay. The evaluation of fatigue performance of SCRs should be conducted through dynamic analyses of load cases considering the environmental loading and fluid/riser/soil interaction. This allows the determination of the long-term time history of local stresses at different points of the structure (hot-spots).

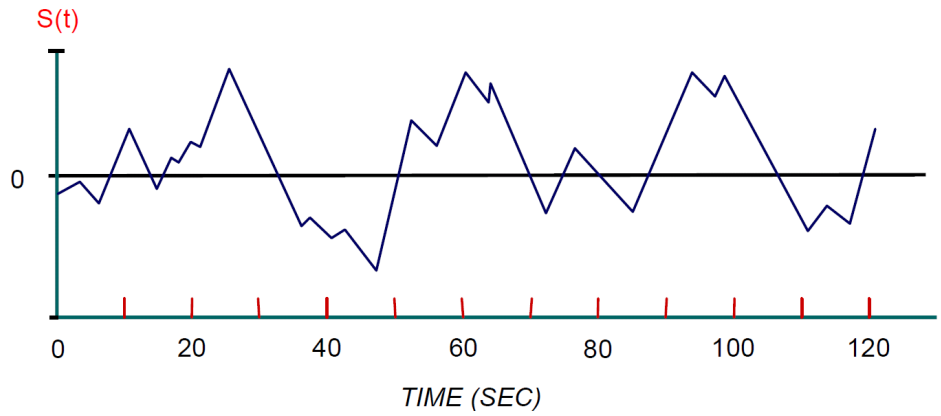

Figure 6.2—1 SCR stress simulation

Stress amplitudes (defined by the difference between successive peaks and valleys in the time response) are subdivided into intervals; each interval of stress amplitude is associated with the number of observed cycles. A probability distribution can then be recognised for each stress cycle, and the estimation of the fatigue life can be performed either through fracture mechanics or through a procedure based on *S-N* curves and Miner's rule, see Figure 6.2—2. The Fracture mechanics approach (crack propagation phase) is used for the monitoring of the crack growth and is more appropriate for the assessment of

specific defects and for inspection planning calculations (i.e., estimates a time history of crack length), while the *S-N* curves approach is indicated for the estimation of overall life of the structure (crack initiation phase) and is the main focus of this study.

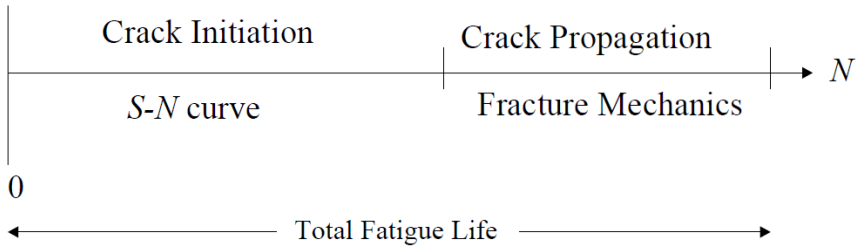

Figure 6.2—2 Comparison between *S-N* and fracture mechanics approach (Ayyub *et al.*, 2002)

6.2.2 *S-N* Fatigue Approach

S-N curves are derived from tests on samples of the material to be characterised where a regular sinusoidal stress is applied by a testing machine, which also counts the number of cycles to failure. The resulting *S-N* curves are presented as a straight line on the log-log scale. The *S-N* fatigue approach is based on the assumption that the fatigue damage accumulation is a linear phenomenon (i.e. follows Miner's rule), as shown in Figure 6.2—3. The high cycle range of fatigue life is approximately above 10^5 cycles, which is usually for marine structures. *S-N* data in the high cycle range tends to follow a log-linear relationship. *S-N*

curves are typically given as straight lines on a log-log scale, as shown in Figure 6.2—4.

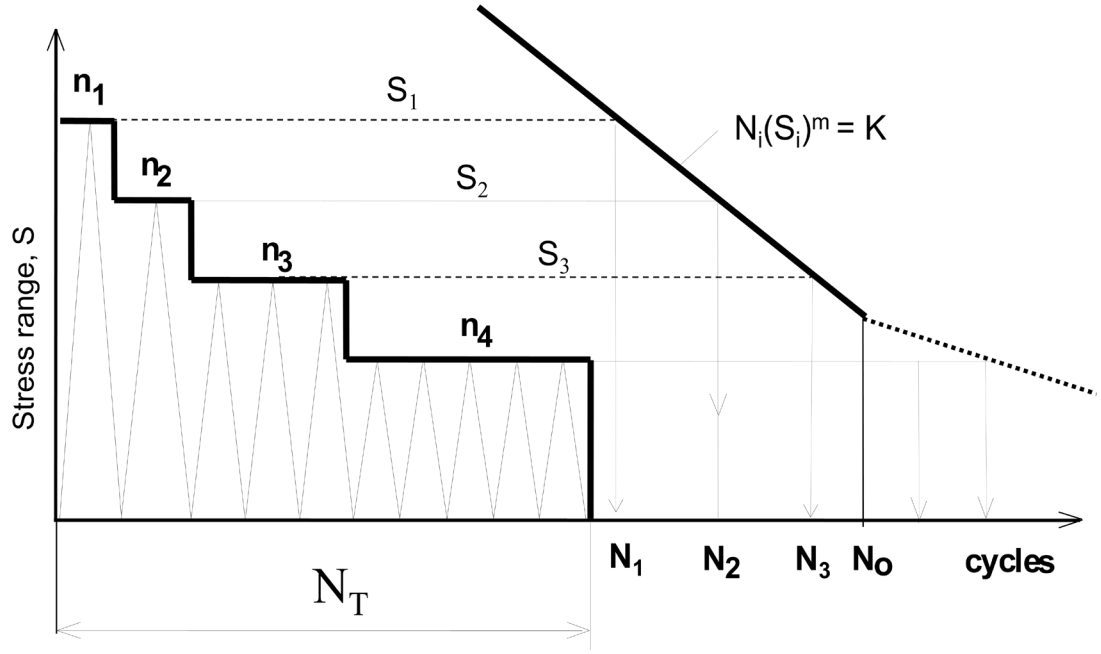

Figure 6.2—3 Procedure for fatigue damage calculation

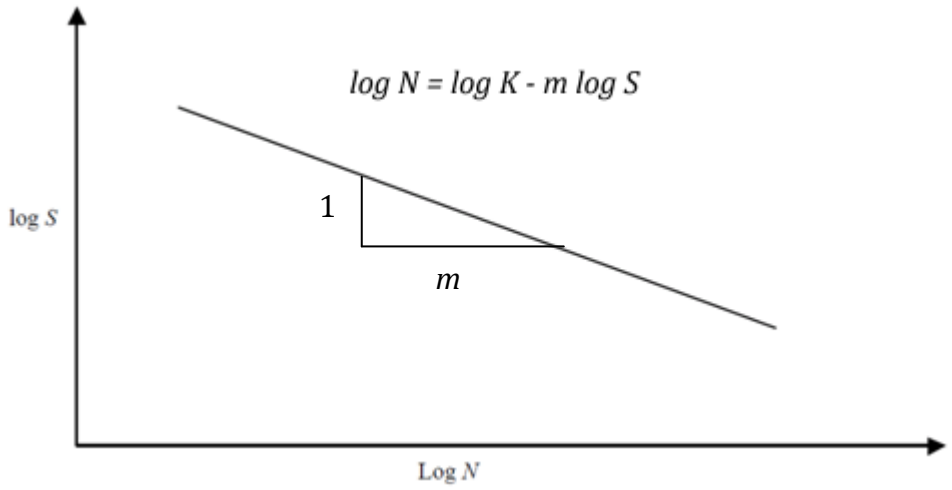

Figure 6.2—4 S-N relationship for fatigue (one slope)

Miner's rule is adopted for accumulation of fatigue damage from stress cycles with variable range:

$$D_{fat} = \frac{n_1 \; cycles \; applied \; at \; S_1}{N_1 \; cycles \; to \; failure \; at \; S_1} + \frac{n_2 \; cycles \; applied \; at \; S_2}{N_2 \; cycles \; to \; failure \; at \; S_2} \ldots + \ldots \frac{n_i \; cycles \; applied \; at \; S_i}{N_i \; cycles \; to \; failure \; at \; S_i}$$

Equation 6.2—1

We can rewrite it as:

$$D = \sum_i \frac{n(S_i)}{N(S_i)}$$

Equation 6.2—2

where $n(S_i)$ is the number of stress cycles with range S_i; $N(S_i)$ is the number of stress cycles to failure. $N(S_i)$ is usually determined from *S-N* curves, which depend on the material. A typical *S-N* curve is shown in Figure 6.2—5.

The basic fatigue capacity is given in terms of *S-N* curves showing the number of stress cycles to failure, *N*, for a given constant stress range, *S*:

$$N = K.S^{-m}$$

Equation 6.2—3

or equivalently, the linear form is:

$$\log(N) = \log(K) - m\log(S)$$

Equation 6.2—4

where K and m represent the fatigue strength coefficient and fatigue strength exponent respectively, both empirical constants are based on experiments; log K is the intercept of log N-axis by S-N curve and N is the predicted number of cycles to failure for stress range S.

The stress range to be used in fatigue damage calculations is found by the application of a stress concentration factor as well as a thickness correction factor to the nominal stress range:

$$S = S_0 \; SCF\left(t_{fat} / t_{ref}\right)^k$$

Equation 6.2—5

where S_0 is the nominal stress range; SCF is the stress concentration factor; $\left(t_{fat} / t_{ref}\right)^k$ is the thickness correction factor; t_{fat} is the average representative pipe wall thickness; $t = t_{\text{ref}}$ is used for thickness less than t_{ref}; t_{ref} is the reference wall thickness equal to 25 mm for welded connections, whilst k is the thickness exponent and is related to the S-N curve (DNV, 2010, DNV, 2005).

Bilinear *S-N* curves in the log-log scale are usually used for representation of the experimental fatigue capacity data, i.e.

$$N = \begin{cases} K_1 . S^{-m_1} & S > S_{SW} \\ K_2 . S^{-m_2} & S \le S_{SW} \end{cases}$$

Equation 6.2—6

where m_1 and m_2 are fatigue exponents (the inverse slope of the bi-linear *S-N* curve) and K_1 and K_2 are characteristic fatigue strength constant defined as the mean-minus-two-standard-deviation curve. S_{sw} is the stress at intersection of the two S-N curves, see Figure 6.2—5, given by

$$S_{SW} = 10^{\left[\frac{\log(K_1) - \log(N_{SW})}{m_1}\right]}$$

Equation 6.2—7

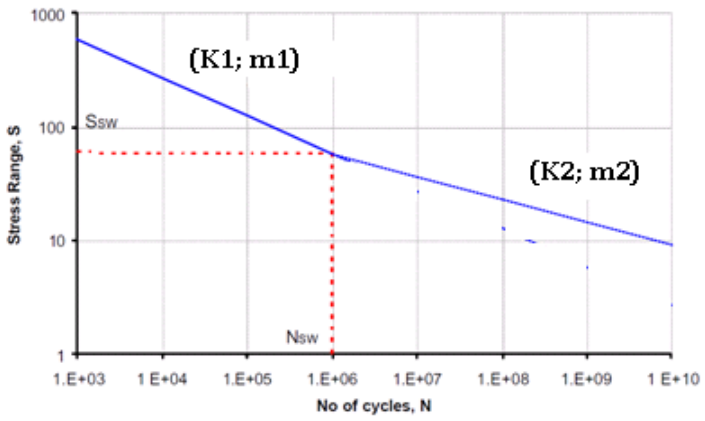

Figure 6.2—5 Basic definition of bi-linear *S-N* curve (DNV, 2010)

6.2.3 Selection of *S-N* Curve

Different *S-N* curves for SCRs have been suggested by design codes for design and installation of offshore structures, such as DNV (2010), DNV (2005) and API (2000). These curves are considered to be conservative (Cao, 2010) and represent the lower bound *S-N* curves for SCR application due to restricting fabrication tolerances, welding procedures, and applied NDT, compared to ordinary offshore steel structures. Table 6.2—1 summarises the most suitable *S-N* curves for SCR fatigue in deepwater. However, it should be noted that the new DNV *S-N* curves are bi-linear (double slopes), which estimate much better fatigue life of SCRs.

Table 6.2—1 Suitable *S-N* curves for SCRs in deepwater

***S-N* Curve**	***m***	**log (*K*) for S_i in MPa**
API X' (API, 2000)	3	10.34
DNV-C-Seawater with Cathodic protection (DNV, 2010)	3 ($N \leq 10^6$ cycles)	12.192
	5 ($N > 10^6$ cycles)	16.32

6.2.4 Determination of Stress Concentration Factor (SCF)

SCF is typically due to the presence of weld (local geometry) and structural detail fabrication (global geometry). The effect of the former together with the residual stress and properties in the heat-affected zone is reflected in the *S-N*

curve to a certain extent. SCFs are component- or detail-specific linear factors that can then be applied to the calculated average component stresses to give local stress values corresponding to particular details within the component. SCF at SCR girth welds arise from geometrical misalignments when pipes are fitted together. SCFs are calculated to consider this mismatch. The determination of SCFs has a significant effect on the fatigue results. The SCF induced by the local axial misalignment, *e*, can be estimated. An empirical formulation based on data fitting is often used (Cao, 2010) and is given as follows:

$$SCF = 1 + 2.6\frac{e}{t_1}\left[\frac{1}{1 + 0.7\left(\frac{t_2}{t_1}\right)^{1.4}}\right]$$

Equation 6.2—8

where t_1 is the wall thickness (thinner tube); t_2 is the wall thickness (thicker tube); and *e* is the pipe eccentricity and is defined as $e = OOR + \frac{t_{thick} - t_{thin}}{2}$, *OOR* is the OD_{max}-OD_{min}. The determination of SCFs has a significant influence on the fatigue results. SCF = 1.0 was suggested with C – *S*-*N* curve by DNV (2010).

6.2.5 Selection of Fatigue Safety Factor

The development of offshore fields moved towards deeper waters where access for structural inspection was practically eliminated. The consequence of SCR failure has been alerted in terms of oil and/or gas stoppage and economic influence, increase the demand for employing fatigue safety factor. The fatigue criterion, which shall be satisfied and can be written as, $D_{fat}.DFF \leq 1$ where D_{fat} is the accumulated fatigue damage (Miner's rule); and *DFF* is the Design Fatigue Factor as shown in Table 6.2—2. SCRs are considered to be non-inspectable; therefore a fatigue life of 20 year service life with a safety factor of 10 (200 year) is required as specified by DNV (2005) and API (1998).

Table 6.2—2 Design Fatigue Factors DFF

Safety class	Low	3.0
	Normal	6.0
	High	10.0

6.3 Wave Loading Fatigue Analysis Technique

Non-linear time domain finite element model is used to analyse semisubmersible and SCR motions. The environmental data input into the analysis is based on a typical NNS scatter diagram. A non-linear seabed model

has been employed as it models the dynamic behaviour of the vertical SCR–seabed interaction on soft clay more precisely than a linear seabed model.

In this Chapter, comprehensive non-linear time domain fatigue analyses are carried out. The SCR dynamic response is established by performing non-linear dynamic response analysis using random irregular waves. Fatigue damage is calculated for the homogenous pipe using a specified *S-N* Curve and rainflow cycle counting see Appendix C. The time domain fatigue analysis procedures are described in Table 6.3—1.

Table 6.3—1 Outlines of time domain fatigue analyses

Procedure	**Depiction**
	Fatigue analyses (OrcaFlex)
Step 1	Divide all wave scatter diagram into a number of representative blocks.
Step 2	A non-linear time domain analysis is carried out for one representative sea state for each of these blocks.
Step 3	For each load case, the time history of response is calculated at the fatigue point, σ_{zz} = Direct tensile stress + Bending stress.
Step 4	Fatigue damage value is calculated corresponding to the time history of response within each load case using rainflow counting procedure.
Step 5	The load case damage values are scaled to allow for the exposure associated with that load case.
Step 6	Finally, these total exposure load case damage values are summed over all load cases to obtain the overall total damage value at that fatigue point, expressed as: $D_{fat} = \sum_{i=1}^{N_s} D_i P_i$

Procedure	Depiction
	Fatigue analyses (OrcaFlex)
	where D_{fat}: Long-term fatigue damage, N_s: Number of blocks of sea-state, D_i: Short-term fatigue damage, and P_i: Sea-state block probability. In this study only 1st order wave effects have been included.

6.4 Case Study Description and Fatigue *S-N* data

The model characteristics and vessel RAOs are fully described in Chapter 5. In practical fatigue calculations for SCRs, the total fatigue damage is the combined damage from first order wave effects, vessel drift motions and VIV, which are analysed dynamically in the time or frequency domain. As noted earlier, the present study considers the effects of the seabed interaction on fatigue performance rather than an accurate estimation of the total fatigue damage. As such, the fatigue analyses have been simplified by considering only the first order wave effects of the semi-submersible in order to clarify clear trends for different soil response parameters. SCR base case as follows;

Configuration	Lateral load case, 90° wave direction
Vessel offset	Mean position
SCF	1.0
S-N curve	DNV-C-Seawater with cathodic protection, see Figure

6.4—1

Sea-state scatter diagram — Northern North Sea

In this study, a series of numerical analyses over a total time simulation length of 3 hr (10800 s) is used for every sea state block. The reduced fatigue bins are initiated from the scatter diagram, presented in Appendix E, by using cubic weighted stress range to save the excessive computation time. Therefore, a cubic weighted mean significant wave height, H_{s3}, will cause the same damage as all the different significant wave heights if $(H_{s3})^3\left(\sum_{i=1}^{NSWH} n_{cycles}\right) = \sum_{sea-state,\,j} n_{cycles}$, where *i=1, 2, 3,…,NSWH*) and *NSWH* is the number of significant wave height during sea state '*j*'. The simplified sea state fatigue blocks are shown in Table 6.4—1. The non-linear soil model parameters used are given in Table 6.4—2.

Table 6.4—1 Sea-state fatigue bins

No.	H_s (m)	T_P (s)	Probability (%)
1	1.32	4.5	3.14
2	2.23	7.5	29.09
3	3.43	10.5	41.82
4	4.54	13.5	22.05
5	5.17	16.5	4.43
6	4.25	19.5	0.43
7	2.91	22	0.04

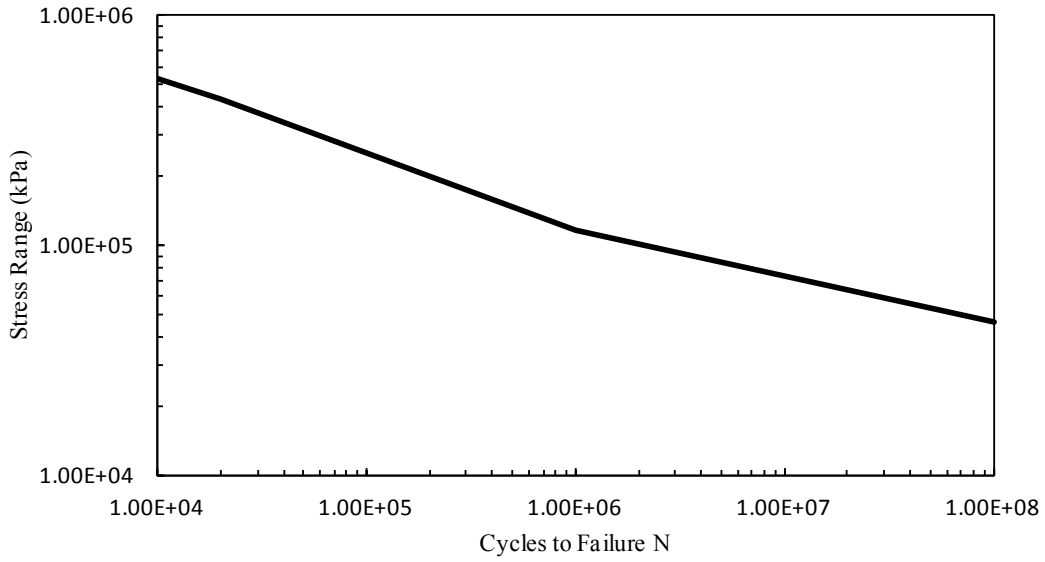

Figure 6.4—1 *S-N* curve (DNV- C – in seawater with cathodic protection)

Table 6.4—2 Non-linear soil model parameters

Parameters	Symbol	Value
Pipe diameter	D	0.273 m
Mudline shear strength (median range)	S_{u0}	2.6 kPa
Shear strength gradient (median range)	S_{ug}	1.25 kPa/m
Saturated soil density	ρ_{soil}	1.5 t/m^3
Power law parameters	a	6.15
Power law parameters	b	0.15
Normalised maximum stiffness	K_{max}	200
Suction ratio	f_{suc}	0.7
Suction decay parameter	λ_{suc}	0.6
Re-penetration parameter	λ_{rep}	0.3

6.5 Results and Discussion – Parametric Study for Fatigue Performance of SCR in the TDZ

6.5.1 Effects of stress concentration factor (SCF)

SCF values can be applied to the calculated stresses to give the local stress value as described before in Equation 6.2—5. This factor depends on the eccentricities, which are presented at each joint during fabrication, as well as pipe wall thickness, *t*. Generally, the eccentricity is assumed to be equal to $\pm$ 10% of '*t*' (Sen, 2006). Therefore, SCF values range from 0.8 to 1.2 are used to investigate their influence on the fatigue life, see Figure 6.5—1. The determination of SCF has a significant effect on the predicted fatigue life. The fatigue life of SCR in the TDZ is decreased with the increase in SCF value. SCF = 1.0 is suggested by *SN* curve C (DNV, 2010). In case of SCF = 0.8, the fatigue life is increased to a value of 494 years (roughly +200% increase) and in case of SCF = 1.2, the fatigue life is decreased to a value of 65 years (roughly – 60%).

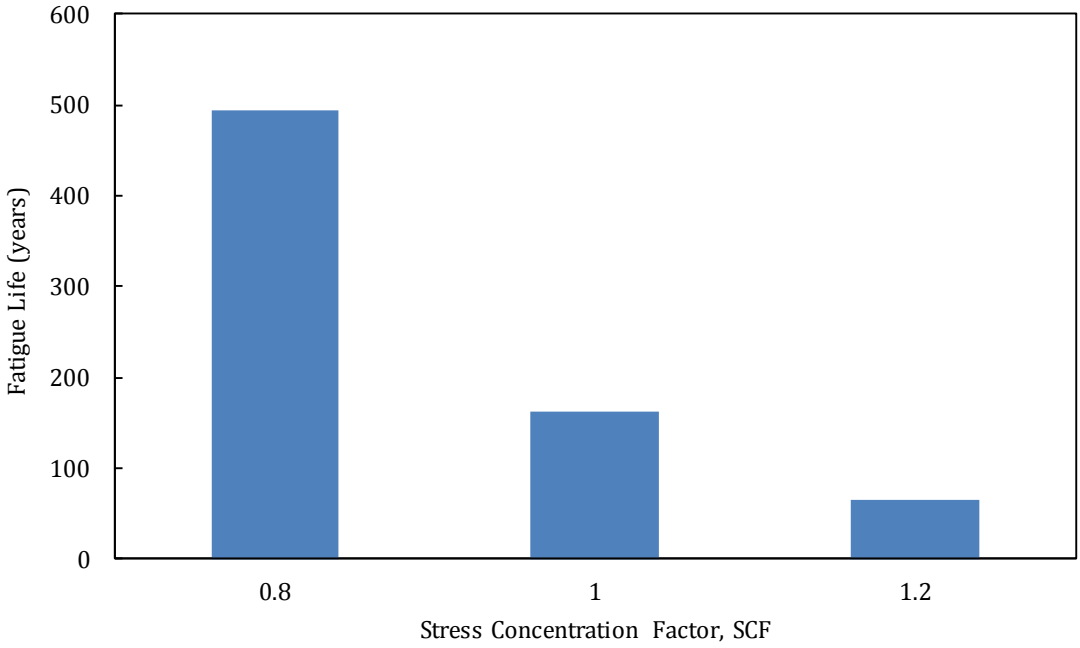

Figure 6.5—1 Fatigue life for SCR in the TDZ for different SCF values

6.5.2 Effects of lateral seabed model

SCR–seabed interaction is modelled as non-linear spring in the vertical direction whilst the Coulomb friction model is used for the lateral direction which is eventually improved to capture the breakout resistance as explained in chapter 4. The fatigue life along the SCR length for the seabed Coulomb model and improved soil model are shown in Figure 6.5—2 and Figure 6.5—3 where the non-linear soil parameters given in Table 6.4—2 are used. The critical locations for fatigue are at the touchdown area and close to the top-end. The shortest fatigue life when the seabed is modelled as Coulomb friction in lateral direction is 161.2 years and 159.9 years when the improved soil model is applied in the

lateral direction at the touchdown zone. The resulting cumulative fatigue damage distribution along the SCR in the TDZ for the worst sea-state blocks is shown in a linear scale in Figure 6.5—4. It is shown that the improved lateral seabed interaction model has small influence on the resulting fatigue life.

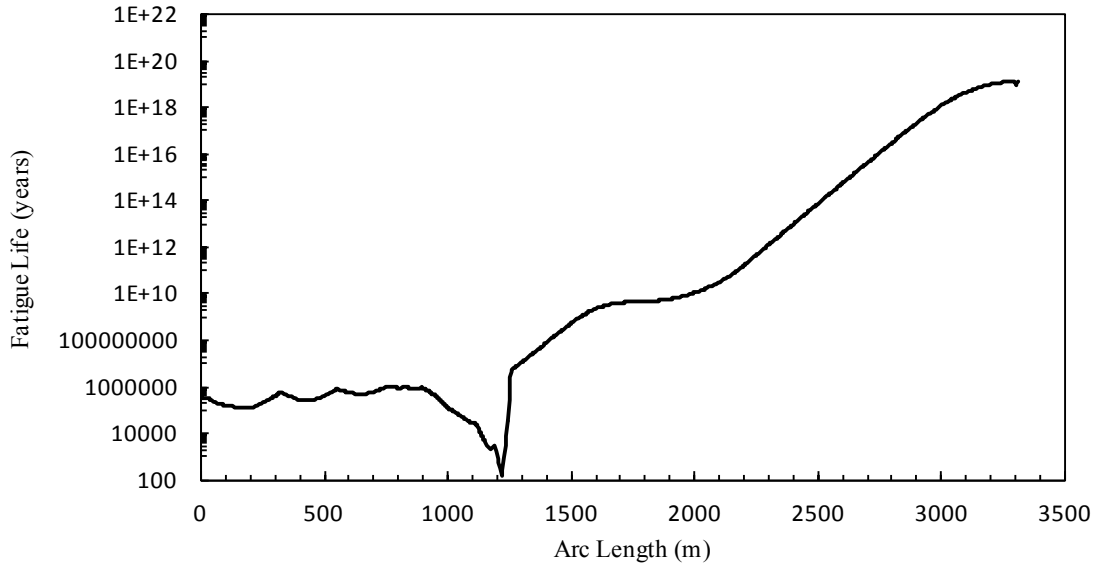

Figure 6.5—2 Fatigue life along SCR arc length measured from vessel with Coulomb model

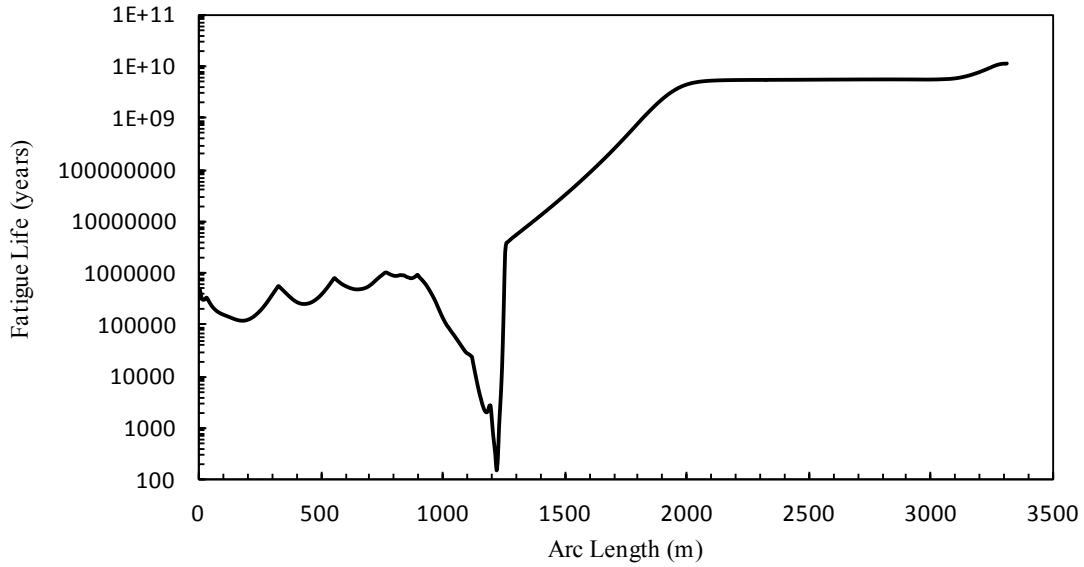

Figure 6.5—3 Fatigue life along SCR arc length measured from vessel with improved model

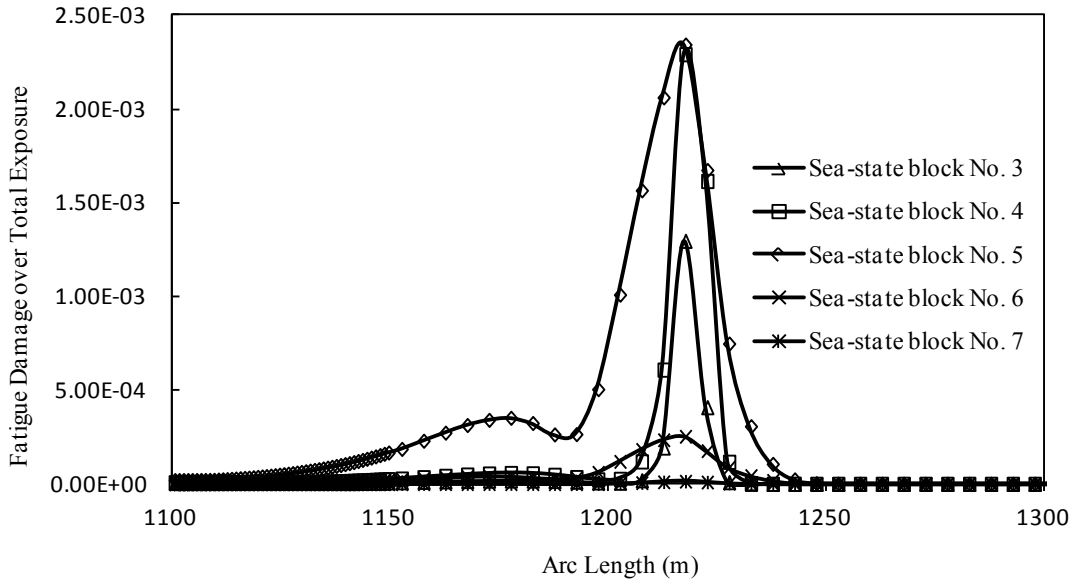

Figure 6.5—4 Fatigue damage over total exposure for worst sea-state block (linear Scale)

6.5.3 Effects of vertical linear seabed model

The SCR–seabed modelling analyses can have a large influence on the predicted riser fatigue life. Fatigue life studies for SCRs are carried out using a linear seabed stiffness in the TDZ, although there is a general awareness that the stiffness will vary along the TDZ, depending on the amplitude of cyclic motions (Clukey *et al*., 2008).

Fatigue analyses are undertaken using a linear soil model with a range of values of linear stiffness (the stiffness equals the spring reaction force, per unit area of contact, per unit depth of penetration). The effect of seabed linear stiffness on the predicted fatigue damage and fatigue life is shown in Figure 6.5—5 and Figure 6.5—6 respectively. High values of soil stiffness (approximately 10,000 $kN/m/m^2$) produce fatigue damage similar to those calculated using a rigid seabed which is clearly concluded from Figure 6.5—6. The effect is significant; higher soil stiffness gives lower predicted fatigue life, whilst lower soil stiffness in contrast may not be representative.

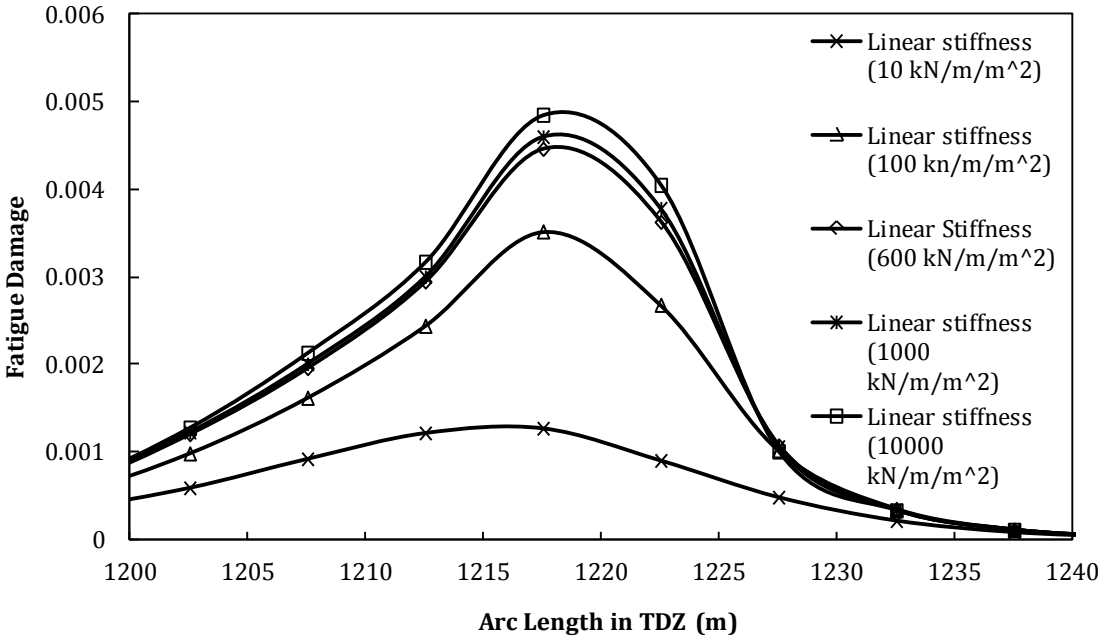

Figure 6.5—5 Effect of linear soil stiffness on SCR cumulative fatigue damage in the TDZ

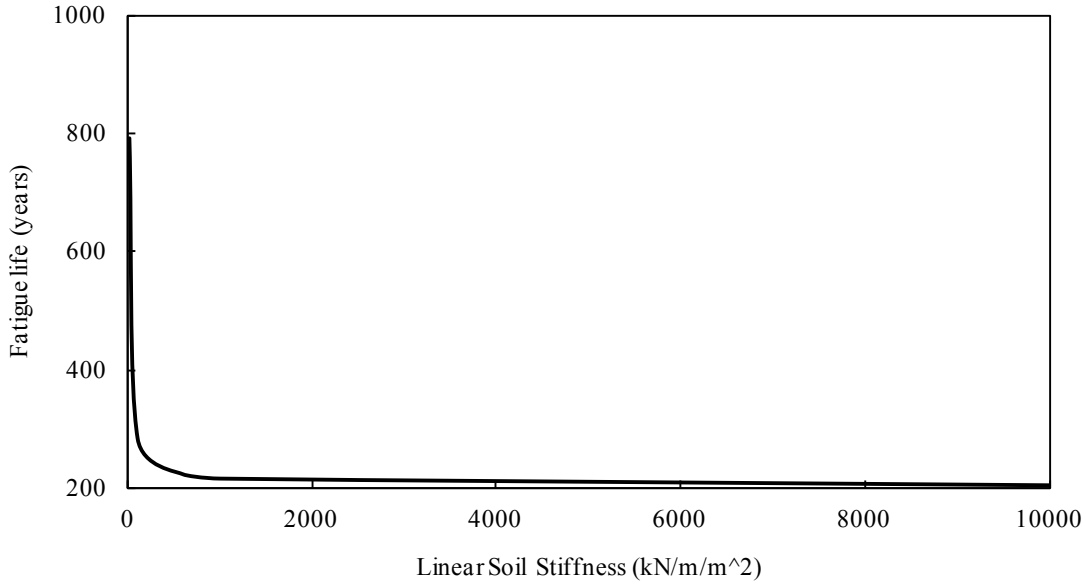

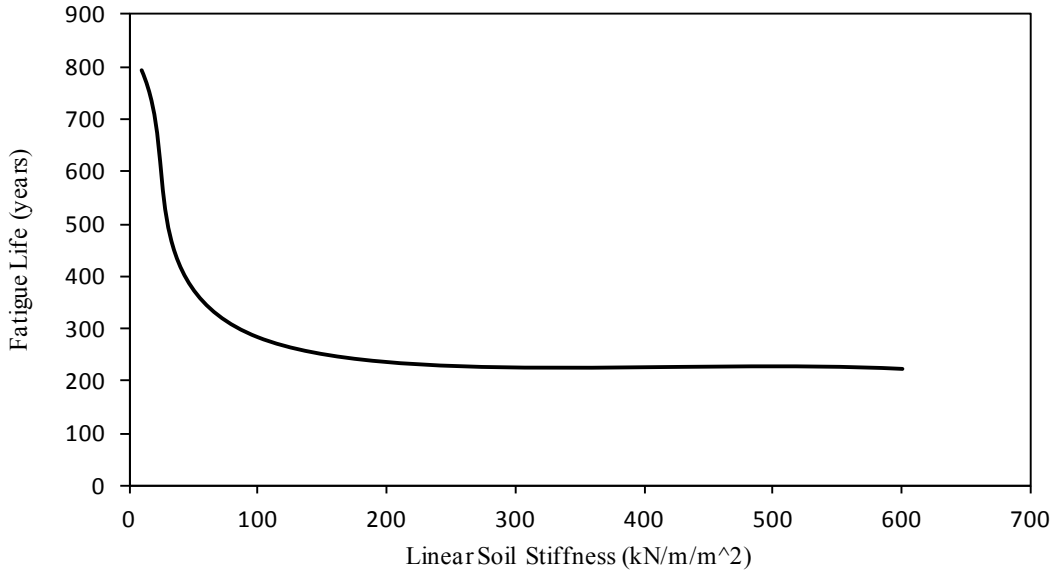

Figure 6.5—6 Linear seabed model: soil stiffness effect on predicted fatigue life

6.5.4 Effects of normalised maximum stiffness, K_{max} (non-linear soil model)

Normalised maximum stiffness, $K_{\max} = (\Delta V/\Delta z)/(V_u/D)$ is the pipe-soil stiffness, *dV/dz*, normalised by the ultimate net bearing pressure at that depth, V_u/D, which is a measure of the effective stiffness since the last reversal in penetration or since penetration started. It has been found (Bridge *et al*., 2004, Aubeny *et al*., 2008, Clukey *et al*., 2008) that K_{max} depends on the cyclic displacement of SCR pipe and it is suggested that the maximum value of $K_{\max}$ is 400 which corresponds to a small cyclic displacement while the lower value of $K_{\max}$ is 20 and corresponds to a large cyclic displacement.

Fatigue analyses are then performed using the non-linear seabed model parameters given in Table 6.4—2 but applying a range of values of the normalised maximum stiffness, $K_{\max}$ = 20, 40, 100, 150, 200, 300 and 400. The predicted fatigue damage and fatigue life are shown in Figure 6.5—7 and Figure 6.5—8 respectively, as a function of the normalised maximum stiffness. As with the non-linear soil model, higher normalised maximum stiffness gives a lower fatigue life of ~151 years compared to lower normalised maximum stiffness which gives a higher fatigue life of ~ 204 years. In addition, the resulting trench profiles for sea-state block No. 3 (H_s=3.43 m, T_p=10.5 s) based on the coupled analysis are shown in Figure 6.5—9 as a function of normalised maximum stiffness.

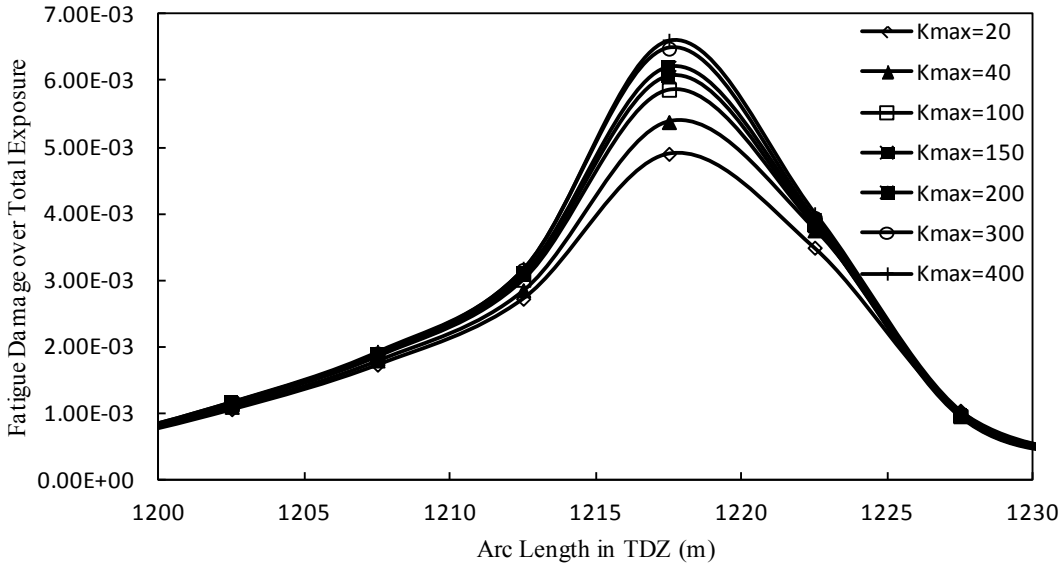

Figure 6.5—7 Normalised maximum stiffness effect on fatigue damage in the TDZ

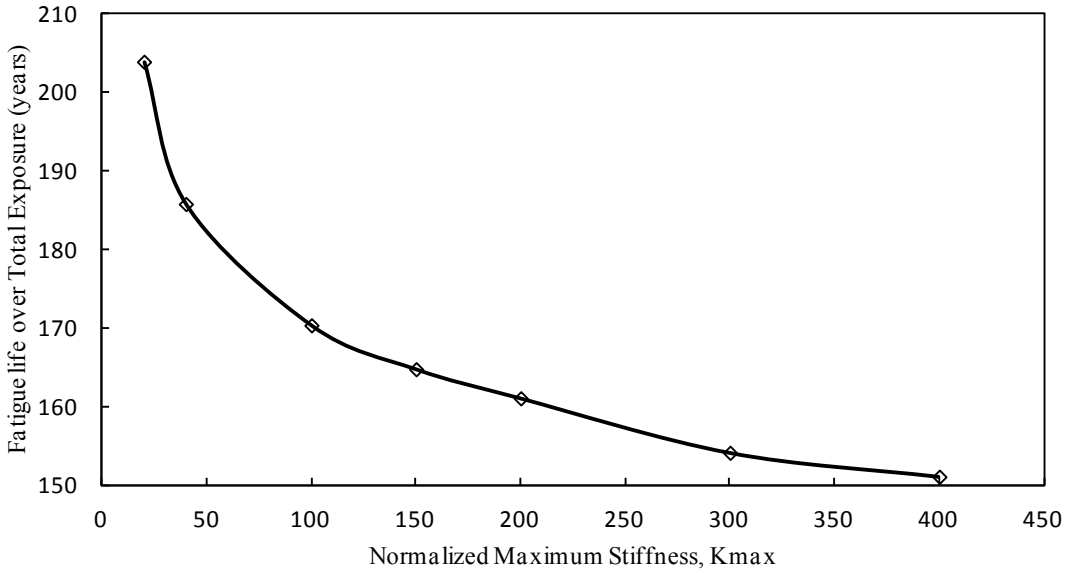

Figure 6.5—8 Normalised maximum stiffness effect on fatigue life in the TDZ at arc length 1217.5 m

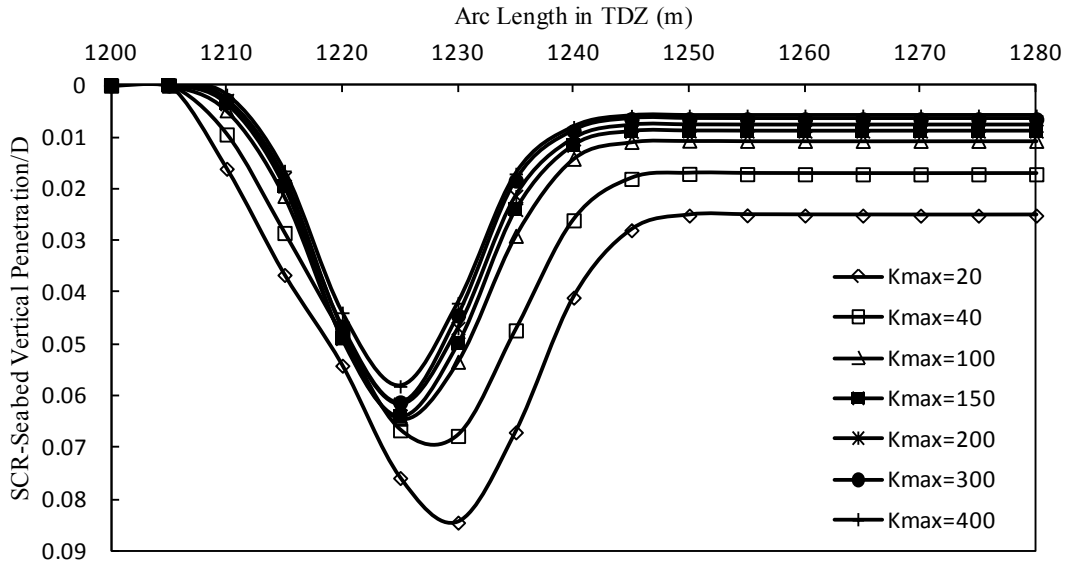

Figure 6.5—9 Normalised maximum stiffness effect on trench deepening in the TDZ

6.5.5 Effect of suction resistance ratio, f_{suc} (non-linear soil model)

The magnitude of suction resistance force mobilised by the non-linear seabed model is mainly controlled by suction resistance ratio f_{suc}. As noted by Randolph and Quiggin (2009), f_{suc} this has been found to depend partly on the soil shear strength and partly on the riser velocity. It also depends on the period of sustained suction as well as the recent history of cyclic motion; therefore, use of a constant factor f_{suc} is a simplification. Because of the very limited experimental data currently available, the non-linear soil model has utilised a range of zero to unity for f_{suc}.

Fatigue analyses are then performed using the non-linear seabed model parameters presented in Table 6.4—2 but with the application of four different levels of the suction resistance ratio, f_{suc} = 0, 0.3, 0.7, 1.0. The evaluation of the suction influence on the cumulative fatigue damage is performed, while sea-state fatigue bins are applied for 10800 sec (3hr) simulation time. Figure 6.5—10 compares the cumulative fatigue damage for different suction ratios varying between zero and unity. The cumulative fatigue damage is roughly doubled between zero and full suction resistance force. The predicted fatigue life near TDP is presented in Figure 6.5—11 as a function of the suction ratio, f_{suc}. The reduction in fatigue life due to soil suction, between upper level, f_{suc}, (full soil suction) and lower level, f_{suc}, (no suction), is approximately 42%, see Figure 6.5—11. The effects of soil suction ratio and normalised maximum stiffness should be combined to show their influence on predicted fatigue life as presented in Figure 6.5—12. If the upper level of normalised maximum soil stiffness is 400, the fatigue life reduces by around 32% when f_{suc} is increased from zero to 0.7. If the normalised maximum stiffness is further reduced to 20, the fatigue life is reduced by around 20% when f_{suc} is increased from zero to 0.7. If the lower level of normalised soil stiffness, 20, is used with no suction effect, fatigue life in TDZ increases by around 22% compared to those calculated using a rigid seabed, while fatigue life in TDZ reduces by around 1.2% with f_{suc}=0.7. Likewise, if the upper level of normalised soil stiffness, 400, is used with no suction effect, fatigue life in TDZ increases by around 8% compared to those

calculated using a rigid seabed, while fatigue life in TDZ reduces by around 27% with f_{suc}=0.7.

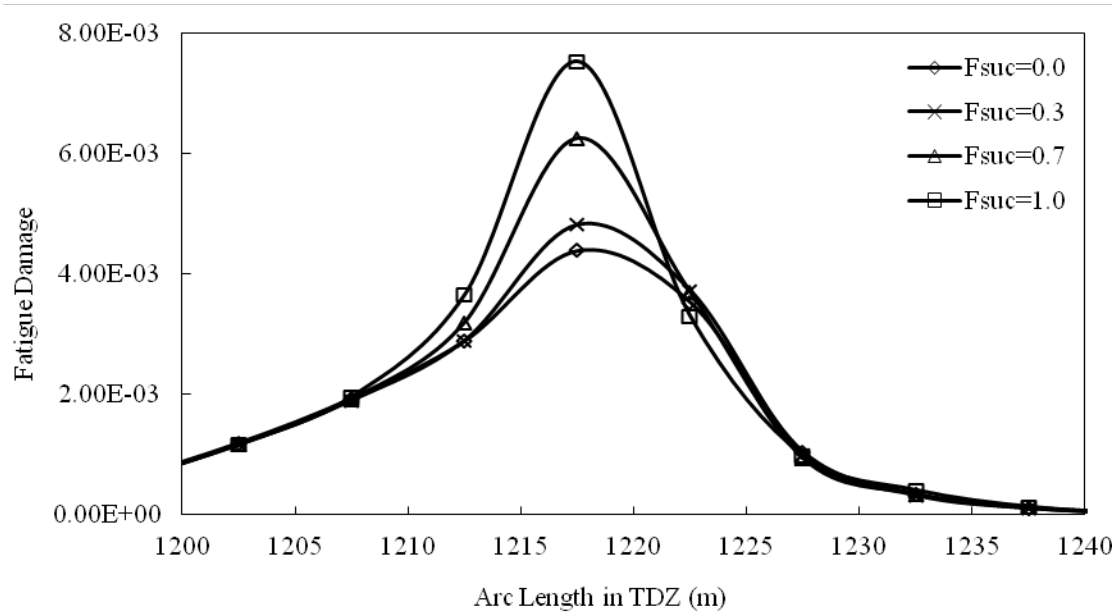

Figure 6.5—10 Cumulative fatigue damage for different suction ratios in the TDZ

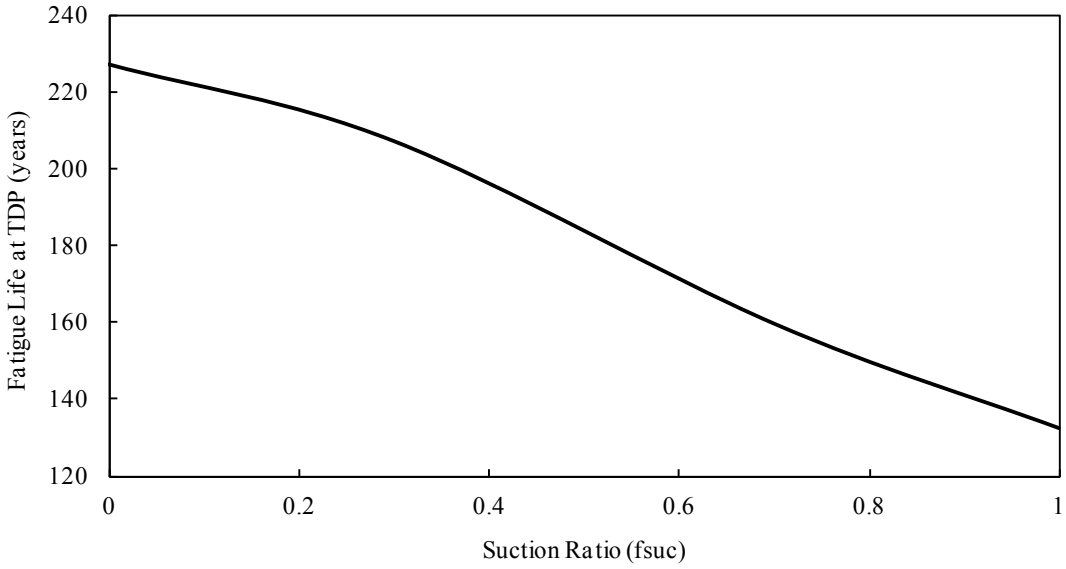

Figure 6.5—11 Suction ratio effect on predicted fatigue life at 1217.5 m arc length (K_{max}=200)

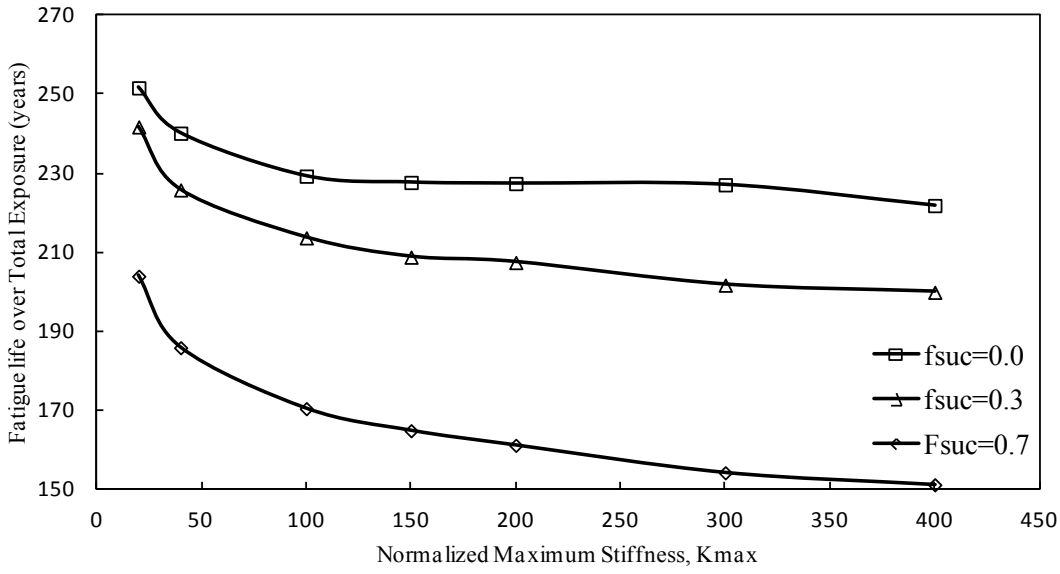

Figure 6.5—12 Influence of maximum normalised stiffness and soil suction ratio on the predicted fatigue life

6.5.6 Effects of normalised re-penetration offset, λ_{rep} (non-linear soil model)

Normalised re-penetration offset, λ_{rep}, controls the delay in mobilising the ultimate soil resistance curve during re-penetration and is presented to capture progressive penetration under cyclic movements. As noted by Randolph and Quiggin (2009), λ_{rep} has a value in the range of 0.1 to 0.5 which fits the experimental data.

Further fatigue analyses are then performed using the non-linear seabed model parameters presented in Table 6.4—2 but with the application of two different levels of normalised re-penetration offset, λ_{rep} = 0.1, 0.5. The effects of normalised re-penetration offset on the cumulative fatigue damage are investigated, and the sea-state fatigue bins are applied for 10800 sec (3hr) simulation time. The predicted fatigue life in the TDZ is shown in Figure 6.5—13 as a function of normalised re-penetration offset, λ_{rep}. The influence of the normalised re-penetration offset parameter and normalised maximum stiffness should be combined to show their effects on the predicted fatigue life. The reduction in fatigue life due to re-penetration offset parameter, between upper level, λ_{rep} = 0.5 and lower level, λ_{rep} = 0.1, is around 5% at which K_{max}=400, see Figure 6.5—13.

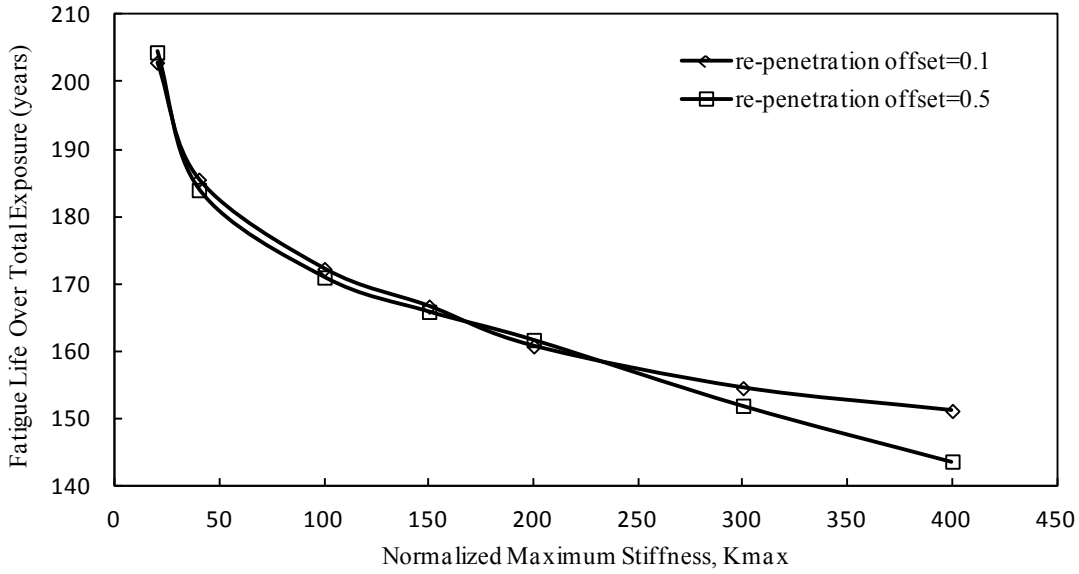

Figure 6.5—13 Influence of normalised re-penetration offset on the predicted fatigue life

6.5.7 Trenching effects

Trench gradual deepening also has significant influence on fatigue life prediction. Cyclic dynamic motions applied be floating production unit have an effect on the gradual variation of trench embedment in the TDZ. Figure 6.5—14 shows the gradual embedment of the SCR in the TDZ under application of a single sea-state block (No. 5 in Table 6.4—1, with H_S = 5.17 and T_P = 16.5 sec), over 3-hour simulation time, for non-linear seabed modelling in vertical direction with undrained shear strength at the mudline of 2.6 kPa and shear strength gradient with depth of 1.25 kP/m.

The resulting cumulative fatigue damage distribution along the SCR in the TDZ under different simulation time lengths is shown in Figure 6.5—15. It is clearly observed that after 8100 sec simulation time length, steady values of cumulative fatigue damage are achieved.

Soil suction ratio also has an effect on the final trench profile under cyclic loading. A comparison of the final seabed trench profiles, under the influence of soil suction ratio, is presented in Figure 6.5—16 which shows that the increase in the soil suction ratio causes deeper penetration under the same load condition and application of a single sea-state block No. 5.

Seabed soil resistance would increase with trench gradual variation and deepening. In addition, the value of suction ratio will influence the distribution of the SCR–seabed resistance in the TDZ. The final seabed resistance envelop under application of a single sea-state block No. 5 is shown in Figure 6.5—17. This figure demonstrates that the suction force is generated in the zone around the TDP. As such, this region is subjected to large cyclic motions.

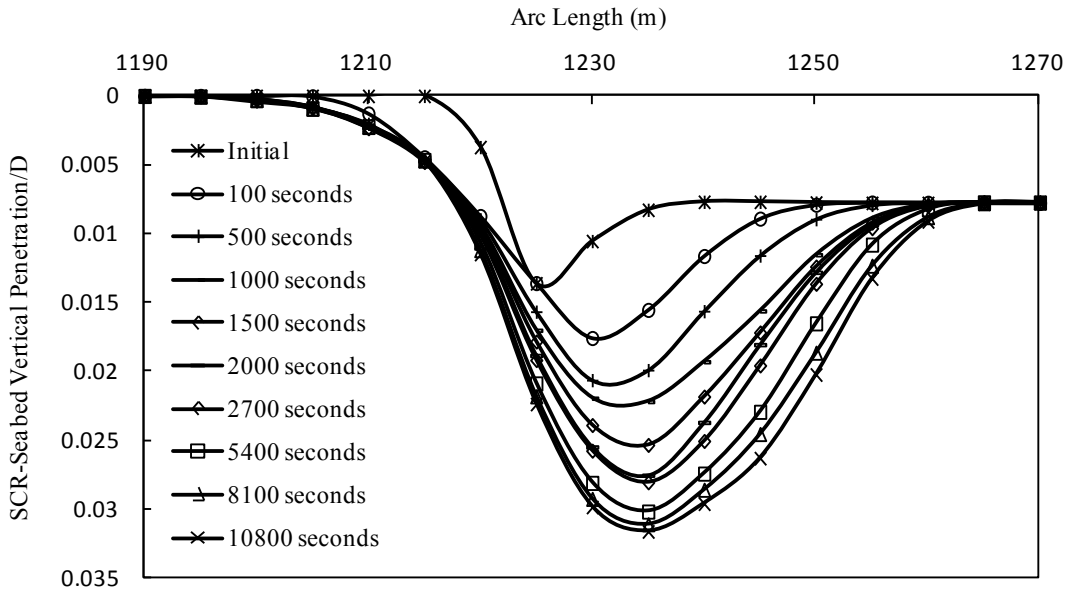

Figure 6.5—14 Gradual deepening of trench profile under single wave application based on coupled analysis

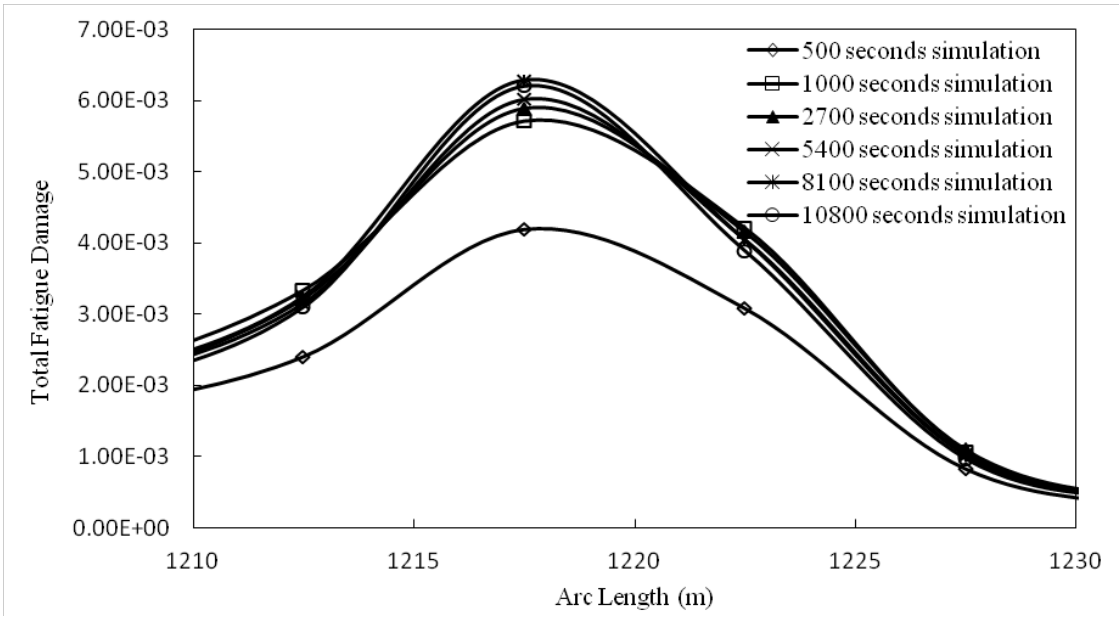

Figure 6.5—15 Cumulative fatigue damage under different simulation time length (linear scale)

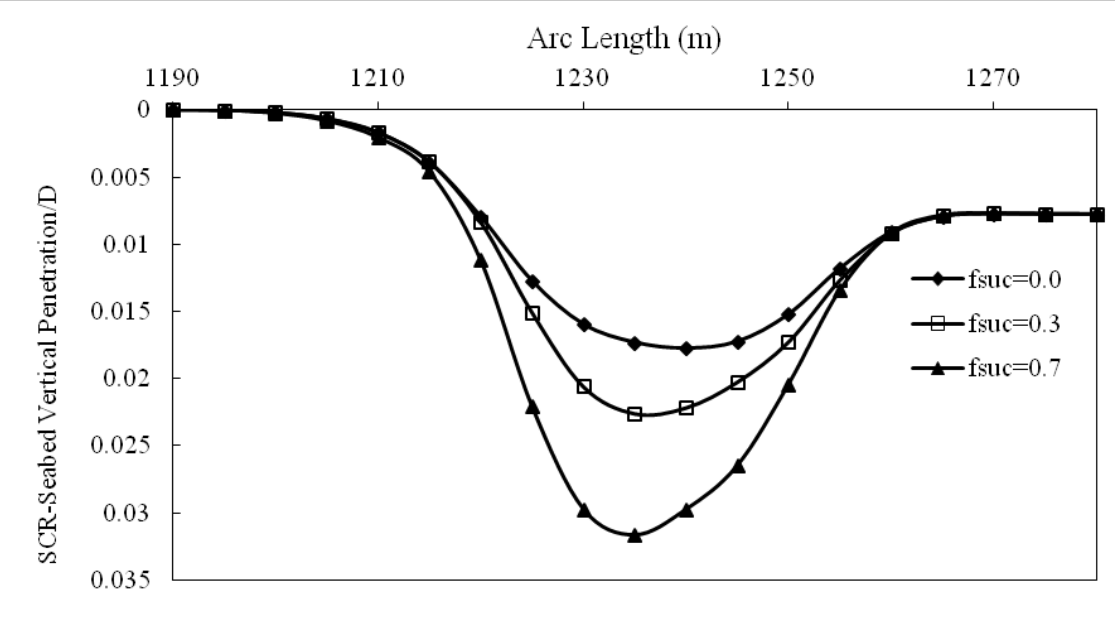

Figure 6.5—16 Final trench profile for various values of suction ratio

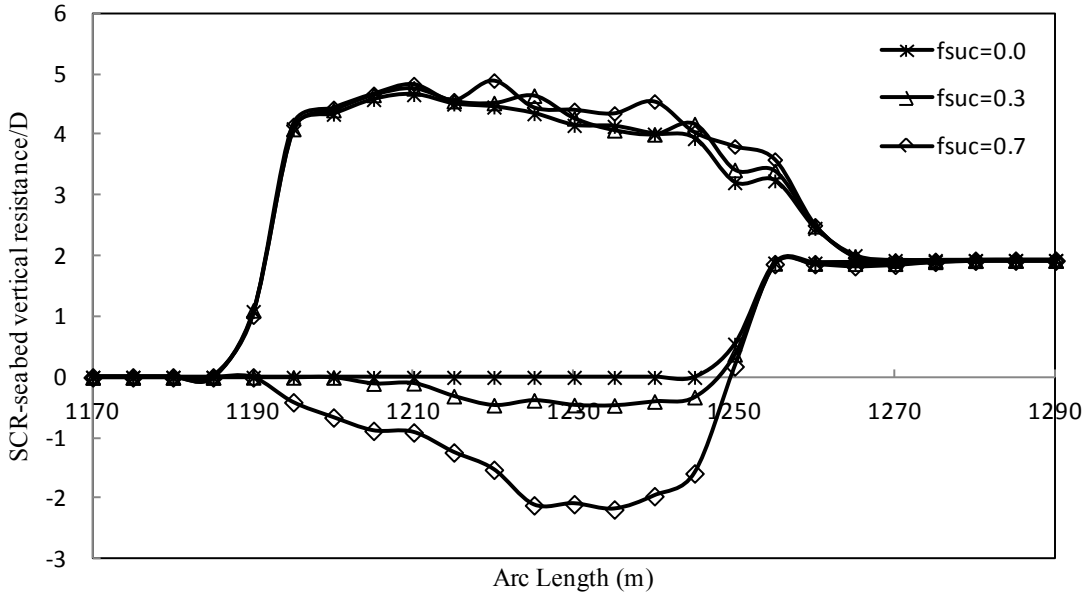

Figure 6.5—17 Seabed resistance envelop for range of suction values

6.6 Conclusion

In this chapter, detailed fatigue analyses of SCR connected to semisubmersible in NNS have been performed. An investigation has also been conducted into the SCR–seabed interaction response and geotechnical parameters' effects on the fatigue performance of SCR near the touchdown point on soft clays. OrcaFlex/Finite element package utilising an adaptive meshing technique is used to model the SCR–seabed interaction. The results of a parametric study of fatigue performance of SCR in the TDZ have been presented using lateral, vertical linear and non-linear SCR–seabed interaction models to investigate how the main geotechnical parameters affect the fatigue life of SCR.

The SCR–seabed interaction analyses allow the effect of physical phenomena such as soil suction forces as well as lateral and vertical seabed stiffness on the SCR performance to be identified and quantified. They also provide a better understanding of the complex physical process of SCR–soil interaction. An outline of the fatigue analysis methodology utilised and the numerical results are presented.

Detailed fatigue analyses are carried out using linear and non-linear seabed springs with cyclic strength degradation and trench deepening for a range of fatigue bins. Global analysis is performed to assess the influence of vertical linear seabed springs, lateral seabed model, non-linear seabed model, gradual

trench deepening into seabed, seabed normalised stiffness, re-penetration offset parameter and soil suction resistance ratio on the fatigue of SCR in the TDZ. A sensitivity study of the linear seabed model and non-linear seabed model including linear soil stiffness, normalised maximum seabed stiffness, soil suction resistance ratio and re-penetration offset parameter are investigated and presented for a wide range of values. The following key observations and conclusions are also drawn from this chapter:

- The lowest SCR fatigue life was found in the TDZ due to the non-linear seabed interaction response
- Compared to the Coulomb friction model, the fatigue life of SCR in the TDZ is slightly affected by improved soil 'tri-linear' model in lateral direction near TDP, while the SCR's flow-line is highly affected by improved lateral soil resistance.
- The seabed linear stiffness has a considerable influence on the assessed fatigue life in the TDZ; higher soil stiffness gives lower predicted fatigue life, conversely lower soil stiffness may not be representative.
- If the non-linear seabed model is used, the fatigue life is reduced by around 44% compared to the linear seabed model with soil stiffness of 100 kN/m/m^2 whilst the fatigue life is also reduced by around 22% compared to the rigid seabed of high seabed stiffness (10,000 kN/m/m^2). This indicates that the SCR-seabed interaction can't be represented by

linear or rigid seabed models and the significance of geotechnical parameters should be investigated.

- Sensitivity studies of normalised maximum stiffness, K_{max} are performed using a wide range of stiffness values. The difference in fatigue life between the upper bound and lower bound of K_{max} is more than 50 years which represents a significant difference for an SCR fatigue life prediction. In addition, K_{max} has a significant effect on the gradual deepening of the trench in the TDZ as also reflected in the fatigue life prediction.
- Soil suction resistance ratio has a significant influence on the final trench profile, seabed resistance and consequently the SCR fatigue life in the TDZ. Higher values of soil suction resistance ratio gives lower fatigue life and the difference in fatigue life between zero suction to full suction ratio is around 100 years. Furthermore, fatigue life prediction is affected by the variation of soil suction with normalised maximum stiffness; as the soil suction ratio increases, the difference in fatigue life increases with the variation of normalised maximum stiffness from low stiffness (K_{max} = 20) to high stiffness (K_{max} = 40) with values up to 50 years for the same soil suction ratio. These results help in interpreting the confounding fatigue life results found by other published studies.
- The normalised re-penetration offset parameter, λ_{rep}, has a negligible effect on the SCR fatigue life for a wide range of K_{max} up to a value of 250,

while λ_{rep} would slightly affect the fatigue life of SCR with high values of K_{max} (K_{max} = 400).

- The influence of the gradual embedment of the riser into the seabed and development of deep trenches on SCR fatigue performance in TDZ has been studied through the use of a hysteretic non-linear seabed model. Gradual deepening of the trench, under random loads and cyclic motions, significantly increases the SCR fatigue damage in the TDZ.

The next chapter will be presenting the probabilistic methodology for fatigue reliability as well as the probability of failure associated with fatigue analysis of SCRs in the TDZ. First order reliability method (FORM) will be used for predicting fatigue reliability index. The influence of uncertainties associated with soil parameters on Reliability-based fatigue will be investigated. In addition, a sensitivity study of influential variables has been carried out.

6.7 References

API 1998. API RP 2RD: Design of risers for floating production systems and tension-leg platforms. American Petroleum Institute

API 2000. API RP 2a: Planning, designing and construction fixed offshore platforms. American Petroleum Institute.

Aubeny, C., Gaudin, C. & Randolph, M. 2008. Cyclic tests of model pipe in kaolin. *Offshore Technology Conference.* Houston, Texas, USA: Society of Petroleum Engineers.

Aubeny, C. P., Biscontin, G. a. & Zhang, J. 2006. Seafloor interaction with steel catenary risers. Texas: Offshore Research Centre, Texas A&M University, College Station, Houston, Final Project Report to Minerals Management Service,Offshore Technology Research Centre Industry Consortium, OTRC Library Number 9/06A173

Aubeny, C. P. a. & Biscontin, G. 2009. Seafloor-riser interaction model. *International Journal of Geomechanics,* Vol. 9, No. 3.

Ayyub, B. M., Assakkaf, I. A., Kihl, D. P. & Siev, M. W. 2002. Reliability-based design guidelines for fatigue of ship structures. *Naval engineers journal,* 114**,** 113-138.

Brennodden, H., Lieng, J., Sotberg, T. & Verley, R. 1989. An energy-based pipe-soil interaction model. *Offshore Technology Conference.* Houston, Texas, USA.

Bridge, C., Laver, K. & Clukey, E. Steel catenary riser touchdown point vertical interaction models. *In:* Offshore Technology Conference, OTC 16628, 2004 Houston, Texas.

Bridge, C. & Willis, N. Steel catenary risers–results and conclusions from large scale simulations of seabed interactions. *In:* International Conference on Deep Offshore Technology, 2002 New Orleans, USA. PennWell.

Bridge, C. D. & Howells, H. A. 2007. Observations and modeling of steel catenary riser trenches. *International Society of Offshore and Polar Engineers (ISOPE)* Lisbon.

Bruton, D., White, D., Cheuk, C., Bolton, M. & Carr, M. Pipe/soil interaction behavior during lateral buckling, including large-amplitude cyclic displacement tests by the safebuck JIP. *In:* Offshore Technology Conference, 2006 Houston, USA.

Cao, J. Fatigue analysis technique of deepwater steel catenary risers. *In:* 29th International Conference on Ocean, Offshore and Arctic Engineering, OMAE 2010, 6-11June 2010 Shanghai, China. ASME.

Cardoso, C. & silveira. Pipe-soil interaction behavior for pipelines under large displacements on clay soils-a model for lateral residual friction factor. *In*, 2010.

Clukey, E., Young, A., Dobias, J. & Garmon, S. Soil response and stiffness laboratory measurements of SCR pipe/soil interaction. *In:* Offshore Technology Conference, 2008 Houston, USA.

DNV 2005. Riser fatigue. *Recommended Practice DNV-RP-F204.* Det Norske Veritas.

DNV 2010. Fatigue design of offshore steel structures. *Recommended Practice DNV-RP-C203.* Det Norske Veritas.

Giertsen, E., Verley, R. and Schroder, K. 2004. Carisima: A catenary riser/soil interaction model for global riser analysis. *23rd International Conference on Offshore Mechanics and Arctic Engineering, OMAE2004-51345*.

Grealish, F., Kavanagh, K., Connaire, A. & Batty, P. Advanced nonlinear analysis methodologies for SCRs. *In:* Offshore Technology Conferecne, OTC 18922, 2007 Houston, Texas, USA.

Karunakaran, D., Meling, T., Kristoffersen, S. & Lund, K. Weight-optimized SCRs for deepwater harsh environments. *In:* Offshore Technology Conference, 2-5 May 2005 Houston, TX, USA.

Langner, C. G. 2003. Fatigue life improvment of steel catenary risers due to self-trenching at the touchdown point. *Offshore Technology Conference.* Houston, Texas, USA.

Leira, B. J., Passano, E., Karunakaran, D., Farnes, K. A. & Giertsen, E. Analysis guidelines and application of a riser-soil interaction model including trench effects. *In:* 23rd International Conference on Offshore Mechanics and Arctic Engineering, OMAE2004-51527, 2004 Vancouver, British Columbia, Canada. ASME.

Lyons, C. Soil resistance to lateral sliding of marine pipelines. *In:* Offshore Technology Conference, 1973 Texas, USA.

Nakhaee, A., and Zhang, J. 2008. Effects of the interaction with the seafloor on the fatigue life of a SCR. *Proceedings of the 18th (2008) International Offshore and Polar Engineering Conference*.

Palmer, A. 2008. Touchdown indentation of the seabed. *Applied Ocean Research,* 30**,** 235-238.

Randolph, M. & Quiggin, P. 2009. Non-linear hysteretic seabed model for catenary pipeline contact. *28th International Conference on Ocean, Offshore and Arctic Engineering, OMAE2009-79259.* Honolulu, Hawaii, USA: Proceedings of the ASME 2009

Sen, T. K. 2006. Probability of fatigue failure in steel catenary riser in deep water. *Journal of Engineering Mechnics*.

Sharma, P. & Aubeny, C. Advances in pipe-soil interaction methodology and application for SCR fatigue design. *In:* Offshore Technology Conference, 2011 Houston, USA.

Thethi, R. & Moros, T. Soil interaction effects on simple catenary riser response. *In:* Proceeding Conference on Deepwater Pipeline & Riser Technology, 2001 Houston, Texas.

Verley, R. & Lund, K. M. A soil resistance model for pipelines placed on clay soils. *In*, 1995. American Society of Mechanical Engineers, 225-225.

Wagner, D., Murff, J., Brennodden, H. & Sveggen, O. Pipe-soil interaction model. *In:* Offshore Technology Conference, April 27-30 1987 Houston, Texas, USA. OTC.

White, D. J., and Cheuk, C. Y. 2008. Modelling the soil resistance on seabed pipelines during large cycles of lateral movement. *Marine Structures,* 21**,** 59-79.

Willis, N. R. T., and West, P. T. J. Interaction between deepwater catenary risers and a soft seabed: Large scale sea trials. *In:* Offshore Technology Conference, 2001 Houston, Texas OTC 13113.

Xia, J., Das, P. K. & Karunakaran, D. 2008. A parametric design study for a semi/SCR system in northern north sea. *Ocean Engineering***,** Ocean Engineering35(2008)1686–1699.

CHAPTER 7

FATIGUE RELIABILITY ANALYSIS OF AN SCR ON SOFT CLAY NEAR TDZ

7.1 Introductory Remarks

The fatigue damage issue of the SCR in the TDZ is significantly affected by the non-linear behaviour of SCR–seabed interaction as explained in the previous chapters, the considerable uncertainty in SCR–seabed interaction modelling and geotechnical parameters, as presented in Chapter 6. This uncertainty highlights the need for answers to the following question: How safe is the fatigue performance of SCRs in the TDZ? This question is best tackled and addressed using the reliability–based fatigue approach, which has thus far not been extensively investigated in the SCR design. A safety factor is usually applied to the fatigue design of SCR to ensure that the estimated fatigue damage is beyond and below the fatigue resistance limit (Miner's index) with an acceptable safety margin; see DNV-RP-F204 (DNV, 2005) for further details. However, the safety factor does not involve the inherent uncertainties associated with the non-linear soil model. Therefore, the safety factor might not be enough to provide the required safety margin which is highlighting the increase in demand for employing the reliability analysis techniques for SCR's structural safety assurance.

In traditional SCR design analyses, the non-linear seabed model and the influence of trench shape is largely ignored. The significance of the seabed interaction and geotechnical parameters on the fatigue performance of SCRs in the TDZ is investigated in Chapter 6. It has been found that seabed stiffness, soil

suction and gradual trench deepening are the most critical parameters that influence the fatigue life of SCRs in the TDZ.

However, it is evident that while many studies have investigated the fatigue performance of SCRs, there are few studies that regard the probability of failure as associated with the current design procedures of the SCR fatigue analysis. Among these studies, Akpan *et al.* (2007), Xia and Das (2008) and Sen (2008) have studied the uncertainties associated with fatigue performance of SCRs. However, both Akpan *et al*. and Sen *et al*. ignored seabed modelling, while Xia *et al*. utilised a linear seabed model.

The ability to quantify the uncertainty of SCRs, especially in the TDZ, which are subject to inherent randomness in loading, material properties, seabed modelling, fatigue characteristics and geometric parameters, is becoming increasingly important in the design and analysis of the SCR. In terms of fatigue, SCRs are very sensitive to seabed modelling. Reliability-based fatigue behaviour provides a method to quantify the reliability of SCRs in the TDZ and to develop a more thorough understanding of the response behaviour of SCR-seabed interaction. The objective of the reliability-based fatigue methodology is to increase the confidence in the design of SCRs in the TDZ.

This study presents the probability of failure associated with the fatigue analysis of SCRs in the TDZ. The probabilistic methodology for fatigue reliability is illustrated. Uncertainties in structural load and material properties are

considered by assigning probability distributions and standard deviations to the deterministic stress levels. Furthermore, fatigue strength parameters, Miner's indices and capacities are modelled as random variables. The first order reliability method (FORM) is used to predict the fatigue-reliability index. The influence of uncertainties associated with soil parameters on reliability-based fatigue is investigated. In addition, a sensitivity study of influential variables has been performed. The SCR Reliability-based fatigue modelling framework is described in Figure 7.1—1.

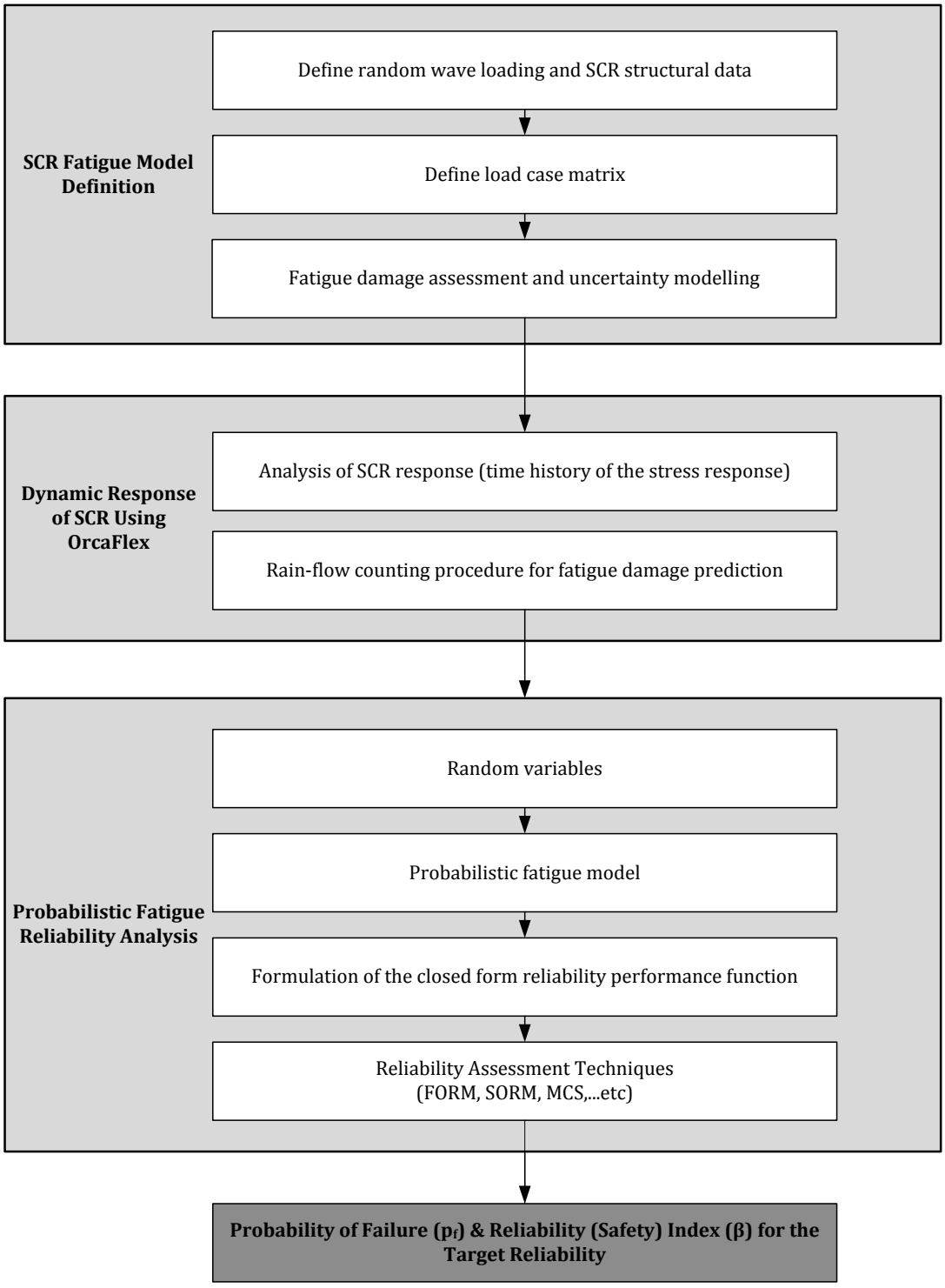

Figure 7.1—1 SCR reliability–based fatigue modelling strategy

7.1.1 Purpose

In many situations, engineers must know the potential effects of any uncertainty behind their decision. This can be evaluated by a review of equations which describe physical relations, or by simple calculations of derivatives and changes in the results for an increment of change in a considered parameter. Reliability methods can be acknowledged as an additional tool for determining data which can be used for a relative comparison of the importance of the different parameters and sensitivities to changes in them.

Reliability analysis is performed when structural safety is a key issue and when safety is to be expressed in terms of a consistent measure. The safety of a structure can be efficiently visualised by using reliable analytical methods which can effectively demonstrate this to other engineers, including those of a different engineering background. Engineers have conventionally linked the safety of structures with safety factors. Obviously, a safety factor is not a good measure of safety level, as it is rarely uniquely defined. In addition, a number of additional parameters are required for the assessment of safety levels such as definition of characteristic strength. Generally, reliability methods are powerful as an engineering tool for verification and means that planned operations of SCR can be performed at an acceptable level of reliability.

7.1.2 Basic Reliability Problem Description

What Is Reliability? As far as the structure integrity is concerned, most of the variables related to the load and resistance are random quantities. The primary concern of the structural analysis is to ensure satisfactory performance of the structure, that is, to ensure that the structure resistance is greater than the load or allowable stresses during the service life of the structure. With regard to the uncertainties of the structural analysis, satisfactory performance cannot be absolutely assured. In contrast, assurance can only be guaranteed in terms of the probability of success in satisfying a certain performance criterion. In engineering terminology, this probabilistic assurance of service performance is assigned to as reliability (Haldar and Mahadevan, 2000). Reliability is the compliment of the failure probability and is a rational measure of safety.

Need for Reliability Evaluation: The conventional approach is to consider the uncertain parameters associated with the structure to be deterministic, whilst also accounting for uncertainties through the use of empirical Safety Factors (SFs). SFs are derived based on past experience but do not absolutely guarantee safety of satisfactory performance of the structure in service. SFs do not provide any information regarding the influence that the different parameters of the system have on safety. Moreover, the engineering structural analysis is a compromise between maximising safety levels and minimising cost. The aforementioned deterministic SFs do not provide adequate information with

which to achieve the optimal use of the available resource to maximise safety. On the other hand, the probabilistic analysis does provide the required information for optimum design by incorporating the experience and expertise in determining the uncertainties.

Measures of Reliability: Reliability is the probability of successful structural performance associated with a particular performance criterion. The widely used term for the measure of reliability is the 'probability of failure'. The reliability or probability of failure should be considered for the individual components against all the performance criteria. For performance criteria in practical structures, the precise evaluation of the probability of failure is difficult to determine. Therefore, an approximation method such as first-order reliability is used for the probabilistic design specification.

The evaluation of the probability of failure of the SCR is established by deciding the specific performance criteria and the relevant load and resistance parameters, referred to as the basic random variables x_i. The failure surface can be defined as $G(x) = 0$. This is the bound between safe and unsafe regions in the design parameter space. Consequently, this surface represents a state beyond which a structure can no longer achieve the function for which it was designed. In structural reliability theory, the failure probability is defined as:

$$p_f = p[G(x) \leq 0] = \int_{G(x) \leq 0} f_x(x) dx$$

Equation 7.1—1

where p_f is the probability of failure; $G(x)$ is the failure function; $G(x) \leq 0$ is a failure state and $G(x) > 0$ a safe state), x is a set of k random basic variables, that is, $[x] = [x_1, x_2 \ldots, x_k]$ *and* $f_X(x)$ the multi-variant density function of x. The evaluation of multiple integral for a range of random variables is extremely complicated. Therefore, the analytical approximation of this integral such as FORM and Second-Order Reliability Method (SORM) are used to compute the integral.

For a component reliability analysis, failure criteria are usually set on the limiting factors of strength and stress of SCR, and are of the form:

$$G(x) = R - S$$

Equation 7.1—2

where R is the component's resistance (or upper limit of strength/behaviour) and S its serviceability (or calculated response distribution from load effects), see Figure 7.1—2. This failure region is shown in Figure 7.1—3 in a diagrammatic comparison of a deterministic and a probabilistic analysis.

The probability of failure depends on the ratio of the mean value of G to its standard deviation. This ratio in commonly known as reliability index and is denoted as β (Haldar and Mahadevan, 2000, Shama, 2009):

$$\beta = \frac{\mu_G}{\sigma_G} = \frac{\mu_R - \mu_S}{\sqrt{\sigma_R^2 + \sigma_S^2}}$$

Equation 7.1—3

The probability of failure, see Figure 7.1—4, in terms of the reliability index can be obtained by rewriting Equation 7.1—1 as:

$$p_f = 1 - \Phi(\beta)$$

Equation 7.1—4

where Φ is the standard normal cumulative distribution function (CDF). The cumulative distribution function describes the probabilities of random variables falls in interval. For example, the probability that the value of x lies in a very small interval from x to $x+\Delta x$. So, although the probability of getting exactly the value x is zero, the probability of being close to x is proportional to $\Phi_x(x)$. Then,

$$P(a \le x \le b) = \Phi_x(b) - \Phi_x(a) = \int_a^b \phi_x(x)dx$$

Equation 7.1—5

Confidence in this probabilistic approach depends on the following factors:

- The ability to accurately evaluate the integral in Equation 7.1—1. The techniques with which to achieve this are described in section 7.3.2.
- The accuracy of the "failure" limit state function. In the reliability analysis, the results can only be judged by the accuracy of the individual modelling components used in the analysis.
- The probabilistic modelling of the uncertainty is associated with the basic random variables. The statistical spread assumed for random variables should reflect their inherent variability.

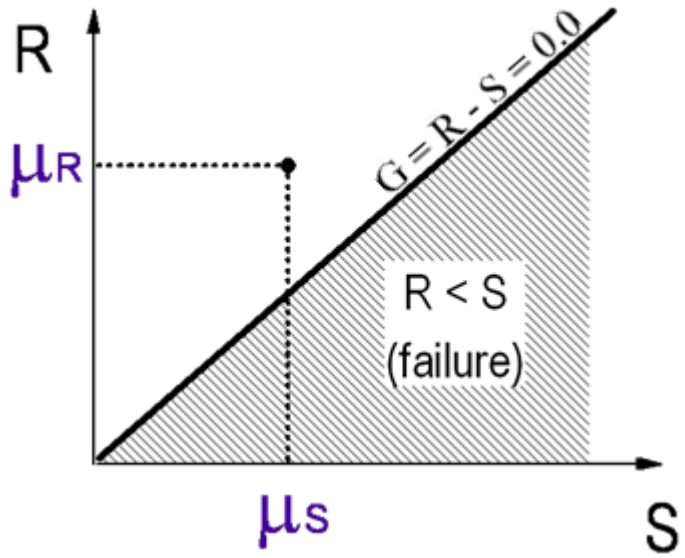

Figure 7.1—2 Stress-resistance limit state function

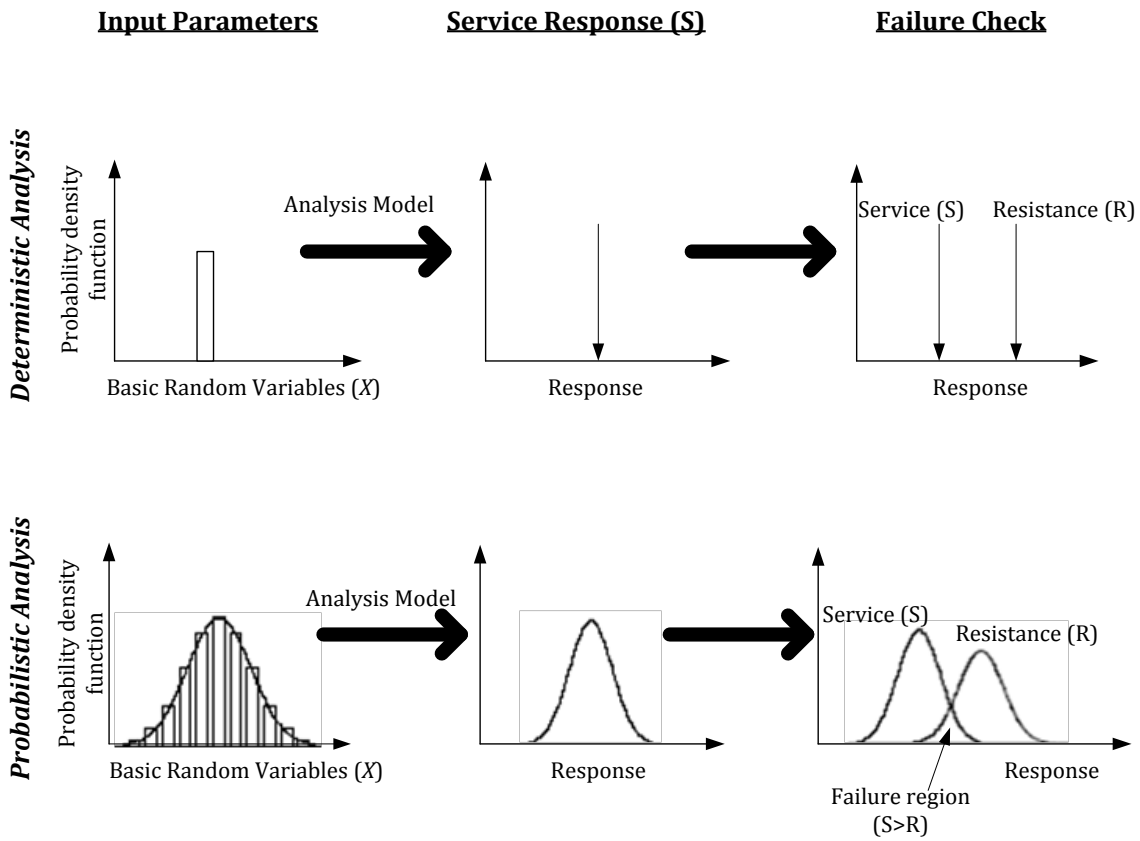

Figure 7.1—3 Description of deterministic and probabilistic approaches

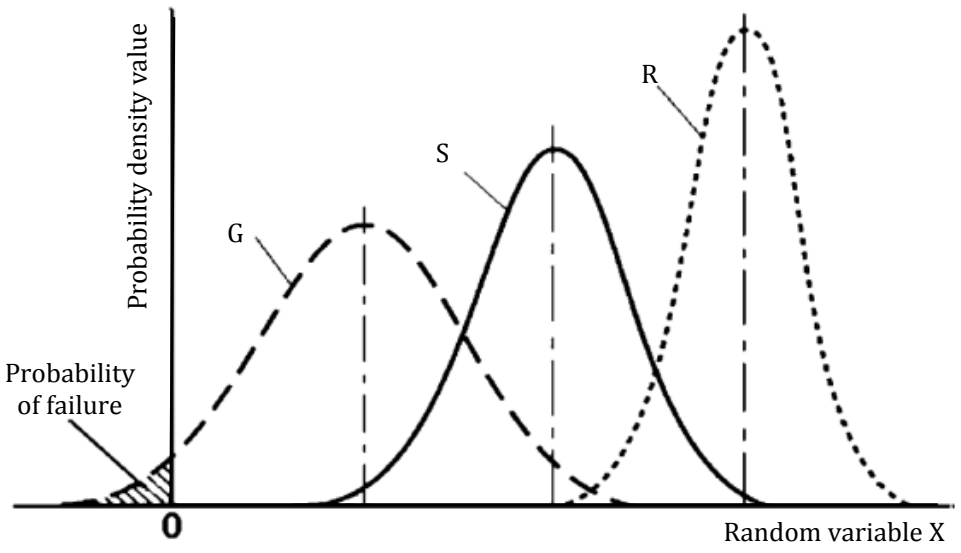

Figure 7.1—4 Concept of probability of failure

7.2 Reliability Analysis Software

7.2.1 Overview of General-Purpose Reliability Analysis Software Packages

The last few decades have seen the creation of several software packages related to the application of the reliability theory to structural engineering. These packages have acted as a crucial guide to the development of the integrated software. Some of the software packages which allow for interaction between the finite element analyses and the probabilistic algorithms are listed in Table 7.2—1. The objective of this table is to provide guidance for engineers and researchers, who are not familiar with any reliability packages for finite element analysis.

The presented packages are known as "general-purpose" packages, which mean that they can deal with a wide bundle of functions, rather than being limited to a specific problem. An assay is made in order to provide an overview of the available software packages, both of commercial and academic nature. This has been achieved by addressing the software codes' developers. The presented software packages are adapted so as they are capable of involving stochastic uncertainty in structural systems incorporating the material properties, geometry, loading and boundary conditions.

Table 7.2—1 General purpose reliability analysis software packages and their features

Software Package	Reliability Analysis Algorithm				Sensitivity	Interaction with FE software	Developer	Reference
	FORM/ SORM	MCS	Advanced MCS	Response surface				
ANSYS PDS & Design Xplorer		•		•	•	ANSYS	ANSYS Company	(Reh *et al.*, 2006)
CalREl/FERUM/OpenSees	•	•	•		•	FEAP/FEDEAS/OpenSees	University of Berkeley (USA)	(Der Kiureghian *et al.*, 2006)
COSSAN		•	•		•	FE_RV	University of Innsbruck (Austria)	(Schuëller and Pradlwarter, 2006)
NESSUS	•	•	•	•	•	ABAQUS, ABAQUS, NASA_GRC, NASTRAN, etc.	Southwest Research Institute, NASA (USA)	(Thacker *et al.*, 2006)
PERMAS-RA/STRUREL	•	•	•	•	•	PERMAS	RCP/University Munich (Germany)	(Gollwitzer, 2006)
PHIMECA	•	•	•		•	ANSYS, ABAQUS, etc.	PHIMECA Engineering SA (France)	(Lemaire and Pendola, 2006)
PROBAN	•	•	•	•	•	SESAM	DNV (Norway)	(Tvedt, 2006)
ProFES	•	•	•	•	•	ANSYS and NASTRAN	Applied Research Associate (ARA) Inc., Southeast Division, Raleigh NC (USA)	(Wu *et al.*, 2006)
UNIPASS	•	•	•	•	•	NASTRAN	PredictionProbe Company (USA)	(Lin and Khalessi, 2006)

7.2.2 Overview of NESSUS - Probabilistic Analysis Software

NESSUS is a modular computer software system and is used to perform probabilistic analysis of structural/mechanical components and systems. NESSUS incorporates state-of-the-art probabilistic algorithms with general-purpose numerical analysis methods to compute the probabilistic response and reliability of engineering systems. Uncertainty in loading, material properties, geometry, boundary conditions and initial conditions can all be simulated. Many deterministic modelling tools can be used such as finite element, boundary element, hydrocodes, and user-defined Fortran subroutines. NESSUS offers and wide range of capabilities, a graphical user interface, and is verified using hundreds of test problems; therefore, NESSUS is used in this study.

In NESSUS, the component reliability of a component is determined considering a single failure mode, where reliability is simply one minus the probability of failure, p_f. NESSUS can compute a single failure probability corresponding to a specific performance value or multiple failure probabilities such that the complete CDF can be constructed. Alternatively, NESSUS can compute a single performance value corresponding to a specific failure probability. The choice of analysis depends on the problem being solved. In addition to the failure probability, NESSUS computes probabilistic importance factors, $\partial\beta/\partial u$, where β is inversely related to p_f and u are the input random variables transformed

into standard normal space, and probabilistic sensitivity factors, $\partial\beta/\partial\theta$, where θ are the parameters of the input random variables, that is, mean value and standard deviation.

7.3 Reliability Assessment Methodology

Structural design has conventionally been based on deterministic analysis. In offshore engineering, roughly all structures and their environments are not deterministic, but rather have probability distributions which reflect the nature of the associated uncertainty. The conventional deterministic method of SCR analysis assumes that all of the factors affecting the strength, fatigue and the load applied to the structure are known and that the strength and load-effects are then known functions of these parameters. Early design codes on deterministic analysis treat the uncertainties in structural analysis by using so-called SFs. High implied SFs are presented by ensuring that the estimates of such parameters are conservative. The objective of this section is to provide an overview of state-of-the-art reliability assessment methodology. The overall objective of structural reliability methods is to quantify these uncertainties and to provide a better basis for decision-making with regards the dimensions of the structure or with respect to maintenance issues.

Generally, the following procedures are proposed for structural reliability evaluation:

- identify the basic resistance and loading variables defining the significant failure problem, of the structure under consideration;
- select resistance models (R) for fatigue strength limit;
- formulate the failure criteria and establish a relevant failure limit state function (G-function)for the failure mode (e.g., fatigue limit state). In simple terms this will be:

  $G = X_R\, R - X_s\, S$

  Equation 7.3—1

  where X denotes modelling accuracy and $G < 0.0$ denotes failure, R and S denotes the resistance and stress models respectively;
- determine and identify the distribution parameters, that is, probability function, standard deviation, location parameter, scale parameter, shape parameter, etc., as appropriate, for each basic variable (if previous experience indicates the variable can be treated as deterministic, this is to be preferred);
- calculate the reliability or the probability of failure of the structure, that is using a FORM procedure, and evaluate the probability that $G < 0$, that is, the probability of failure p_f, and the corresponding reliability index β given by:

$$\beta = -\Phi^{-1}\left(P_f\right)$$

Equation 7.3—2

Equation 7.3—2 is used to:

- ✓ calculate sensitivity measures, and
- ✓ assess the structure reliability against the given target reliability.

7.3.1 Levels of Reliability in Rational Approach

With regards to the rational approach, structural safety assurance should be based upon the probabilistic parameters of both resistance and stress. It is evident that neither the stress '*S*' nor the resistance '*R*' can be represented by a single value. Both are functions of several random variables and can only be treated probabilistically. The stress or loading, *S*, normally refers to the maximum value of loading likely to occur over the expected service life of the structure. The resistance or strength, *R*, represents a limiting state beyond which th structure is expected to fail or collapse. However, the probabilistic approach can be divided into two methods:

a. Full-Probabilistic Approach (Level 3 method)

With this method, the safety assurance is based on a complete probabilistic analysis for all of the structural systems or individual components. The complete probabilistic information of both stress and resistance is required,

together with the target failure probabilities. The probability of failure of a structure can be estimated by the integration of the joint probability distributions of the design variables involved in the load and resistance of the structure defining the failure domain. However, it is difficult to determine the joint probability density function of the variables in the actual engineering structures.

b. Semi-Probabilistic Approach

With this method, a semi-probabilistic approach is presented. A consistent method such as FORM and SORM are developed and used to assess the safety of the structures. However, because of the approximations to the failure surface and the distribution information of random variables, this approach, whilst very efficient, is not exact. This method is generally divided into two levels:

- **Safety index approach (Level-2 method)**

  Structural safety is ensured by a safety index compatible with acceptable probability of failure.

- **Partial safety factor approach (Level-1 method)**

  Structural safety is ensured by a number of partial safety factors, taking into account the variation of maximum loading and

minimum resistance. The uncertainties of parameters are modelled by their characteristic values for each design variable.

7.3.2 Overview of Reliability Analysis Techniques

The evaluation of the probability of failure which is the estimate of convolution integral can be conducted in the following ways:

a. Direct integration (only in some special cases)
b. Simulation techniques, such as using Monte Carlo Simulation (MCS), and
c. Analytical approximation: these can be grouped into two types: FORM and SORM.

As mentioned in the previous section, the evaluation of p_f using Equation 7.1—1 is known as the full distributional approach and is the fundamental equation of reliability analysis. Generally, the evaluation of multiple integrals is extremely complicated. The exact analytical solution of this integral cannot generally be carried out except for very simple models, with alternative techniques being needed for complex problems in reliability analysis. These alternative methods are analytical approximation or simulation techniques which can more simply compute this integral.

In simulation techniques, each random variable is sampled several times to introduce its real distribution according to its probabilistic nature. The

method commonly employed for this purpose is called MCS. For each simulated vector of random variables *x*, a complete numerical experiment must be performed. As the majority of structural analysis problems are complex and computationally time-consuming, this requires a prohibitively large number of complete runs to produce a result with statistical confidence.

The latter type, the analytical approximation, can be grouped into two types, namely the FORM and SORM. The limit state of interest can be linear or non-linear functions of the basic random variables. In FORM, the failure function (or the response surface) is approximated by a first order (linear) function in standardised Gaussian space at the most probable failure point. In standardised Gaussian space this is the point physically closest to the origin (the mean point). SORM is similar to FORM except for the fact that curvature is considered by fitting a second order (non-linear) function. In this study, FORM has been employed to evaluate the reliability-based fatigue of SCR in the TDZ. A brief description of FORM, SORM and MCS is presented in Appendix G.

7.3.3 Choice of Reliability Method

The applicability of a particular method depends, as in all mathematical modelling, on the problem at hand and on the objective of the analysis. In Appendix G, a number of important characteristics of the methods are presented in order to assist the user in selecting the most appropriate method for the problem at hand. The following issues are important to the selection of a method:

- The objective of the analysis.
- The number of random variables involved.
- The computational cost of evaluating the event (e.g. limit state) function.
- The properties of the event function, namely existence, continuity and differentiability.
- The reliability level of interest.

A reliability method which introduces an acceptable estimate of the reliability for the structure or structural components shall be used. Analytical approximation techniques (i.e., FORM and SORM) can be used when the limit state is a linear function and verified by simulation. When the number of basic random variables is under 5, the integral methods can be used to verify the results of analytical methods and simulation methods. Generally, simulation methods can be used to verify the results of other methods. A local reliability estimate using FORM at a single design point can be verified by a SORM

estimate. The choice of method to evaluate the SCR structural reliability can be summarised as follows:

- For linear failure limit state function or p_f <0.05, the analytical FORM and SORM for reliability estimates are suggested.
- For the number of random variables < 5, the direct integration method is suggested.
- The other cases, with the exception of those mentioned above, are evaluated by means of simulation techniques (e.g., MCS).
- In case of implicit limit state function, FORM, SORM or the response surface method can be used.

This study uses the analytical approximation FORM for reliability-based fatigue analysis. The motivations and choice of suitable reliability method are presented in Appendix G.

7.3.4 Target Reliability Level

Target reliability is a standard that must be fulfilled in the design or service of a structure to ensure that certain safety levels are sustained, as shown in Figure 7.3—1. Wirsching and Chen (1988) stated that the target reliability, β_T, is equal to 4.26 is recommended on an annual basis. It is generally more practical to work with lifetime probabilities of failure than with annual values. The target reliability level of β_T = 3.71 is a recommended value for structural lifetime of

approximately 20 to 30 years. A reliability analysis can be applied to verify that the required target reliability is achieved for the considered structural element. One of the main issues in this context relates to the possibility that uncertainties incorporated in the structural reliability analysis (SRA) will deviate from those that occur in real life because substantial errors may occur in real life along with a lack of knowledge regarding statistical uncertainty modelling.

The target reliability (safety) for the SRA should be appropriately selected based on factors such as consequence of failure, relevant design codes, accessibility for inspection and repair, and so on. The design is safe if $\beta > \beta_T$ where β is the reliability (safety) index as evaluated from SRA, and β_T is the target reliability (safety) index. The recommended target reliability (safety) indices and the corresponding annual probability of failure for marine risers and pipelines are summarised in a number of recommended practise codes (DNV, 2002, DNV, 2001-amended 2009, DNV, 1992, DNV, 2005). The acceptable target reliability indices and probability of failure values are introduced in Table 7.3—1, based on DNV (DNV, 1992, DNV, 2005).

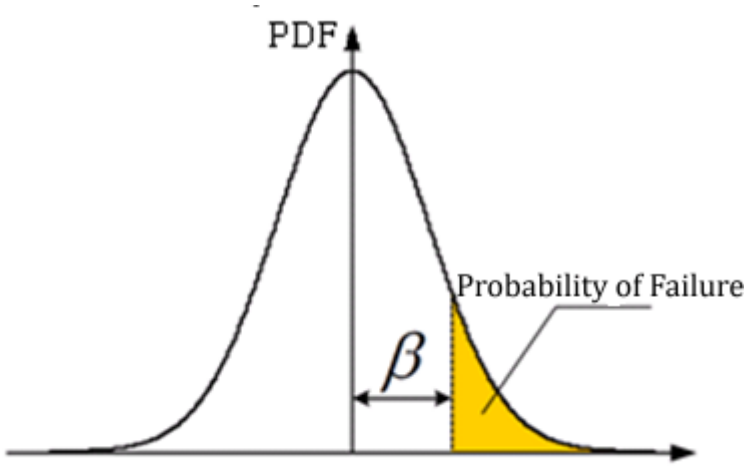

Figure 7.3—1 Target Reliability index corresponding to structural safety

Table 7.3—1 Values of acceptable probabilities of failure (p_f) and target reliabilities (β) for fatigue limit state of marine risers

Safety class (Consequence of failure)			
	Low (Not Serious)	p_f	10^{-3}
		β	3.09
	Normal (Serious)	p_f	10^{-4}
		β	3.71
	High (Very Serious)	p_f	10^{-5}
		β	4.26

7.4 Reliability-Based Fatigue Strategy

7.4.1 Fatigue Damage Assessment

Here, the primary concern is the fatigue damage produced from random loading, as this loading is the most applicable to offshore structures. The fatigue damage assessment can be described as follows:

$$N(S)^m = K$$

Equation 7.4—1

where N is the number of stress cycles required to produce fatigue failure at an applied stress level; S_i denotes the applied stress level, typically described in terms of a stress range; and both 'K' and 'm' represent the fatigue strength coefficient and fatigue strength exponent respectively, both of which are empirical material constants. For a specific stress range S_i ($i=1, 2, 3,\ldots,NSR_j$), where NSR_j is the number of applied stress ranges during sea state 'j':

$$N_i(S_i)^m = K$$

Equation 7.4—2

from which it follows that the corresponding number of cycles to failure is given by:

$$N_i = \frac{K}{(S_i)^m}$$

Equation 7.4—3

This relationship is commonly referred to as the 'stress-life' or '*S-N*' curve approach, see Figure 7.4—1. The *S-N* curve approach is commonly used in conjunction with the Palmgren-Miner rule, a linear damage accumulation rule which suggests that the accumulated damage fraction, D_i, resulting from the application of n_i cycles of stress range S_i is given by:

$$D_i = \frac{n_i}{N_i}$$

Equation 7.4—4

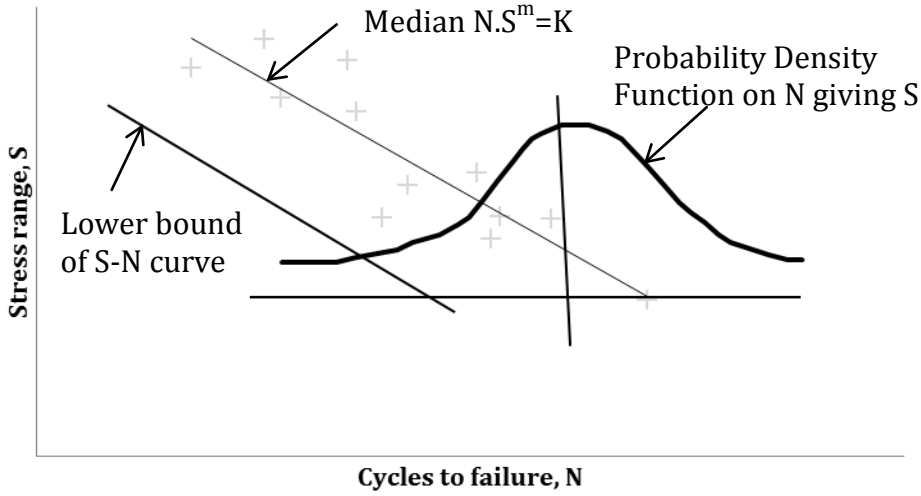

Figure 7.4—1 Definition of *S-N* curve (log-log scale)

a. Fatigue Damage Based on N_T

For applied stresses below a material's endurance limit (S_{end}), it is assumed that damage will be negligible. Consider an offshore structure subjected to loads during a sea state '*j*' of timeframe T_j. The total number of applied stress cycles during sea state '*j*' is given by $(N_T)_j$, where as follows:

$$\left(N_T\right)_j = \sum_{i=1}^{NSR_j} n_i$$

Equation 7.4—5

From the above equations, the total damage accumulated during sea state '*j*' is as follows:

$$D_j = \sum_{i=1}^{NSR_j} D_i = \sum_{i=1}^{NSR_j} \frac{n_i \left(S_i\right)^m}{K} = \frac{\left(N_T\right)_j}{K} \sum_{i=1}^{NSR_j} \frac{n_i \left(S_i\right)^m}{\left(N_T\right)_j}$$

Equation 7.4—6

where f_i is the probability that a single stress range within sea state '*j*' will have magnitude S_i (i.e., the fraction of the total stress cycles of a given sea state that are applied at stress range S_i) and in addition, the probability density curve (or histogram) for the applied stress range associated with each sea state is essentially defined as follows:

$$\left(f_i\right)_j = \left(\frac{n_i}{N_T}\right)_j \text{, where } \sum_{i=1}^{NSR_j}\left(f_i\right)_j = 1$$

Equation 7.4—7

It follows from Equation 7.4—4 that the total damage accumulation during sea state '*j*' can also be computed using the following relation:

$$D_j = \frac{\left(N_T\right)_j}{K}\sum_{i=1}^{NSR_j}\left(f_i\right)_j\left(S_i\right)_j^m$$

Equation 7.4—8

The accumulation of fatigue damage throughout a series of relevant sea states is dependent not only on the distribution of applied stresses within each sea state but also on the relative frequency of occurrence of individual sea states. The fatigue damage accumulated at a given structural location within timeframe T_T can be expressed as follows:

$$D_{tot} = \sum_{j=1}^{NSS} p_j D_j = \sum_{j=1}^{NSS} p_j \left(\frac{\left(N_T\right)_j}{K}\sum_{i=1}^{NSR_j}\left(f_i\right)_j\left(S_i\right)_j^m\right)$$

Equation 7.4—9

where D_j denotes the damage accumulation during sea state, '*j*', f_i and S_i (i=1,2,3,…,NSR_j) define the probability density curve for the applied stresses within each sea state and T_j represents the duration of sea state '*j*' (usually

expressed in terms of elapsed time or applied cycles). The probability of occurrence associated with sea state '*j*' is denoted by p_j and given by the ratio T_j/T_T, where $T_T = \sum_{j=1}^{NSS} T_j$, (*j*=1, 2, 3,... *NSS*); *NSS* represents the number of relevant sea states. It is noted that *K* and *m* are empirical constants which may be treated as random variables to reflect the uncertainty in structural capacity and material properties. It is further noted that the stress S_i is typically randomly distributed because of uncertainties in environmental parameters and structural loading.

b. Fatigue Damage Based on Life Time (T)

It is evident from Equation 7.4—2, Equation 7.4—3 and Equation 7.4—5 that fatigue damage is given by the following expression:

$$D = \frac{N_T S^m}{K}$$

Equation 7.4—10

where N_T is the total number of cycles in time, *T*, and *S* is the random variable denoting the fatigue stress range. Here, the distinction between the actual stress ranges in the pipe, S_a, and the estimated stress range, *S*, should be highlighted. It is assumed that $S_a = B.S$, where *B* is a random variable that quantifies modelling error. The average frequency of the stress cycles can be defined as follows:

$$f_0 = \frac{N_T}{T}$$

Equation 7.4—11

Then, the expression for fatigue damage (Wirsching, 1984, Wirsching, 1987) (Fatigue damage at time *T*) can be written as follows:

$$D = \frac{TB^m \Omega}{K}$$

Equation 7.4—12

where *B* is a factor to account for the uncertainties in estimating fatigue stresses from oceanographic data; Ω is the stress parameter defined by $\Omega = f_0 \sum_i \left(f_i S_i^m \right)$

where f_0 is the average frequency of stresses; S_i is the stress range; and f_i is the fraction of total stress ranges that S_i is acting.

7.4.2 Formulation of Limit State Models

a. Closed Form Limit State Based on Fatigue Damage

Reliability analysis methods are easy to implement if the limit state function $G(x)$ is an explicit function of the load and resistance-related input random variable x. In the case of the FORM, when an explicit function is available, it is easy to compute the derivatives of $G(x)$ with respect to random variables x to proceed with the search for the minimum distance point on the limit state, see Appendix G for minimum distance point concept and search procedure. The limit state function for the fatigue reliability of deep and ultra-deep offshore structures can be defined as follows (Akpan *et al*., 2007):

$$G(x) = B_R\Delta - B_S D_{tot}$$

Equation 7.4—13

This equation can be rewritten using Equation 7.4—9 as follows:

$$G(x) = B_R\Delta - B_S \sum_{j=1}^{nss} p_j \left(\frac{(N_T)_j}{K} \sum_{i=1}^{NSR_j} (f_i)_j \left(SCF.t_f.S_{oi} \right)_j^m \right)$$

Equation 7.4—14

$$S_i = S_{oi}\left(SCF.t_f\right)$$

Equation 7.4—15

where x is the vector of random variables; B_R denotes the modelling uncertainty factor applied to the fatigue resistance limit Δ (also known as Miner's index); B_S represents the bias factor associated with the fatigue damage calculation itself; S_{oi} is the nominal stress range whose level is given by Equation 7.4—15; *SCF* is the structural stress concentration or stress concentration factor and t_f is the thickness factor. The thickness factor is given as follows:

$$t_f = \left(\frac{t}{t_{ref}} \right)^k$$

Equation 7.4—17

where t is the pipe thickness; and t_{ref} is the reference thickness for the *S-N* curve, which is 25mm, as indicated by DNV (DNV, 2010). The determination of the *SCF* has a significant effect on the fatigue damage of the SCR. An empirical formulation based on data fitting is often used (Cao, 2010) and is given as follows:

$$SCF = 1 + 2.6 \frac{e}{t_1} \left[\frac{1}{1 + 0.7 \left(\frac{t_2}{t_1} \right)^{1.4}} \right]$$

Equation 7.4—18

where t_1 is the wall thickness (thinner tube); t_2 is the wall thickness (thicker tube); and e is the pipe eccentricity, which is defined as $\pm 10\%$ of t (Sen, 2008). The SCR has a uniform thickness hence $t = t_1 = t_2$. Using Equation 7.4—14 for a reliability analysis, this study assumes that:

- The empirical constants '*K*' and '*m*' are based on the *S-N* curve and are the same for all locations along the SCR; and
- The deterministic fatigue evaluations obtained using OrcaFlex software will be used for reliability-based fatigue analysis in the form of stress levels and frequency of occurrence.

b. Closed Form Limit State Based on Fatigue Life Time

Significant uncertainty exists in the factors of the fatigue damage expressions. Assuming that each uncertainty can be quantified, an expression for reliability can be derived based on the work of Wirsching (1979) and Wirsching (1984). Miner's rule states that failure under irregular stress ranges occurs when fatigue damage $D \geq 1.$ However, random fatigue experimental results have suggested that it is appropriate to describe fatigue failure more generally as $D \geq \Delta$, where Δ is a random variable denoting damage at failure, which quantifies modelling error associated with Miner's rule. Uncertainties in fatigue strength, as evidenced by scatter in the *S-N* data, are accounted for by considering K to be a random variable and m is considered to be deterministic.

Inaccuracies in fatigue stress estimation are described by the random variable *B*.

Let *T* denote time to fatigue failure. If $D = \Delta$, the basic damage expression of Equation 7.4—12 can be expressed in terms of time to failure as follows:

$$T = \frac{\Delta K}{B^m \Omega}$$

Equation 7.4—19

As *Δ*, *K*, and *B* are random variables. The intended service life of the structure can be defined as T_s. Therefore, the probability of fatigue failure of a joint is given as follows:

$$p_f = P(T \le T_s)$$

Equation 7.4—20

The fatigue failure occurs when the random variable *T*, is smaller than the service life of the structure, T_s. Thus, the performance (limit state) function is expressed as follows:

$$G(x) = T - T_s = \frac{\Delta K}{B^m \Omega} - T_s$$

Equation 7.4—21

7.5 Uncertainty Modelling

This section provides general guidance regarding the uncertainty modelling for an SCR structure in a deepwater environment.

7.5.1 Choice of Random Variables and Their Predicted Variability

To quantify uncertainty in the modelling of SCRs, it is necessary to define a set of *basic* variables that govern the dynamic response of the structure. The term basic is used to emphasise the fact that these quantities represent the most fundamental variables in the analysis calculation. This process of defining values for all input variables is performed in a deterministic calculation with single values attributed. In a probabilistic approach, the uncertainty of the fundamental random variables is addressed.

There are distinctive types of uncertainties in the basic random variables which must be considered. These include (ABS, 2001, Ditlevsen and Madsen, 2007):

- *Physical uncertainty*: is due to inherent variability of the properties in nature. Loads, material properties and dimensions are all examples of basic variables which, if measured, would exhibit physical fluctuation which could be described in terms of a probabilistic distribution or stochastic process.
- *Statistical uncertainty*: as the physical variability can only be quantified from example data, which is often sourced from a small sample size.

Uncertainty arises due to the inferences drawn from these limited observations. Statistical uncertainties are produced from incomplete information of variables and will be a function of the utilised distribution function, the applied estimation technique and the value of the distribution parameters. The probability distribution function and the corresponding statistical estimators may be different for various samples. This uncertainty can be reduced by the addition of information regarding the variable in terms of its statistical significance.

- *Modelling uncertainty:* besides the randomness and uncertainty associated with the input variables, uncertainty exists in the mechanical model set up to formulate the response. This uncertainty is due to imperfections and idealisations made in the physical model formulations for load and resistance as well as choices of probability distribution types for representation of uncertainties. This type of uncertainty is associated with the difference between the numerical models and the real behaviour of SCR. This *modelling uncertainty* involves not only uncertainty of model components, but also the response of the complete model. It results in the difference between actual and predicted results.

7.5.2 Random variables influencing the fatigue response of SCR

Before a set of basic random variables is chosen to represent the loading and physical uncertainties in fatigue life calculations of SCRs, an investigation of the

random variables used in literature is conducted. The aim is to determine which variables can be important in the fatigue analysis of the SCR. For a reliability analysis, it is important that the mean value and coefficient of variation (COV) for each variable be specified. Table 7.5—1 outlines the results and gives some indication of possible distributions, mean values and *COV*s. The uncertainties associated with fatigue damage evaluation can be categorised as follows:

- Numerical modelling of SCR involves uncertainty;
- The basic data of *S-N* curve is exposed to statistical scatter;
- Miner's rule, which is used to determine the fatigue damage accumulation, is exposed to uncertainty; and
- Fatigue stress levels involve uncertainty as they are based on load history.

Fatigue damage prediction of the SCR includes many sources of uncertainty. The main sources of uncertainty, based on Equation 7.4—14, can be categorised as follows:

- B_R, the modelling uncertainty factor;
- Δ, fatigue resistance limit (Miner's Rule);
- m, empirical fatigue strength exponent;
- K, empirical fatigue strength coefficient;
- B_s, the bias factor associated with the fatigue damage calculation itself;
- S_i, fatigue stress levels (MPa);

- *SCF,* stress concentration factor; and
- *t,* Pipe wall thickness.

Fatigue Resistance Limit & Modelling Error: Miner's rule states that fatigue failure under irregular stress ranges occurs when fatigue damage $D \geq 1$. Random fatigue experimental results have suggested that it is appropriate to introduce fatigue failure more generally as $D \geq \Delta$, where Δ is a random variable denoting damage at failure. The modelling uncertainty factor, B_R, is associated with Δ, which quantifies the error associated with Miner's rule. The reasons behind the difficulty of quantifying modelling error are obvious. Subjective uncertainty depends on:

- The general method of analysis used;
- how well a numerical model describes stress and strength;
- the site of the structure;
- time, because the engineer's degree of confidence improves as knowledge improves;
- the location of the joint in the structure;
- the magnitude of the load applied; and
- the phase of design and development under consideration.

While it may be difficult to define characteristic statistics for the offshore industry, it should be noted that the reliability alternative to the blanket factor of the safety approach requires that the modelling error be quantified. In

summary, values of B_R = 0.70 and *COV* = 0.50 are considered to be reasonable for general applications (Wirsching, 1984).

***S-N* Curve Parameters & Inaccuracy in fatigue damage estimation:** The *S-N* curve shows the relationship between the stress range and the number of stress cycles to failure when the amplitude of cyclic loading is constant. If the loading is irregular, Miner's rule is used. The basic data from which the *S-N* curve is characterised is subject to scatter. Uncertainties in fatigue strength are accounted for by considering the fatigue strength coefficient, *K*, and fatigue strength exponent, *m,* to be random variables to justify the scatter in the material behaviour. In previous studies, as described in Table 7.5—1, *K* could be considered to have a lognormal distribution. Several studies have considered *m* to be deterministic, while others assume it to have a lognormal distribution. Inaccuracies in fatigue damage estimation are described with the bias factor, B_S. Typical examples for the types of statistical variations that are placed on the SCR fatigue model in reliability studies are shown in Table 7.5—1.

Fatigue Stress Levels: The bias and uncertainty of stress range levels are substantial parameters in the probabilistic fatigue analysis. This is because these parameters are highly uncertain and the stress ranges are also greatly escalated in the fatigue damage equation by the empirical constant, *m*, of the *S-N* curve (Stahl and Banon, 2002). This uncertainty is reflected in values previously used in literature, with *COV*s of 40%. Distributions used to describe the effect

fatigue strength exponent, *m*, on an SCR fatigue performance have also been listed in Table 7.5—1.

Table 7.5—1 Basic random variables of interest in the probabilistic fatigue reliability analysis of SCR

	Basic Variable	Mean Value	Distribution	COV (%)	Reference	Notes
Modelling Uncertainty Factor	B_R	1.0	Weibull	25	Akpan *et al.*, (Akpan *et al.,* 2007)	used in an example calculation of Steel Compliant Riser
		0.7	Lognormal	50	Wirsching (Wirsching, 1984)	for example of fatigue design process in welded joints of steel offshore structures
		0.9	Lognormal	25	Wirsching *et al*. (Wirsching and Chen, 1988)	for example of fatigue design of marine structures (TLP tendons)
		1.0	Weibull	30	Xia & Das (Xia and Das, 2008)	for example of fatigue analysis of SCR
Fatigue Resistance Limit (Miner's Index)	**Δ**	1.0	Weibull	25	(Akpan *et al.*, 2007)	used in an example calculation of Steel Compliant Riser
		1.0	Lognormal	30	(Sen, 2008, Nazir, 2008)	for example of fatigue analysis of SCR in deepwater
		1.0	Lognormal	30	(Wirsching, 1984, Wirsching and Chen, 1988)	Based on analysis of variable amplitude test data
		1.0	Weibull	30	(Xia and Das, 2008)	for example of fatigue analysis of SCR
		1.0	Lognormal	30	(Khan, 2007)	for example of fatigue analysis of marine riser

	Basic Variable	Mean Value	Distribution	COV (%)	Reference	Notes
***S-N* Curve Parameters**	Fatigue strength exponent (m)	3.74	Lognormal	10	(Akpan *et al.*, 2007)	used in an example calculation of Steel Compliant Riser (Based on X' *S-N* curve)
		3.0	Deterministic	-	(Sen, 2008)	for example of fatigue analysis of SCR in deepwater
		3.0	Deterministic	-	(Wirsching, 1984)	for example of fatigue design of marine structures (TLP tendons)
		3.0	Lognormal	25	(Xia and Das, 2008)	based on *S-N* curve defined by DNV-seawater cathodic curve
		3.0	Deterministic	-	(Khan, 2007)	for example of fatigue analysis of marine riser
		3.0	Deterministic	-	(Leira *et al.*, 2003)	based on *S-N* curve class E
	Fatigue strength Coeff. (K)	2.5E+13	Lognormal	10	(Akpan *et al.,* 2007)	based on X' *S-N* curve
		1.46E+10	Lognormal	67	(Wirsching, 1984)	based on API RP 2A, data set 'F'
		1.23E+12	Lognormal	56	(Sen, 2008)	based on sample *S-N* curve
		5.81E+11	Lognormal	10	(Xia and Das, 2008)	based on *S-N* curve defined by DNV-seawater cathodic curve

	Basic Variable	Mean Value	Distribution	COV (%)	Reference	Notes
		1.73E+12	Lognormal	50	(Wirsching and Chen, 1988)	based on UK Den *S-N* curves-F- for welded joints
		5.27E+12	Lognormal	63	(Khan, 2007)	based on Proper *S-N* curve from API-RP2A for marine riser
		3.88E+12	Lognormal	63	(Leira *et al.*, 2003)	based on *S-N* curve class E
Bias Factor Associated with Fatigue Damage Calculation	B_S	1.0	Lognormal	25	(Akpan *et al.*, 2007)	used in an example calculation of Steel Compliant Riser
		0.9	Lognormal	25	Sen (Sen, 2008)	for example of fatigue analysis of SCR
		1.0	Lognormal	30	(Xia and Das, 2008)	for example of fatigue analysis of SCR
		1.0	Lognormal	20	(Khan, 2007)	for example of fatigue analysis of marine riser
Fatigue Stress Levels (MPa)	S_i		Gumbel	40	(Akpan *et al.*, 2007)	the applied stress data is discretised into stress ranges and cycles which affect cumulative damage

7.6 Case Study

7.6.1 Problem Description

The SCR model, which is attached to the semisubmersible as shown in Figure 7.6—1, is used for both deterministic and reliability analyses. A non-linear soil model approach for seabed reactions can result in significant variations in the estimated stresses of SCRs in the TDZ. These stresses can govern fatigue loading on the SCR. This study is focused on comparisons made between the linear and non-linear riser–seabed interaction model, as well as the effect on estimated stress near the TDP. Seabed interaction models are presented in Chapter 4, while soil parameter sensitivities and their effect on the fatigue life have been discussed in Chapter 6 based on deterministic fatigue analysis. As presented in Table 7.6—1, the non-linear soil model parameters are used for reliability-based fatigue analysis.

This study uses the deterministic fatigue results accounting for the effects of riser–seabed interaction effects for probabilistic reliability assessment. At the TDP, the fatigue response is mainly driven by the floating platform heaves and their induced motions. With this in mind, the study is focused on the semisubmersible platform, which poses more challenges in terms of motions that affect the TDP fatigue life (Yue *et al.*, 2010, Campbell, 1999, Deka *et al.*, 2010).

Table 7.6—1 Non-linear soil model parameters

Parameters	Symbol	Value
Pipe diameter	D	0.273 m
Mudline shear strength (median range)	S_{u0}	2.6 kPa
Shear strength gradient (median range)	S_{ug}	1.25 kPa/m
Saturated soil density	ρ_{soil}	1.5 t/m^3
Power law parameters	a	6.15
Power law parameters	b	0.15
Normalised maximum stiffness	K_{max}	200
Suction ratio	f_{suc}	0.7
Suction decay parameter	λ_{suc}	0.6
Re-penetration parameter	λ_{rep}	0.3
Soil buoyancy factor	f_b	1.5

7.6.2 Deterministic SCR Fatigue Model

The main requirements for deterministic fatigue calculations are summarised as follows:

a. The wave environment defined by the wave scatter diagram; and

b. The floating unit responses in terms of both first order and low frequency motions.

Fatigue analysis of SCRs has been addressed in several studies, including those by Hatton & Willis (1998), Campbell (1999), Karunakaran *et al.* (1999), and Karunakaran & Meling *et al.* (2005). Fatigue life in the TDZ is a critical design aspect of the SCR; this is the area in which geotechnical considerations become important. The significance of SCR-seabed interaction on the fatigue life of SCR in the TDZ is discussed and investigated in Chapter 6. The main sources of fatigue damage are the first-order vessel motions, slow-drift motions and VIV. A deterministic fatigue analysis comprises three major steps:

a. Analysis of stresses induced by random sea which is characterised by a wave scatter diagram;
b. Application of rain-flow counting (RFC) in a time domain analysis, which gives the stress cycles and stress range; and
c. Application of Miner's rule (cumulative damage theory), which is used to determine the fatigue damage.

7.6.3 SCR Probabilistic Fatigue Model

As shown in Figure 7.6—1, the SCR model, attached to a semisubmersible at a depth of 910 m, is used for both deterministic and reliability-based fatigue analyses. Probabilistic fatigue calculations only include the effect of first-order

vessel motion. The characteristics of the SCR model are provided in Table 7.6—2. A typical sea-state scatter diagram in the NNS is used. The resultant simplified sea-state fatigue bins are shown in Table 7.6—3.

The software OrcaFlex (Orcina, 2010) is used for the time domain analyses of the SCR. The SCR response time history is irregular with time. Therefore, the time domain analyses are followed by RFC (Lindgren, 1987, Ariduru, 2004) to break down the irregular time history into equivalent stress of block loading in the TDZ. The number of stress cycles in each block is conventionally listed in a stress range histogram, which can be used in Miner's calculation to obtain fatigue damage of the SCR in the TDZ. Time domain analyses are performed for the SCR in the TDZ and are followed by the FORM to predict the fatigue reliability index. The procedures for Reliability-based fatigue analyses are outlined in Table 7.6—4.

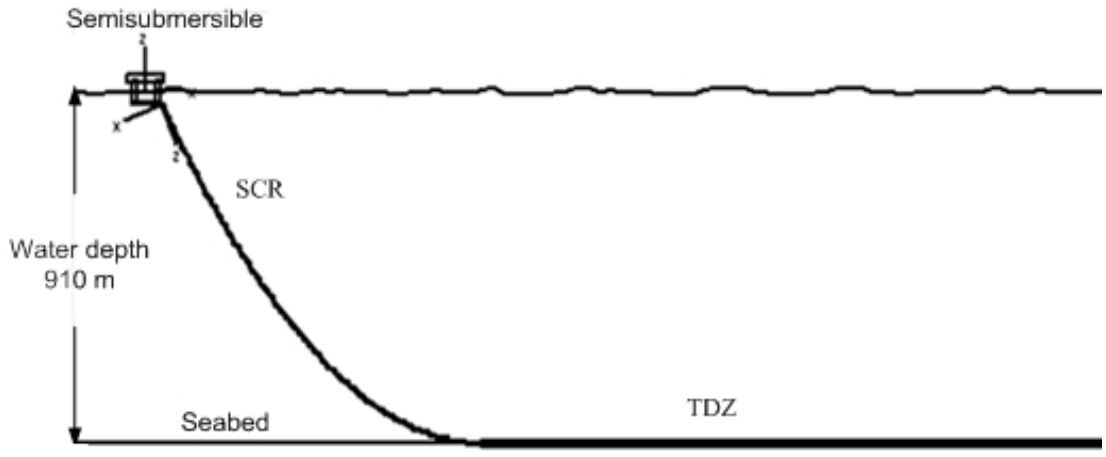

Figure 7.6—1 SCR attached to semisubmersible

Table 7.6—2 Characteristics of SCR

Outer diameter	273mm (10.75 inch)
Wall thickness	20.6 mm (0.812 inch)
Riser total length	3310 m
Hang-off angle	20°
Internal fluid density	0.8 t/m^3
Coating thickness	0.075 m
Coating density	0.8 t/m^3
Minimum yield strength	551.58 MPa
Sea-state scatter diagram	NNS
Vessel position	Mean position

Table 7.6—3 Sea-state fatigue bins

No.	H_S (m)	T_P (s)	Probability (%)
1	1.32	4.5	3.14
2	2.23	7.5	29.09
3	3.43	10.5	41.82
4	4.54	13.5	22.05
5	5.17	16.5	4.43
6	4.25	19.5	0.43
7	2.91	22	0.04

Table 7.6—4 Outlines of Probabilistic fatigue analyses

Procedure	Depiction
	Fatigue analyses (OrcaFlex)
Step 1	Divide all wave scatter diagram into a number of representative blocks.
Step 2	A non-linear time domain analysis is carried out for one representative sea state for each of these blocks.
Step 3	For each load case, the time history of response is calculated at the fatigue point, σ_{zz} = Direct tensile stress + Bending stress.
Step 4	Fatigue damage value is calculated corresponding to the time history of response within each load case using a rainflow counting procedure.
Step 5	The load case damage values are scaled to allow for the exposure associated with that load case.
Step 6	Finally, these total exposure load case damage values are summed over all load cases to obtain the overall total damage value at that fatigue point, expressed as: $D_{fat} = \sum_{j=1}^{NSS} D_j P_j$ where D_{fat} = Long-term fatigue damage, NSS = Number of blocks of sea-state, D_j = Short-term fatigue damage, and P_j = Sea-state block probability. In this paper only 1st order wave effects have been included.
Reliability-based fatigue analyses	
Step 7	• Fatigue Damage is given by: $D_{tot} = \sum_{j=1}^{NSS} p_j D_j = \sum_{j=1}^{NSS} p_j \left(\frac{(N_T)_j}{K} \sum_{i=1}^{NSR_j} (f_i)_j (S_i)_j^m \right)$ • The limit state function for SCR can be defined as $G(X) = B_R \Delta - B_s D_{tot}$ and this can be rewritten as:

	$$G(X) = B_R\Delta - B_S\sum_{j=1}^{nss} p_j\left(\frac{(N_T)_j}{K}\sum_{i=1}^{NSR_j}(f_i)_j(S_i)_j^m\right)$$ • Evaluate the probability of failure $p_f = p[G(x)\le 0]$

7.6.4 Distributions of Random Variables Used in Reliability Analysis

The probability distribution for a random variable expresses the uncertainty in that variable. Regression of available observations for a quantity will not always present a sufficient amount of information to allow for interpretation of the distribution type for the uncertainty. The choice of the distribution type will influence the reliability analysis; and thus, proper choice of the distribution type is often crucial (Veritas, 1992).

Normal or lognormal distribution is conventionally used when no detailed information is available. However, a random variable cannot have a negative value in many engineering issues due to the physical aspects of the problem. The lognormal distribution automatically eliminates the possibility of negative values. It has been also demonstrated that the lognormal is a valid model for a wide variety of structural design variables (Wirsching, 1984).

With Offshore structures, the extreme values of random variables are of particular importance. The largest (maxima) and smallest (minima) values of random variables have received a great deal of attention and are now often used for engineering design applications. When constructing an extreme value

distribution, if different sets of samples are obtained, one can select the extreme values from each sample set, either the maxima or minima values, and then construct a different distribution for the extreme values. Hence, the distribution of a considered variable governs the form of the corresponding extreme distribution. The comprehensive mathematical aspects of extreme value distributions are presented in Kotz and Nadarajah (2000).

As the sample size grows and approaches infinity, the distribution of the largest or the smallest values may asymptotically approach a mathematical distribution function in some cases, if the samples are identically distributed and statistically independent. The asymptotic extreme value distributions for both maxima and minima are categorised into three types; Type I, Type II, and Type III extreme value distributions.

The Type I extreme value distribution of the largest value is also known as the Gumbel distribution or simply the Extreme Value Distribution (EVD) in reliability engineering applications. The Gumble distribution is conventionally used in the analysis of extreme values of environmental loads and survival analysis.

The Weibull distribution, which is known as the Type III extreme value distribution in case of smallest value, is commonly used to describe the material strength and life-time characteristics of parts and components (Haldar and Mahadevan, 2000). It is worth noting that the Gumbel distribution relates to

maxima (*largest* extreme value), while the Weibull model relates to minima (*smallest* extreme value).

Based on previous studies, see Table 7.5—1, basic random variables have been chosen for the reliability analysis. The total number of variables used for reliability analysis is 62. Table 7.6—5 outlines these variables, their distribution type (formulation can be found in Appendix F), mean values and *COV*'s.

Table 7.6—5 Distributions of random variables used in reliability analysis

Random Variable	Mean Value	COV (%)	Probability Distribution
B_R	1.0	25	Weibull
B_S	1.0	25	Lognormal
Δ	1.0	25	Weibull
m	3 for S_i < 116E3 kPa 5 for S_i >116E3 kPa	10	Lognormal
K	$10^{12.192}$ for S_i <116E3 kPa $10^{16.32}$ for S_i >116 E3 kPa	10	Lognormal
S_i (kPa)	0.0007 – 92000	40	Gumbel
t (m)	0.0205	3	Lognormal
SCF	Given by Equation 7.4—17	_	Deterministic

7.7 Results and Discussion

7.7.1 Probabilistic Fatigue Reliability analysis Results

The purpose of this case study is to investigate the reliability-based fatigue for SCRs in the TDZ based on different geotechnical parameters. The uncertainties are assigned to the random variables, which are utilised in a probabilistic fatigue analysis. A description of the random variables is provided in Table 7.6—5.

The analysis is performed for 7 sea state load cases with 3 wave headings (0°, 90° and 180°) while the vessel is in the mean position. The stress ranges and accumulated fatigue damage results from linear, rigid and non-linear seabed models for SCR interaction are used in the reliability analysis. All reliability-based fatigue analyses are conducted using the FORM.

The TDP is proven to be a fatigue high spot for the SCR. Hence, the results of the reliability-based fatigue analysis, such as probability of failure, the corresponding reliability index and the deterministic fatigue life, results in the TDZ at an arc length of 1217.5 m are presented. These results are introduced in Table 7.7—1 for different wave headings, including seabed non-linearity. The deterministic fatigue analyses are conducted using the OrcaFlex program, while the general purpose reliability analysis tool NESSUS (Thacker *et al*., 2006) is used for the probabilistic reliability prediction. Table 7.7—1 presents a comparison between the deterministic and probabilistic influence of the fatigue

exponent and *SCF*. Furthermore, a comparison is made between the aforementioned closed-form limit state functions, which are based on fatigue damage and fatigue life, and their influence on the safety index.

The reliability analysis results are based on deterministic fatigue models in which the vessel is in the mean position and the seabed soil is modelled as non-linear in the vertical and lateral directions. The effect of the formulation of limit state function on the reliability indices is presented in Figure 7.7—1, where *m* and *SCF* are considered to be deterministic.

The results for all wave directions indicate that sea state load cases with a wave direction of 90° are the most critical in terms of fatigue. Evidently, the safety indices and the corresponding probabilities of failure for the fatigue damage and fatigue life limit state formulations are different. These results indicate that the safety indices depend on the formulation of the limit state equation as well as the distribution of random variables in the limit state.

Table 7.7—1 Reliability–based fatigue analysis results at TDP

Wave direction	Fatigue Life (years)	*m* and *SCF* (Deterministic)				*m* and *SCF* (Random)			
		FD* $(P[D > \Delta])$		FL $(P[T < T_s])$		FD $(P[D > \Delta])$		FL $(P[T < T_s])$	
		p_f	β	p_f	β	p_f	β	p_f	B
0°	175.13	5.9E-5	3.85	1.7E-2	2.1	0.187	0.89	0.315	0.48

Wave direction	Fatigue Life (years)	*m* and *SCF* (Deterministic)				*m* and *SCF* (Random)			
		FD* $(P[D > \Delta])$		FL $(P[T < T_s])$		FD $(P[D > \Delta])$		FL $(P[T < T_s])$	
		p_f	β	p_f	β	p_f	β	p_f	B
90°	161.15	1.8E-4	3.57	2.9E-2	1.9	0.193	0.87	0.321	0.464
180°	200.36	4.6E-5	3.91	1.5E-2	2.17	0.178	0.92	0.3	0.52

**FD and FL represent formulation of the limit state based on the fatigue damage and fatigue life respectively*.

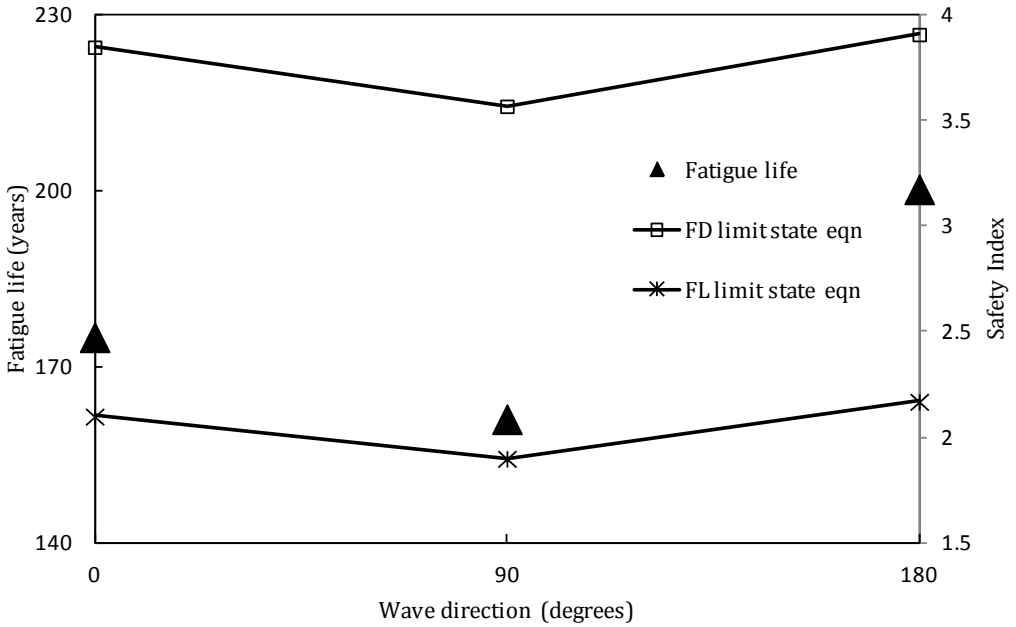

Figure 7.7—1 The influence of the wave direction on the safety index and fatigue life

The Probabilistic importance factors predicted through the reliability analysis are described in the pie charts depicted in Figure 7.7—2 and Figure 7.7—3.

These pie charts suggest that the fatigue strength exponent '*m*' is the dominant uncertainty parameter which most significantly affects the reliability of SCR in the TDZ while the dominant uncertainty parameter is the stress range S_i when *m* is deterministic.

The structural reliability index increases dramatically to around 3.57 (p_f = 1.8E-4), when *m* is considered deterministic, whilst S_i is the most important factor, and the reliability index drops to around 0.87 (p_f = 0.193) in cases where *m* has a random distribution and *COV*= 10 %. Therefore, it is clearly observed that the structural reliability and probabilistic importance factors of the basic random variables (B_R, B_S, Δ, *K* and S_i) are a significant function of the randomness of *m*.

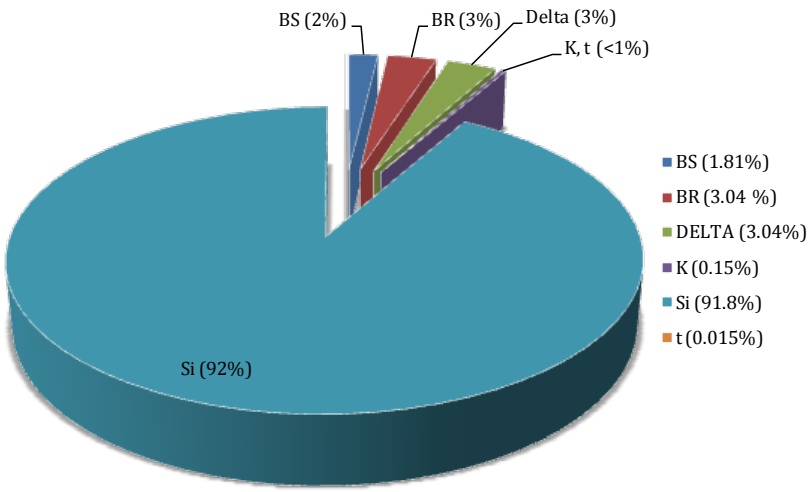

Figure 7.7—2 Probabilistic importance factors (%) for random variables at the TDP when *m* is deterministic and wave heading 90 deg

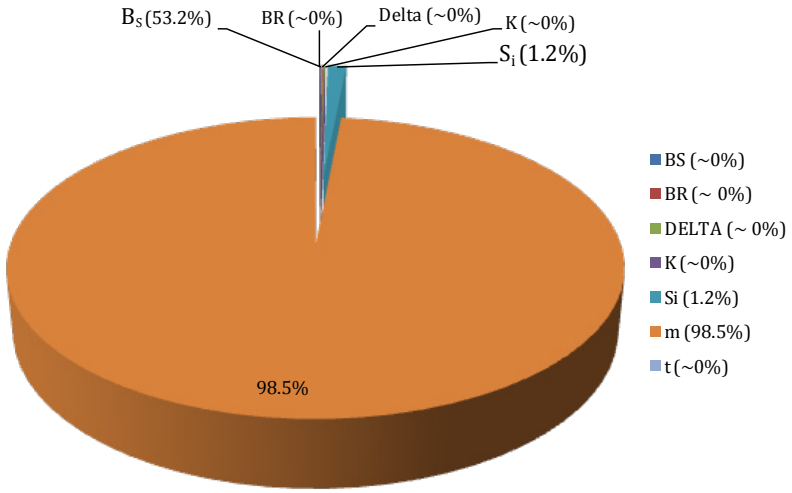

Figure 7.7—3 Probabilistic importance factors (%) for random variables at the TDP, wave heading 90 deg

7.7.2 Sensitivity of Reliability Index

The sensitivity of the SCR structural response to the input variables is calculated and used in the FORM. The fundamental concept of the FORM, that is, the search for design point or checking point, only requires the value and gradient of the performance function at each iteration. The value of the performance function is available from the deterministic structural analysis. The gradient is calculated using sensitivity analysis. In the case of explicit closed-form functions, the gradient is simply determined by analytical or numerical differentiation of the performance function with respect to each random variable.

In deterministic analysis, sensitivity is defined as the derivative of Z, where $Z = G(x)$, with respect to X; $\partial Z / \partial X_i$, which measures the change in the performance

due to change in the design parameter. In probabilistic analysis the sensitivity measure is $\partial p/\partial \theta_i$, which measures the change in the probability relative to the change in a distribution parameter (e.g., mean and standard deviation).

Another useful probability sensitivity analysis is the determination of the relative importance of the random variables. This can be achieved by performing several probabilistic analyses in which one of the random variables is treated as a deterministic variable (i.e., by reducing the standard deviation to zero) for each analysis. Based on the resulting probability changes, the relative importance of the random variables can be determined. Repeated analyses, however, may be very time consuming for large numbers of random variables.

A more efficient way of evaluating the relative importance of the random variables is based on the location of the checking point (also referred to as the design point, the minimum distance point, or the most probable point (MPP) of failure). At the MPP, $u^* = \left(u_1^* + u_2^* + \ldots . u_n^*\right)$, see Appendix G, the first-order probability estimate is $p_{f,FORM} = p\left[g_u(u) \le 0\right] = \Phi(-\beta)$ where:

$$\beta^2 = u_1^{*2} + u_2^{*2} + \ldots . u_n^{*2}$$

Equation 7.7—1

The unit normal vector at the MPP of the *g*=0 surface is defined as:

$$\alpha = -\frac{\nabla g}{|\nabla g|}$$

Equation 7.7—2

The α vector is positive towards the direction of decreasing g (i.e., to failure region). The sensitivity factors are projections of the α vector to the u-axes. Thus, they are the directional cosines of the α vector as shown in Figure 7.7—4, and can be written as:

$$\alpha_i = \frac{u_i^*}{\beta}$$

Equation 7.7—3

The directional cosines satisfy the following rule:

$$\alpha_1^2 + \alpha_2^2 + \ldots \alpha_n^2 = 1$$

Equation 7.7—4

which implies that each α_i^2 is a measure of the contribution to the probability (since the probability is related to β); higher α (in magnitude) indicates higher contribution. Thus, the sensitivity factors provide first-order information on the importance of the individual random variable.

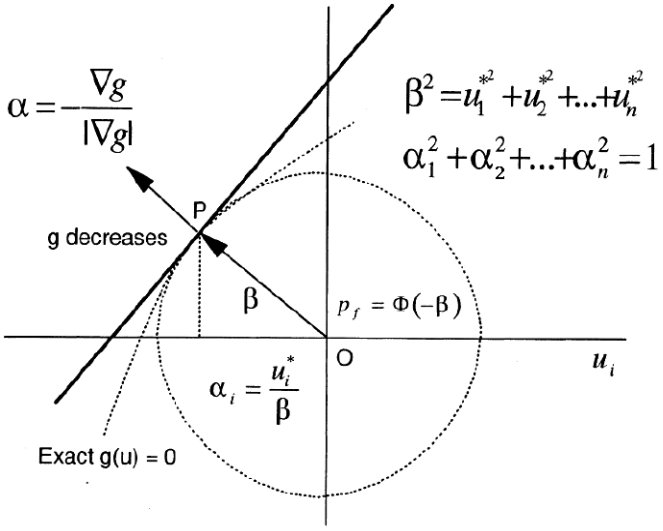

Figure 7.7—4 Definition of sensitivity factors

In general, sensitivity factors depend on the g-function as well as the input probability distributions. In a CDF analysis, the sensitivity factors will usually be different for different responses or probability levels. This is because the performance sensitivity or the approximate standard deviation may be different for different response or probability levels.

Because the above probabilistic sensitivity analysis is based on the first-order reliability method, α is a good probability sensitivity measure only if $\Phi(-\beta)$ is a good approximation to the true probability. Based on MPP, other sensitivity measures with respect to a distribution parameter (mean or standard deviation) or a limit-state function parameter, can be computed based on the sensitivity factors, the distribution, and the distribution transformation.

However, the probabilistic importance factors (pie chart) are the direction cosines to the most probable point in the transformed space as previously

presented. These factors provide a relative importance of the variables' contribution to the probability of failure. These factors are not available for sampling based probabilistic methods.

a. Sensitivity of Safety Index to Sea-States Fatigue Bins

The influence of individual sea-state fatigue bins on the reliability index is shown in Figure 7.7—5. The sea-state fatigue results for a 90° wave heading are based on the fatigue life limit state function (assuming the SCR service life T_s = 20 years), where m and SCF are constants. Sea-state #5 has the highest probability of failure (lowest safety index) because of the high stress ranges and the probability of occurrence associated with this sea-state.

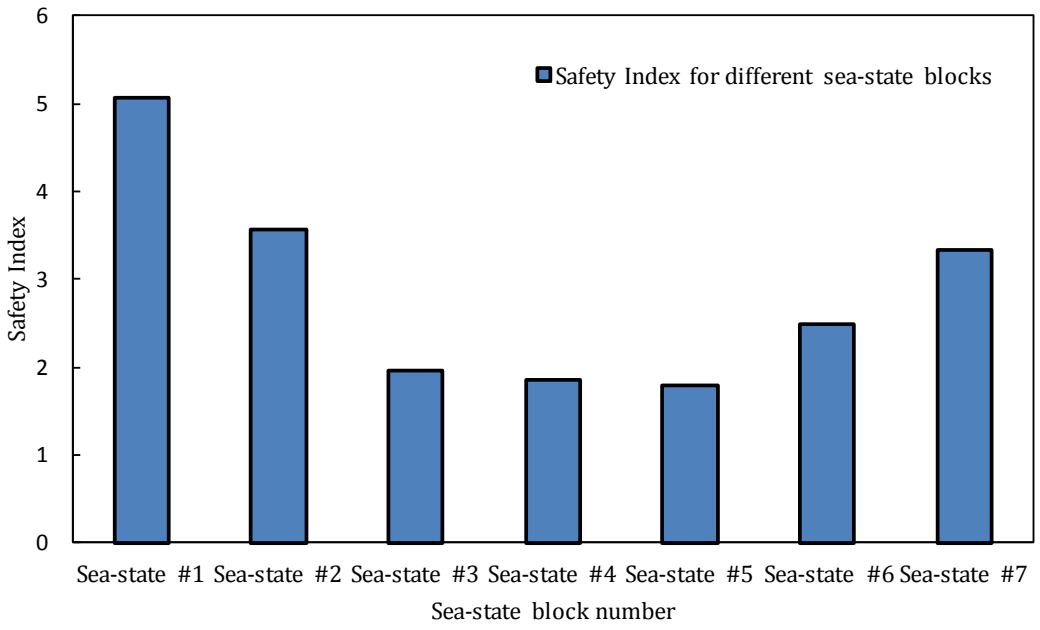

Figure 7.7—5 Influence of sea-states on the reliability index

b. Sensitivity of Safety Index to Fatigue Strength Exponent

A sensitivity study for the fatigue strength exponent '*m*' is performed to depict the influence of the chosen *COV* as shown in Figure 7.7—6, while the mean values of the reliability index are presented in Figure 7.7—7. Consequently, additional attention should be devoted to better calibration of '*m*' for the catenary riser and flow-lines in the TDZ. Furthermore, the stress range, 'S_i', has significant importance because it is a function of all sea blocks; and therefore, considerable efforts should be directed towards calibration of this parameter.

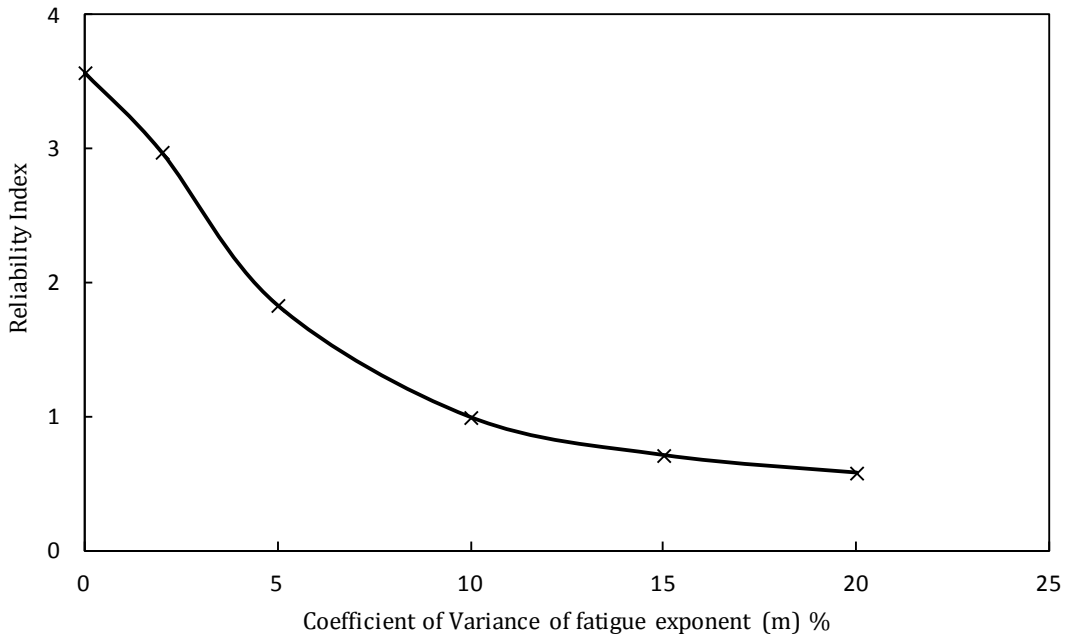

Figure 7.7—6 The influence of the *COV* of fatigue exponent '*m*' on the reliability index

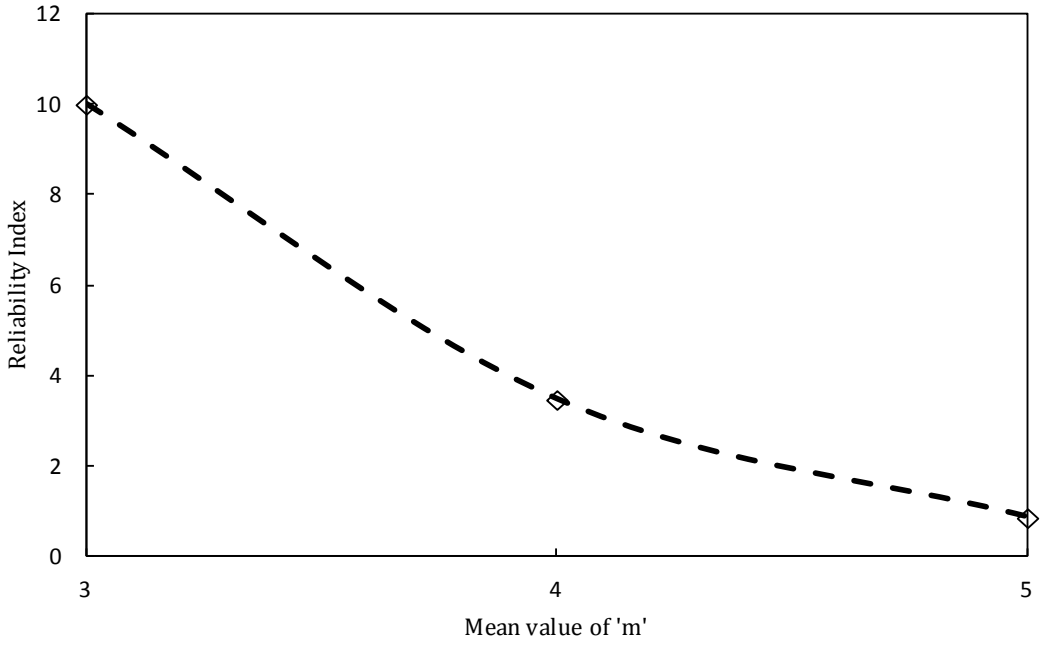

Figure 7.7—7 Effect of the fatigue strength exponent '*m*' mean value on the reliability index

c. Sensitivity of Safety Index to Linear Seabed Model

The interaction modelling of SCRs with seabed soil can have a significant influence on the safety level of SCRs in the TDZ. Therefore, to predict the influence of the common linear seabed modelling on the safety index of the SCR in the TDZ and compare this with that of the non-linear seabed model, the deterministic fatigue sea-states models of the SCR are implemented using linear seabed stiffness for SCR interaction in the TDZ. Deterministic fatigue analyses are performed using a linear soil model with a range of values of linear stiffness extending from linear low stiffness to rigid seabed (high values of soil stiffness approximately 10,000 kN/m/m^2). The influence of the linear seabed model

interaction with the SCR on the deterministic fatigue life and the reliability (safety) index are presented in Figure 7.7—8. The lower linear stiffness soil model yields a higher fatigue life and a higher safety index of the SCR compared to the rigid seabed model for SCR interaction in the TDZ. The change in the safety index of the SCR from low linear stiffness to rigid soil model is 16%. It is necessary to consider the uncertainty in soil stiffness when modelling the SCR–seabed interaction.

Furthermore, the reliability (safety) index is evaluated using limit sate function based on fatigue life, see Equation 7.4—20. API RP 2RD (API, 1998) code recommends for a component which can and will be inspected with low pollution risk, the design life should be at least 3 time the service life (SF=3). In addition, for all locations that cannot be inspected or where safety and pollution are significant, the design fatigue life should be at least 10 times the service life (SF=10) as described by API RP 2RD & API RP 2A (API, 1998, API, 2000). This means that the field life=20 years; when SF=0 means that Design Life=20 years, SF=2 means that Design Life=40 years, SF=4 means that Design Life=80 years, SF=6 means that Design Life=120 years, and SF=10 means that Design Life=200 years.

Reliability index and probability of failure for the range of linear stiffness seabed models are shown in Figure 7.7—9 and Figure 7.7—10 assuming that the field life=20 years. If Linear low stiffness=10 kN/m/m^2 and SF=0.0,

Reliability index and p_f (2.517, 5.92E-3), p_f = 1E-03 is recommended by DNV as the lower safety Class. Reliability index as a function of the linear seabed and SF is presented in Figure 7.7—11. The linear stiffness = 100, 10000 kN/m/m^2 and has a low safety index for high safety class SF which are very low compared to the DNV target safety index.

However, it should be stated that in order to evaluate the safety index due to fatigue in SCR, the system effects such as floating platform motion, and riser tension, must be involved. A direct comparison with API RP 2RD (API, 1998) cannot be conducted at this stage as the system effects have not been involved.

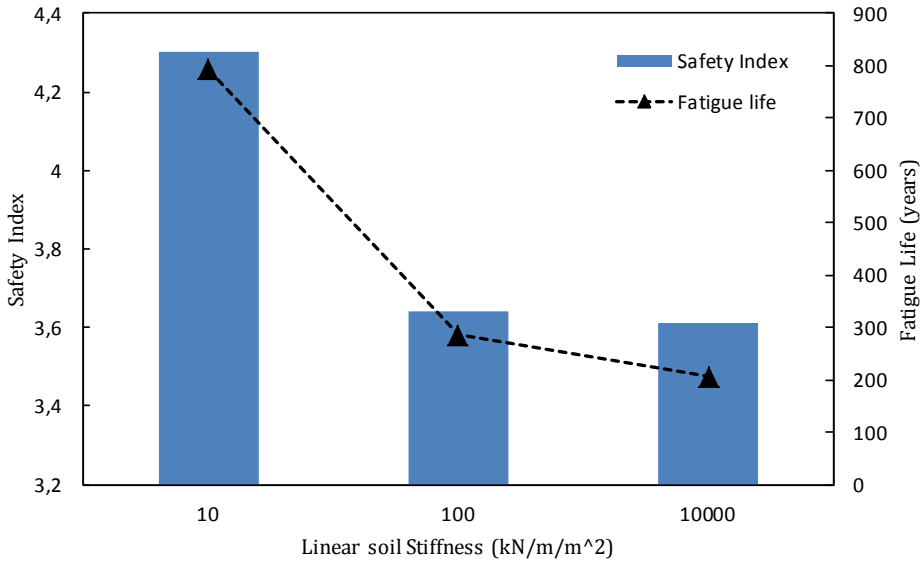

Figure 7.7—8 Effect of the linear stiffness on the safety index of SCR in the TDZ

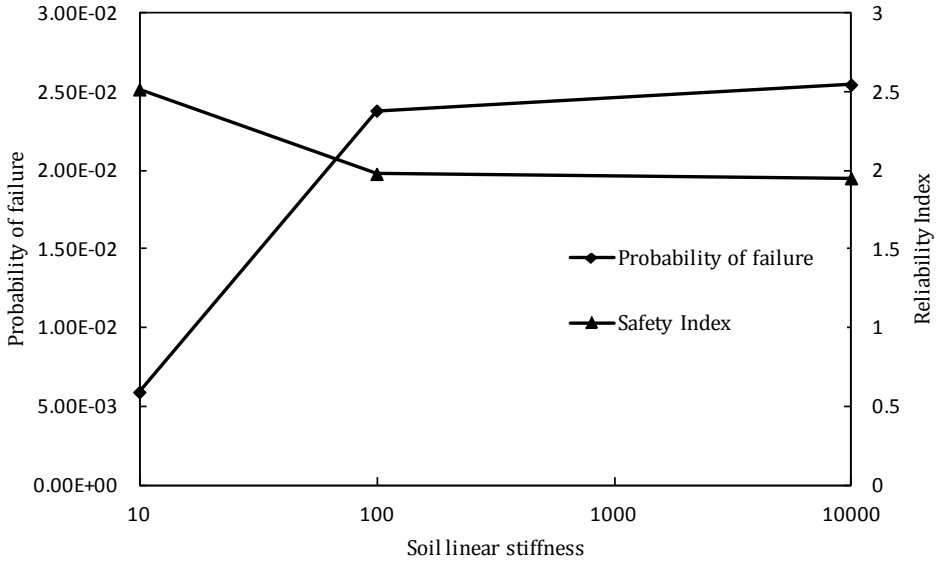

Figure 7.7—9 Reliability index and probability of failure for linear seabed model (Design life =20 years, i.e., SF=0)

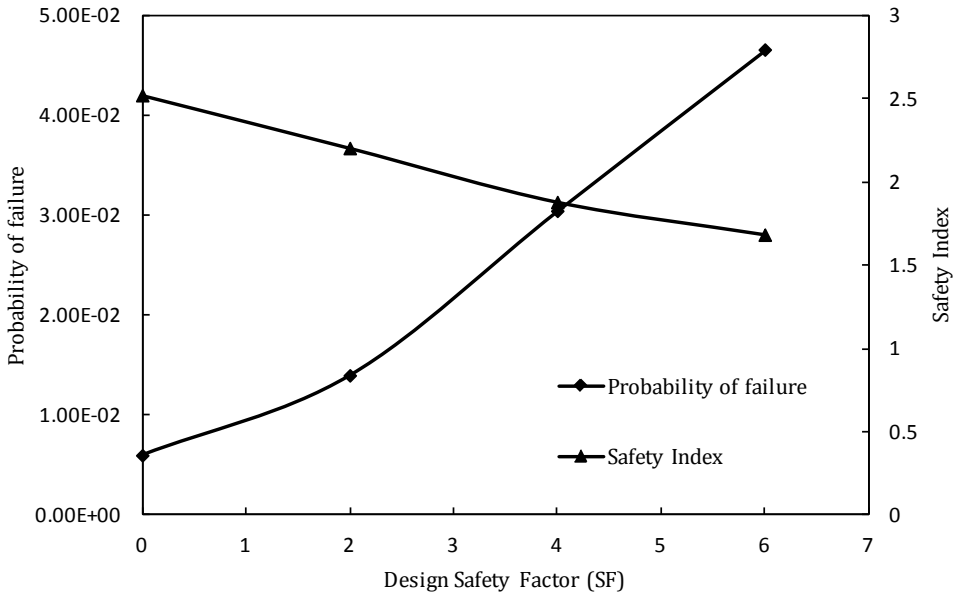

Figure 7.7—10 Reliability index and probability of failure as a function of the safety factor for linear seabed = 10 kN/m/m²

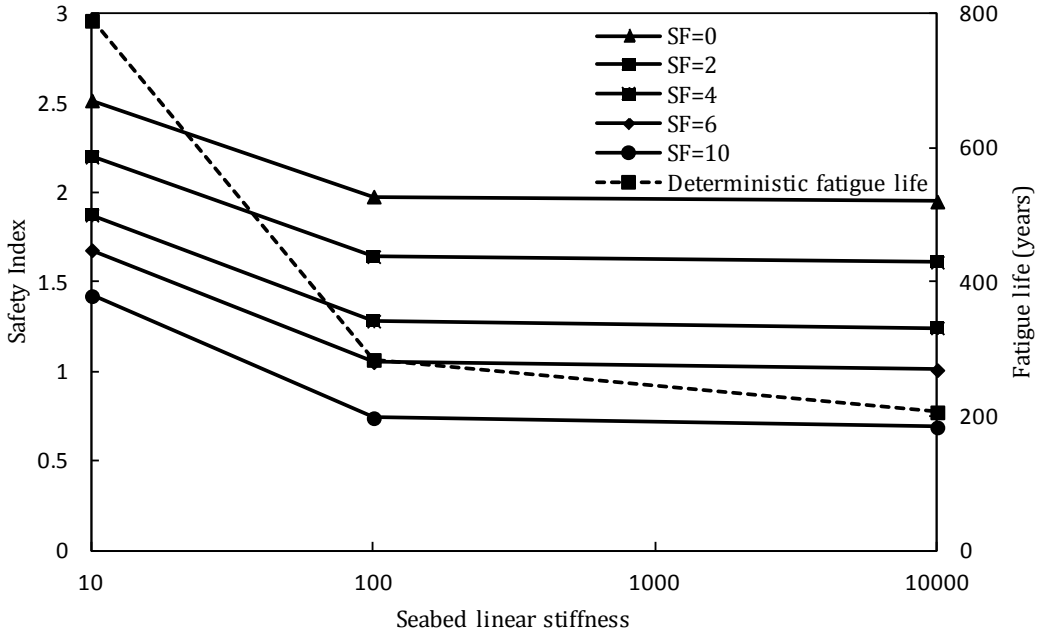

Figure 7.7—11 Safety index for different linear seabed stiffness by utilising a range for safety factors

d. Sensitivity of Safety Index to Non-linear Seabed Model Parameters

Figure 7.7—12 shows that the effect of the SCR–seabed model interaction on the probability of failure also influences the safety level of the SCR structure in the TDZ. The non-linear seabed model (using non-linear soil parameters in Table 7.6—1) introduces a higher probability of failure (low safety index) than does the linear high stiffness (Rigid) seabed, while the linear low stiffness seabed model gives a very low probability of failure (high safety class) compared to the non-linear model. The probability of failure occurring with a linear low stiffness is 95% less than that calculated using the non-linear seabed.

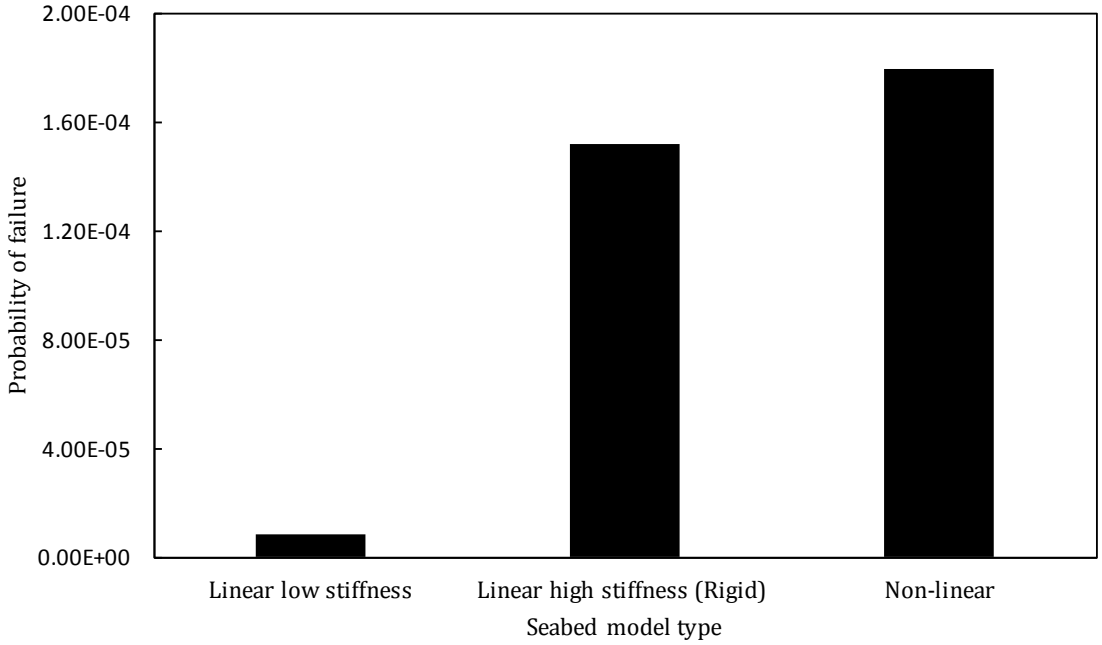

Figure 7.7—12 Probability of failure corresponding to the soil model type

As shown in Table 7.6—1, the non-linear seabed model has several parameters that influence the seabed response model. The non-linear seabed model, represented by the *V-z* curve and described in Chapter 4, is proven to be more realistic in terms of capturing the SCR–seabed interaction. Although fatigue analyses show that the fatigue damage is very sensitive to the seabed stiffness and soil suction, these parameters have not yet been evaluated with a great degree of confidence.

From Figure 7.7—13, it is evident that fatigue life decreases with an increase in normalised maximum stiffness, K_{max}; hence, a high K_{max} produces a low safety index, while *m* and *SCF* are assumed to be deterministic. by observing the soil suction shown in Figure 7.7—14, it is clear that the soil suction ratio, f_{suc}, can

influence the fatigue performance of SCRs in the TDZ and reduce the fatigue life. As previously presented in Chapter 6, the increase in the soil suction ratio increases the trench deepening in the TDZ, which decreases the safety index of the structure. It has been determined that variations in seabed non-linear parameters such as normalised maximum stiffness, K_{max}, soil suction, f_{suc}, and seabed trench deepening can have a significant influence on the uncertainty of SCRs fatigue damage in the TDZ. However, the effect of soil suction is subject to hysteresis effects such as cyclic loading, pull-out velocity and consolidation of soil, which can have a significant influence on the maximum soil suction force. The soil suction effect is assumed to be constant; therefore, the uncertainty associated with the dynamic suction effect warrants further research.

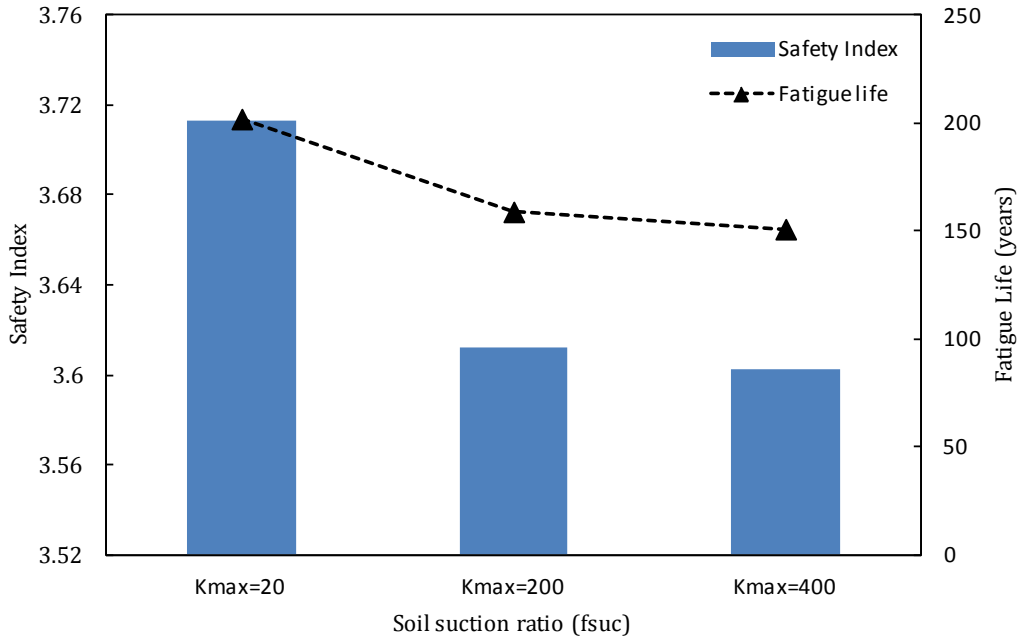

Figure 7.7—13 Effect of normalised maximum stiffness, *K*max, on the safety index, *β*

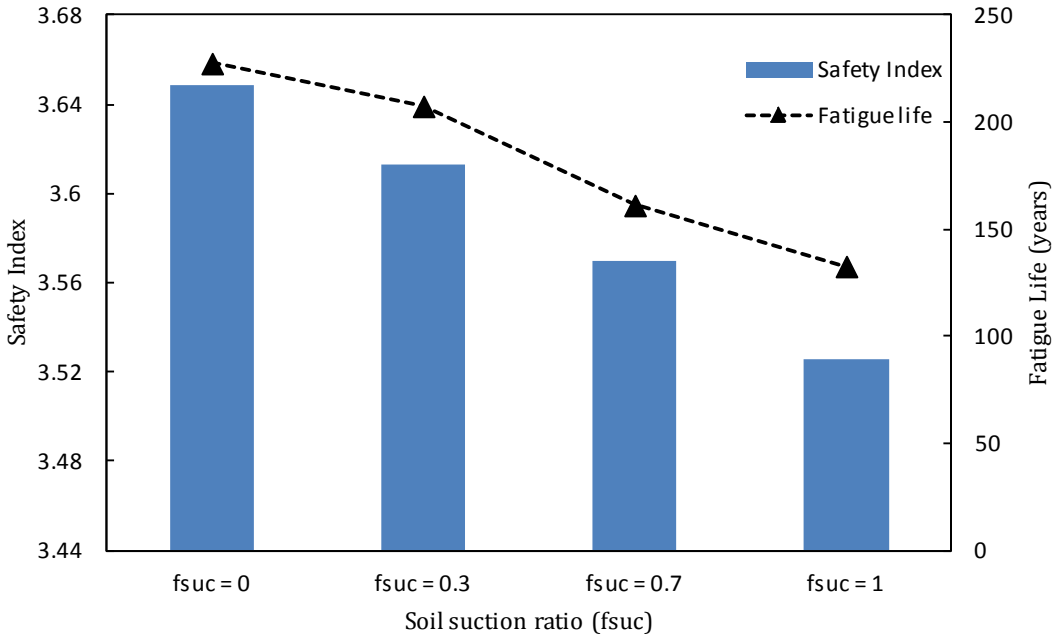

Figure 7.7—14 Effect of soil suction ratio on the safety index

7.8 Concluding Remarks

Reliability analysis is a rational technique for the evaluation of structural integrity and safety in comparison to the traditional SF method. This method considers the statistical nature of uncertainty in each random variable and gives guidance regarding the selection of the parameter values with a way to sustain the desired level of safety. The sensitivity of each variable on the structure response can be evaluated using these reliability analysis techniques. Sensitivity measures assist a designer in selecting the appropriate variable to adjust for a better service performance.

This chapter has presented an overview of the reliability procedure practiced in the offshore industry, briefly illustrating the basic techniques of reliability analysis. This study has developed and demonstrated practical procedures and techniques for determining the probabilistic fatigue reliability of SCRs. Additionally, this study implements a methodology for reliability assessment of SCRs which uses deterministic fatigue results as the starting point in conjunction with analytical reliability techniques such as the FORM. The case study involves an SCR that is attached to a semi-submersible and interacts with the non-linear seabed.

Uncertainty is involved in both the stress and resistance components and is well documented in the literature as characterising the probabilistic nature of reliability-based fatigue analysis. In the stress component, uncertainty arises

due to the uncertainty associated with the scatter in *S*–*N* curve data, wall thickness, eccentricity of the welded joint, *SCF*, uncertainty in estimation of fatigue stresses and the presence of a random variable which quantifies modelling error. Uncertainty in the strength part of the limit state function is due to the modelling error associated with Miner's rule. The safety index indicates the level of safety and whether the probability of failure is small enough to be acceptable. The limit state function may be extended further to include other uncertainties in the fatigue loading part. There is no limit on the number of uncertainties. This is seen as a way forward for a rational design of SCR with seabed interaction.

Furthermore, a sensitivity Study has been conducted to provide insight into the effect of the seabed modelling approach and geotechnical parameters on the fatigue reliability index of SCRs in the TDZ. The following conclusions can be drawn based on this study:

- The reliability-based fatigue strategy has been summarised and conducted for an SCR in deepwater and based on the deterministic fatigue analysis results. The limit state model presented can be used to perform a risk analysis for SCRs and offshore structures.
- The reliability assessment technique accounts for various sources of uncertainties included in the fatigue analysis of SCRs. It should be noted that the uncertainties in the SCR's loadings, material properties,

associated structural parameters and marine environment have been accounted for by specifying a maximum extreme load value distribution (Gumbel) and a high value of *COV* for the stress levels which is known as lump strategy. In Reliability analysis, Gumbel distribution is usually used in the analysis of extreme values of environmental loads and survival analysis.

- Two different reliability-based fatigue strategies are utilised; the first strategy is the limit state model based on fatigue damage, while the second is the limit state model based on fatigue life. These limit state models are applied to the SCR that is attached to the semisubmersible at the top-end and interacts with the seabed in the TDZ. The case studies are used to investigate (a) the effect of the wave direction, (b) the effect of the formulation of limit state model, (c) the uncertainty effect of the fatigue exponent *m* and the stress concentration factor *SCF*, (d) the effect of individual sea-states on the safety level of the structure, and (e) the effect of the SCR–seabed interaction in which the seabed is modelled as a linear low/high stiffness or non-linear seabed model.
- For case study (a), the lowest reliability index is 3.57, where the limit state model is based on fatigue damage, *m* and *SCF* are deterministic and the wave direction is 90°. The investigated case study has demonstrated that the 90° wave direction is more critical in terms of fatigue performance. Reliability analysis using the limit state function based on

the fatigue damage presents a small probability of failure, which means that the reliability index is acceptable when compared to the target reliability given in Table 7.3—1.

- For case study (b), the formulation of the limit state function can dramatically influence the reliability (safety) index of the SCR structure in a component reliability analysis. The reliability index is reduced from 3.57 in cases where the limit state model is based on fatigue damage, to 1.9 in cases where the limit state model is based on fatigue life and *m* and *SCF* are deterministic.
- For case study (c), assuming that *m* and *SCF* have deterministic values, the lowest reliability index will be 3.57. The index is significantly reduced to 0.87 in cases where it is assumed that they have an uncertainty distribution and the limit state model is based on fatigue damage. The investigated case studies have shown evidence that the uncertainty in the fatigue exponent strength, *m*, has the largest influence on the reliability-based fatigue of SCRs. Sensitivity studies have shown that the probabilistic importance of the fatigue strength coefficient, *K*, is low. It should be noted that *K* and *m* are correlated random variables. This correlation has not been considered in this study.
- Parametric sensitivity studies of *m* indicate that the reliability analysis is very sensitive to the uncertainty associated with parameters such as *COV*

and the mean value of *m*. Therefore, this study highlights the need for a better probability calibration of *m*.

- Sensitivity studies have also been presented and reveal that the most important random variable is the stress levels, S_i; where *m* and *SCF* are deterministic, which captures the uncertainties associated with loading and material properties.
- For case study (d), individual sea-state fatigue bins are considered to determine the most critical sea-state load cases for the safety of the structure. The importance of the individual sea-state lies in the fact that the high stress levels and the probability of occurrence are associated with the individual sea-states.
- For case study (e), the seabed modelling approach significantly affects the reliability-based fatigue analysis. In the case of a linear seabed, the low-stiffness seabed gives a reliability index of approximately 4.3, and decreases to a value of approximately 3.6 in cases where there is a high-stiffness linear seabed. The non-linear seabed model gives a higher probability of failure than those that arise from the linear low and high stiffnesses. This result clearly implies the conservatism of the linear and rigid seabed modelling with SCR interaction. However, it should be noted that careful attention should be directed towards selecting the values of the non-linear seabed parameters. These parameters can affect the safety

of the structure, due to the wide range of values for critical seabed parameters.

This study provides insight into the significance of geotechnical, *S-N*, and modelling error parameters. In addition, this study has revealed that the uncertainties associated with seabed parameters and *S-N* scatter data significantly affect the fatigue reliability of SCRs in the TDZ. The most critical seabed parameter is the normalised maximum stiffness $K_{\max}$ and f_{suc} which require better calibration of their value for clay soil. The fatigue reliability analysis is conducted using FORM. The chosen values for the seabed parameters are based on recent literature and experimental data.

7.9 References

ABS 2001. Guide for building and classing subsea pipeline systems and risers. USA: American Bureau of Shipping.

Akpan, U., Koko, T., Rushton, P., Tavassoli, A. & Else, M. Probabilistic fatigue reliability of large diameter steel catenary risers (SCR) for ultra-deepwater operations. *In:* Proceedings of the 26th International Conference on Offshore Mechanics and Arctic Engineering, 2007 California, USA. ASME.

API 1998. API RP 2RD: Design of risers for floating production systems and tension-leg platforms. American Petroleum Institute

API 2000. API RP 2A: Planning, designing and construction fixed offshore platforms. American Petroleum Institute.

Ariduru, S. 2004. *Fatigue life calculation by rainflow cycle counting method.* Master of Science, The Graduate School of Natural and Applied Sciences of Middle East Technical University.

Campbell, M. The complexities of fatigue analysis for deepwater risers. *In:* Deepwater Pipeline Conference, March 1999 New Orleans, USA.

Cao, J. Fatigue analysis technique of deepwater steel catenary risers. *In:* 29th International Conference on Ocean, Offshore and Arctic Engineering, OMAE 2010, 6-11June 2010 Shanghai, China. ASME.

Deka, D., Campbell, M., Kakar, K. & Hays, P. Advances in deepwater riser technology: Gulf of mexico wet tree deepwater riser concepts with sour service. *In:* Offshore Technology Conference, 2010 Houston, USA.

Der Kiureghian, A., Haukaas, T. & Fujimura, K. 2006. Structural reliability software at the university of california, berkeley. *Structural safety,* 28**,** 44-67.

Ditlevsen, O. & Madsen, H. O. 2007. *Structural reliability methods*, Wiley Chichester.

DNV 1992. Classification notes No. 30.6 structural reliability analysis of marine structures.

DNV 2001-amended 2009. DNV-OS-F201: Dynamic risers. Det Norske Veritas.

DNV 2002. Dnv RP F201: Recommended practice design of titanium risers. Det Norske Veritas.

DNV 2005. Riser fatigue. *Recommended Practice DNV-RP-F204.* Det Norske Veritas.

DNV 2010. Fatigue design of offshore steel structures. *Recommended Practice DNV-RP-C203.* Det Norske Veritas.

Gollwitzer, S. 2006. Permas-ra/strurel system of programs for probabilistic reliability analysis. *Structural safety,* 28**,** 108-129.

Haldar, A. & Mahadevan, S. 2000. *Reliability assessment using stochastic finite element analysis*, Wiley.

Khan, R. A. a. A., S. Dynamic response and fatigue reliability analysis of marine riser under random loads. *In:* Proceedings of the 26th International Conference on Offshore Mechanics and Arctic Engineering, OMAE2007-29235, 2007 San Diego, California, USA.

Kotz, S. & Nadarajah, S. 2000. *Extreme value distributions: Theory and applications*, World Scientific Publishing Company.

Leira, B. J., Meling, T. S., Larsen, C. M., Berntsen, V., Stahl, B. & Trim, A. 2003. Assessment of fatigue safety factors for deep-water risers in relation to viv. *Journal of Offshore Mechanics and Arctic Engineering,* 127**,** 353.

Lemaire, M. & Pendola, M. 2006. Phimeca-soft. *Structural safety,* 28**,** 130-149.

Lin, H. Z. & Khalessi, M. 2006. General outlook of unipass (tm) v5. 0: A general-purpose probabilistic software system. *Structural safety,* 28**,** 196-216.

Lindgren, G. a. R., I. 1987. Rain flow cycle distributions for fatigue life prediction under gaussian load processes. *Fatigue & Fracture of Engineering Materials & Structures* Vol. 10, No. 3, pp.251-260.

Nazir, M., Khan, F. and Amyotte, P. 2008. Fatigue reliability analysis of deep water rigid marine risers associated with morison-type wave loading. *Stochastic Environmental Research and Risk Assessment (2008) 22:379-390***,** 379-390.

Orcina 2010. Orcaflex user manual *Orcina,* version 9.4a, UK.

Reh, S., Beley, J. D., Mukherjee, S. & Khor, E. H. 2006. Probabilistic finite element analysis using ansys. *Structural safety,* 28**,** 17-43.

Schuëller, G. & Pradlwarter, H. 2006. Computational stochastic structural analysis (cossan)-a software tool. *Structural safety,* 28**,** 68-82.

Sen, T. K., Brown, K. and Root 5-8 May 2008. Fatigue in deep water steel catenary risers - a probabilistic approach for assessment of risk. *Offshore Technology Conference.* Houston, Texas, USA.

Sen, T. K., Brown, K. and Root 2008. Fatigue in deep water steel catenary risers - a probabilistic approach for assessment of risk. *Offshore Technology Conference.* Houston, Texas, USA.

Shama, M. 2009. Basic concept of the factor of safety in marine structures. *Ships and Offshore Structures,* 4**,** 307-314.

Stahl, B. & Banon, H. Fatigue safety factors for deepwater risers. *In:* International Conference on Offshore Mechanics and Arctic Engineering, 2002 Oslo, Norway. ASME.

Thacker, B. H., Riha, D. S., Fitch, S. H. K., Huyse, L. J. & Pleming, J. B. 2006. Probabilistic engineering analysis using the nessus software. *Structural safety,* 28**,** 83-107.

Tvedt, L. 2006. Proban-probabilistic analysis. *Structural safety,* 28**,** 150-163.

Veritas, N. 1992. *Structural reliability analysis of marine structures*, Det Norske Veritas.

Wirsching, P. H. 1984. Fatigue reliability for offshore structures. *Journal of Structural Engineering,* 110**,** 2340-2356.

Wirsching, P. H. 1987. Fatigue design criteria for tlp tendons. *Journal of Structural Engineering,* 113**,** 1398.

Wirsching, P. H. & Chen, Y. N. 1988. Considerations of probability-based fatigue design for marine structures* 1. *Marine Structures,* 1**,** 23-45.

Wu, Y. T., Shin, Y., Sues, R. H. & Cesare, M. A. 2006. Probabilistic function evaluation system (profes) for reliability-based design. *Structural safety,* 28**,** 164-195.

Xia, J. & Das, P. K. 2008. Probabilistic fatigue reliability analysis of deepwater steel catenary risers. *Proceedings of the ASME 27th International Conference on Offshore Mechanics and Arctic Engineering.* Estoril, Portugal: OMAE.

Yue, B., Campbell, M., Walters, D., Thompson, H. & Raghavan, K. 2010. Improved SCR design for dynamic vessel applications. *Proceedings of the ASME 2010 29th International Conference on Ocean, Offshore and Arctic Engineering, OMAE2010-20406.* Beijing, China.

CHAPTER 8

DISCUSSIONS AND RECOMMENDATIONS FOR FUTURE RESEARCH

8.1 Introductory Remarks

The research work introduced in this thesis attempts to address the issues related to the SCR–seabed interaction response and their effects on the dynamic structural behaviour, fatigue assessment and safety of the SCR. This chapter begins by briefly recapping the thesis and the major results achieved in the research work undertaken, whilst also highlighting the novelties of this investigation. The chapter will conclude with a number of recommendations for future research which it is hoped will serve as a guide for future endeavours.

8.2 Broader View of the Thesis

This thesis begins by critically reviewing SCR analysis techniques with special focus on the SCR–seabed interaction response. Several factors affect the SCR response with seabed interaction in the TDZ. Following evaluation of the previous research work, experimental results and model simulation, the significant key parameters influencing the TDZ response are identified. In addition, it is proposed that the modelling methodology for lateral interaction be combined with the vertical model through cyclic motions for determining the SCR response.

Generally, SCR analysis techniques use either a rigid or linear surface in order to model the seabed response. This study finds that using a rigid surface to model the seabed produces conservative fatigue results compared to the linear seabed.

Furthermore, current seabed models neither account for the non-linearity with seabed, including the trenching effects within the TDZ, nor suction soil effects, both of which can influence the SCR maximum stress and the fatigue damage assessment.

The main goal of this thesis is to evaluate the effects of the SCR–seabed interaction response on the global response of SCR. This involves the examination of non-linearity in the response model of SCR–seabed interaction and trenching effects of SCR. Also of vital importance is the uncertainty of geotechnical parameters and their influence on the dynamic structural behaviour and the reliable estimates of the fatigue life of SCR in the TDZ. This study also develops and presents a practical methodology as well as procedures for the reliability–based fatigue analysis assessment of an SCR.

Throughout this research, realistic techniques for modelling the seabed response are studied and investigated in order to predict the global dynamic response and structural behaviour of SCR in the TDZ. This study discusses the significance of SCR–seabed soil interaction in the design of SCR for deepwater applications and reports the results of analyses carried out on a SCR on soft clay in 910 m depth of water using the commercial code OrcaFlex for non-linear time domain simulation with a robust meshing technique. Indeed, the present study involves the investigation of the vertical embedment and large lateral movements of the SCR in the TDZ. We also present results from numerical

simulations of the global responses of the SCR, taking into account a critical point at the TDZ. During simulations, the seabed is modelled using a hysteretic non-linear model in vertical seabed direction, bilinear and tri-linear soil model in the lateral seabed direction.

The challenges regarding fatigue damage assessment of SCR in the TDZ are primarily rooted in the non-linear behaviour of SCR–seabed interaction, considerable uncertainty in SCR–seabed interaction modelling and geotechnical parameters. SCR–seabed response is critical for a reliable estimation of the fatigue life in the TDZ. Various design approaches pertaining to the lateral pipe–soil resistance model are discussed. The techniques which can be used to cover these aspects and to develop an advanced SCR–seabed lateral interaction model are outlined. These techniques have been applied in the FE model which can be used to analyse the lateral SCR–seabed interaction under hydrodynamic loading. This study investigates the sensitivity of fatigue performance to geotechnical parameters through a parametric study. In this research, global analyses are performed in order to assess the influence of vertical linear seabed springs, the lateral seabed model and the non-linear seabed model, including trench evolution into seabed, seabed normalised stiffness, re-penetration offset parameter and soil suction resistance ratio on the fatigue life of SCR in the TDZ.

The ability to quantify the uncertainty of SCRs, especially in TDZ subject to inherent randomness in loading, material properties, seabed modelling, fatigue

characteristics and geometric parameters, is becoming increasingly important in the design and analysis of SCR. In terms of fatigue, SCRs are very sensitive to seabed modelling. Reliability-based Fatigue behaviour provides a means by which to quantify the reliability of SCR in the TDZ and to develop a further understanding of the response behaviour of SCR-seabed interaction. The objective of reliability-based fatigue methodology is to increase the confidence in the design of SCR in TDZ.

This study presents the probability of failure associated with fatigue analysis of SCRs in the TDZ. The probabilistic methodology for fatigue reliability is illustrated. Uncertainties in structural load and material properties are considered by assigning probability distributions and standard deviations to the deterministic stress levels. Furthermore, fatigue strength parameters, Miner's indices and capacities are modelled as random variables. FORM is used to predict the fatigue reliability index. The influence of uncertainty parameters on reliability-based fatigue is also investigated. In addition, a sensitivity study of influential variables is carried out.

8.3 Contributions & Achievement of Research Objectives

The following sections will discuss the contributions of this work to the field of offshore structures in general and SCR research in particular whilst also providing details of the objectives achieved.

8.3.1 Main Contributions

The research undertaken in this thesis provides a new perspective regarding the importance of the topic of SCR with seabed interaction in the TDZ. The main contributions of this research work are:

a. **Adopting a fresh methodology for SCR–seabed interaction modelling**

The non-linear seabed model for SCR interaction in the TDZ is utilised in both vertical and lateral direction. Recent times have seen the development of a non-linear pipe–seabed interaction model in vertical direction based on experimental results. Furthermore, the improved (tri-linear) SCR–seabed interaction model in lateral direction is utilised, and depends on an empirical model developed from test results. The improved lateral seabed model mimics the effects of soil strength and load history of the catenary pipeline as well as the associated pipe embedment on the lateral seabed soil resistance. Better characterisation of the SCR–seabed interaction model, with accurate prediction of soil stiffness and riser penetration enables us to obtain global riser dynamic performance and fatigue assessment of SCR in the TDZ with improved accuracy.

b. Effects of the uncertainty in the geotechnical parameters and the development of the trench into seabed on the dynamic response, structural behaviour and fatigue performance of SCR in the TDZ

The SCR–seabed interaction analyses make it possible to identify and quantify the effect of physical phenomena such as soil suction forces and seabed stiffness as well as geotechnical parameters on the SCR performance. The non-linear seabed model as well as the influence of the trench shape and geotechnical parameters influences on the fatigue performance of SCRs in the TDZ are investigated. The seabed parameters used in SCR analysis can have a significant influence on the global riser response as well as the fatigue life in the TDZ and can also lead to conservative fatigue damage.

c. Probabilistic approach for fatigue assessment of SCRs in the TDZ

In this thesis, a practical methodology and procedures for reliability-based fatigue analysis is developed. The uncertainty of SCR, especially in the TDZ, which is subject to inherent randomness in loading, seabed modelling and fatigue characteristics is investigated. Reliability-based fatigue performance provides a means by which to quantify the reliability of SCR in the TDZ and to develop a more thorough understanding of the response behaviour of SCR-seabed interaction whilst also increasing confidence in the design of SCR in the TDZ. The novelty of the reliability approach lies primarily in the comprehensive consideration of uncertainty in the fatigue assessment of SCR. Efficient

algorithms for uncertainty modelling and processing, together with the sophisticated computational tool for SCR response analysis, facilitate a reliable prediction of fatigue behaviour and assessment of the structural reliability. The introduced limit state model can be used to perform a risk analysis for SCR and offshore structures.

8.3.2 Research Objectives Achieved

As discussed below, the aims and objectives of this study, as outlined in Chapter 2 have, broadly speaking, been successfully achieved:

- This venture begins with an extensive review of the scientific literature pertaining to SCR–seabed interaction. During this phase, a deeper understanding of the subject is developed. This is followed by a critical review of existing SCR–seabed interaction modelling approaches.
- Using the knowledge acquired from the literature review, non-linear SCR–seabed vertical interaction models are applied with the cyclic motions of the SCR using a finite element model. The seabed soil introduces a complex resistance to SCR movement in the vertical and lateral direction, meaning that the seabed soil effects are best captured by the more rigorous non-linear model. The vertical non-linear seabed model response allows the effect of physical phenomena such as soil suction forces and vertical seabed stiffness on the SCR performance to be identified and quantified. This also provides a better understanding of

the complex physical process of SCR-soil-fluid interaction. The TDZ response involves the degradation of the seabed soil stiffness (i.e., the seabed soil tends to lose strength and stiffness with an increase in plastic embedment during cyclic oscillations). Indeed, cyclic loading is addressed by the analyses conducted for this thesis.

The improved lateral seabed resistance to SCR movement consists of sliding resistance between the riser and seabed as well as the passive resistance of the soil. The developed model is based on an existing empirical formula. This empirical formula is established based on test results. The improved lateral model is applied so as to model the lateral movements with cyclic motions in the FE model. Furthermore, developing a better realisation of the lateral SCR-soil interaction model improves the dynamic response of soil stiffness and riser penetration which in turn affect global riser dynamic performance in the TDZ.

- The key geotechnical and non-linear seabed modelling parameters are identified and the influence of the trench development into seabed under dynamic cyclic motions is also investigated. A parametric study is conducted to evaluate the effect of soil parameters on the dynamic structural behaviour and fatigue performance of SCR in the TDZ.

  The comprehensive approach adopted throughout this study for seabed model introduces a severe dynamic response and fatigue assessment of

SCR in the TDZ, which is traceable from many perspectives. The investigation of the key parameters provides a more thorough identification and confidence for an efficient and effective evaluation of SCR dynamic response in the TDZ.

- The reliability-based fatigue assessment framework is developed and advised. The basic philosophy is to investigate the seabed non-linearity and geotechnical parameters' effects using advanced deterministic tools, within a probabilistic reliability-based fatigue which systematically accounts for inherent uncertainties. Such an approach has improved the understanding of SCR behaviour in the TDZ and ultimately leads to more effective management of the risks associated with SCR design.

8.4 Recommendations for Future Research

During this study, a number of areas are identified which may warrant further investigation in order to improve our general understanding of SCR analysis. These areas are summarised as follows:

a. SCR Global dynamic analysis

Throughout this thesis, OrcaFlex is used for the uncoupled riser analysis with wave loading applied. The global dynamic analysis is required to determine the overall structural behaviour of the SCR through fully coupled analysis using a program with more control options and source accessibility for riser dynamic

analysis and soil modelling, thus exposing the riser system to environmental loading conditions and floater motions. The coupled analysis can be clarified as simultaneous analysis of the motions of the floating platform, risers and mooring lines using the hydrodynamic model of the floating platform coupled with a 3D finite element or lumped mass model which represents the non-linear hydrodynamic and structural dynamic behaviour of the mooring lines and risers. The finite element solution employed for structural analysis should account for coupling effects together with non-linearity and seabed contact problems combined with in-line and lateral transverse floating unit motions.

b. SCR–seabed interaction

Oscillations of the floating structure and the dynamic loads on the SCR are critical for fatigue assessment analysis as shown in this study. The most severe fatigue damage is located near to and in the TDZ. The lateral seabed model resistance to SCR movement is also investigated as well as its influences on the dynamic response and fatigue analysis. The next step is to apply the lateral non-linear seabed model to the finite element model in order to investigate the influence of the lateral soil resistance model on the lateral buckling analysis of the SCR in the TDZ. Such lateral buckling can have a serious consequence for the integrity of the SCR pipeline.

c. Fatigue assessment of SCR in the TDZ

This thesis utilises the *S-N* approach for fatigue analysis in order to evaluate the fatigue life of SCR in the TDZ. It would be desirable to use the Fracture Mechanics (FM) approach for crack growth assessment which would signify a substantial understanding of the different parameters in the fatigue damage process. FM represents a potential tool which can be used to clarify the gradual development of the crack and therefore account for the effect of inspection and possible repair at the different stages of crack growth.

d. Reliability analysis of SCR

A closed-form reliability-based fatigue limit-state model is developed and is used to evaluate a reliable estimate of the fatigue life of SCRs. The uncertainties regarding the environmental loading and structural parameters are accounted for indirectly by assigning extreme random distributions to the stress levels. It is therefore desirable to develop a strategy which directly assigns the inherent uncertainties to the environmental loading and material properties as well as structural parameters. Furthermore, the results should then be compared to those obtained in this study. It is recommended to include the critical uncertainty in stochastic dynamic analysis and reliability assessment of SCRs as part of the coupled system with floating platform and mooring. Such an approach for the reliability assessment of SCRs would involve advanced simulation methods based on Response Surfaces (RS) and/or Monte Carlo

Simulation (MCS) in a numerically efficient manner. This ensures that the analysis assessment is more confident and avoids approximation errors introduced by conventional methods. It should be noted that such an approach would be more expensive and time-consuming when compared to the approach introduced in this thesis. However, the inclusion of uncertainties in loading, material and structural and seabed non-linearities will make the evaluation of the probability of failure significantly more realistic. Moreover, this approach could serve to further validate the approach employed in this study. The reliability analysis discussed in Chapter 7 has been mainly concerned with a single failure model defined by a single limit state equation. SCRs, however, involve several modes of failure, i.e., there is a possibility that an SCR structure may fail in one or more of multiple possible failure scenarios. It is therefore desirable to conduct system reliability for the SCR. The system reliability deals specifically with combining the probabilities of failure to determine the total reliability of SCR structure as a system.

8.5 Concluding Remarks

This chapter presents the novelty of the present research work, while also identifying its contributions to the filed in question. The aims and objectives achieved are presented before final recommendations for further future research are outlined.

The following chapter will summarise the conclusions of this thesis.

CHAPTER 9

CONCLUSIONS

9.1 Introductory Remarks

This thesis is concerned with the modelling of an SCR with seabed interaction on soft clay when subjected to random waves. Analysis techniques have been developed in the three main areas outlined in the research aims: SCR–seabed interaction modelling; influences of the uncertainty in the geotechnical parameters as well as the development of the trench in the seabed on the dynamic response, structural behaviour and fatigue performance of SCRs in the TDZ, and the probabilistic approach for fatigue assessment of SCRs in the TDZ. This chapter is summarising the main findings and conclusions drawn by the thesis.

9.2 Concluding Statements – Main Findings

In overall terms, the main concluding statements drawn from the research work undertaken in this thesis are summarised and introduced as follows.

9.2.1 Dynamic Response of an SCR with Seabed Interaction under Random Loads

In this study the vertical embedment and large lateral movements of the SCR in the TDZ were investigated. The results of numerical simulations of the global responses of the SCR considering a critical point at the TDZ are presented. During the dynamic analysis the seabed has been modelled using a hysteretic

non-linear model in a vertical seabed direction along with bilinear and tri-linear soil models in the lateral seabed direction. The following findings were concluded:

- The semisubmersible offsets govern and influence the maximum von Mises stress at the TDP and the maximum tension at the SCR's top end. The most critical section for von Mises stress along the SCR is in the TDZ, and the dynamic analyses indicated the maximum variation of bending moment near the TDZ depends on the excursion and cyclic motions of the floating production unit.

- The non-linear soil model captures the entity of varying soil stiffness and soil cyclic degradation, thereby allowing the re-penetration, uplift and suction effects. The investigation of soil stiffness degradation was influential in evaluating the structural dynamic performance and trench development in the TDZ.

- SCR's flow-line movements at the seabed which are driven by the oscillation of the floating production unit were affected by the dynamic response of the SCR. The non-linear soil model is used to assess the changes in the vertical soil resistance through the SCR's flow-line in contact with the seabed. The maximum dynamic vertical seabed resistance/D was 19.4, which is nearly eight-times the static value. It has been found that the TDZ responses result in the degradation of the

seabed soil stiffness loading and give evidence of the dynamic SCR penetration in the TDZ due to cyclic loading.

- The main conclusion from SCR–seabed lateral interaction is that soil resistance to lateral SCR motions is more complex than simple coulomb friction. The improved lateral soil model mimics the effects of soil strength and load history of the catenary pipeline and the associated pipe embedment on the lateral seabed soil resistance. It is proven that the employing of the improved lateral SCR-soil interaction model with accurate prediction of soil stiffness and riser penetration with cyclic loading enables us to obtain dynamic global riser performance in the TDZ with better accuracy.

9.2.2 Significance of Seabed Interaction on Fatigue Assessment of an SCR in Touchdown Zone

The challenges regarding fatigue damage assessment of the SCR in the TDZ are mainly due to the non-linear behaviour of SCR–seabed interaction, considerable uncertainty in SCR–seabed interaction modelling and geotechnical parameters. Various design approaches pertaining to the lateral pipe–soil resistance model are discussed. This study investigates the sensitivity of fatigue performance to geotechnical parameters through a parametric study. In this study, global dynamic analyses are performed in order to assess the influence of vertical linear seabed springs, the lateral seabed model and the non-linear seabed

model; including trench evolution into seabed, seabed normalised stiffness, re-penetration offset parameter and soil suction resistance ratio on the fatigue life of the SCR in the TDZ. The following conclusions can be drawn from the fatigue analysis performed:

- Using rigid seabed modelling for fatigue assessment of the SCR in the TDZ introduces conservative fatigue damage in comparison with a linear seabed surface as the high contact force near the TDZ increases the peak stress and consequently reduces the number of cycles to failure and increases the fatigue damage. The linear seabed surface modelling can distribute the reaction force along the TDZ distance across the seabed and reduce the peak stress.

- The seabed linear stiffness has a considerable influence on the assessed fatigue life in the TDZ; higher soil stiffness gives a lower predicted fatigue life, conversely lower soil stiffness may not be representative. This indicates that the seabed interaction with an SCR is not as simple as linear or rigid seabed models and is a testament to the significance of seabed non-linearity and geotechnical parameters.

- The fatigue damage of the SCR in the TDZ has been proven to be a critical design aspect where the geotechnical consideration becomes important. The fatigue analyses results prove that the confounding results indicated by the previous research studies on the SCR in the TDZ are because of

different geotechnical parameters imposed with soil model and trench development. The trench deepening and the gradual embedment of riser and soil stiffness have a substantial influence on the fatigue life of SCR in the TDZ.

- The lateral seabed model marginally affected the fatigue life of SCR in the TDZ and can be considered to have a negligible influence on the fatigue assessment.

9.2.3 Fatigue Reliability Analysis of an SCR on Soft Clay Near The TDZ

In terms of fatigue, SCRs are very sensitive to the seabed modelling technique. Reliability-based Fatigue behaviour provides a method to quantify the reliability of the SCR in the TDZ and develop further understanding of the response behaviour of the SCR-seabed interaction. The objective of reliability-based fatigue methodology is to increase the confidence in the design of the SCR in the TDZ. This study introduces the probability of failure associated with fatigue analysis of SCRs in the TDZ. The probabilistic methodology for fatigue reliability is illustrated. Uncertainties in structural load and material properties are considered by assigning probability distributions and standard deviations to the deterministic stress levels. Furthermore, fatigue strength parameters, Miner's indices, and capacities are modelled as random variables. The influence of the probabilistic analysis approach, as an extension of the deterministic analysis,

was investigated using the FORM. The influence of uncertainties parameters on the Reliability-based fatigue are investigated. In addition, a sensitivity study of influential variables has been performed. The following conclusions can be drawn:

- The limit state model and a procedure for the reliability-based fatigue analysis of the SCR in the TDZ has been developed and performed. This model can be employed as a risk analysis tool for the SCR analysis assessment, leading to a safer and more cost effective design of the SCR system. It should be noted that the formulation of the limit state function and the parameters selected for stochastic variables can dramatically influence the failure probability of the SCR structure in component reliability analysis.

- The investigated case studies have indicated that the uncertainty in *S-N* characteristics, especially fatigue exponent strength *m*, has the highest influence on the reliability-based fatigue of the SCR. Parametric sensitivity studies of *m* indicate that the reliability analysis is very sensitive to the uncertainty associated to the parameters such as COV and the mean value of *m*. Therefore, the need for better probability calibration of *m* is highlighted.

- The seabed modelling approaches significantly affect the reliability-based fatigue analysis. The non-linear seabed model gives the highest

probability of failure in comparison with other seabed modelling approaches (i.e., linear and rigid seabed). Consequently, careful attention should be undertaken for the calibration of geotechnical and non-linear parameters such as normalised maximum stiffness and soil suction ratio. These parameters can dramatically influence the safety of the structure because of the wide range values for seabed parameters, and this is critical.

- The main benefit of employing the reliability-based fatigue analysis framework is to increase the confidence in analysis and reduce the likelihood of the failure of the SCR with seabed interaction, thereby minimising the risk of the loss of the containment with the associated environmental impact. The reliability approach also assisted in the determination of the factors that have a significant effect on the probability of failure under cyclic loading in the TDZ.

9.3 Concluding Remarks

The modelling and analysis of the SCR is challenging because of its complexity in seabed interaction and the inherent non-linearity and geotechnical parameters. It is proven that the current modelling of seabed interaction with the SCR, whether using a linear or rigid seabed, is simplified with the field observation of trench deepening of the SCR pipe and the soil suction effects in the TDZ. More robust modelling techniques for SCR–seabed interaction provide a better

account for seabed stiffness, soil suction effects and passive resistance which can be used to improve the evaluation of fatigue performance and dynamic structural behaviour while also assessing the significance of soil parameters on a global analysis of the SCR. Only with confidence in seabed interaction modelling and better calibration of geotechnical parameters values can one have confidence in the final analysis results. In this thesis, several techniques have been combined to achieve what is believed to be a realistic modelling of the SCR with seabed interaction.

APPENDIX A

DERIVATION OF CATENARY EQUATION

A.1 Introductory Remarks

The SCR is a freely hanging line connecting to the floating platform and extending down to the seabed. This chapter reviews the basic mechanics of a catenary. This appendix presents the derivation of equations which can be used to evaluate the geometric properties and forces on an SCR.

A.2 Basic Differential Equation

SCRs are horizontal at the lower end generally within about 8-20° of the vertical at the top end. Hence, their total profile and curvature cannot be even remotely analyzed using small-angle deflection theory. They can, of course, be analyzed by defining local axes for which the angles do not evolve by more than 10°, which is the limit normally accepted for small-angle deflection theory. It is, however, simpler to abandon (x, y) coordinates and use (θ, s) coordinates instead, as defined in Figure A—1, where θ is the angle with the horizontal and s is measured from the touchdown point (TDP). The basic differential equation governing curvature and deflections of tensioned beams subject to large deflections is derived in the following section.

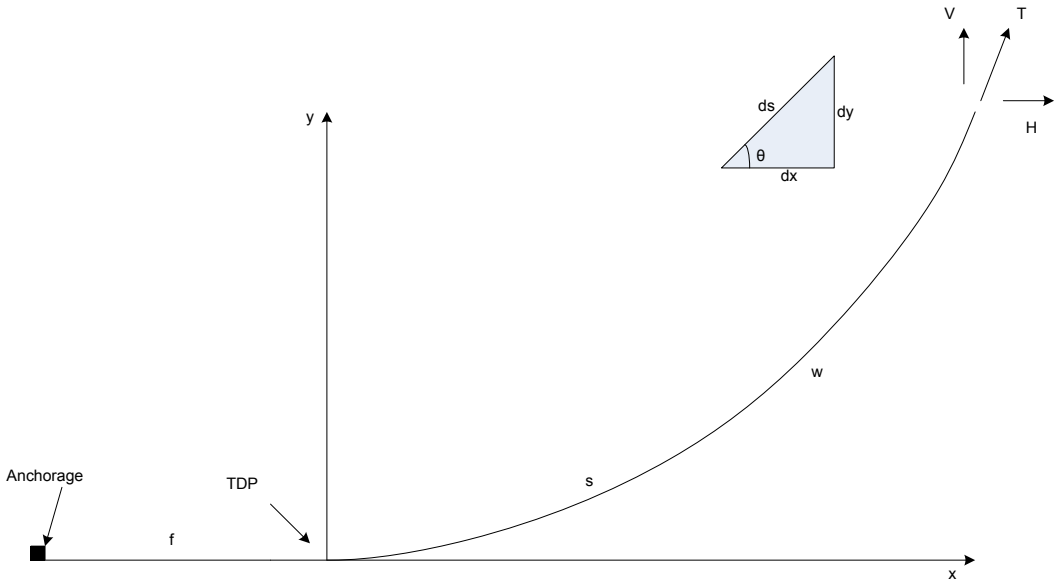

Figure A—1 Catenary axes and symbols

A.2.1 Tensioned-Beam Equation for Small-Angle Deflections

The differential equations governing the static deflected shape of a tensioned beam can be deduced very simply by considering the balance of forces acting on a short segment. In Figure A—2 shows a short segment of tensioned beam oriented close enough to the vertical (within 10°) for small-angle deflection theory to be applicable.

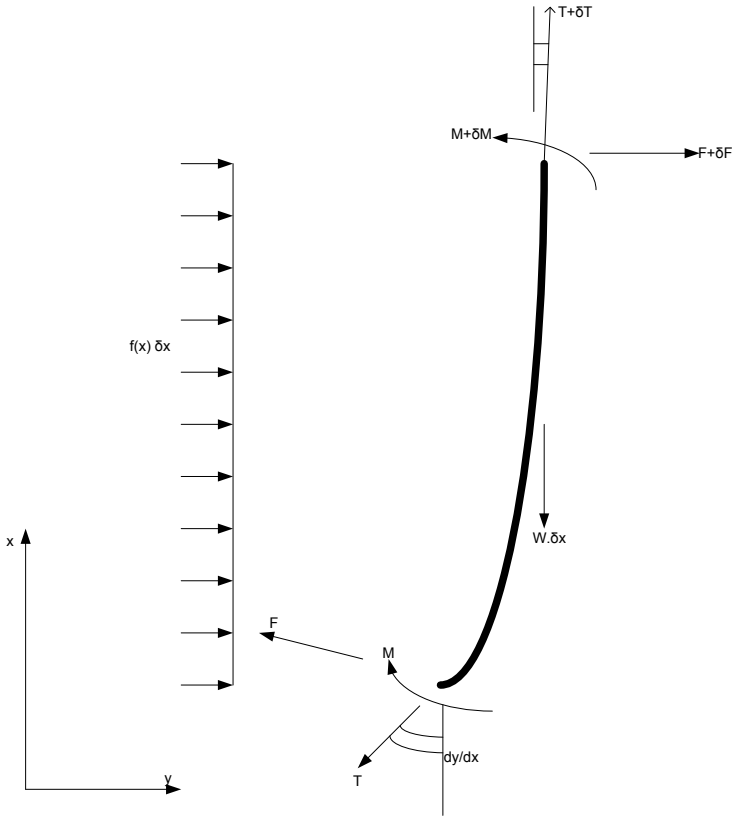

Figure A—2 Tensioned beam- forces acting on a segment of length δx

Considering static forces acting on a beam segment of length δx and resolving in Y-direction gives:

$$-F\frac{dy}{dx}+F\frac{dy}{dx}+\delta F\frac{dy}{dx}-T\frac{dy}{dx}+T\frac{dy}{dx}+\delta T\frac{dy}{dx}+f(x)dx=0.0$$

Equation A—1

After reduction

$$\delta F \frac{dy}{dx} + \delta T \frac{dy}{dx} + f(x)dx = 0.0$$

Equation A—2

For small-angle

$$dF + \delta(T \frac{dy}{dx}) + f(x)dx = 0.0$$

Equation A—3

where F is the shear force, T dy/dx is the horizontal component of axial tension, and $f(x)$ is the external lateral load.

Dividing Equation A—3 by dx,

$$\frac{dF}{dx} + \frac{d}{dx}(T \frac{dy}{dx}) + f(x) = 0.0$$

Equation A—4

$$\because \textit{shear force F is related to the moment by } F = \frac{dM}{dx}$$

$$\therefore \frac{d^2M}{dx^2} + \frac{d}{dx}(T \frac{dy}{dx}) + f(x) = 0.0$$

Equation A—5

Equation A—5 applies to all tensioned-beams with small-angle deflections and is the most general from the governing equation.

For special case of a beam made of elastic materials with bending stiffness EI, $M = -EI\frac{d^2y}{dx^2}$,

$$\therefore \frac{d^2}{dx^2}\left(EI\frac{d^2y}{dx^2}\right) - \frac{d}{dx}\left(T\frac{dy}{dx}\right) - f(x) = 0.0$$

Equation A—6

for the case of tensioned beam with constant *EI*, Equation A—6 becomes,

$$EI\frac{d^4y}{dx^4} - \frac{d}{dx}\left(T\frac{dy}{dx}\right) - f(x) = 0.0$$

Equation A—7

For near-vertical tensioned beams, $\frac{dT}{dx} = w$ where *w* is the weight of segment per unit length. Equation A—7 can be rewritten as

$$EI\frac{d^4y}{dx^4} - \frac{dT}{dx}\left(\frac{dy}{dx}\right) - T\frac{d^2y}{dx^2} - f(x) = 0.0$$

Equation A—8

$$\therefore EI\frac{d^4y}{dx^4} - w\left(\frac{dy}{dx}\right) - T\frac{d^2y}{dx^2} - f(x) = 0.0$$

Equation A—9

This equation used for near-vertical risers made of elastic materials with constant bending stiffness and with three assumptions:

- for near-vertical risers,
- for elastic materials, and
- constant bending stiffness

For a beam with uniform bending stiffness, the basic is as follows:

$$EI\frac{d^3\theta}{ds^3} - T\frac{d\theta}{ds} + w\cos\theta + f(s) = 0.0$$

Equation A—10

Where $w\cos\theta$ and $f(s)$ are the respective component of the self-weight and the in-plane current load, acting perpendicular to the catenary axes; T is the tension. Since the curvature is given by $1/R = \mathrm{d}\theta/\mathrm{d}s$, Equation A—10 can be rewritten as,

$$EI\frac{d^2}{ds^2}\left(\frac{1}{R}\right) - T\left(\frac{1}{R}\right) + w\cos\theta + f(s) = 0.0$$

Equation A—11

A.3 Catenary Curve

A catenary curve can be defined by the equation:

$$y = c\cosh(x/c) \qquad \textit{(c is a constant)}$$

Equation A—12

The curve and co-ordinate system used are shown in Figure A—3. The constant is determined by iteration using surface boundary condition y=*c*+*b* when *x*=*a*. All iterations are carried out using MatLab software. Table A—1 lists a selection of catenary equation constants for a range of horizontal and vertical offsets.

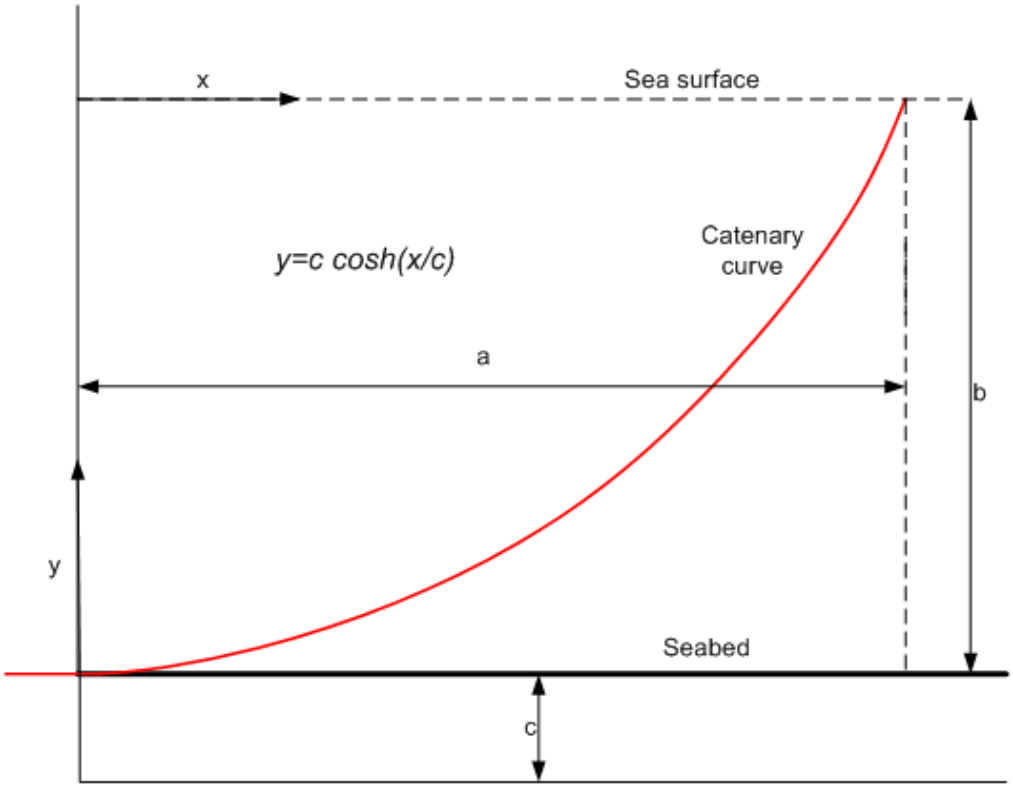

Figure A—3 Catenary Curve and coordinate system

Table A—1 Constant values of catenary equation

Horizontal projection (a) (m)	Catenary constant (c)			
	depth b=1000 m	b=1500 m	b=2000 m	b=2500 m
750	383.3	304.1	264.3	239.9
1000	618.8	475.7	404.4	363.1
1250	911.6	683.3	572.6	506.8
1500	1263.5	928.1	766.5	671.3
1750	1675.6	1211.24	988	857.1
2000	2148.64	1533.4	1237.5	1064.7
2250	2683.2	1895.3	1515.8	1294.5
2500	3279.3	2297.2	1823.2	1546.9
2750	3937.5	2739.7	2160.2	1822.3
3000	4657.7	3223	2527	2120.9

A.4 Cable Catenary Equations

The cable catenary has zero bending stiffness and zero current load. Figure A—1 shows the axes and the forces acting on a simple catenary, with origin at the TDP. Angle θ is measured from the horizontal; T is the catenary effective tension, with vertical component V and horizontal component H; w is the apparent weight per unit length; and s is the arc length measured from the TDP.

The vertical force at any point is equal to the apparent weight of the suspended length (V=ws), measured from the TDP. Also, at any point, ds/dx=T/H, and dy/dx=V/H. The following relationships can be deduced from the top-end forces in Figure A—1:

$$\frac{ds}{dx} = T/H = \frac{\sqrt{H^2 + V^2}}{H} = \frac{\sqrt{H^2 + (ws)^2}}{H} = \sqrt{1 + \left(\frac{ws}{H}\right)^2}$$

Equation A—13

$$\frac{dy}{dx} = \frac{V}{H} = \frac{ws}{H} = \tan\theta$$

Equation A—14

The standard catenary equations can be derived from Equation A—13 and Equation A—14. Equation A—13 lead to Eqn (5.3), which when evaluated leads to Equation A—15:

$$\int_0^s \frac{ds}{\sqrt{1+\left(ws/H\right)^2}} = \int_0^x dx$$

Equation A—15

$$\frac{ws}{H} = \sinh\left(\frac{wx}{H}\right)$$

Equation A—16

Substitution of Equation A—16 into Equation A—13 gives Equation A—17:

$$\frac{T}{H} = \cosh\left(\frac{wx}{H}\right)$$

Equation A—17

Equation A—14 and Equation A—16 lead to Equation A—18 and, hence, to Equation A—19:

$$\int_0^y dy = \int_0^x \sinh\left(\frac{wx}{H}\right) dx$$

Equation A—18

$$\frac{wy}{H}+1=\cosh\left(\frac{wx}{H}\right)$$

Equation A—19

Therefore, from Equation A—17 and Equation A—19,

$$\frac{T}{H}=\frac{wy}{H}+1=\cosh\left(\frac{wx}{H}\right)$$

Equation A—20

The curvature ($1/R$ = $\mathrm{d}\theta/\mathrm{d}s$) is given by differentiating the last equality of Equation A—14, which which gives Equation A—21 and Equation A—22:

$$\frac{w}{H}\frac{ds}{d\theta}=\sec^2\theta=\frac{T^2}{H^2}$$

Equation A—21

$$\frac{1}{R}=\frac{d\theta}{ds}=\frac{wH}{T^2}$$

Equation A—22

We can derive catenary equations by another way considering Figure A—4 which shows an element of a catenary of constant submerged weight per unit length $w=mg$ hanging freely and assumed to be inextensible. A differential

equation for this variation is obtained by taking both horizontal and vertical equilibrium of the forces acting on the line element of Figure A—4. Thus;

horizontally;

$$\frac{d}{ds}\left(T\cos\theta\right)=0.0$$

Equation A—23

Vertically;

$$\frac{d}{ds}\left(T\sin\theta\right)=mg$$

Equation A—24

Taking cos θ = dx/ds and sin θ = dy/ds and substituting them into Equation A—23 and Equation A—24 respectively gives

$$\frac{d}{ds}\left(T\frac{dx}{ds}\right)=0.0$$

Equation A—25

$$\frac{d}{ds}\left(T\frac{dy}{ds}\right)=mg$$

Equation A—26

By integrating Equation A—25,

$$T\frac{dx}{ds} = H$$

Equation A—27

where *H* is the horizontal component of tensile force. From Equation A—26 and Equation A—27 then,

$$\therefore H\frac{d^2y}{dx^2} = mg\frac{ds}{dx}$$

Equation A—28

The geometric constrain:

$$ds = \sqrt{dx^2 + dy^2} \quad then \frac{ds}{dx} = \sqrt{1 + \left(\frac{dy}{dx}\right)^2}$$

Equation A—29

From Equation A—28 and Equation A—29 and let $P = dy/dx$, hence

$$\therefore H\frac{dp}{dx} = mg\sqrt{1 + p^2}$$

Equation A—30

By integrating both sides of Equation A—30, then the expression becomes:

$$\sinh^{-1} P = \frac{mg}{H}x + c_1$$

Equation A—31

$$\therefore P = \frac{dy}{dx} = \sinh\left(\frac{mg}{H}x + c_1\right)$$

Equation A—32

Further integration gives:

$$y = \frac{H}{mg}\cosh\left(\frac{mg}{H}x + c_1\right) + c_2$$

Equation A—33

where c_1 and c_2 are constants to be determined from the boundary conditions;

$y = 0$ when $x = 0$, and

$y = 0$ when $x = l$ where l is the span of hanging catenary.

$$c_1 = -\frac{mg}{H}\frac{l}{2}$$
$$c_2 = -\frac{H}{mg}\cosh\left(\frac{mg}{H}\frac{l}{2}\right)$$

Equation A—34

Therefore the solution is:

$$y = \frac{H}{mg}\left[\cosh\left(\frac{mg}{H}x - \frac{mg}{H}\frac{l}{2}\right) - \cosh\left(\frac{mg}{H}\frac{l}{2}\right)\right]$$

Equation A—35

It should be noted that if a catenary riser is to have zero slope at the point of the seabed contact then from Equation A—32 it is shown that a constant c_1 must also be zero. Equation A—35 can be checked by applying zero slope condition by putting c_1 = 0.0 and hence:

$$y = \frac{H}{mg}\cosh\left(\frac{mg}{H}x\right)$$

Equation A—36

The component H/w is constant along the catenary line and if it is replaced by the constant c, Equation A—36 becomes identical to the mathematical expression defining a catenary curve given in Section A.3, Equation A—12.

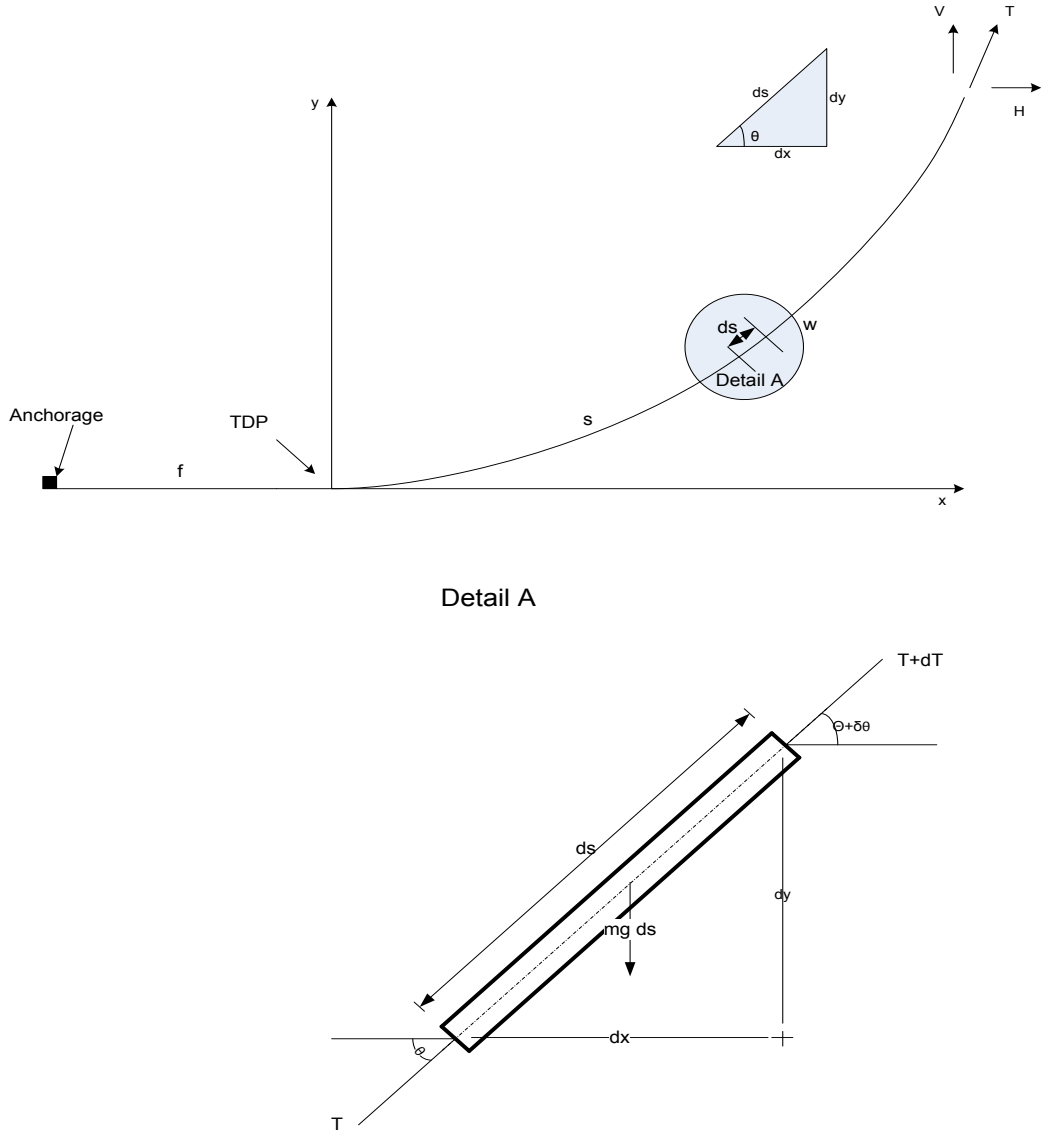

Figure A—4 Definition diagram for an element of catenary curve

A.5 Curvature and Bending Moment

The beam cross-section of any shape and is symmetrical about the vertical axis shown in Figure A—5. Assuming that the plane sections remain plane, if the beam is bent in the vertical plane to radius R, then the axial strain at distance z from the neutral axis N-A will be equal to z/R, with corresponding stress Ez/R, where E is the Young's modulus of elasticity. The stress action on the strip of width b, of the height δz, and at distance z from the neutral axis N-A induces moment $\delta M = bz^2\,\delta z/R$ about the neutral axis N-A. Integration over the complete cross-section then yields,

$M = \frac{EI}{R}$ where I is the second moment of area

Equation A—37

Figure A—5b shows the global deformation of length δs of beam, bent to radius R. The angle $\delta\theta$ turned through is related to δs by $\delta s = R\delta\theta$. Hence, the curvature at any point on a curve can be expressed analytically as:

$$\frac{1}{R} = \frac{d\theta}{ds}$$

Equation A—38

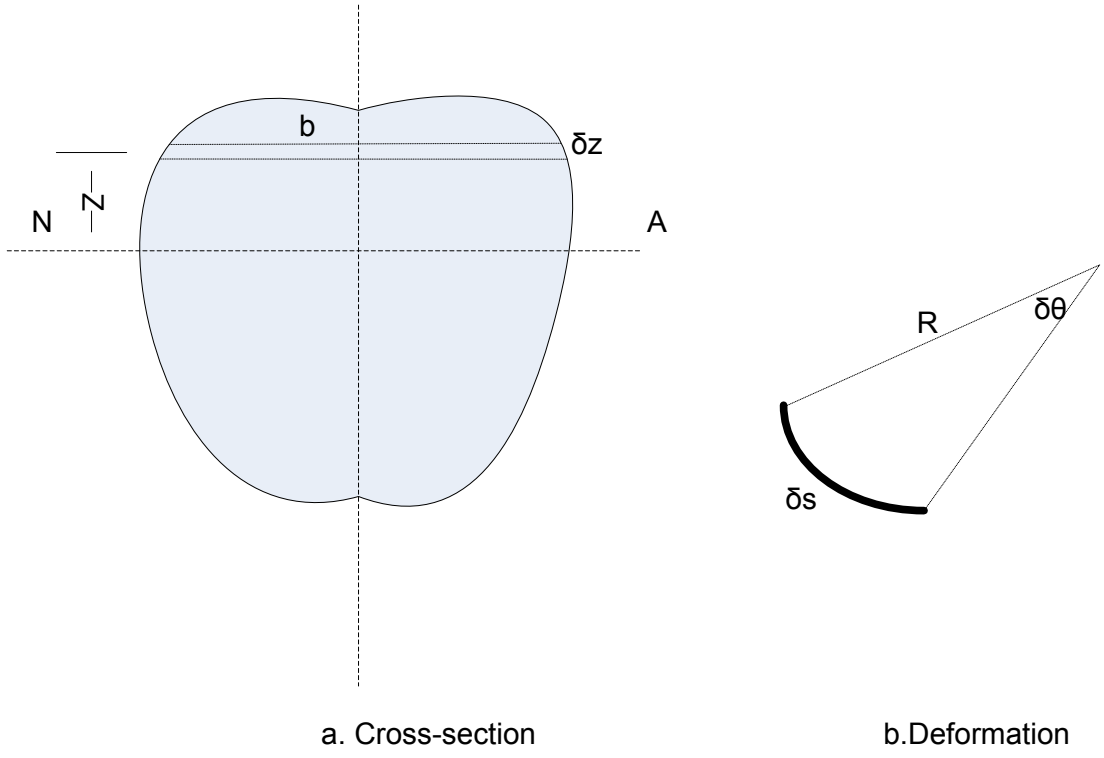

Figure A—5 Beam sketches

If δs is assumed to be very small both the arc and chord lengths between the two points can be considered equal and hence:

$$\frac{dy}{dx} = \tan\theta$$

Equation A—39

$$\frac{dx}{ds} = \cos\theta$$

Equation A—40

If Equation A—39 is differentiated with respect to s an exact relationship between curvature and curve geometry can be obtained:

$$\frac{d\theta}{ds} = \frac{1}{R} = \frac{d^2y/dx^2}{\left[1+\left(dy/dx\right)^2\right]^{3/2}}$$

Equation A—41

On knowing the equation $y = f(x)$ of the curve, the first and second differential derivatives can be calculated and subsequently substituted into the above formula in order to obtain $1/R$, the following fundamental relationship can be used:

$$\because \frac{1}{R} = \frac{M}{EI}$$

Equation A—42

Therefore,

$$\frac{M}{EI} = \frac{d^2y/dx^2}{\left[1+\left(dy/dx\right)^2\right]^{3/2}}$$

Equation A—43

The catenary equation $y = f(x)$ is defined before in Equation A—12, then

$$\frac{dy}{dx} = \sinh\left(\frac{x}{c}\right)$$
$$\frac{d^2y}{dx^2} = \frac{1}{c}\cosh\left(\frac{x}{c}\right)$$
$$\therefore \frac{M}{EI} = \frac{1}{c\cosh^2\left(\frac{x}{c}\right)}$$

Equation A—44

At the seabed ($x = 0$):

$$\frac{M}{EI} = \frac{1}{c}$$

Equation A—45

At the water surface ($x = a$):

$$\frac{M}{EI} = \frac{1}{c\cosh\left(\frac{a}{c}\right)}$$

Equation A—46

An expression for bending moment can be formulated by substituting Equation A—32 and its differential derivative into Equation A—43 and hence:

$$M = \frac{w\,EI}{H\cosh^2\left(\frac{w}{H}x + c_1\right)}$$

Equation A—47

This equation can be checked by first substituting $c = H/w$ and $c_1 = 0$ and then comparing to Equation A—46. The bending stress resulting from this moment can be established using fundamental relationship:

$$\sigma_b = \frac{M}{z}$$

Equation A—48

where Z is the section modulus; and I is the second moment of area.

A.6 Appendix Summary

This chapter reviews the basic mechanics of a catenary and derive its governing equations. Catenary constant c can be calculated using iteration for a range of horizontal values and also for a range of water depth and can be used in further calculations to assess the horizontal component of tensile force H.

Curvature $(1/R)$ is maximum at the TDP ($x = 0$, $s = 0$), where it is equal to w/H. This should be no surprise since the part of the catenary adjacent to the TDP can be treated as a horizontal cable subject to vertical load w and axial tension H.

APPENDIX B

ANALYSIS PROGRAM USED IN THESIS

B.1 Overview of OrcaFlex

An overview of the components of the dynamic structural analysis program used in this thesis is described here. Named OrcaFlex, it is capable of considering the major non-linearities in marine riser response. OrcaFlex is the world's leading package for the dynamic analysis of offshore marine systems.

B.1.1 Elements of an OrcaFlex System Model

To analyse a marine riser system using OrcaFlex, we first build a mathematical model of the real-world system, using the various modelling facilities provided by OrcaFlex. The model consists of the marine environment to which the system is subjected, plus a variable number of objects chosen by the user, placed in the environment and connected together as required. The objects represent the structures being analysed and the environment determines the current, wave excitation, etc, to which the objects are subjected. The following types of objects are available in OrcaFlex and detailed description of each type of object are given by Orcina (2010).

Metocean Data

The marine environment model includes:

a. **Seabed**: Represented as a linear or non-linear surface, usually a plane (not necessarily horizontal).

Linear Seabed Model theory

The linear soil model theory is given by:

$V=K_nAd$

Equation B—1

Where V=normal seabed reaction force, K_n=seabed normal stiffness, A= penetrator contact area, and d= depth of penetration into the seabed.

Non-Linear Seabed Model Theory

The model consists of a "backbone curve" which defines the maximum plastic resistance of the soil as function of penetration. The max soil resistance, V, per unit length is given by equation:

$$P_1 = N_c S_u D \approx a\left(\frac{z}{D}\right)^b S_u D$$

Equation B—2

where S_u is the shear strength at pipe invert, D is the pipe diameter, z is the depth to the pipe invert from free surface, N_c is a bearing capacity factor, (a,b) are parameters fitted results of finite element analyses.

b. **Current**: Multiple sets of current profiles can be used, each with magnitude and rotation varying with depth, see Figure B—1.

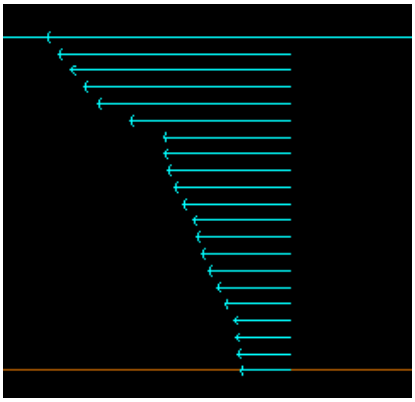

Figure B—1 Example of current varying with water depth

c. **Waves:** can use multiple wave trains. Wave models available include a simple linear (sinusoidal) wave, several non-linear regular waves, a number of wave spectra for modelling random seas, user defined components and time histories of wave elevation, see Figure B—2. Directional wave spreading for wave spectra can be included.

Regular Waves

- Airy
- Dean
- Stokes 5th
- Cnoidal

Irregular (Random) Waves

Setting up a random sea state

- JONSWAP and ISSC Spectra,
- Ochi-Hubble Spectrum,

- Torsethaugen Spectrum,
- Gaussian Swell,
- User-Defined Spectrum.

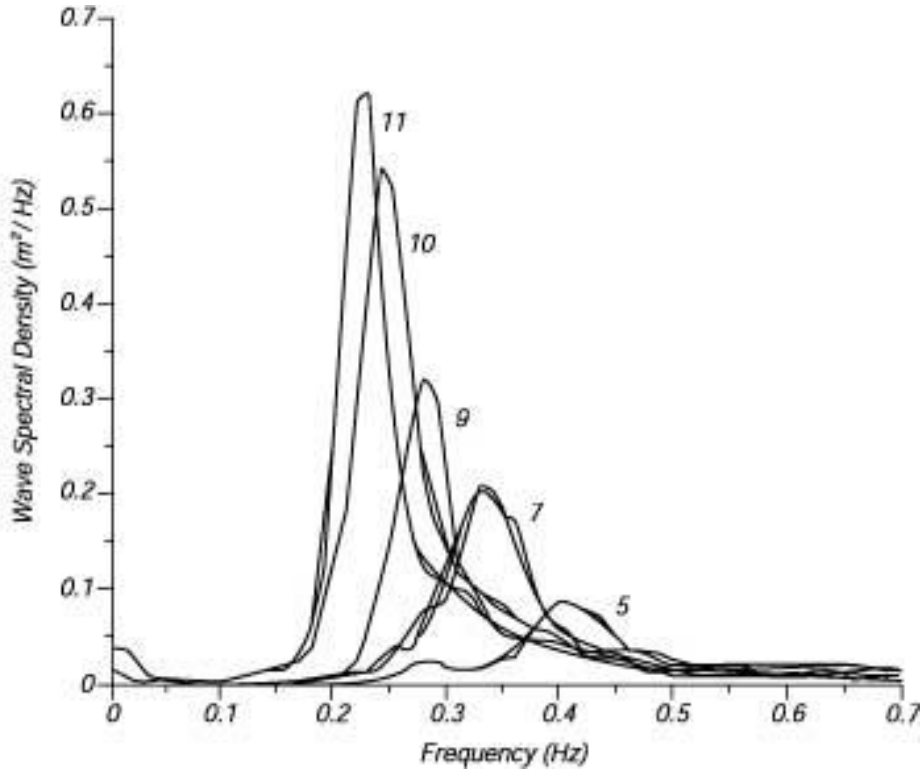

Figure B—2 JONSWAP wave spectrum for different peak enhancement factor (Whitford, 2002)

d. Wind: can be constant, spectral or time history files can be used if necessary.

Vessels

Vessels object are used to model ships, floating platforms; see Figure B—3 and Figure B—4, barges, etc. They are rigid bodies whose motions can be:

- prescribed by user-specified Displacement Response Amplitude Operators (RAOs), see Figure B—5, for each of the 6 degrees of freedom (surge, sway, heave, roll, pitch and yaw).
- calculated from Load RAOs for each of the 6 degrees of freedom.
- prescribed with a user-specified time-varying forward speed and rate of turn. Special facilities are also provided for mooring analysis.
- imposed from user defined time history motion files, which are readily imported.
- the low frequency (slow drift) motion can also be calculated in the time domain.

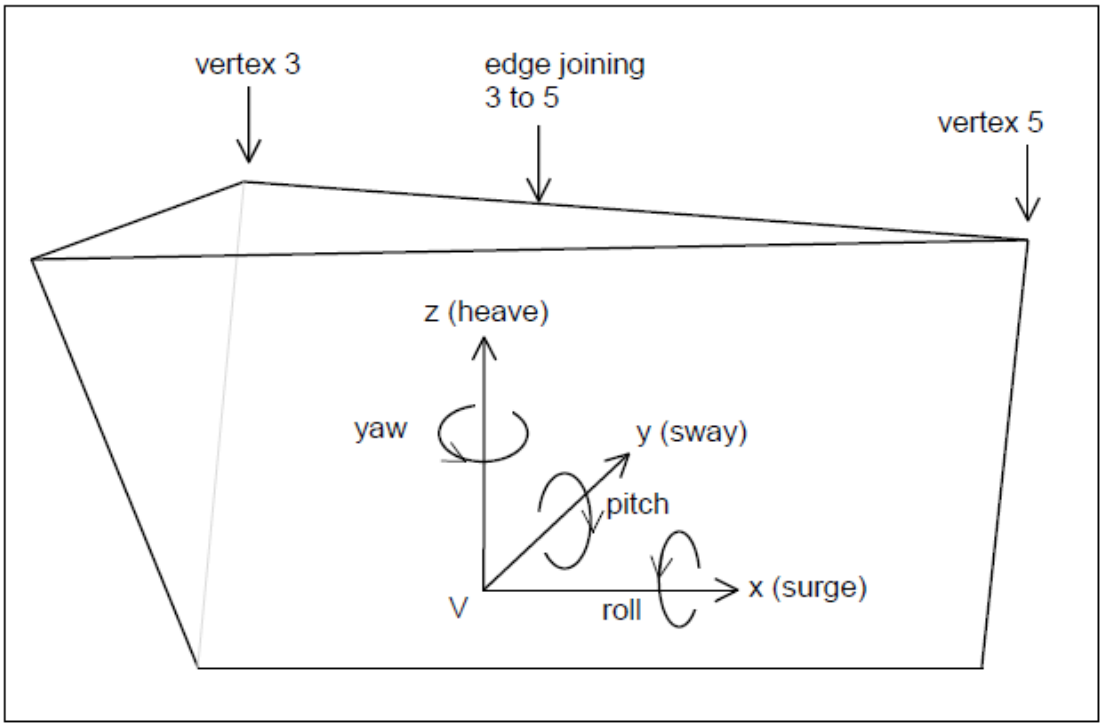

Figure B—3 Schematic of vessel model

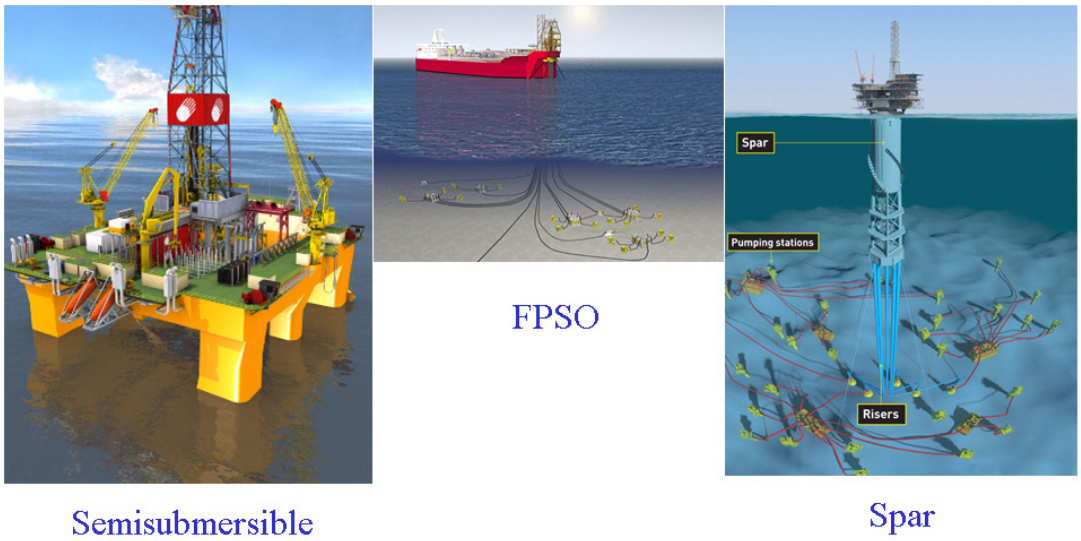

Figure B—4Examples of floating platforms

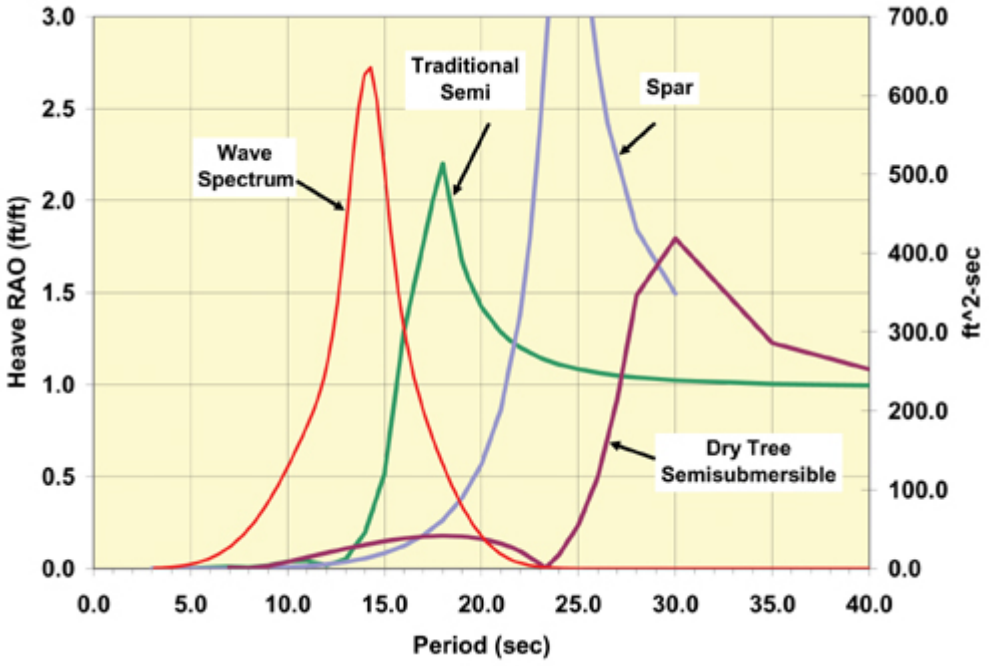

Figure B—5 Typical heave RAO's for different floater types

Lines

Lines are flexible linear elements used to model cables, hoses, chains or other similar items. Lines are represented in OrcaFlex by a "lumped mass" finite element model, see Figure B—6. The mass, volume and hydrodynamic properties of the associated length of line are assigned to a node, and a series of springs and dampers are defined to represent the axial, bending and torsional stffnesses and associated damping properties. As long as your 'line' can be characterised with these properties it can be modelled in OrcaFlex.

Typical applications include: Risers (TTRs, SCRs, flexibles, umbilicals, etc), moorings (chain, wire rope, etc), hoses, towed systems, installation analysis (including pipelines), etc. Line properties may vary along the length, so that a single line may be used to represent a chain/wire/chain mooring cable or a marine riser incorporating eg, buoyant section(s). Line ends may be fixed or free, or attached to other objects such as Vessels or Buoys, and ends can be disconnected in the course of simulation.

Line theory

- In OrcaFlex, the transfer of the physical riser into a line model that can be used in calculations is done by dividing the actual riser into segments.
- The line is divided into a series of line segments which are then modelled by straight massless model segments with a node at each end. The model segments only model the axial and torsional properties of the line. The other properties (mass, weight, buoyancy etc.) are all lumped to the nodes, as indicated by the arrows in Figure B—6.

Nodes

Each node is effectively a short straight rod that represents the two half-segments either side of the node. The exception to this is end nodes, which have only one half-segment next to them, and so represent just one half-segment.

Each line segment is divided into two halves and the properties (mass, weight, buoyancy, drag etc.) of each half-segment are lumped and assigned to the node at that end of the segment.

Forces and moments are applied at the nodes – with the exception that weight can be applied at an offset. Where a segment pierces the sea surface, all the fluid related forces (e.g. buoyancy, added mass, drag) are calculated allowing for the varying wetted length up to the instantaneous water surface level.

Segments

Each model segment is a straight massless element that models just the axial and torsional properties of the line. A segment can be thought of as being made up of two co-axial telescoping rods that are connected by axial and torsional spring+dampers.

The bending properties of the line are represented by rotational spring+dampers at each end of the segment, between the segment and the node. The line does not have to have axial symmetry, since different bend stiffness values can be specified for two orthogonal planes of bending.

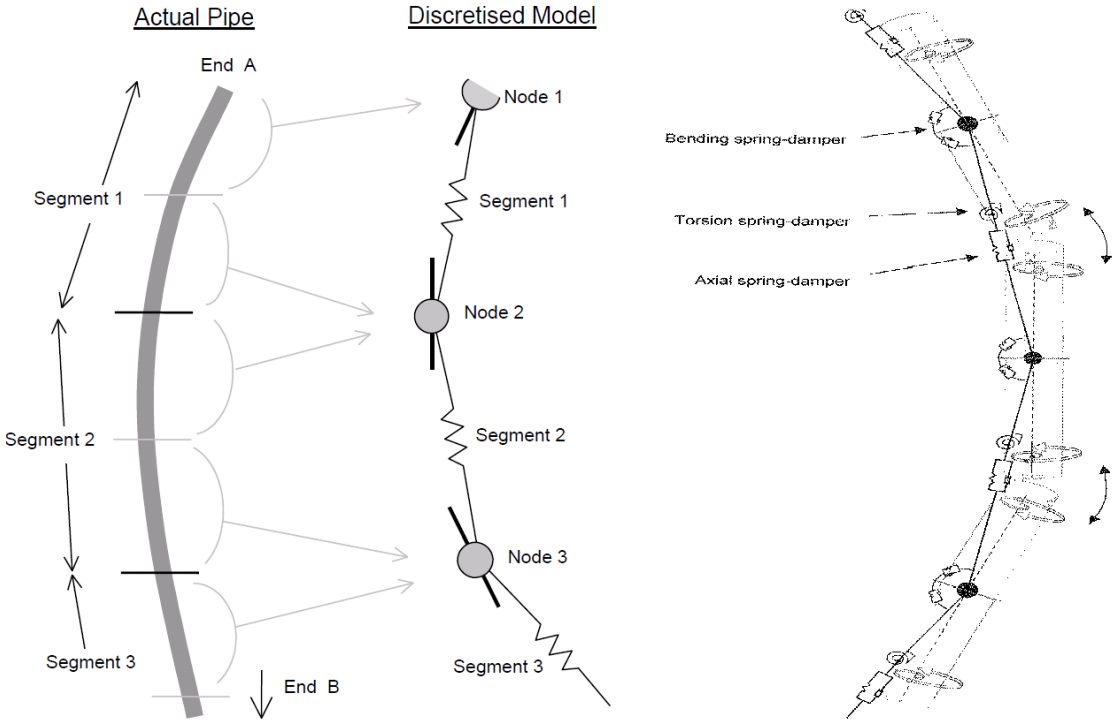

Figure B—6 OrcaFlex line model

Morison's Equation

OrcaFlex calculates hydrodynamic loads on lines and buoys using an extended form of Morison's Equation (Barltrop, 1998). Mrorison's equation was originally formulated for calculating the wave loads on fixed vertical cylinders. There are two force components, one related to water particle acceleration (the 'inertia' force) and one related to water particle velocity (the 'drag' force). For moving objects, the same principle is applied, but the force equation is modified to take account of the movement of the body. The extended form of Morison's equation used in OrcaFlex is:

$$F_w = \left(\Delta a_w + C_a \Delta a_r\right) + 0.5\rho V_r \left|V_r\right| C_D A$$

Equation B—3

where F_w is the wave force; Δ is the mass of fluid displaced by the body; a_w is the fluid acceleration relative to earth; C_a is the added mass coefficient for the body; a_r is the fluid acceleration relative to the body; ρ is the density of water; V_r is the fluid velocity relative to the body; C_D is the drag coefficient for the body; and A is the drag area.

The term in parentheses is the inertia force, the other is the drag force. The drag force is familiar to most engineers, but the inertia force can cause confusion. The inertia force consists of two parts, one proportional to fluid acceleration relative to earth (the 'Froude-Krylov' component), and one proportional to fluid acceleration relative to the body (the 'added mass' component).

To understand the Froude-Krylov component, imagine the body being removed and replaced with an equivalent volume of water. This water would have mass Δ and be undergoing an acceleration a_w. It must therefore be experiencing a force Δ. a_w. Now remove the water and put the body back: the same force must now act on the body. This is equivalent to saying that the Froude-Krylov force is the integral over the surface of the body of the pressure in the incident wave, undisturbed by the presence of the body.

The 'added mass' component is due to the distortion of the fluid flow by the presence of the body. A simple way to understand it is to consider a body accelerating through a stationary fluid. The force required to sustain the acceleration may be shown to be proportional to the body acceleration and can be written:

$$F = (M + C_a\Delta)a$$

Equation B—4

where F is the total force on the body; M is the mass of the body; $C_a\Delta$ is a constant related to the shape of the body and its displacement; and a is the acceleration of the body.

Another way of looking at the problem is in terms of energy. The total energy required to accelerate a body in a stationary fluid is the sum of the kinetic energy of the body itself, and the kinetic energy of the flow field about the body. These energies correspond to the terms ($M.a$) and $C_a.\Delta.a$ respectively.

Static Analysis

There are two objectives of a static analysis:

- To determine the equilibrium configuration of the system under weight, buoyancy, hydrodynamic drag loading, etc.
- To provide a starting configuration for dynamic simulation

In most cases, the static equilibrium configuration is the best starting point for dynamic simulation and the two objectives become one. However there are occasions where this is not so and OrcaFlex provides facilities for handling these special cases.

Dynamic Analysis

At the start of the time simulation, the initial positions and orientations of all objects in the model, including all nodes in all lines, are known from the static analysis. The forces and moments acting on each free body and node are then calculated. Forces and moments considered include:

- Weight
- Buoyancy
- Hydrodynamic drag and added mass
- Tension and shear
- Bending and torque
- Contact forces
- Forces applied by links and winches

The equation of motion is then formed for each node and free body:

$$\{M\}.\{x''\}=\{F\}$$

Equation B—5

where $\{M\}$ is the mass matrix for the node or body, including added mass terms, $\{x''\}$ is the acceleration vector, and $\{F\}$ is the total force vector. The equation is solved for acceleration vector which is then integrated. . At the end of each time-step, the positions and orientations of all nodes and free bodies are again known and the process is repeated.

B.2 OrcaFlex software Validation against API Bulletin 16J

A validation of OrcaFlex against other computer softwares has been carried out using the analysis cases described in the American Petroleum Institute's (API) Bulletin on 'Comparison of analyses of Marine Drilling Risers' (Bul 16J). A number of the analysis cases have been constructed in OrcaFlex and the results obtained have been compared with the results published by the API, which represent a summary of results from other riser softwares. In general, the OrcaFlex show good agreement within the results obtained from the other riser softwares, dilate of the analysis cases are given below.

B.2.1 Explanation of API cases

Frequent element is a riser which starts from a point some 30 ft off the seabed rising up to a vessel, to which it is connected some 50 ft above the mean water level.

The analyses cases have the following alternatives:

- Water depths

Four different water depths (500 ft, 1500 ft, 3000 ft and 6000 ft);

- Waves

    a. Periodic waves

    Two different current profile/wave height combination for the 500 ft, 1500ft and 3000 ft cases;

    b. Random waves

    One current profile/wave height combination for the 500 ft, 1500ft and 3000 ft cases;

- Connections

    a. Connected cases

        - Lower end: lower ball joint pin connection;
        - Upper end: pin connection to a tensioner ring with two different top tensions for the 500 ft, 1500 ft and 3000 ft cases (only one top tension for the 6000 ft case) with a different static offset per water depth;

- Riser filled with drilling mud;

b. Disconnected cases:

- Lower end: Lower Marine Riser Package (LMRP) incorporating a lower ball joint;

  - *Lower marine riser package data*

LMRP length, feet	10
Weight in air, pounds	150000
Weight in seawater, pounds	120000
C_d, drag coefficient	0.7
C_m, mass coefficient	1.5
Effective diameter for current and wave forces, inches	36

- Upper end: no tensioner ring, simply pinned and no static offset;
- Riser filled with seawater.

B.2.2 Specifications of main data

Vertical distances	Mean water level to riser support ring	50 ft
	Seafloor to Lower Ball-Joint (LBJ)	30 ft
Riser data	Riser pipe outside diameter	21 in
	Riser pipe inside diameter	20 in
	Modulus of Elasticity E	30×10^6 psi
	Weight, 50 ft riser joint, complete in air	8800 lb
	Weight, 50 ft riser joint, complete in seawater	7660 lb
Densities	Drilling mud	89.8 lb/cu.ft
	Seawater	64 lb/cu.ft
Hydrodynamic force constants	Drag coefficient C_D	0.7
	Mass coefficient C_M	1.5

Excitation	*Dynamic-Periodic Regular Wave*		
	H, wave height, peak to trough, feet	20	40
	T, wave period, seconds	9	12.8
	Vessel surge amplitude (peak to peak), feet	4	26.7
	Vessel surge phase angle, degrees	-90	-90
	Current profile	A	B

Current Profile

A. Linear, 2 knots at mean water level, 0.4 knot at LBJ.

B. Linear, 2 knots at mean water level, 0.4 knot at LBJ.

B.2.3 Results

The analysed connected riser contains mud and is connected to a frictionless ball-joint at the lower end. Waves are assumed to perform in the direction of the positive offset, and the upper end is subjected to horizontal vessel motions. Only regular wave analysis is carried out, and the horizontal motion of the vessel (surge) is sinusoidal with the same period as the wave. Top tension is constant. Figure B—7 shows a typical riser configuration.

The results for static and dynamic analysis are detailed in the API bulletin. For static analysis cases see which Compare the results from OrcaFlex model with API average values. For the results of the dynamic analysis carrying out a regular wave analysis (harmonic excitation), time integration will give a steady

state solution after a short transient period. The results from this steady state motion of the riser model are identified by the envelopes (maximum and minimum values) of the riser deflection and bending stress.

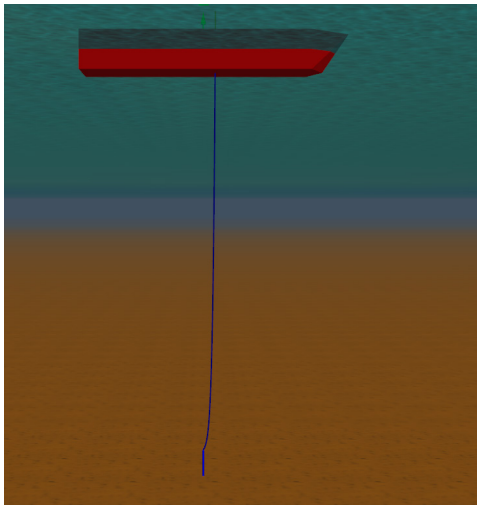

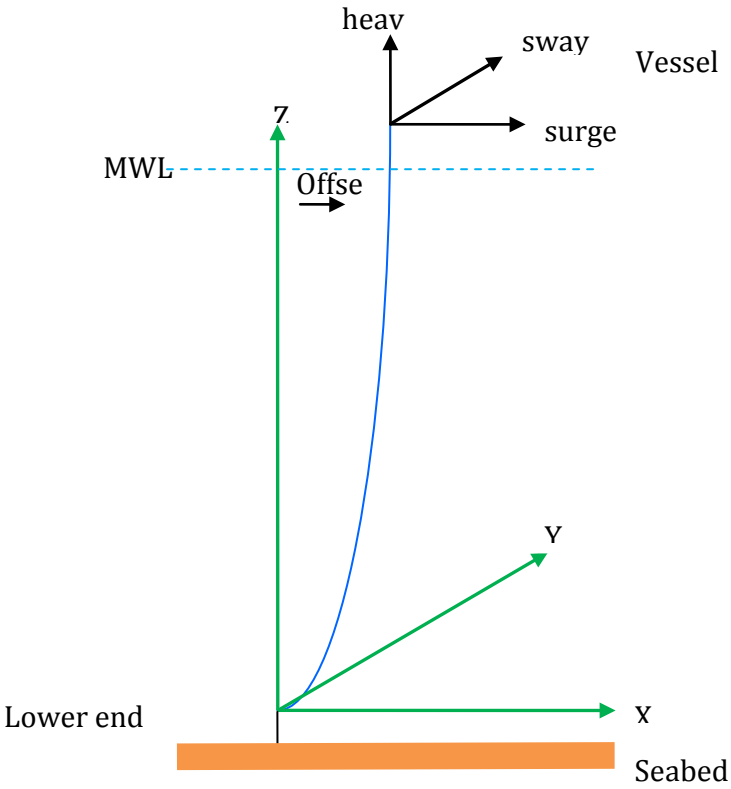

Figure B—1 System coordinate

Table B—1 Comparison of OrcaFlex results with mean API results – API Bul 16J

Analysis case ID	Max bending stress (ksi)		Max bending stress location above BOP		Max total stress (ksi)		Max total stress location above BOP (ft)		ngle from vertical (degrees)			
									LBJ		Top	
	API mean	Orcaflex model	API mean	Orcaflex model	API mean	OrcaFlex model	API mean	OrcaFlex model	API mean	OrcaFlex model	API mean	OrcaFlex model
500-A-1-S	2.05	1.80	127.4	126.54	5.41	5.69	444.9	487.33	2.51	2.4	1.00	1.07
500-A-2-S	1.14	1.01	126.27	126.54	7.75	7.56	470.91	495	2.17	2.11	1.22	1.25
500-B-1S	3.59	2.9	168	169.25	7.19	6.81	369.67	379.62	3.28	3.01	0.19	0.23
500-B-Free-S	1.59	1.46	391.20	392.92	7.19	7.4	413.20	418.75	-0.03	-0.031	-1.04	-0.92

Table B—2 The regular wave dynamic analysis is performed for the following connected riser cases

Case	500-20-2-D	500-40-1-D	1500-20-2-D
Water depth (feet)	500	500	1500
Riser length (feet)	520	520	1520
Top tension (Kips)	240	170	600
Static offset (feet)	15	15	45

Table B—3 The regular wave dynamic analysis is performed for the following disconnected riser cases:

Case	500-40-Free-D	1500-40-Free-D	3000-40-Free-D
Water depth (feet)	500	1500	3000
Riser length (feet)	520	1520	3020
Top tension (Kips)	Disconnected	Disconnected	Disconnected
Static offset (feet)	0	0	0

The following parameters are used for the difference approximation:

Table B—4 Connected cases parameter approximation

Case	500-20-2-D	500-40-1-D	1500-20-2-D
No. of riser element	158	520	926
Length of riser element (ft)	3.281	1.00	1.64
Time step (s)	0.1	0.1	0.1

Table B—5 Disconnected Cases parameter approximation

Case	500-40-Free-D	1500-40-Free-D	3000-40-Free-D
No. of riser element	624	1520	3020
Length of riser element (ft)	0.833	1.00	1.00
Time step (s)	0.1	0.1	0.1

The results from the connected riser dynamic analysis simulations are shown in Figure B—9 : Figure B—20, as previously mentioned results are compared to the corresponding API curves. The graphs show both the output obtained from OrcaFlex and representations of the output obtained from the other softwares involved in the original API analysis. API BUL 16J curves are indicated as black curves representing the minimum and maximum values (form an envelope) of the indicated variable, against arc length, observed over a wave period. The results show a good agreement with API curves.

To illustrate some properties of the disconnected cases (freely hanging riser) see Figure B—8, a simulation of disconnected riser model is carried out with a free lower-end (i.e. the riser is disconnected from BOP base at the seafloor). Furthermore, the riser is now assumed to be filled with sea water instead of drilling mud. The simulation results of the regular wave analysis described in Figure B—15 : Figure B—20, with the same excitation as mentioned before. As denoted, the amplitude of the bending stress has increased.

In general, and with few oddities, the OrcaFlex model output lies comfortably within the envelopes. Possible evokes of oddities:

a. Important assumptions in the establishment of the models due to abstruse specifications in API Bul 16J document.
b. The time-domain approach affiliate by OrcaFlex allows for more elaborated modelling of non-linear effects.

c. The essence on which specific results were accepted or rejected by API document is not discussed in the API document, and no justification is presented.

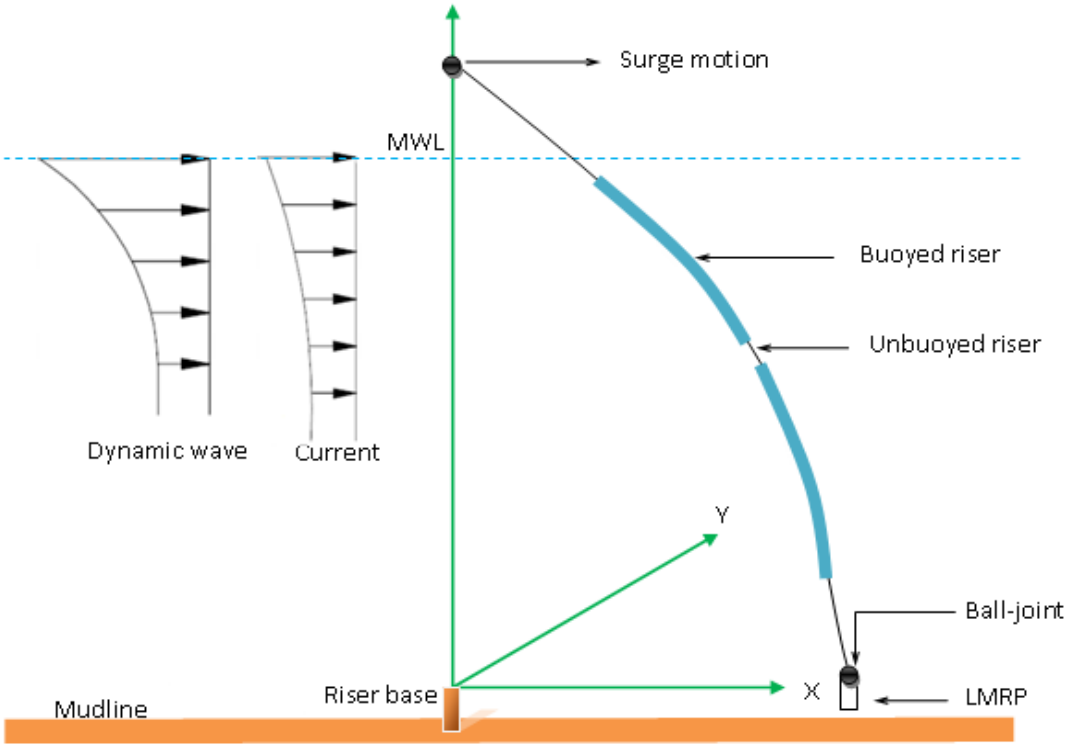

Figure B—8 Disconnected riser

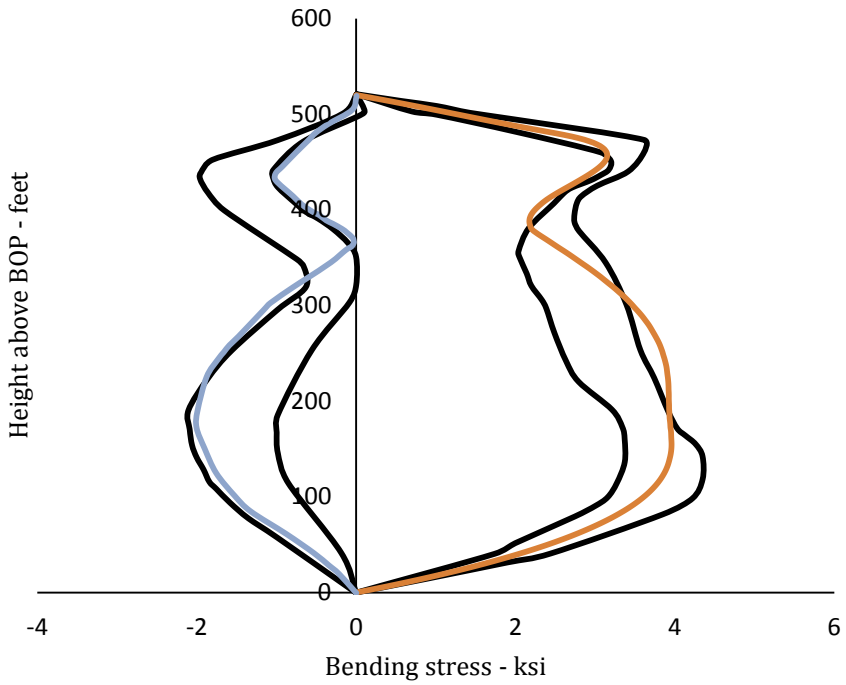

Figure B—9 Bending stress 500-20-2-D

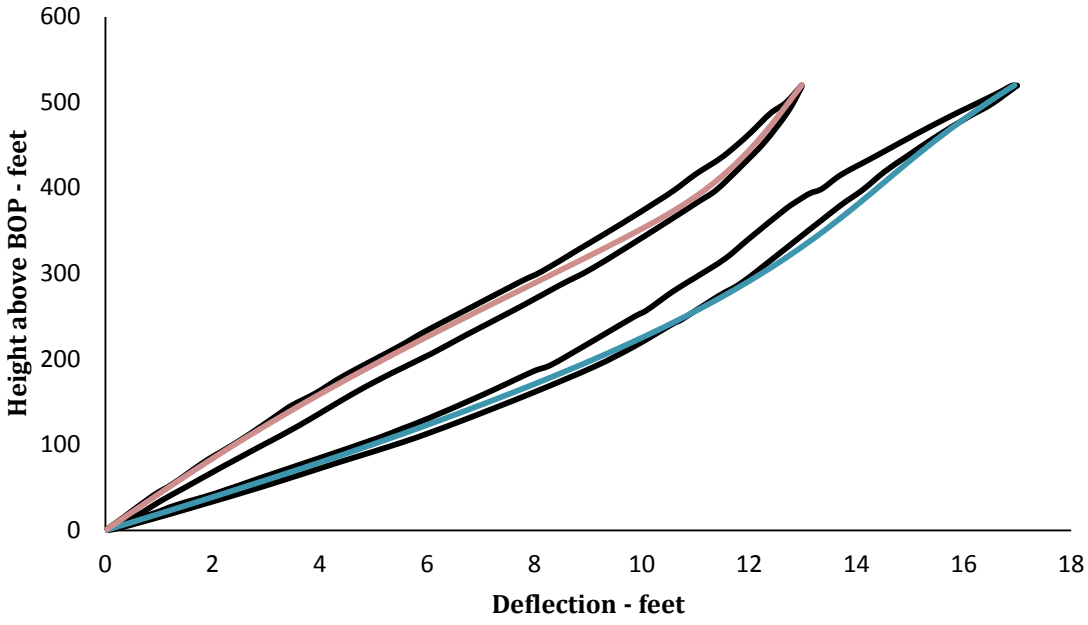

Figure B—10 Deflection 500-20-2-D

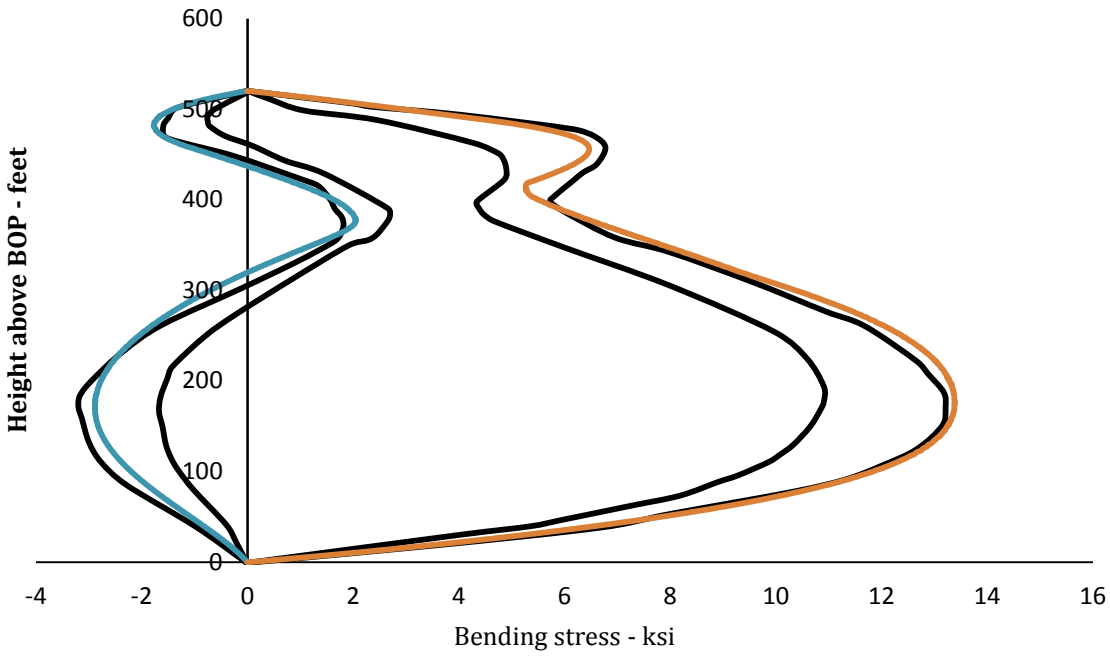

Figure B—11 Bending stress 500-40-1-D

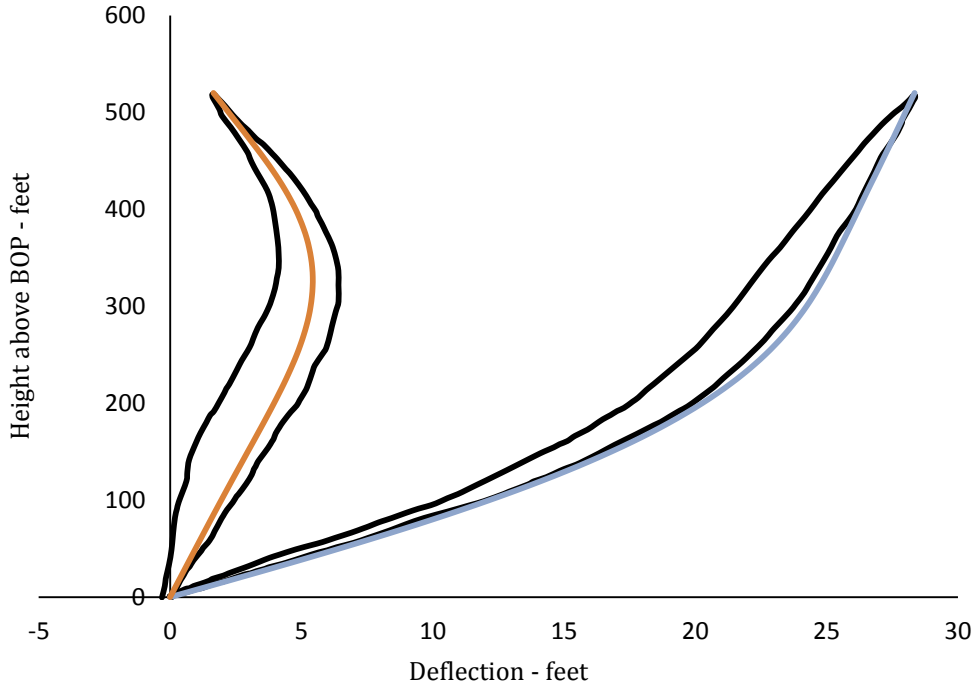

Figure B—12 Deflection 500-40-1-D

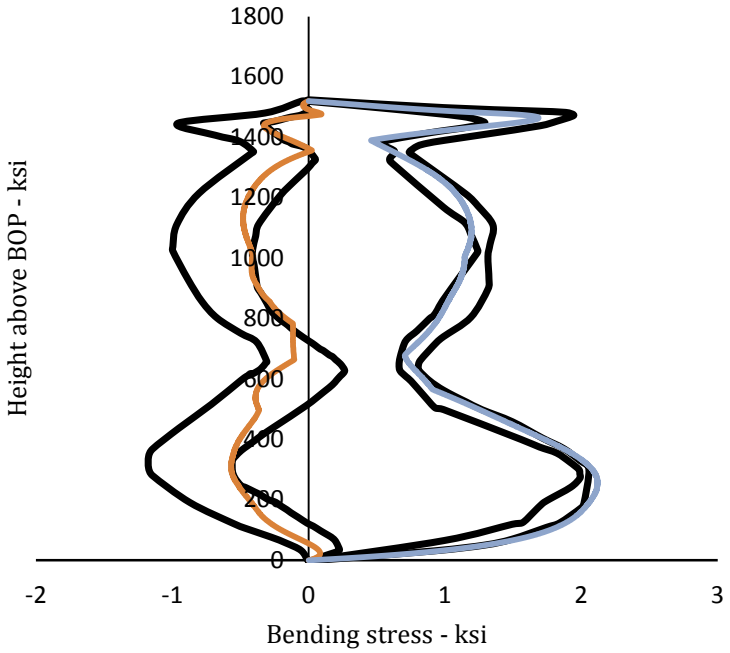

Figure B—13 Bending stress 1500-20-2-D

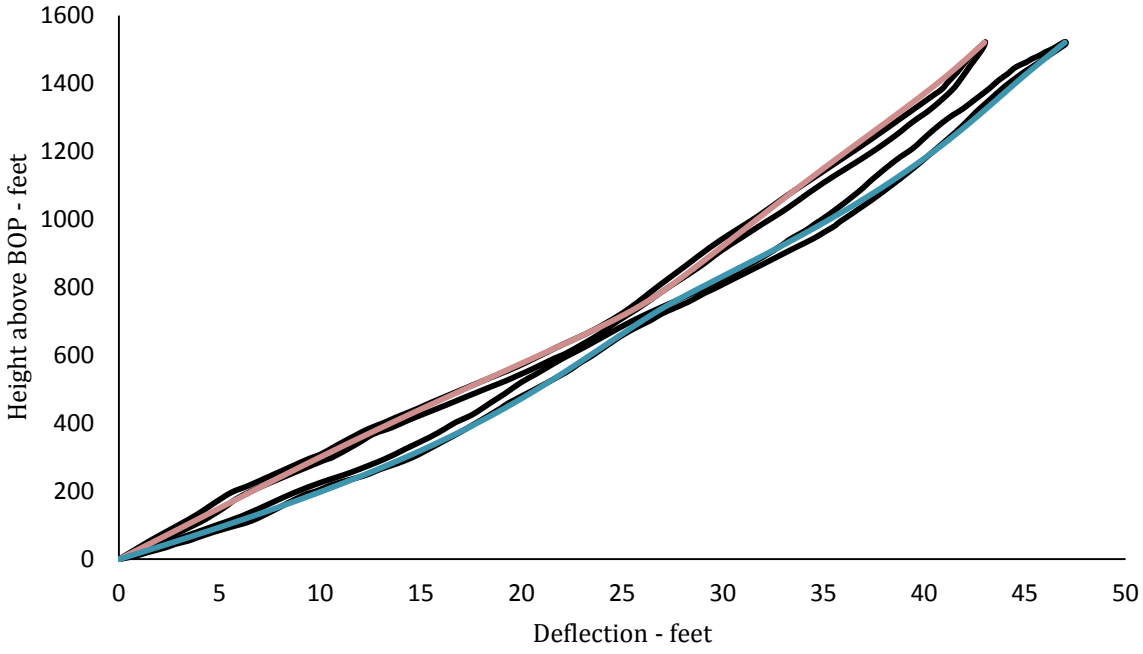

Figure B—14 Deflection 1500-20-2-D

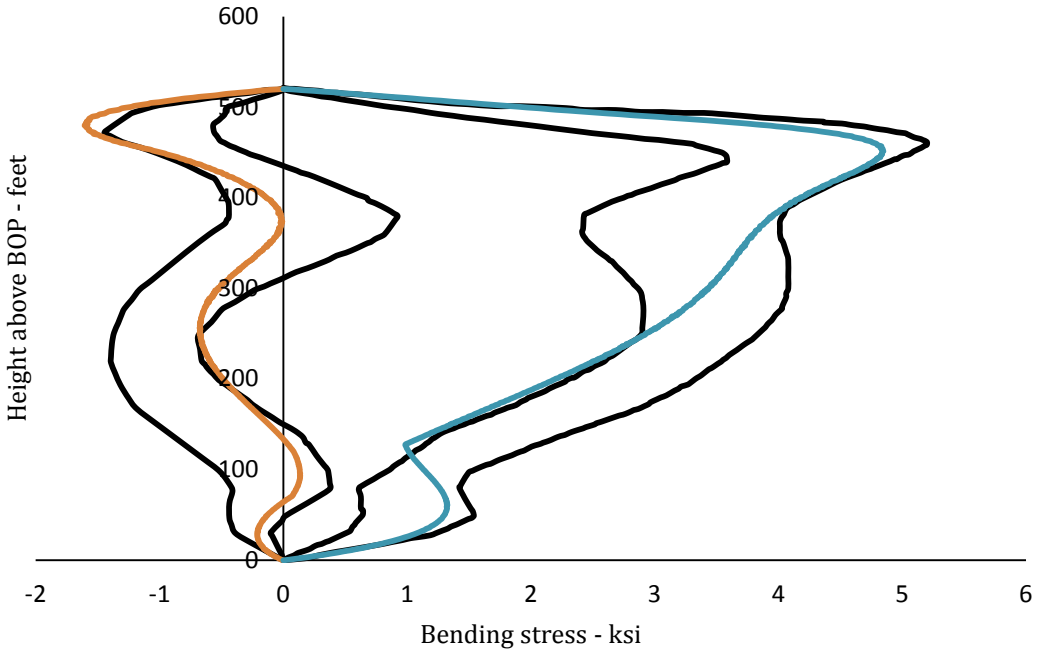

Figure B—15 Bending stress 500-40-Free-D

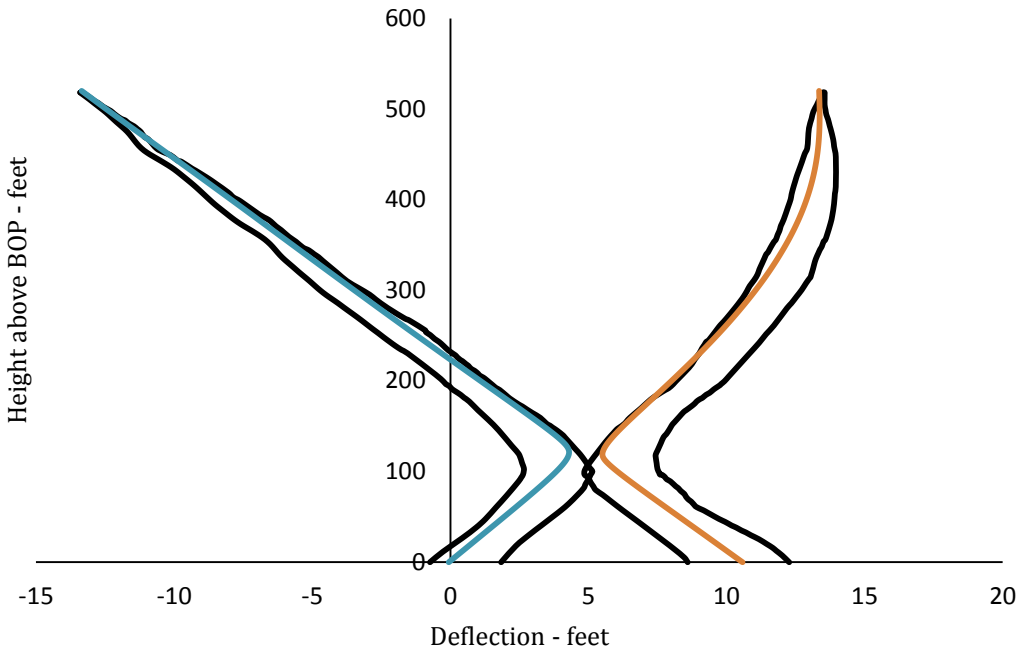

Figure B—16 Deflection 500-40-Free-D

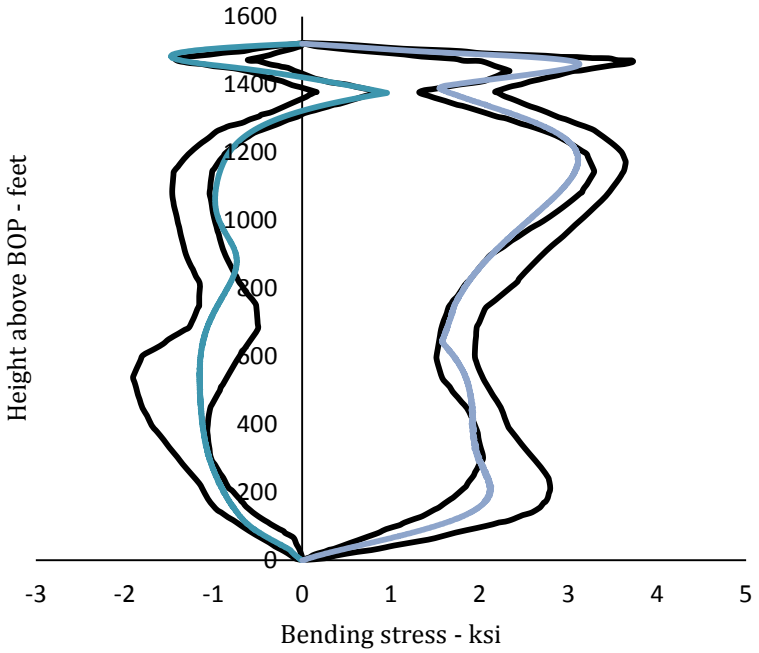

Figure B—17 Bending stress 1500-40-Free-D

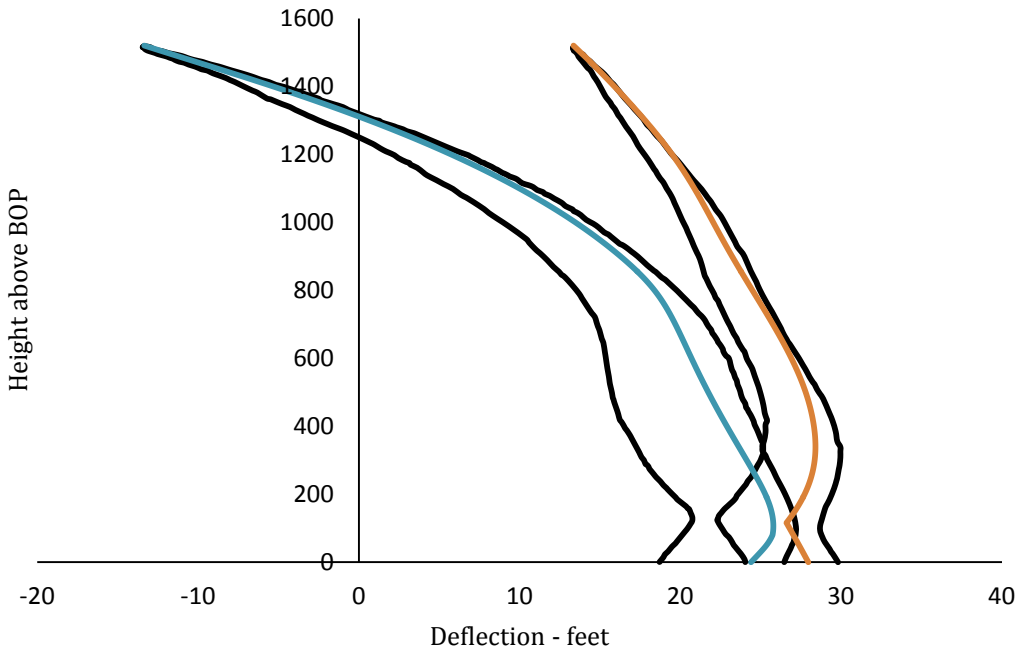

Figure B—18 Deflection 1500-40-Free-D

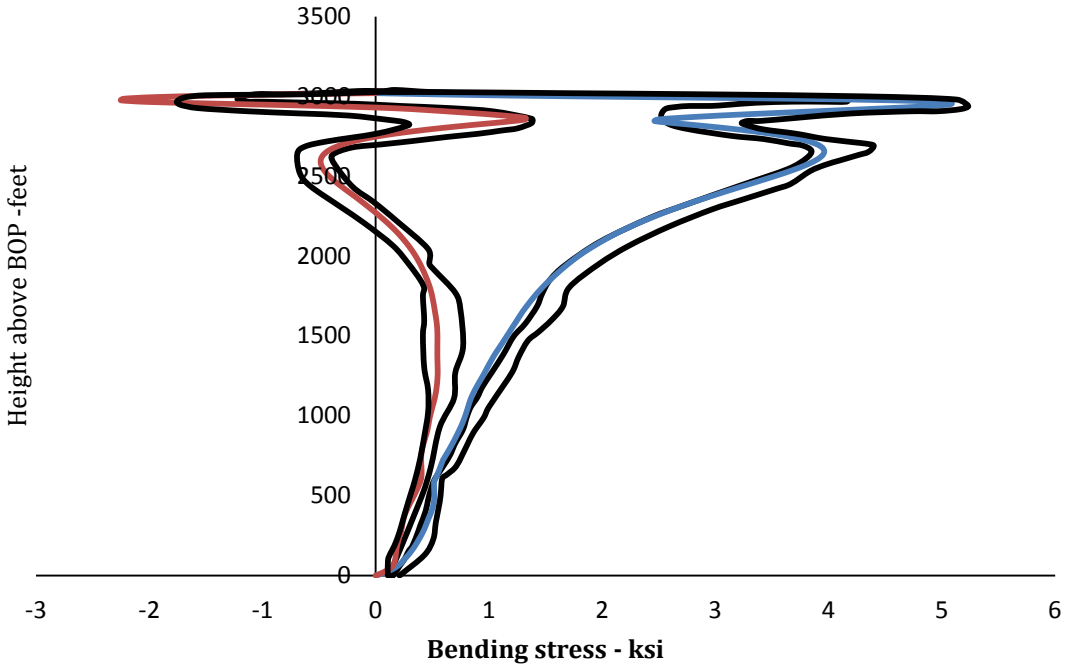

Figure B—19 Bending stress 3000-40-Free-D

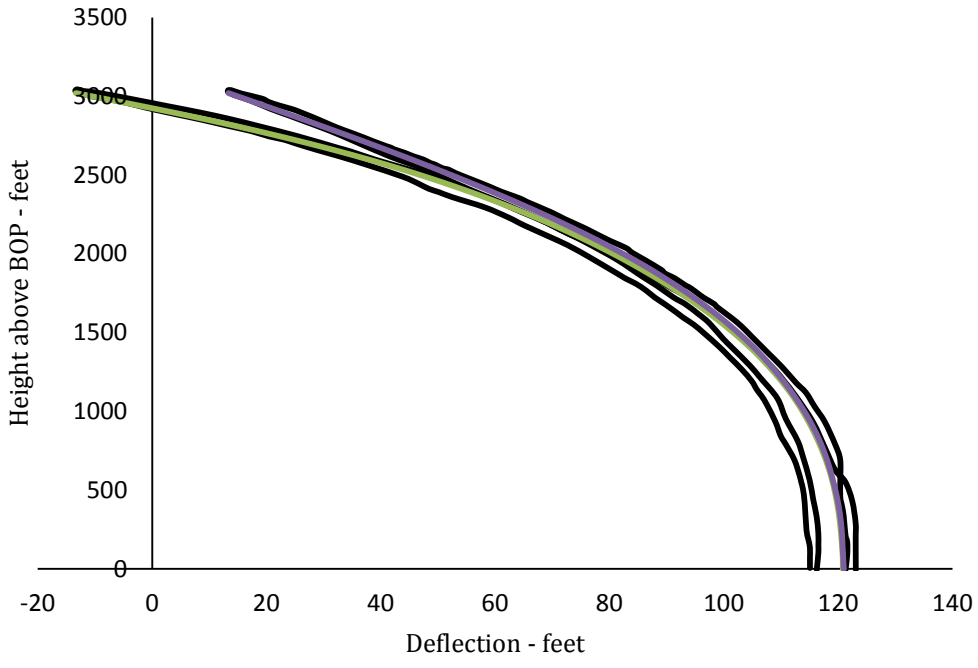

Figure B—20 Deflection 3000-40-Free-D

B.3 Appendix Summary

An overview of the elements of an OrcaFlex model has been presented. This is followed by OrcaFlex software validation using API Bulletin 16J cases. Both static and dynamic results are detailed in the API bulletin. We concentrate here on the dynamic results. The graphs presented show both the output obtained from OrcaFlex and representations of the output obtained from the other programs involved in the original API test. In general, and with few exceptions, the OrcaFlex output lies comfortably within the envelopes.

B.4 References

API 1982. American Petroleum Institute Bulletin on Comparison of Marine Drilling Riser Analyses. API Bulletin. 16J, Washington.

Barltrop, N. D. P. 1998. *Floating structures: A guide for design and analysis*, Oilfield Publications, Incorporated.

Orcina 2010. Orcaflex user manual *Orcina,* version 9.4a, UK.

Whitford, D. J. 2002. Teaching ocean wave forecasting using computer-generated visualization and animation--part 1: Sea forecasting. *Computers & geosciences,* 28**,** 537-546.

APPENDIX C

RAINFLOW COUNTING METHOD

C.1 Introductory Remarks

This appendix presents the cycle counting technique which can be used to reduce a complicated variable amplitude loading history into a number of discrete simple constant amplitude loading events which in turn are associated with fatigue damage.

C.2 Rainflow Counting

Various methods of cycle counting have been proposed to convert the irregular load histories to blocks of constants amplitude cycles. These counting methods can be subdivided into two categories; one-parameter cycle counting methods (i.e., level crossing counting, peak counting and range counting methods): and two-parameter cycle counting methods (i.e. Rainflow counting RFC) (Lee, 2005). One of the preferred methods in the rainflow counting method and is widely accepted technique of cycle counting in fatigue analysis for damage assessment in engineering components and structures. .

Rainflow cycle counting method has initially been proposed by Matsuiski and Endo (1968) in Japan and become known as rainflow method (Singh and Ranganath, 2007, Lindgren, 1987, Rychlik, 1987). RFC method is based on the analogy of raindrops falling on a pagoda roof and running down the edges of the roof. The RFC method is briefly described n the following.

A stress time series of peaks and valleys is considered with the time axis as shown Figure C—1 and in this method the lines connecting peaks and valleys fall from a series of pagoda roofs. The rainflow method applies general rules to produce stress cycles, as follows:

- Each rainflow begins at the beginning of the time series and successively at the inside of every peak and valley.
- Rainflow initiating at a peak (or a valley) drops down until it reaches opposite a peak more positive (or a valley more negative) than the peak (or the valley) it started from.
- Rainflow also stops when it meets the rainflow from a roof above.
- Rainflow must terminate at the end of the time series.
- The horizontal length of each rainflow is counted as a half cycle with that stress range.

As shown in Figure C—1, the first rainflow starts from the beginning at 1 as a valley, the second one from the peak 2, the third one from the valley 3, and so on. The end at 10 is considered as a peak herein. There are totally 9 half cycles can be extracted from this time series.

The rainflow initiating at the valley 1 drops down at 2 and ends at 4 because the following valley 5 has a smaller value than the initial point 1. Therefore, a half cycle of 1-2-4 has been identified. The same rule can be applied to determine the half cycle of 5-6.

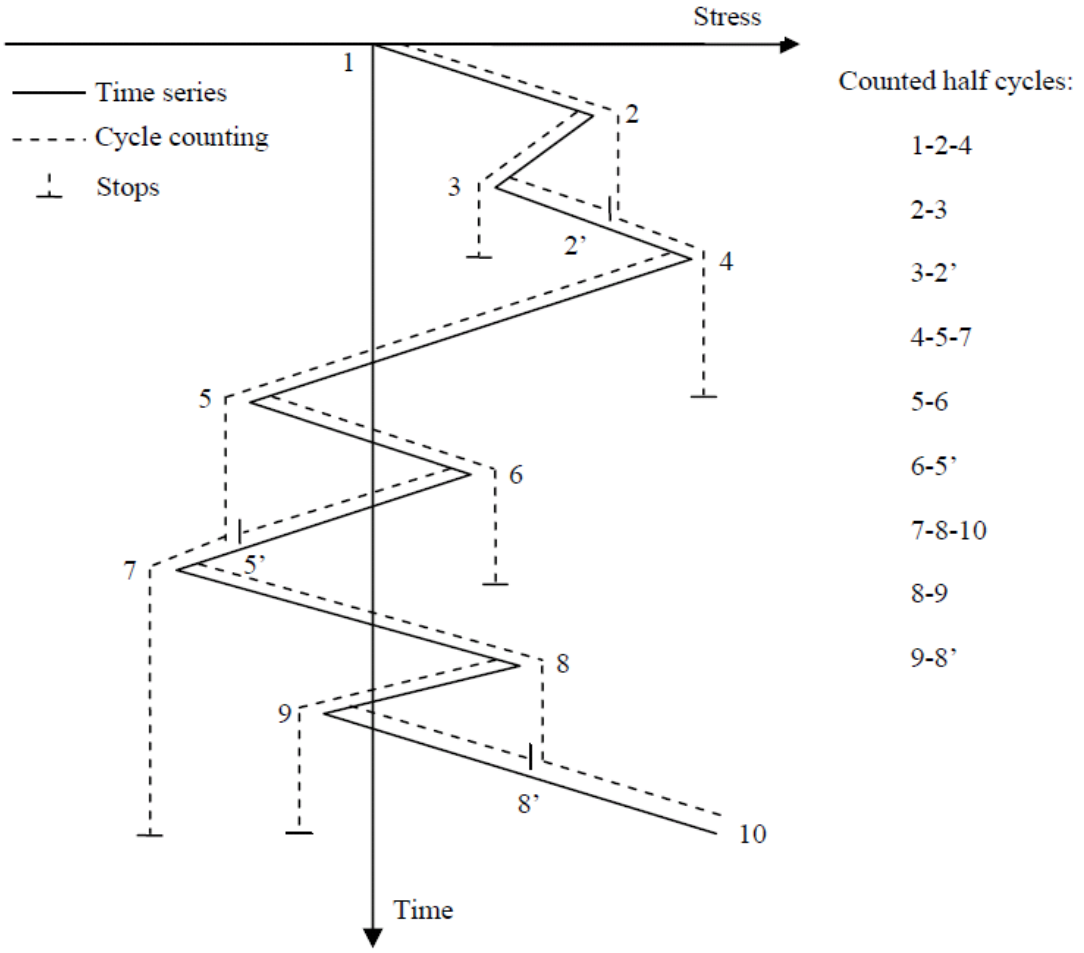

Figure C—1 Illustration of rainflow cycle counting method

The second rainflow starts from 2 and stops at 3, which leads to a half cycle of 2-3, because the following peak 4 has larger value than 2. Similarly, the half cycles of 4-5-7 and 8-9 can be extracted based on the same rule due to the largest peak at 10.

The half cycles of 3-2', 6-5' and 9-8' are determined because the rainflows started at 3, 6 and 9, respectively, meet the rainflows from roofs above.

The half cycle of 7-8-10 is formed because the time series ends at 10.

When all of the half cycles have been identified, the horizontal length of each cycle is used as an effective stress range to calculate the fatigue damage based on Miner's rule fatigue accumulation.

C.2 Appendix Summary

This appendix presented the original proposal of the rainflow cycle counting algorithm. RFC is now generally regarded as the method leading to the best estimation of the fatigue life. A number of algorithms have been proposed due to the great importance of the RFC.

C.3 References

Lee, Y. L. 2005. *Fatigue testing and analysis: Theory and practice*, Butterworth-Heinemann.

Lindgren, G. a. R., I. 1987. Rain flow cycle distributions for fatigue life prediction under gaussian load processes. *Fatigue & Fracture of Engineering Materials & Structures* Vol. 10, No. 3, pp.251-260.

Rychlik, I. 1987. A new definition of the rainflow cycle counting method. *International journal of fatigue,* 9**,** 119-121.

Singh, K. & Ranganath, V. 2007. Cycle counting using rainflow algorithm for fatigue analysis.

APPENDIX D

COATING OF SCR

D.1 Introductory Remarks

This appendix presents an overview of the SCR coating and insulation.

D.2 SCRs Coating

Polymeric external coatings are generally used on flowlines and risers for corrosion protection, mechanical protection and thermal insulation. The most common coating systems used in offshore oil and gas industry are:

- Multilayer polypropylene (PP) or polyethylene (PE)
- Polyurethane / syntactic polyurethane (PU)
- Rubber coating

The different coating systems have various density limits which are qualified for deepwater offshore industry. Rubber coating is classified as high density coating system while PP and PU classified as low density coating system.

A multilayer technology is applied to achieve the various functional requirements for SCR system. Five-layer syntactic PP coating has been used in deepwater projects with coating thickness ranging from 34-102 mm (Karunakaran *et al.*, 2005, Deka *et al.*, 2010), see Figure D—1. The normal coating density is ranging from 750-950 kg/m^3.

The five-layer syntactic PP coating consists of (Karunakaran *et al.*, 2005, Bai and Bai, 2010):

- 1st Layer - Fusion bond epoxy
- 2nd Layer - PP adhesive
- 3rd Layer - Solid PP
- 4th Layer - Syntactic PP
- 5th Layer - Solid PP

The functions of the five-layers are:

- 1st to 3rd Layer – for corrosion protection
- 4th Layer – for buoyancy and thermal insulation
- 5th Layer – provide protective top coating

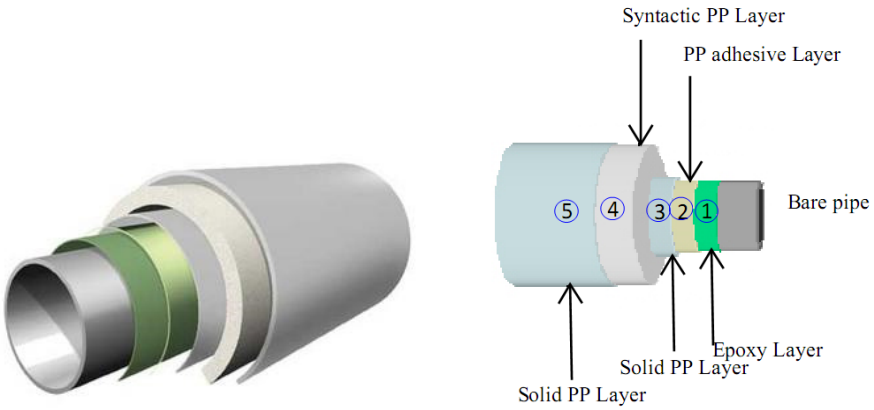

Figure D—1 Five-layer syntactic PP (Jukes *et al.*, 2008, Grosjean *et al.*, 2009, CHAPMAN and SHUKLA, 2012)

D.3 Appendix Summary

This appendix reviewed the coating layers and its characteristics for SCRs.

D.4 References

Bai, Y. & Bai, Q. 2010. *Subsea engineering handbook*, Gulf Professional Publishing.

CHAPMAN, M. & SHUKLA, K. 2012. Non-chemical solutions enhance flow assurance options. *Offshore,* 72.

Deka, D., Campbell, M., Kakar, K. & Hays, P. Advances in deepwater riser technology: Gulf of mexico wet tree deepwater riser concepts with sour service. *In:* Offshore Technology Conference, 2010 Houston, USA.

Grosjean, F., Bouchonneau, N., Choqueuse, D. & Sauvant-Moynot, V. 2009. Comprehensive analyses of syntactic foam behaviour in deepwater environment. *Journal of materials science,* 44**,** 1462-1468.

Jukes, P., Wang, S. & Wang, J. The sequential reeling and lateral buckling simulation of pipe-in-pipe flowlines using finite element analysis for deepwater applications. *In*, 2008. International Society of Offshore and Polar Engineers, P. O. Box 189, Cupertino, CA, 95015-0189, USA.

Karunakaran, D., Meling, T., Kristoffersen, S. & Lund, K. Weight-optimized scrs for deepwater harsh environments. *In*, 2005.

APPENDIX E

NORTHERN NORTH SEA SCATTER TABLE

E.1 Scatter Table

Table E—1 Joint frequency of significant wave height and spectral peak period for the NNS (Faltinsen, 1999)

H_s (m)	Spectral peak periods (T_p)																			
	3	4	5	6	7	8	9	10	11	12	13	14	15	16	17	18	19	21	22	**Sum**
1	59	403	1061	1569	1634	1362	982	643	395	232	132	74	41	22	12	7	4	2	2	8636
2	9	212	1233	3223	5106	5814	5284	4102	2846	1821	1098	634	355	194	105	56	30	16	17	32155
3	0	8	146	831	2295	3896	4707	4456	3531	2452	1543	901	497	263	135	67	33	16	15	25792
4	0	0	6	85	481	1371	2406	2960	2796	2163	1437	849	458	231	110	50	22	10	7	15442
5	0	0	0	4	57	315	898	1564	1879	1696	1228	748	398	191	84	35	13	5	3	9118
6	0	0	0	0	3	39	207	571	950	1069	885	575	309	142	58	21	7	2	1	4839
7	0	0	0	0	0	2	27	136	347	528	533	387	217	98	37	12	4	1	0	2329
8	0	0	0	0	0	0	2	20	88	197	261	226	138	64	23	7	2	0	0	1028
9	0	0	0	0	0	0	0	2	15	54	101	111	78	39	14	4	1	0	0	419
10	0	0	0	0	0	0	0	0	2	11	30	45	39	22	8	2	1	0	0	160
11	0	0	0	0	0	0	0	0	0	2	7	15	16	11	5	1	0	0	0	57
12	0	0	0	0	0	0	0	0	0	0	1	4	6	5	2	1	0	0	0	19
13	0	0	0	0	0	0	0	0	0	0	0	1	2	2	1	0	0	0	0	6
14	0	0	0	0	0	0	0	0	0	0	0	0	0	1	0	0	0	0	0	1
15	0	0	0	0	0	0	0	0	0	0	0	0	0	0	0	0	0	0	0	0
Sum	68	623	2446	5712	9576	12799	14513	14454	12849	10225	7256	4570	2554	1285	594	263	117	52	45	100001

Table E—2 Determination of 100-year wave height in NNS by assuming wave period 16 seconds

j	H_{sj}	n_j	p_j	$\exp(-2*H^2/H_{sj}^2)$	$\exp(-2*H^2/H_{sj}^2)*p_j$
1	0.5	22	0.00022	0	0
2	1.5	194	0.00193998	2.8208E-288	5.4723E-291
3	2.5	263	0.00262997	3.0348E-104	7.9815E-107
4	3.5	231	0.00230998	1.53025E-53	3.53484E-56
5	4.5	191	0.00190998	1.12213E-32	2.14324E-35
6	5.5	142	0.00141999	4.09271E-22	5.81159E-25
7	6.5	98	0.00097999	4.86078E-16	4.76352E-19
8	7.5	64	0.00063999	3.14786E-12	2.01461E-15
9	8.5	39	0.00039	1.1096E-09	4.32741E-13
10	9.5	22	0.00022	6.77911E-08	1.49139E-11
11	10.5	11	0.00011	1.35407E-06	1.48946E-10
12	11.5	5	5E-05	1.28189E-05	6.40939E-10
13	12.5	2	2E-05	7.23245E-05	1.44648E-09
14	13.5	1	9.9999E-06	0.000281841	2.81838E-09
15	14.5	0	0	0.000837095	0

The conclusion of the preceding table is,

P(H)	0.999999995
Q = 1-P(H)	5.07009E-09
N (number of response cycles)	197234997.2
Return Period (Years)	99.99999858
$H_s = H_{max} / 1.75$	15.59561339

Therefore, the 100-year sea state is:

- significant wave height H_s 15.6 m
- corresponding wave peak period T_p 16

E.2 Formulation of JONSWAP wave spectrum

The spectral density function for the JONSWAP (Joint North Sea Wave Project) spectrum can be written as:

$$S_\zeta(w_0) = \alpha g^2 w_0^{-5} e^{-\frac{5}{4}\left(\frac{w_p}{w_0}\right)^4} \gamma^{e^{-\frac{1}{2}\left(\frac{w_0 - w_p}{\sigma w_p}\right)^2}}$$

The wave spectrum parameters are

α – Spectral parameter (generalized Phillips' constant), $\alpha = 1.2905 \frac{H_s^2}{T_z^4}$

The spectrum parameter α is also computed as

$$\alpha = \frac{5}{16} \frac{H_s^2 w_p^4}{g^2} (1 - 0.287 \ln \gamma)$$
$$= 5.061 \frac{H_s^2}{T_p^4} (1 - 0.287 \ln \gamma)$$

H_s – significant wave height which is approximately equal to the average of the highest one third of the waves

g – acceleration of gravity

w_0 – wave frequency (rad/sec), *$w = 2\pi/T_w$*

T_w – wave period

w_p – peak frequency, $w_p = 2\pi/T_P$

T_P – peak or significant wave period (period with maximum energy density)

T_z – zero up-crossing wave period, $\frac{T_p}{T_z} = 1.407\left(1 - 0.287\ln\gamma\right)^{1/4}$

γ – peakedness parameter

σ – spectral width parameter, $\sigma = 0.07$ for $w_0 < w_p$ and $\sigma = 0.09$ for $w_0 > w_p$

The Pierson-Moskowitz spectrum appears for $\gamma = 1$.

where H_s is the significant wave height. A standard value of the peackedness parameter γ is 3.3. However, amore correct approach is to relate the peakedness parameter to the significant wave height and the peak period:

$$\begin{aligned} \gamma &= 1.0 && T_p \geq 5\sqrt{H_s} \\ &= \exp\left(5.75 - 1.15\frac{T_P}{\sqrt{H_s}}\right) && 3.6\sqrt{H_s} \leq T_P < 5\sqrt{H_s} \\ &= 5.0 && T_P < 3.6\sqrt{H_s} \end{aligned}$$

E.3 References

Barltrop, N. D. P., A. J. Adams and M. Hallam. 1991. *Dynamics of fixed marine structures*. Butterworth-Heinemann Oxford.

Faltinsen, O. M. 1999. *Sea loads on offshore structures,* Cambridge, Cambridge University Press.

APPENDIX F

STATISTICAL DISTRIBUTIONS

F.1 Introductory Remarks

This appendix contains the statistical distributions used to represent the probabilistic variability of the basic random variables used in Chapter 7.

F.2 Probability distributions

Normal Distribution

Probability density function:

$$f_X(x) = \frac{1}{\sigma\sqrt{2\pi}} \exp\left[\frac{-1}{2}\left(\frac{x-\mu}{\sigma}\right)^2\right] \quad \text{where} \quad -\infty < x < \infty$$

Equation F—1

Cumulative distribution function:

$$F_X(x) = \int_{-\infty}^{x} \frac{1}{\sigma\sqrt{2\pi}} \exp\left[\frac{-1}{2}\left(\frac{t-\mu}{\sigma}\right)^2\right] dt \quad \text{where} \quad -\infty < x < \infty$$

Equation F—2

This integral can not be evaluated in closed form, however, by using the substitution $s = (t - \mu)/\sigma$ and $dt = \sigma ds$, Equation F—2 becomes

$$F_X(x) = \int_{-\infty}^{\frac{x-\mu}{\sigma}} \frac{1}{2\pi} \exp\left[-\frac{1}{2}s^2\right] ds$$

Equation F—3

The standard normal distribution function used is defined by:

$$\Phi_X(x) = \int_{-\infty}^{x} \frac{1}{\sqrt{2\pi}} \exp\left[\frac{-t^2}{2}\right] dt$$

Equation F—4

Lognormal Distribution

If the random variable $Y = \ln(X)$ is normally distributed (and μ_Y is a real number and $\sigma_Y > 0$) then X is lognormally distributed.

Probability density function:

$$f_X(x) = \frac{1}{\sigma_Y \sqrt{2\pi}} \frac{1}{x} \exp\left[-\frac{1}{2}\left(\frac{\ln(x)-\mu_Y}{\sigma_Y}\right)^2\right] \qquad \text{where } 0 \le x \le \infty$$

Equation F—5

Cumulative distribution function

$$F_x(x) = \Phi\left(\frac{\ln(x)-\mu_Y}{\sigma_Y}\right)$$

Equation F—6

where F is the standard normal distribution of Equation F—4.

Gumbel Distribution

The Gumbel distribution, also known as the *Extreme Value Type I* distribution, and has the following probability density function:

$$f(x) = \frac{1}{\sigma}\exp\left(-z-\exp^{(-z)}\right)$$

Equation F—7

where $z=(x-\mu)/\sigma$, μ is the location parameter, and σ is the distribution scale ($\sigma>0$).

Cumulative distribution function

$$F_x(x) = \exp\left(-\exp^{(-z)}\right)$$

Equation F—8

Weibull Distribution

The Weibull distribution, also known as the *Extreme Value Type III* distribution, first appeared in his papers in 1939. The two-parameter version of this distribution has the density function

$$f(x)=\frac{\alpha}{\beta}\left(\frac{x}{\beta}\right)^{\alpha-1}\exp\left(-\left(\frac{x}{\beta}\right)^{\alpha}\right)$$

Equation F—9

The Weibull distribution is defined for x>0, and both distribution parameters (α - shape, β - scale) are positive.

APPENDIX G

RELIABILITY ANALYSIS TECHNIQUES

G.1 Introductory Remarks

Reliability theory for structures is concerned with the rational treatment of uncertainties in structural engineering and with the methods for assessing the safety and serviceability of structures. It has become a design tool in some cases with the objective of achieving a more uniform and consistent reliability within a class of structures or structural systems. Modern reliability methods provide an alternative design approach by assigning probability distributions to the uncertain variables for computation of the probability of exceeding various limit states and for comparison of this probability with a required reliability level. This appendix presents an overview of reliability calculation techniques.

G.2 Overview of reliability calculation techniques

Methods required for the evaluation reliability analysis:

i. *First Order Reliability Methods* (FORM): The failure function (or the RS) is approximated by a first order function in standardised Gaussian space at the most probable failure point. In standardised Gaussian space this is the point physically closest to the origin (the mean point).

ii. *Second Order Reliability Methods* (SORM): Similar to FORM except that curvature is considered by fitting a second order function.

iii. *Monte Carlo Simulation (MCS)*: Briefly, it uses randomly generated samples of the input variables for each deterministic analysis, and estimates response

statistics and reliability after numerous repetitions of the deterministic analysis. The efficiency of the simulation can be improved by variance reduction techniques. Monte Carlo method can easily handle problems with implicit and closed-form performance functions. As long as an algorithm (a black box, such as a commercial finite element program) is available to compute the structural response, given the values of the input variables, the Monte Carlo method can easily evaluate G(x) for each deterministic analysis and therefore compute the failure probability after performing several deterministic analyses. However, if the deterministic structural analysis is time-consuming, as in the case of structures with numerous finite elements, the Monte Carlo simulation may be impractical.

FORM and SORM will be discussed briefly in the following sections.

G.3 Analytical approximation methods

The analytical approximation methods are generally categorized into the First Order Reliability Method (FORM) and the Second Order Reliability Method (SORM). In these approximation methods, the original problem is first transformed into a standard normal probability space and the failure probability is then calculated by converting the original hyperplane failure surface into the tangential and quadratic approximations. Transformation to the standard normal space is of importance in a reliability analysis because the

reliability index in this space has a geometry interpretation as the shortest distance to origin.

G.3.1 Transformation to the standard Normal space

In the approximation methods, the reliability calculation should be carried out in the standard independent normal space. Since the original basic random variables are in general not mutually independent and normally distributed, a procedure is required to transform the vector of basic variables, *x*, into a vector of independent standard normal variables, *u*. In most cases the Rosenblatt transformation procedure can be performed, i.e.

$$u_1 = \Phi^{-1}\left[F_1\left(x_1\right)\right]$$
$$u_2 = \Phi^{-1}\left[F_2\left(x_2 \middle| x_1\right)\right]$$
.
.
.
$$u_n = \Phi^{-1}\left[F_n\left(x_n \middle| x_1, x_2, \ldots, x_{n-1}\right)\right]$$

Equation G—1

where $\Phi(\ )$ is the standard normal distribution and $F_i\left(x_i\right)$ is the cumulative distribution of x_i conditional on $x_1, x_2, \ldots, x_{n-1}$.

This transformation is usually carried out numerically step by step, i.e. the first step x_1 is transformed into a standard normal variable and followed in the

second step by a transformation of $x_2 | x_1$ into standard normal variables and this procedure is continuing to the end, see Figure G—1. When the variables are mutually independent, this transformation reduces to:

$$u = \Phi^{-1}\left[F_x(x)\right]$$

Equation G—2

The inverse transformation is:

$$x = F_x^{-1}\left[\Phi(u)\right]$$

Equation G—3

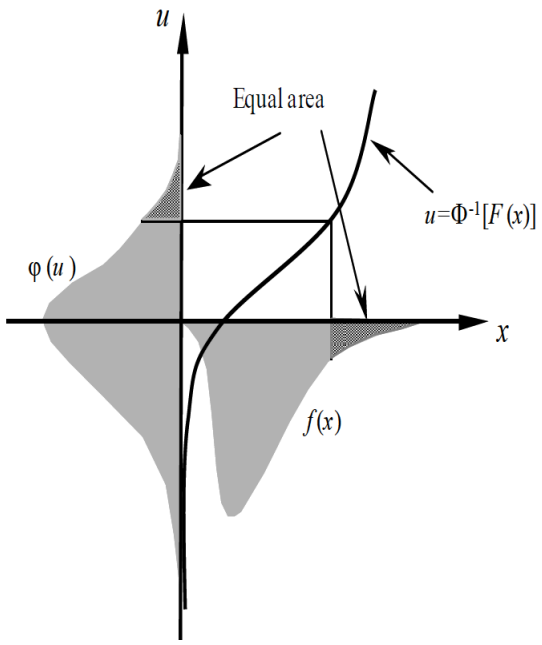

Figure G—1 Transformation of single random variable into Normal standard space

Using he above transformation, the entire g(*x*)-function can be transformed to g(u) and allow the probabilistic analysis to be performed in the u-space. Numerically, however, the *x*-to-*u* or *u*-to-*x* transformations are needed only at points required to find the Most Probable Point (MPP), construct polynomials, and perform importance sampling. The advantage for transforming to the u-space is that probabilistic analysis becomes mathematically more tractable. The drawback is that the involved transformation.

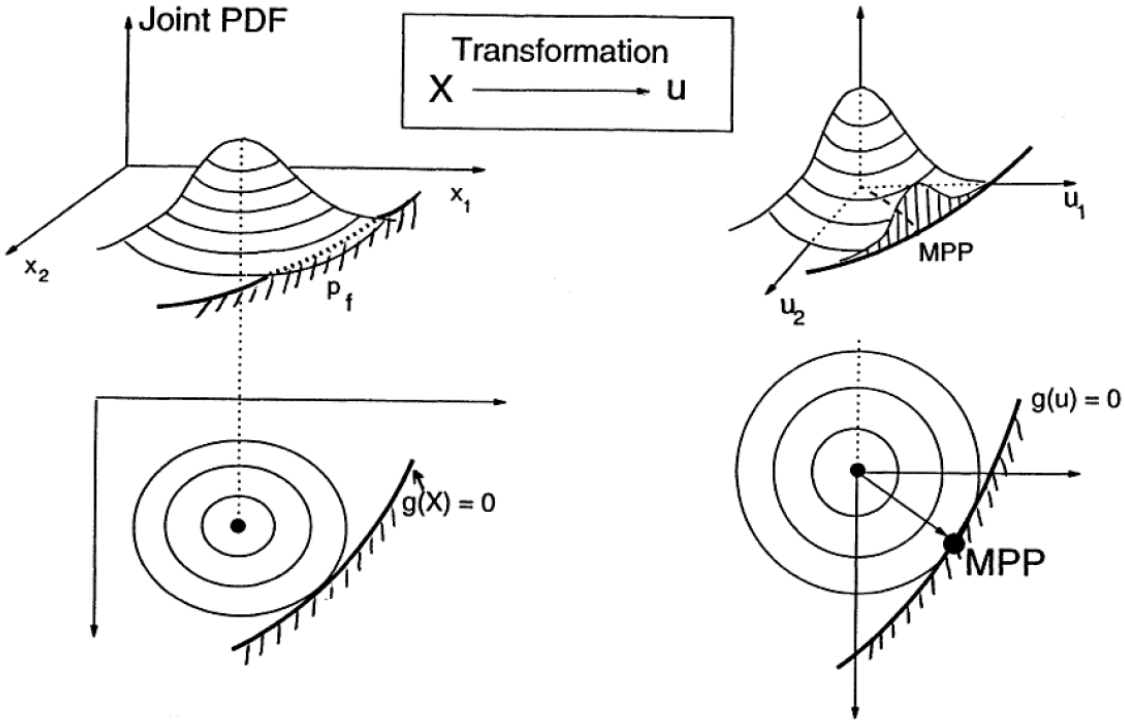

Figure G—2 Most Probable Point (MPP) (Haldar and Mahadevan, 2000a)

G.3.2 First Order Reliability Method (FORM)

In the first order reliability method, the random variables are firstly transformed into the standard normal space by one of the methods explained in the previous section and the failure surface is then replaced by its tangent hyperplane. The reliability index in this space is defined as the shortest distance between this tangent hyperplane and origin and an iteration procedure must be carried out to search for the shortest distance. The FORM probability solution is based on the linearisation of the g-function at the MPP in the u-space. The first-order polynomial, $g_1(u)$, is:

$$g_1(u) = a_0 + \sum_{i=1}^{n} a_i \left(u_i - u_i^*\right)$$

Equation G—4

Given $g_1(u)$, the probability of failure is a function of the minimum distance to the plane defined by g_1 in u-space:

$$p_f = \Phi(-\beta)$$

Equation G—5

Where β is computed from

$$\beta = \frac{\mu_g}{\sigma_g} = \frac{a_0 + \sum_{i=1}^{n} a_i \mu_i}{\sqrt{\sum_{i=1}^{n} a_i^2 \sigma_i^2}}$$

Equation G—6

where β is the first order reliability index and defined as the shortest distance from the origin to the failure surface and its sign is determined as the sign of $g_u(0)$, Figure G—3. A negative β means the origin is in the failure region (i.e., for the $p_f > 0.5$ case). α vector is positive from MPP to the origin and α_i is the component of the unit normal to the failure surface with direction towards the failure space (direction cosine). The closest point to the origin on the failure surface is defined as the design point, u^*. Figure G—4 summarises the FORM results.

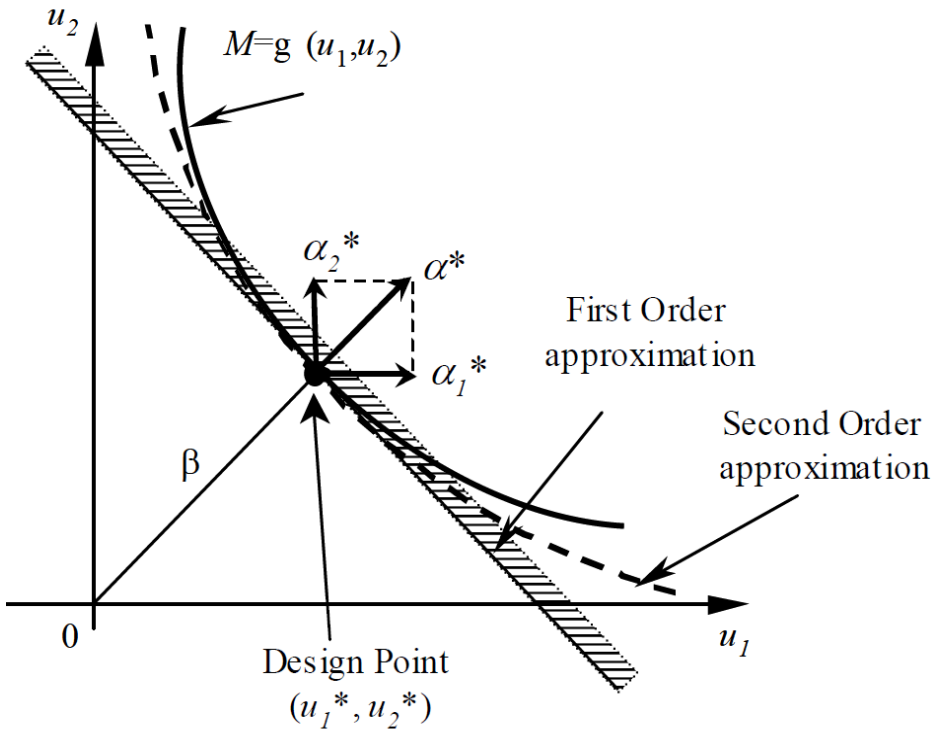

Figure G—3 First and second order approximation of limit state in standard Normal space (Ditlevsen and Madsen, 1996)

By minimizing this function, the design point can be determined with $u_i^* = \beta\alpha_i^*$ in such a way that the component of the unit vector is given by

$$\alpha_i^* = -\frac{\partial g_u\left(u_i^*\right)/\partial u_i^*}{\left[\sum_{j=1}^{n}\left(\partial g_u\left(u_j^*\right)/\partial u_j^*\right)\right]^{1/2}}$$

Equation G—7

The direction cosine α_i^* is a measure of the sensitivity of the reliability index to change in the corresponding random variable, u_i^*. Furthermore, a positive α-

value indicates a load variable and a negative α-value indicates a resistance variable. The quantity $\left(\alpha_i^*\right)^2$ is commonly attributed to the importance factor of the variable and the value is an indication of the uncertainty fraction that can be associated with the corresponding random variable.

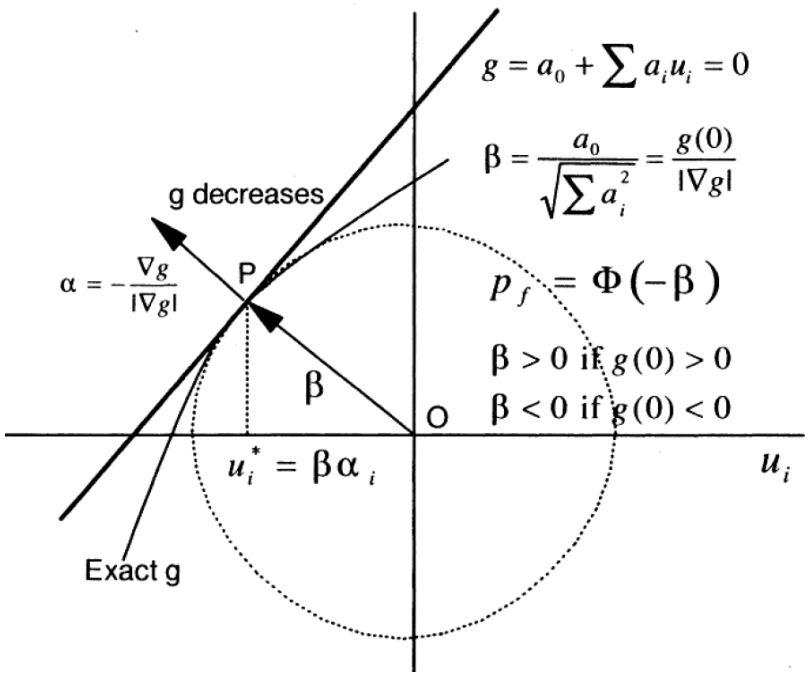

Figure G—4 First Order Reliability Method

The failure probability according to this method can be determined with $p_{f,FORM} = p[g_u(u) \le 0] = \Phi(-\beta)$. In the iteration procedure of the FORM approach for finding the shortest distance from the origin, care should be given to the search algorithm because sometimes the iteration process leads to the global maximum instead of minimum. Furthermore, for failure surfaces with several minimum points, the iteration procedure may only focus on one of the

local minima instead of a global one (local minimum). It thus becomes necessary to try several starting points for the iteration routine or generally apply another procedure such as MCS to determine the failure probability.

In the case of a highly nonlinear failure surface, the FORM algorithm sometimes may not represent the exact failure probability content and other procedures such as SORM or Monte Carlo Simulation techniques will be more essential and proper than using the FORM method.

MPP Search Procedure

The MPP is the key approximation point for the MPP-based methods. Therefore, the identification of the MPP is an important task. Generally, the identification of the MPP can be solved by many optimisation problem (i.e., find the minimum distance point subject to g=0) and can be solved by many optimisation methods. The procedure used for MPP search is summarised in the following steps (Haldar and Mahadevan, 2000b):

I. Assume an MPP x^*.
II. Compute equivalent normal distributions for the non-normal random variables at x^*.
III. Construct a linear g-function using x^* as the expansion point.
IV. Based on the equivalent normal distributions, compute the minimum distance and the updated MPP in the u-space.

V. Repeat steps II to IV until the MPP converges.

In III , the equivalent normal distribution is computed by the Rackwitz-Fiessler which matches the CDF's and the PDF's for the original and the equivalent normal distribution at the MP point,

$$F_x\left(x^*\right)=\Phi\left(u^*\right)$$

Equation G—8

and

$$f_x\left(x^*\right)=\frac{\phi\left(u^*\right)}{\sigma_N}$$

Equation G—9

where

$$u^*=\frac{x^*-\mu_N}{\sigma_N}$$

Equation G—10

The parameters μ_N and σ_N are the mean and the standard deviation of the approximate normal and $\phi(\cdot)$ is the standard normal PDF.

From the above three equations, the approximate normal parameters can be derived as:

$$\sigma_N = \frac{\phi\left[\Phi^{-1}\left(F_x\left(x^*\right)\right)\right]}{f_x\left(x^*\right)}$$

Equation G—11

$$\mu_N = x^* - \Phi^{-1}\left[F_x\left(X^*\right)\right]\sigma_N$$

Equation G—12

The above iteration algorithm has been found to be quite efficient and robust. Many other algorithms have been proposed in the literature. However, just like using any optimisation methods, there is no guarantee that the procedure will always converge.

G.3.3 Second Order Reliability Method (SORM)

The FORM method presented in the previous section, generally gives accurate results for practical engineering problems.

$$g_2(u) = a_0 + \sum_{i=1}^{n} a_i\left(u_i - u_i^*\right) + \sum_{i=1}^{n} b_i\left(u_i - u_i^*\right)^2 + \sum_{i=1}^{n}\sum_{j=1}^{i-1} c_{ij}\left(u_i - u_i^*\right)\left(u_j - u_j^*\right)$$

Equation G—13

The definition of $g_2(u)$ requires $n(n-1)/2$ second order derivatives. The second-order coefficients can be computed by numerical differentiation in NESSUS. Breitung derived the following asymptotic formula for large β:

$$p_{f,SORM} \approx \Phi(-\beta)\prod_{i=1}^{n-1}(1-\beta k_i)^{-1/2}$$

Equation G—14

where κ_i for i=1,2,..,n-1 are the main curvatures of the limit state at the design point. The SORM reliability index can therefore be estimated with,

$$\beta_{SORM} = -\Phi^{-1}(p_{f,SORM})$$

Equation G—15

The first and second-order methods, as well as other MPP-based methods (including the advanced first-order and the convolution method) attempt to approximate the original g-functions by simple functions.

G.4 Probability Sensitivity Analysis

Because all input random variables do not have equal influence on the statistics of the output, the probability sensitivity analysis can be used to quantify the influence of each basic random variable. In deterministic analysis, sensitivity is defined as $\partial Z/\partial X_i$, which measures the change in the performance due to the

change in a design parameter. In probabilistic analysis the sensitivity measure is $\partial p/\partial \theta_i$, which measures the change in the probability relative to the change in a distribution parameter (e.g., mean and standard deviation).

Another useful probability sensitivity analysis is the determination of the relative importance of the random variables. This can be done by performing several probabilistic analyses in which one of the random variables is treated as a deterministic variable (i.e., by reducing the standard deviation to zero) for each analysis. Based on the resulting probability changes, the relative importance of the random variables can be determined. Repeated analysis may be very time consuming for large numbers of random variables.

A more efficient way of evaluating the relative importance of the random variables is based on the location of the MPP. At the MPP, $u^* = \left(u_1^*, u_2^*, \ldots, u_n^*\right)$, the first-order probability estimate is $\Phi\left(-\beta\right)$where

$$\beta^2 = u_1^{*2} + u_2^{*2} + \ldots u_n^{*2}$$

Equation G—16

The unit normal vector at the MPP of the g=0 surface is defined as:

$$\alpha = -\frac{\nabla g}{|\nabla g|}$$

Equation G—17

The α vector is positive towards the direction of decreasing g (i.e. to the failure region). The sensitivity factors are the projections of the α vector to the u-axes. Thus, they are the directional cosines of the α vector as shown in Figure G—5, and can be written as:

$$\alpha_i = \frac{u_i^*}{\beta}$$

Equation G—18

The directional cosines satisfy the following rule:

$$\alpha_1^2 + \alpha_2^2 + \ldots \alpha_n^2 = 1$$

Equation G—19

Which implies that each α_i^2 is a measure of the contribution to the probability (since the probability is related to β); higher α (in magnitude) indicates higher contribution. Thus, the sensitivity factors provide a first-order information on the importance of the individual random variable.

It can be shown that in the u-space,

$$|\alpha_i| \propto \left(\frac{\partial g}{\partial u_i} \right)_{u^*}$$

Equation G—20

And in the X-space,

$$|\alpha_i| \propto \left(\frac{\partial g}{\partial X_i} \right)_{x^*} \sigma_i$$

Equation G—21

where σ_i is the normal (or approximate normal for non-normal distribution) standard deviation. It can be concluded that the sensitivity factors are function of both the deterministic sensitivity and the uncertainty (characterised by the standard deviation).

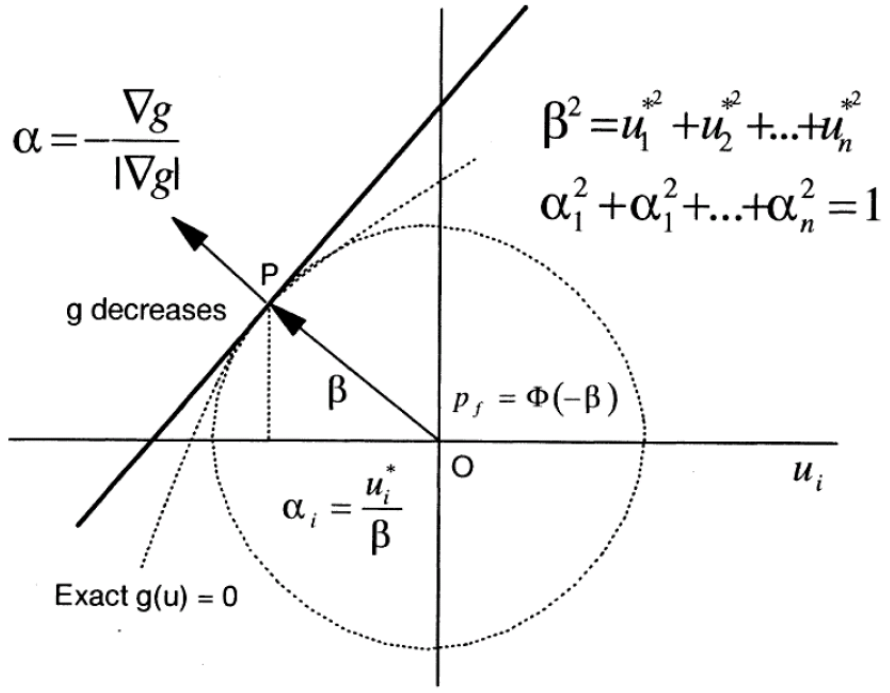

Figure G—5 Definition of sensitivity factors

In general, the sensitivity factors depend on the g-function as well as the input probability distributions. Because the above probabilistic sensitivity analysis is based on the first-order reliability method, α is a good probability sensitivity measure only if $\Phi(-\beta)$ is a good approximation to the true probability.

G.5 Appendix Summary

This appendix discussed briefly the reliability analysis techniques with special focus on FORM and SORM. The analytical solution of the reliability integral cannot be generally carried out except for very simple models and alternative techniques are needed for complex problems in reliability analysis. The alternative methods are

analytical approximations, MCS and numerical integration methods. The applicability of a particular method depends, as in all mathematical modelling, on the problem at hand and on the objective of the analysis.

G.5 References

Ditlevsen, O. & Madsen, H. O. 1996. *Structural reliability methods*, Wiley Chichester.

Haldar, A. & Mahadevan, S. 2000a. *Probability, reliability, and statistical methods in engineering design*, John Wiley & Sons, Incorporated.

Haldar, A. & Mahadevan, S. 2000b. *Reliability assessment using stochastic finite element analysis*, Wiley.

APPENDIX H

PAPERS

The papers written based on this thesis and submitted to journals or presented for conference are as follows:

1. Elosta, H., Huang, S., Incecik, A. 2012. Dynamic Response of Steel Catenary Riser/Seabed Interaction under Random Loads" *Submitted to Ocean Engineering Journal*.
2. Elosta, H., Huang, S., Incecik, A. 2012. Significance of Seabed Interaction on Fatigue Assessment of Steel Catenary Riser in Touchdown Zone. Submitted to *Journal of Marine structures*.
3. Elosta, H., Huang, S., Incecik, A. Reliability-Based Fatigue Analysis of Steel Catenary Riser in the Touchdown Zone. To be submitted to *Journal of Ship and Offshore Structures*.
4. Elosta, H., Huang, S., Incecik, A. 2013. Seabed Interaction Modelling Effects on the Global Response of Catenary Pipeline: A Case Study. *International Conference on Offshore Mechanics and Arctic Engineering, OMAE*10782, France.

Conference Presentations:

1. Reliability–Based Fatigue Analysis of Steel Catenary Riser with Seabed Interaction in the Touchdown Zone, Marine Technology Postgraduate Conference (MTPC), Glasgow, UK, 7th-8th June 2012.
2. Effects of Seabed on Steel Catenary Riser, Marine Technology Postgraduate Conference (MTPC), Newcastle, UK, 10th-11th June 2010.